Particle shape anisotropy and its effects in AlNiCo and Fe-Cr-Co magnet alloys.

GRAY, P.

PARTICLE SHAPE ANISOTROPY AND ITS EFFECTS IN ALNICO AND Fe-Cr-Co MAGNET ALLOYS

A thesis for the degree of

DOCTOR OF PHILOSOPHY

by

P. GRAY

submitted to the COUNCIL for

NATIONAL ACADEMIC AWARDS

May 1978

Department of Metallurgy,

Sheffield City Polytechnic &

Swift Levick & Sons Ltd.

PREFACE

The work reported in this thesis is intended as a contribution to the understanding of the magnetic and associated metallurgical characteristics and behaviour of those permanent magnet alloys which owe their properties to the presence of a finely distributed ferromagnetic phase based on iron in a non-ferromagnetic or lesser ferromagnetic matrix phase. The most commercially important examples of this are the Alnico alloys which have been available for more than fourty years and provide the "backbone" of the alloy permanent magnet industry at this time. The work reported here is concentrated not only on alloys in this system but also includes work on another alloy system, the Fe-Cr-Co system in which, as only relatively recently discovered, some alloys behave, both magnetically and metallurgically, in a very similar manner to the Alnicos.

During the course of this work I have attended two conferences on permanent magnets and magnetism. These were "The Third European Conference on Hard Magnetic Materials" held in Amsterdam in 1974, and "The Second I.E.E. Conference on the Advances in Magnetic Materials and Applications" held in London in 1976. I presented a paper at both these conferences covering certain aspects of the work now fully reported in this thesis. These papers have since been published in the proceedings of these conferences. In addition I have attended a course on numerical methods which was part of a M.Sc. course in Metallurgy. The course consisted of lectures and practical work including digital and analogue computing methods in about ten three hour weekly sessions. I also attended several series of lectures at degree level on relevant special subjects including theory of spinodal decomposition and other metallurgical transformations, and basic theory of magnetism.

I would like to express my gratitude to Swift Levick & Sons Ltd., for generously allowing time to be spent on the experimental work. It gives me great pleasure to thank my supervisors, Dr. H. W. Rayson of The Sheffield City Polytechnic and Dr. D. Hadfield of Swift Levick & Sons Ltd., for their valuable advice, helpful discussions and encouragement throughout.

Finally I would like to thank my wife Jackie for bearing with me throughout the course of this work and for typing the draft and final copies of the thesis itself.

ABSTRACT

This thesis is the result of a comparative investigation of two alloy systems from which useful permanent magnet properties can be achieved by suitable heat treatment. Alnico alloys, and in particular a Fe-Al-Ni-Co alloy, are compared with Fe-Cr-Co alloys.

The most striking observation throughout this work has been the great similarity in magnetic behaviour and metallurgical structure of the Alnico type alloys and the Fe-Cr-Co alloys.

The alloys studied, although they display additional idiosyncrasies peculiar to the individual alloy, all, with the support of TEM observations, behave magnetically (specifically the properties of magnetic anisotropy and coercivity) in a manner consistent with a common transformation mechanism. The evidence supports the view that this mechanism is spinodal decomposition, which initially produces an homogeneous, fine shape-anisotropic particle microstructure, and by subsequent diffusion during heat treatment achieves a highly ferromagnetic state; all of which are necessary conditions for good permanent magnet properties. The results indicates that some contribution to the magnet properties may ensue from further elongation of the particles with prolonged heat treatment. However the evidence indicates that elongated particles aligned, to an extent allowed by crystallographic conditions, with the direction of the applied field during the early stages of heat treatment are produced as the initial spinodal decomposition product, consistent with the theoretical predictions for this mechanism.

The rotational hysteresis loss and rotational hysteresis integral specify curling as the mode of magnetisation reversal in a Fe-Cr-Co alloy after heat treatment to produce the optimum magnetic state.

The behaviour of remanence and coercivity for Alcomax 111 and an Fe-Al-Ni-Co alloy suggests a possible proportional relationship between coercivity and the saturation magnetisation of the particles during tempering at 600°C. Coherent magnetisation reversal of the particles will give such a relationship at intermediate coercivity levels if it is assumed that some of the matrix magnetisation can reverse prior to the particle magnetisation.

CONTENTS

TABLES

XVIII Rotational hysteresis losses at indicated magnetic fields for alloy C1 heat treated to optimum magnetic condition [96]

XIX Experimental and theoretical predictions for the number of band electrons in the 4S band and the atomic percent of non-ferromagnetic solute element to reduce the magnetisation to zero in two component ferromagnetic solvent metal systems [115]

XX Fractional saturation (average composition) of a cylinder during diffusion [126]

FIGURES

19. (a) Free energies of formation of the α and σ phases in the system Fe-Cr (114), and (b) revised low-temperature phase diagram of the Fe-Cr system (113,114,115,116,117). [58]

20. (a) Vertical section of Fe-Cr-Co system at 15 wt.% Co and (b) vertical section of Fe-Cr-Co-Nb-Al system at 15 wt.% Co, 1 wt.% Nb and 1 wt.% Al (106). [59]

21. The assumption that $\partial^2 G/\partial C^2$ is independant of composition is equivolent to fitting the free-energy function to a parabola. [61]

22. Schematic evolution of concentration profiles to illustrate the difference between nucleation and growth and spinodal decomposition. [65]

23. Demagnetisation curves for samples of Alnico 5 after cooling at 1.5°C per second with magnetic field on for various times (120). [67]

24. (a) Variation of both structural parameters of α' particles and magnetic properties of Alnico 5 after cooling in a magnetic field interupted by quenching and after further tempering (140); and (b) coercivity of alnico isothermally aged measured at the ageing temperature and at R.T after tempering (70). [67]

25. Zijlstra's (51) magnetic anisotropy results for polycrystalline samples of Alnico 5 aged for various times and temperatures. [70]

26. Zijlstra's (51) magnetic anisotropy results for single crystals of Alnico 5 aged for various times and temperatures. [70]

27. Permanent magnet jig for heat treatment of Fe-Cr-Co magnets. [75]

28. Schematic diagram of electromagnet used for experiments with permanent magnet samples and discs. [75]

29. Temperature record from permanent magnet jig after placing into the furnace. [77]

30. Salt bath and attendant power supplies. [78]

31. Steel strip jig for holding rod specimens during salt bath heat treatment. [79]

32. Jig used for grinding thin disc specimens on 600-800 grit paper. [81]

33. Sketch of torque magnetometer with disc sample in position. [81]

34. Current v. gap field strength for Sucksmith type electromagnet used for torque magnetometry. [81]

35. Constructional details of top protractor assembly of torque magnetometer. [82]

36. Torque curve for a polycrystalline disc of 2.5% silicon iron (large grain size). [83]

37. The top half of the torque magnetometer set up for determination of the characteristic frequency of oscillation in torsion of the torque wire. [84]

38. Torque curves for disc of alloy C1 optimaly heat treated and tempered, showing rotational hysteresis. [85]

39. (a) Demagnetisation curve of alloy A1 sample aged 15 min. at 800°C and tempered showing shear produced by the reluctance of the test circuit; and (b) accuracy of remanence measurements as a function of measured coercivity using hysteresigraph. [88]

40. Electrochemical polarisation curve for alloy A1 discs in a 10% chromate solution in methanol. [90]

41. Alloy A1 - magnetic properties after cooling at various rates and after tempering. [92]

42. Alloy C1 - magnetic properties after various times and temperatures after tempering. [93]

43. Hysteresis loops for alloys A1 and C1 after isothermal ageing for short periods in a magnetic field, measured both parallel and perpendicular to the ageing field direction. [94]

44. Torque curves for alloys A1 and C1 after isothermal ageing for short periods in a magnetic field at 800°C and 650°C respectively. [95]

45. Optical micrograph of alloy A1. [97]

46. Dependence of microhardness on ageing time for alloy C1 isothermally aged at 650°C in a magnetic field. [97]

47. Variation of intrinsic coercivity with particle diameter (schematic). [99]

48. (a) Angles of deviation of individual anisotropy constants K; from reference direction. (b) Integration over the solid angle defining the range of orientations of the particles. [104]

49. The value of apparent remanence and magnetic anisotropy constant for an assembly of identically shaped particles with long axes distributed uniformally at angles up to ϕ_n from the easy axis. [103]

50. Variation of shape anisotropy factor ($N_a - H_c$) with axial ratio of a prolate spheroidal particle. [110]

51. Variation of saturation magnetisation of solid solutions of various metallic elements in nickel and cobalt. [115]

52. Variation of saturation magnetisation of solid solutions of various metallic elements in iron. [115]

53. Variation of Log (m - 0.7) with log (t') for $x = 1.07$ and $x = 1.00$. [121]

54. Ratio of components of terms making up t' as a function of ($N_a - N_c$). [121]

55. Variation particle dimensional ratio, m, with ageing time. [122]

56. Variation of ($N_a - N_c$) with the reciprocal cube root of the ageing time as measured by theoretical parameters with $x = 1.00$ and $x = 1.07$. [123]

57. Variation of $(N_a - N_c)$ with the reciprocal cube root of the ageing time as measured by theoretical parameters with $x = 1.00$ and $x = 0.93$. [124]

58. Expected changes in anisotropy with ageing time t' for Zijlstra's particle elongation mechanism and comparison with particle diffusion mechanism. [124]

59. Diffusional behaviour for a system of particles for various mechanism and possible combinations of such mechanisms. [127]

60. Schematic miscibility gap, binary or pseudobinary section and linear change of saturation magnetisation with composition. [129]

61. Variation of magnetic anisotropy with ageing time for Alcomax 111. [131]

62. Variation of magnetic anisotropy with ageing time for Alloy A1. [131]

63. Variation of magnetic anisotropy with ageing time for alloy C1. [131]

64. Variation of the logarithm of the anisotropy with ageing time for alcomax 111. [131]

65. Variation of the logarithm of the anisotropy with ageing for alloys A1 and C1. [131]

66. Variation of the magnetic anisotropy of Alcomax 111 with reciprocal cube root of ageing time. [132]

67. Variation of the magnetic anisotropy of alloy A1 with reciprocal cube root of ageing time. [132]

68. Variation of the magnetic anisotropy of alloy C1 with the reciprocal cube root of ageing time. [132]

69. Variation of saturation magnetisation with ageing time in a magnetic field for alloys A1, C1 and Alcomax 111. [135]

70. Zijlstra's magnetic anisotropy results (51) for polycrystalline Alnico 5 samples, plotted against the reciprocal cube root of the ageing time. [137]

71. Zijlstra's magnetic anisotropy results (51) for single crystal samples of Alnico 5 plotted against the reciprocal cube root of the ageing time. [137]

72. Schematic diagram illustrating changes in saturation magnetisation with composition for different temperatures and subsequent diffusion for two phases within the miscibility gap. [138]

73. Zijlstra's magnetic anisotropy results for polycrystalline Alnico 5. $\sqrt{K_s}$ v. ageing time to power $-\frac{1}{3}$. [140]

74. Zijlstra's magnetic anisotropy results for single crystals of Alnico 5. $\sqrt{K_s}$ v. ageing time to power $-\frac{1}{3}$. [140]

75. Mean axial ratio of particles v. ageing time to the power 0.26 from Zijlstra's polycrystalline Alnico 5 data. [141]

76. Mean axial ratio of particles v. ageing time to the power 0.26 from Zijlstra's single crystal Alnico 5 data. [141]

77. Variation of Z_q - transformed correlation coefficient for (a) K_s v. t^{-q} and (b) $\sqrt{K_s}$ v. t^{-q}. [141]

78. Variation of Z - transformed correlation coefficient for K_s^n v. $t^{-1/3}$. [142]

79. Zijlstra's magnetic anisotropy results (51) at the shorter ageing times for polycrystalline samples of Alnico 5. [144]

80. Zijlstra's magnetic anisotropy results (51) at the shorter ageing times for single crystals of Alnico 5. [144]

81. Alloy C1 after quenching from solution and ageing for 2 minutes at 650°C in a magnetic field, light field image at extinction contours. [148]

82. Alloy C1 after 2 minutes at 650°C in a magnetic field, dark field image. [148]

83. Alloy C1 after 3 minutes at 650°C in a magnetic field. [148]

84. Alloy C1 after 9 minutes at 650°C in a magnetic field. [148]

85. Alloy C1 after 60 minutes at 650°C in a magnetic field. [148]

86. Alloy C1 after 30 minutes at 650°C in a magnetic field followed by tempering for 2 hours at 600°C plus 4 hours at 580°C plus 16 hours at 560°C. [148]

87. Alloy C1 after 30 minutes at 650°C in a magnetic field and cooled in the magnetic jig. [151]

88. Alloy C2 as quenched showing nitrides on dislocation segments. [151]

89. Alloy C2 as quenched showing nitrides homogeneously precipitated. [152]

90. Alloy C2 heat treated in hydrogen, solution heated, quenched and then aged for 15 minutes at 643°C in a magnetic field. [152]

91. Alloy C2 heat treated in hydrogen, solution heated, quenched and then aged for 30 minutes at 643°C in a magnetic field. [152]

92. Alloy C2 heat treated in hydrogen, solution heated, quenched, aged for 30 minutes at 643°C in a magnetic field and then tempered for 2 hours at 600°C. [152]

93. Alcomax 111 solution heated and cooled at 20°C/min in a magnetic field followed by tempering. [153]

94. Alnico solution heated and cooled at about 150°C/min followed by tempering. [153]

95. Alcomax 111 solution heated, quenched and then aged for 2 minutes at 800°C without a field. [154]

96. Alcomax 111 aged for 5 minutes without a field. [154]

97. Alcomax 111 aged for 15 minutes without a field. [154]

98. Alloy A1, solution heated, quenched and aged for 5 minutes at 800°C in a magnetic field. [154]

99. Alloy A1 aged for 15 minutes at 800°C in a magnetic field. [155]

100. Alloy A1 aged for 15 minutes at 800°C in a magnetic field. [155]

101. Alloy A1 aged for 48 hours at 600°C (without a field). [156]

102. Variation of Curie point with saturation magnetisation for a number of iron and nickel solid solution systems. [160]

103. Variation of coercivity with ageing time for C1 at 650-660°C and alloy A1 and Alcomax 111 at 800°C. [162]

104. Variation of H_{CJ} with time ($t^{\frac{1}{2}}$) of tempering at 600°C after previous ageing at 800°C without a magnetic field for samples of alloy A1. [162]

105. Variation of H_{CJ} with time ($t^{\frac{1}{2}}$) of tempering at 600°C after previous ageing at 800°C in a magnetic field for samples of alloy A1. [162]

106. Variation of H_{CJ} with time $^{\frac{1}{2}}$ ($t^{\frac{1}{2}}$) of tempering at 600°C after previous ageing at 800°C without a magnetic field for samples of Alcomax 111. [162]

107. Alloy A1 aged at 800°C J_r v. H_{CJ} after tempering periods of from 0 - 407 hours at 600°C. [163]

108. Variation of remanence with coercivity for samples of Alcomax 111 aged at 800°C and tempered at 600°C for from 0 - 420 hours. [163]

109. Possible way in which the higher magnetisation inside the particle can be closed by displacement of magnetic moments in the ferromagnetic matrix around the particle. [164]

110. Measurement of magnetic flux through two planes in a system containing both ferromagnetic particles and matrix. [166]

111. Observed rotational hysteresis loss as a function of H_e, the applied field for alloy C1 after optional ageing and tempering. [169]

112. Magnetisation curve in the direction of the applied field during ageing of alloy C1 after optional ageing and tempering. [169]

113. Observed rotational hysteresis loss curve as a function of internal field, H_i, for alloy C1 after optional ageing and tempering. [170]

114. Observed rotational hysteresis loss curve W_r v. $\frac{1}{H_i}$ for alloy C1 optimally aged and tempered. [170]

115. Theoretical curves (48, 60) for rotational hysteresis loss W_r for reversal of magnetisation by coherent rotation, curling, and fanning for aligned and random assemblies of particles as a function of the reduced field. [173]

116. Rotational hysteresis integral for long cylindrical particles reversing magnetisation coherently, by curling or by buckling, calculated for aligned and randomly oriented particles. [173]

117. The variation of coercivity with particle diameter for e.s.d. particles, iron wire, elongated iron particles and iron whiskers (56, 178). [173]

INTRODUCTION

The objectives of the work outlined in this thesis has been to use magnetic measurements, assisted by electron microscopy and other measurements, in an attempt to gain further insight into the details of the alloy transformations and morphological changes which are responsible for the permanent magnetism of both the Alnico alloys which are based on the Fe-Ni-Al system, and some Fe-Cr-Co alloys, which behave magnetically in a very similar way.

Initially Chapter 1, outlines the basic principles which account for ferromagnetism in these alloys and considers under what conditions permanent magnetism can be expected to occur with particular emphasis on the particle shape anisotropy mechanism. The chapter goes on to discuss the background literature on Alnico and Fe-Cr-Co alloys, and alloy systems generally which are considered to owe their permanent magnetism to internal particle shape anisotropy. The basic theoretical ideas of possible metallurgical transformations and other changes in such alloys to account for the morphology of the structure responsible for the occurrence of permanent magnetism are also considered.

Chapter 2 contains a description of the preparation of the alloys and samples used, and the equipment and techniques employed, which include magnetic property determinations and transmission electron microscopy over a range of heat treatment conditions. Chapter 3 outlines the results obtained from this work. Chapters 4 and 5 develops some theoretical ideas, which are required in order to properly make use of both the practical results of this work and the work of previous investigators.

A discussion of the practical results is presented in Chapter 6 in the light of the various alternative theories for (a) the metallurgical transformation mechanisms responsible for the permanent magnetism in the first place, (b) the behaviour of the magnetic properties and what these predict for both the mechanism of decomposition and for the evolution of the morphology of the microstructure and (c) the mechanism of magnetic reversal both at various stages in the development of the metallurgical structure and in the optimum state.

The conclusions arising from these considerations are put forward in Chapter 7.

Throughout the course of this investigation reference is frequently made to measurements of the various magnetic properties normally determined for permanent magnets (and ferromagnetic materials generally). It may therefore be useful here to give some brief description of these properties and their measurement and significance.

Magnetic field strength, H, is determined by, or equivalent to, the effect produced by a current flowing through a wire wound into an (infinitely) long coil of N turns per metre. The S.I. unit of field strength is therefore A/m and a magnetic field or magnetising force exists inside the centre of the coil or solenoid in the direction of its long axis when carrying a current of, A, ampere

$$\text{i.e.} \quad H = N I \quad A/m$$

This infinite solenoid may be replaced by a toroidally wound solenoid as shown in the diagram.

A change in magnetic flux, Φ, causes an E.M.F. in volts, V, to be induced in a coil of N turns

$$\text{i.e.} \quad V = - N \frac{d\Phi}{dt}$$

The significance of the minus sign is that if the E.M.F. causes a current to flow, then this will be in a direction that produces a flux that tends to neutralise the change in I. The unit of flux is called the weber and the flux density, B, being the flux per unit area of that plane for which the flux is the normal, is measured in weber/square metre, which also has the special name, tesla.

An E.M.F. can be induced not only by changes in field strength, but also by changes in magnetisation, J, of the substance through which the field is passing. i.e. B is composed of the sum of two effects i.e. $B = J + \mu_0 H$

Where J is also measured in units of tesla (in the Kennelly system), and when specifically referring to magnetisation in these units connected by the above formula, it is conventional to use the term magnetic polarisation to describe J. The magnetic constant, $\mu_0 = 4\pi \times 10^{-7}$ in units of Tm/A allows field strength in the form of $\mu_0 H$ also to be quoted in units of tesla. This is the convention accepted by the International Union of Pure and Applied Physics and embodied in the 1969 Report of the Royal Society, Symbols, Signs and abbreviations, and is used throughout this report. (There is an alternative system however, the Sommerfield system in which $B = \mu_0(H + M)$. Here M, the magnetisation is expressed in A/m like H).

It is evident from the foregoing that H, being a force, and B, being the flux through a specific area, are (together with J) vector quantities necessitating, as well as a magnitude for each of these quantities, the knowledge of a direction as well. In a magnetic material B and H can vary independently. Their principal directions do not have to be in the same direction, but theory is usually limited to cases in which they are either parallel or antiparallel.

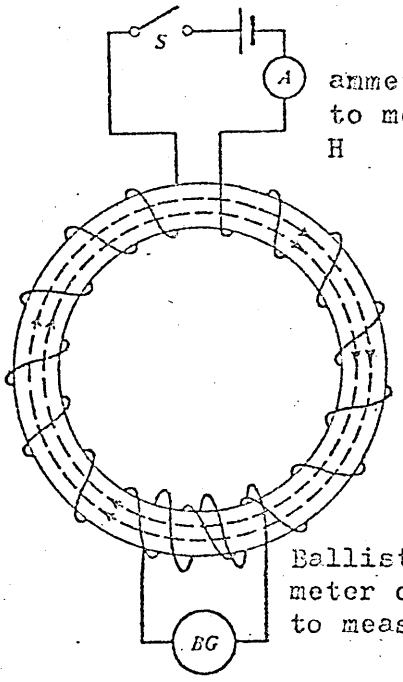

Circuit for magnetic testing of a ring specimen. Dashed lines indicate flux.

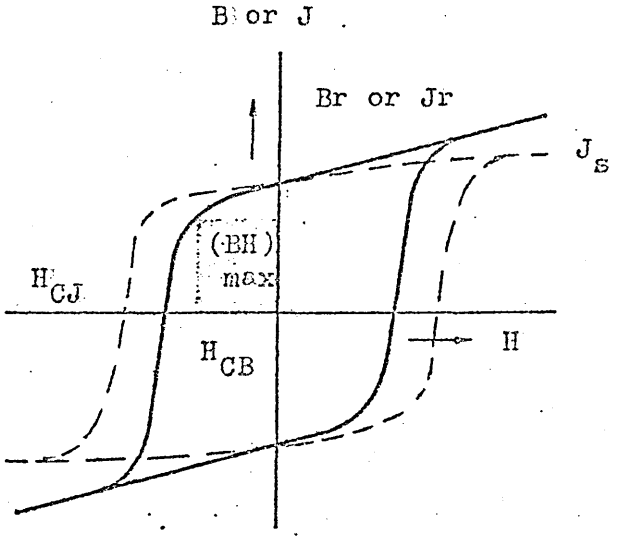

Major magnetic hysteresis loop of a permanent magnet material

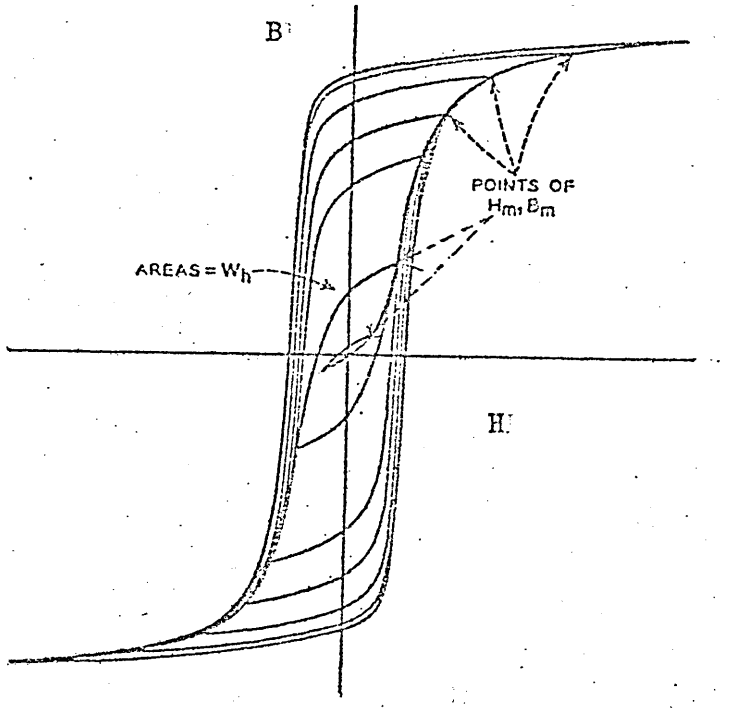

Magnetic hysteresis loops for a ferromagnetic specimen.

Suppose the toroid in the diagram is filled with a ring of ferromagnetic material having a uniform cross-section. Suppose further that the material is initially unmagnetised and a magnetising field is applied and gradually increased. If B is plotted against H a magnetisation curve passing through the points Bm, Hm is obtained as included in the lower diagram. H can be stopped at any level Hm and reversed through zero to -Hm and then back again to Hm. The result is an enclosed loop and if this is performed for a series of progressively increasing values of Hm a series of hysteresis loops of progressively increasing area are produced as shown in the lower diagram. The area enclosed by the loop for any particular Hm includes all loops for lesser Hm values. It can be seen that the changes in B lag behind those of H so that there is always some remanent B when H = 0, and some negative application of H to reduce B to zero.

Up to a point the larger is H_m then the larger the hysteresis loop, but when H_m reaches a value sufficient to saturate the magnetic material the area of the loop ceases to grow as illustrated in the diagram. B at H = 0 and H at B = 0 reach constant values known as the remanence, B_r, and coercivity, H_{CB}, respectively. This largest hysteresis loop is known as the major hysteresis loop, or just THE hysteresis loop.

Alternatively instead of B, J may be plotted against H, and since B and J are both measured in the same units both major loops are sometimes shown on the same graph as illustrated in the upper right hand diagram. It can be seen that when the material has become magnetically saturated at high values of H the J - H curve becomes, for most practical purposes, a straight horizontal line, wereas B continues to increase at all increasing values of H.

In fact J still continues to increase very slowly with increasing H at high field strengths, however this is so gradual as not to be detectable by most permanent magnet test equipment. The value of J at high H, once J has reached this almost constant value is known as the saturation magnetisation or saturation polarisation, Js.

Also, extrapolation of the linear region back to H = 0 gives the value of J known as the spontaneous magnetisation which is, however, for most ferromagnetic alloys, virtually identical to J_s.

The major hysteresis loops for B v. H and J v. H at H = 0 intersect, at this point B = J, i.e. $B_r = J_r$. B_r and J_r are thus interchangeable symbols for remanence. The negative field required to reduce J to zero is H_{CJ}, the intrinsic coercivity. H_{CJ} is in practice only a little larger than H_{CB} so long as $H_{CB} \ll B_r$.

The second quadrant of the hysteresis loop with B positive and H negative, i.e. from B_r to H_c inclusive, the demagnetisation curve, is particularly important for describing the quality of a permanent magnet material. There is a point along this part of the curve for which the product of B and H has a maximum value. This point the (BH) max has the dimensions of joule per metre ^{3} (J/m^3) and is also known as the energy product, although it is numerically double the actual maximum energy which may be stored in the magnet.

Most of the above magnetic properties (and others not covered here) are of great use to the engineer or designer who wishes to make use of permanent magnets and also provide some problems for the physicist or metallurgist in trying to explain and predict their values. However, one of the aforementioned properties, J_s, is more directly and simply related to the electronic structure and therefore the composition of the ferromagnetic phase or phases in such materials.

It is this property, and other properties also measured in the presence of high magnetic fields (notably the magnetic anisotropy energy, which under certain circumstances can give information on the variation of the saturation magnetisation of the constituents of the material) that is used here to help to understand the behaviour of such permanent magnet alloys, and forms the basis for the experimental work.

CHAPTER 1 - REVIEW

Ferromagnetism and permanent magnet alloys based on fine particle anisotropy

1.1. Ferromagnetism

1.1.1. Saturation magnetisation and the electronic structure of metals

The band theory of the electronic structure of solids currently provides the most acceptable model for ferromagnetism in the transition metals and the alloys of these metals.

When applied to magnetic problems, the band theory is often referred to as the Stoner collective electron theory (1) or the Itinerant-Electron model. The latter because the existence of ferromagnetism in metals and alloys requires the band to be narrow which also implies some tendency for atomic locallisation of the electrons. The band theory, as applied to ferromagnetic alloys is conveniently summerised by Cottrell (2).

The exchange energy is extremely sensitive to interatomic distance as shown by the Bethe-Slater relationship in Fig 1. the band width is also strongly dependent on interatomic spacing as shown for 3d and 4s bands of the transition metals in Fig 2. The kinetic energy difference between individual levels is small when the atoms are far enough apart in the crystal lattice, and if the interatomic distance is also sufficient to cause the exchange integral to become positive (Fig 1.) and to have a sufficiently high value such that the kinetic energy required for an electron at the Fermi surface to jump to the next highest level and reverse its spin is smaller than the resulting reduction in exchange energy, then the electron will spontaneously flip to this condition to minimise the total energy.

The unfilled 3d band of the transition metals is sufficiently narrow that, depending on the lattice constant for the individual

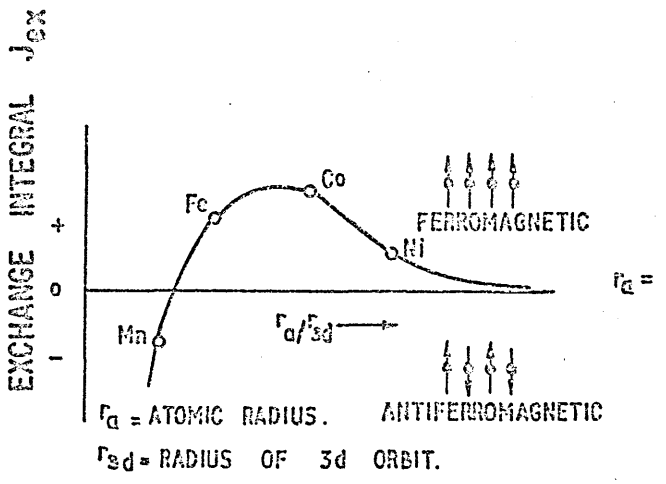

FIG. 1 BETHE-SLATER CURVE (SCHEMATIC)

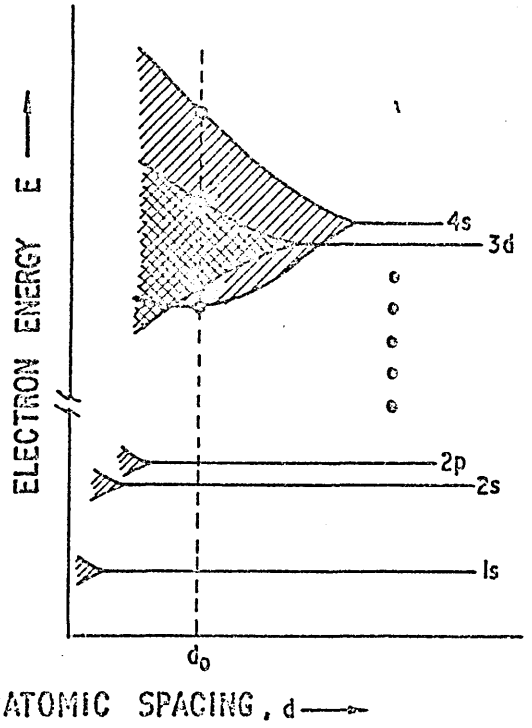

FIG. 2 SPLITTING OF ELECTRON ENERGY LEVELS AS THE INTERATOMIC DISTANCE d DECREASES.

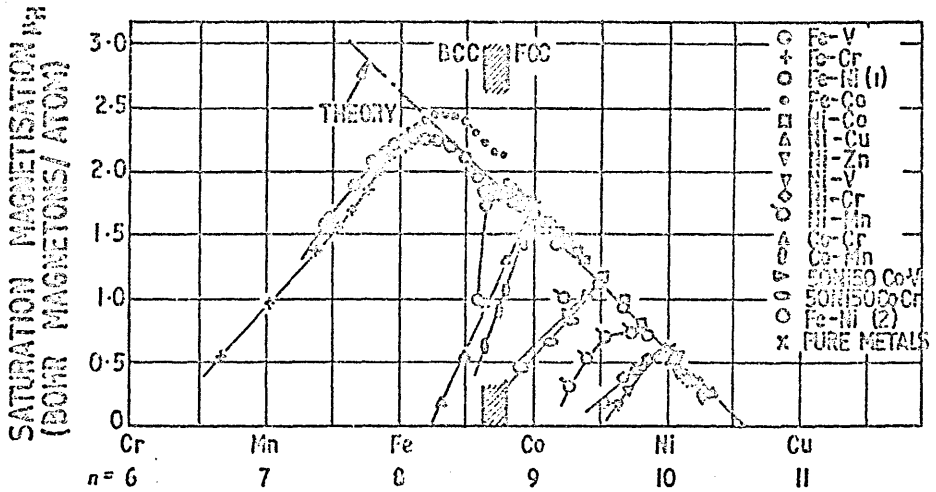

FIG. 3 DEPENDENCE OF THE SATURATION MAGNETISATION OF ALLOYS ON THE NUMBER n OF (3d + 4s) ELECTRONS PER ATOM (SLATER - PAULING CURVE). AFTER CHIKAZUMI. [13]

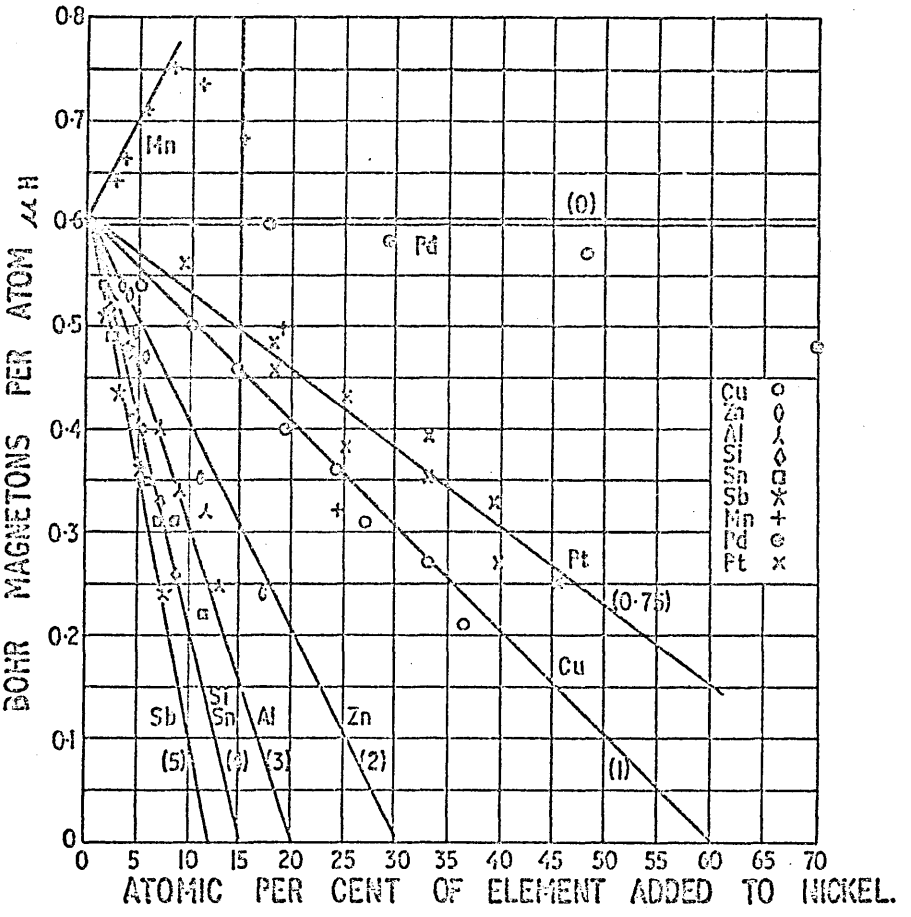

FIG. 4. MAGNETIC MOMENT PER ATOM FOR SOLID SOLUTIONS OF METALS IN NICKEL AS A FUNCTION OF ATOMIC CONCENTRATION OF SOLUTE.

metals, they are ferromagnetic or antiferromagnetic as shown on the curve in Fig 1.

The theory accounts for the saturation magnetisation of elements such as iron nickel and cobalt which, expressed as Bohr magnetons per atom, have non-integral values. As shown in Table 1, when the conditions of interatomic spacing and band width are right, which is apparently the case for the above three metals, as many electrons as possible from one subband will transfer to fill the available levels in the other. This behaviour also occurs with many of the alloys of these metals as shown by the Slater-Pauling Curve (3,4) (Fig 3) in which many of the points follow approximately the relationship

$$\mu_H = (10 + x - n) \quad \ldots\ldots\ldots\ldots (1.1)$$

where μ_H is the saturation magnetisation in Bohr magnetons per atom and n is the number of (3d + 4s) electrons. 10 represents the total number of electrons per atom that the 3d band can contain and x = 0.6 is the normal level of electrons expected in the 4s band. Further considerations and possible explanation for this behaviour and the behaviour in Fig 3 are given in Chapter 5.

This principle that electrons from the valence shell may transfer to the 3d shell according to some prescribed rule was also noticed by Stoner (5) from the experimental results of Sadron (6) and Marian (7) for alloys of nickel, not only with other transition metals with 4s valence electrons, but also with metals having 3s or 5s valence electrons such as silicon and antimony etc. (Fig 4) (8). These again are linear relationships of magnetisation with composition in accordance with equation (1.1) with X = 0.6.

This almost universal linear behaviour of changes in magnetisation with composition in solid solutions in which no structural

TABLE I

Number of electrons antl vacancies (holes) in various shells in metal atoms near iron in the periodic table,

EJJ5MKNT	Number of electrons in foil ow in, T shells :—				Total:	Hole: In :~		Excess holes in 3d-over 3d+
	3df	3d-	4S+	45-		3d+	3d-	
Cr	2,7	2.7	0.3	0.3	6	2,3	2.3	0
Mn	3,2	3.2	0.3	0.3	7	1,8	1.8	0
Fe	4.8	2.8	0,3	0,3	8	0.18	2.4	2,22
Co	5	3.3	0.35	0.35	9	0	1.7	1.71
Ni	5	4.4	0.3	0.3	10	0	0.0	0.60
Cu	5	5	0.5	0,5	11	0	0	u

.....

transformations occur may possibly be explained (Chapter 5) by transfer of electrons between the various unfilled bands.

Even where the relationship is not quite linear, straight lines can often be fitted over quite large changes of composition. Use is made of this expected proportionality of saturation magnetisation with compositions in subsequent chapters.

This presentation of the Itinerant model is naturally a simplified one in at least two respects. Firstly the band concept begins to break down somewhat when applied to narrow bands. As already stated, in these bands electrons tend to have a measure of localisation at atomic sites and a model which successfully takes this into account has yet to be formulated. Secondly thermal effects have been ignored. Thermal energy will reduce to some extent the perfect spontaneous magnetisations at $0^{\circ}K$ by disturbance of the spin orientations. However for temperatures well below the Curie point the reduction is only relatively slight as seen by inspection of the magnetisation temperature curves for iron and cobalt in Fig 5 in which the magnetisation is reduced by less than 3% from $0^{\circ}K$ to $300^{\circ}K$. J - T curves for many single phase ferromagnetic alloys when plotted as $\frac{J_s}{J_o}$ against $\frac{T}{T_c}$, where J_s is the saturation intensity of magnetisation in tesla at absolute temperature T, J_o is the saturation at 0 K, and T_c is the Curie temperature, are very similar and, as long as the Curie temperature is of the order of that of iron (i.e. $\gtrsim 700^{\circ}C$) then thermal effects on the level of the saturation magnetisation of most ferromagnetic solid solution alloy will be equally small at ambient temperatures.

1.1.2. The Domain Concept

The classical theory of ferromagnetism by Weiss (9) was originally advanced assuming localised electrons completely bound to

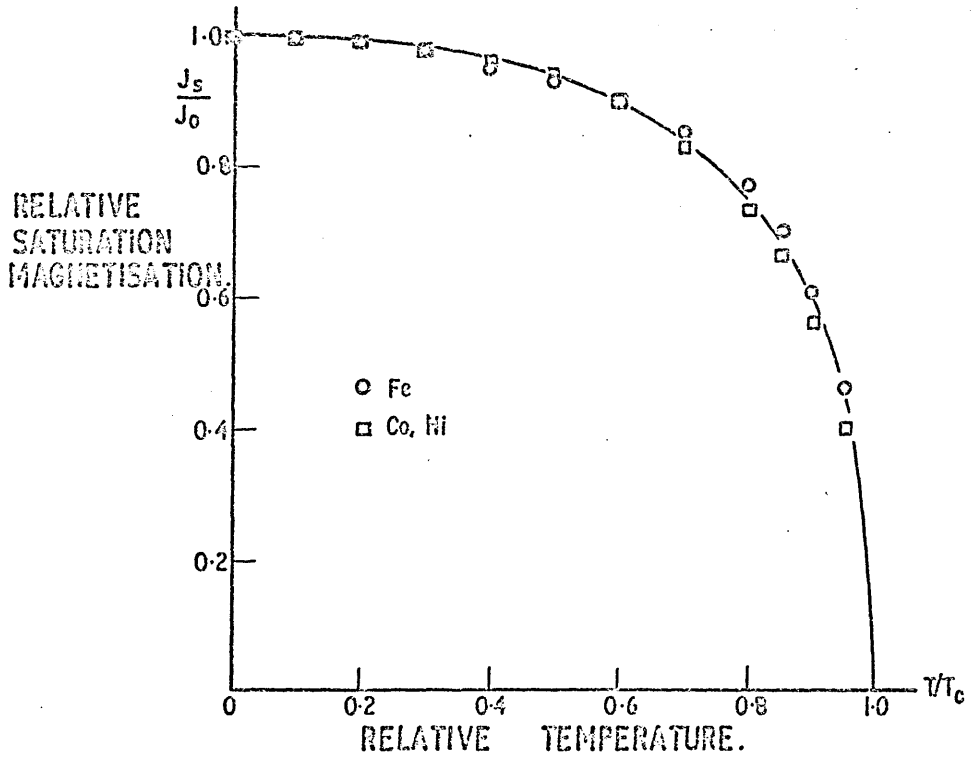

FIG. 5. RELATIVE SATURATION MAGNETISATION OF Fe, Co AND Ni AS A FUNCTION OF RELATIVE TEMPERATURE.

J_S SATURATION MAGNETISATION.
J_0 " " AT 0° K
T - TEMPERATURE.
Tc - CURIE TEMPERATURE.

atomic sites and is therefore now known not to be strictly applicable to metals and alloys. He postulated a " molecular field" or force proportional to the true spontaneous saturation magnetisation - now known to be due to the exchange energy - which tends to align the individual electron spins of each "ferromagnetic" atom within the lattice.

Opposing this effect is thermal energy which was taken into account in the Weiss theory by a Boltzman distribution between the "molecular field" and the temperature. The basic theory has since been modified to some extent in detail, but not in principle, by quantum considerations and can be used to explain non-metallic para - and ferromagnetism.

Weiss also recognised that two new ideas were necessary to explain the ease with which ferromagnetic substances could be magnetised. The existence of a "molecular field" or exchange energy to cause spontaneous magnetism does not by itself explain why some external field, be it small in comparison with the fields necessary to magnetise paramagnetic materials, is still necessary to magnetise ferromagnetic materials, which by this principle alone should be (almost) fully magnetised even in the absence of any applied magnetic field.

The further idea presented by Weiss was that ferromagnetic materials are in fact always fully magnetised. However the substance itself is internally sub-divided into regions, called domains (or Weiss domains), within which the material is fully magnetised in a particular direction, but the direction of magnetisation varies from domain to domain either randomly or in such a way that in many instances a piece of ferromagnetic material appears, outwardly, to be un-magnetised because the various magnetic orientation of the individual domains cancel out to produce a net zero magnetisation.

There have, of course, been numerous observations of the magnetic structure of ferromagnetic materials to amply confirm this fact, which was originally deduced purely from the external magnetic behaviour of these materials, and the presence of domains are still expected whether a localised theory of ferromagnetism such as that of Weiss, or a band theory is applicable.

A ferromagnetic material tends to arrange its domain configuration so that the net magnetisation is zero in order to minimise the magnetostatic energy or demagnetising field of the ferromagnetic specimen as a whole. At any point inside the magnet the energy per unit volume produced by reaction between the magnetisation or magnetic moment per unit volume, J, (in tesla) and the external field, H, (in A/m) is (10)

$$E_H = -JH \quad \ldots\ldots\ldots\ldots (1.2)$$

This is the mean for all domains and inside an individual domain the magnetisation is saturated so that

$$E'_H = -HJ_s \cos \phi \quad \ldots\ldots (1.3)$$

where ϕ is the angle between H and J_s. For zero applied field this energy, E_H, is also zero. However if H inside the material is taken to include the self demagnetising field H_d then for zero applied field the energy is $E_p = \frac{1}{2} H_d J \quad \ldots\ldots\ldots\ldots (1.4)$

For ellipsoidal shapes, H_d within the specimen is also uniform and can be simply expressed in terms of J,

$$H_d = -N J/\mu_o \quad \ldots\ldots\ldots (1.5)$$

where μ_o is a constant known as the magnetic constant equal to $4\pi \times 10^{-7}$ TA/m, and N is purely a function of the shape of the specimen and, for ellipsoidal particles is tabulated in numerous sources (11,12,13,8). This demagnetising energy is thus the driving force for the reduction of the mean magnetisation towards zero and the source of the energy necessary to generate the domain configuration.

Within any ferromagnetic material there are at least two regions of magnetisation -

(a) the region inside the domain

(b) the region at the interface between adjacent domains known as domain walls (or Bloch walls).

1.1.3. Magnetic anisotropy

It has already been stated that the magnetisation within domains is essentially complete (i.e. saturated) and deviates little in direction from point to point within the domain. However the principles governing in which direction the domain as a whole is magnetised has not yet been considered.

The crystal structure itself, presence of directional ordering within the crystal, anisotropy in the exchange energy, internal stresses, magnetostatic interaction due to the shape of the specimen and the domains, and any applied external field can all influence the direction of magnetisation of individual domains. The direction of magnetisation will in fact be such as to minimise the energy of the system as a whole. All these factors tend to impose a preferred direction, or directions for the magnetisation and as such have characteristic anisotropy energies which are referred to as -

crystal anisotropy
shape anisotropy
stress anisotropy etc.

Ferromagnetic alloys generally have intrinsic preferred crystallographic directions of magnetisation. Magnetisation curves measured in different directions for crystals of iron, nickel and cobalt (14, 15) are shown in Fig 6. In the body centred cubic lattice of iron a comparatively small magnetising field in any <100> cube edge will magnetise the crystal to saturation. Application of an external field in a direction other than an easy one will cause the

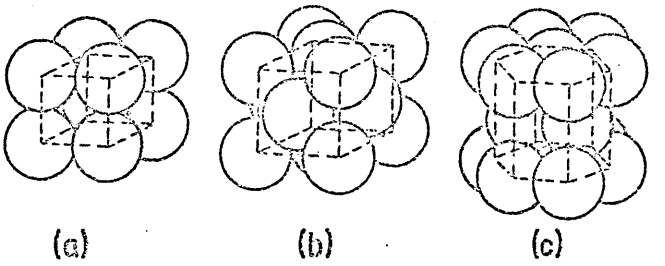

FIG.6. CRYSTAL STRUCTURES OF (a) IRON, (b) NICKEL AND (c) COBALT.

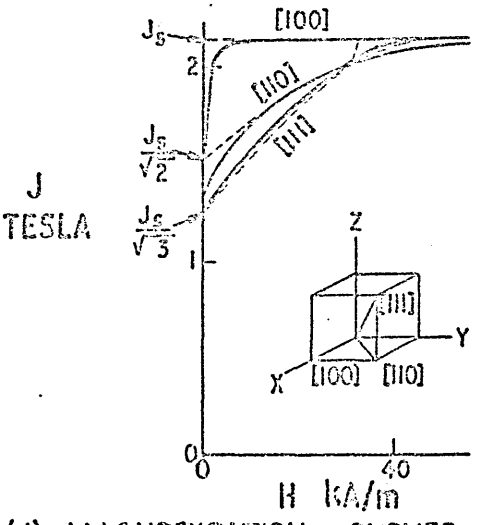

FIG. 6 (d) MAGNETISATION CURVES FOR IRON SINGLE CRYSTALS (HONDA AND KAYA)[14] THE BROKEN LINES ARE THEORETICAL.

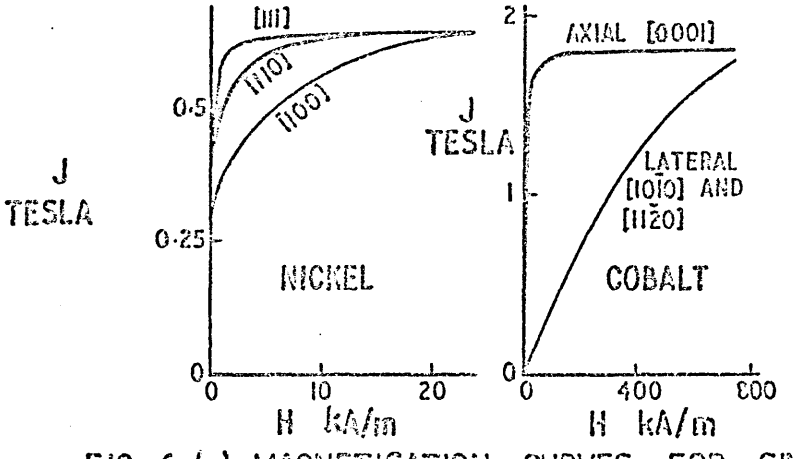

FIG. 6 (e) MAGNETISATION CURVES FOR SINGLE CRYSTALS OF NICKEL AND COBALT (KAYA)[15]

magnetisation within the domain to rotate reversibly against the crystalline forces which tends to hold it in a $\langle 100 \rangle$ position. Energy is therefore stored in the crystal when J_s is directed in a non-easy direction. Because crystalline solid state theory does not yet offer a complete explanation of the crystal anisotropy energy E it is necessary to use a series expansion of the direction cosines of J_s relative to the cubic crystal axes to define a number of anisotropy constants

$$E = K_o + K_1 (\alpha_1^2\alpha_2^2 + \alpha_2^2\alpha_3^2 + \alpha_3^2\alpha_1^2) + K_2 (\alpha_1^2 \alpha_2^2 \alpha_3^2) + \ldots\ldots \quad (1.6)$$

where α_1 α_2 and α_3 are the direction cosines for the angles between the crystal axes and J_s, and K_o, K_1, and K_2 are the anisotropy constants. Because only changes in energy are usually considered K_o can be ignored, and constants from higher terms than the one containing K_2 are not needed, indeed K_2 is sometimes so small that the term involving it can be neglected.

Sometimes for crystals with a uniaxial preferred direction, such as in hexagonal crystals, typified by cobalt in which the hexagonal c - axis is the direction of easy magnetisation, the magnetisation in all directions perpendicular to the preferred direction, are found, within the accuracy of measurement, to be equally hard. Under these circumstances the crystal anisotropy energy depends only on a single angle, θ, between the J_s vector and the preferred axis. In hexagonal crystals it is customary to write the equation for E in terms of powers of sin θ rather than cosines and E simplifies to

$$E = K_o + K_1, \sin^2\theta + K_2 \sin^4\theta + \ldots\ldots \quad (1.7)$$

For uniaxial stress or shape anisotropy effects, it may, in the simplest possible cases, be possible to analyse the anisotropy energy and obtain equations which are also of the type

$$E = K \sin^2\theta \quad \ldots\ldots\ldots\ldots \quad (1.8)$$

For shape effects E_s is the magnetostatic energy and the corresponding shape anisotropy constant K_s is given by

$$K_s = \frac{1}{2\mu_0}(N_a - N_c)\ J^2 \quad \ldots\ldots\ldots \quad (1.9)$$

where N_a and N_c are the demagnetising factors (11,12,13,8) for the equatorial and polar directions respectively of ellipsoidally shaped samples.

For internal stresses and where changes in lattice parameter can be induced by magnetisation, E is the magnetoelastic energy, E_{me}, and the corresponding stress anisotropy constant K_σ is given by $\frac{3}{2}\lambda\sigma$ where σ is the magnitude of the stress and λ is the saturation magnetostriction constant.

Anisotropies induced by directional magnetic ordering are of the same form as other uniaxial anisotropies governed by equations similar to (1.7) or (1.8).

Any or all of these anisotropy effects (and others not considered here) may contribute to establishing one or a number of preferred directions of magnetisation within an individual domain. For example if two uniaxial anisotropies which are given, except for constant terms, by expressions of the form of equation (1.9), with easy axes at some angle α ($\neq 90^\circ$), to each other then it can be shown that they are together equivalent to a new uniaxial preferred axis (see chapter 4).

An anisotropy <u>field</u> H_A may, for mathematical convenience, be defined (analogous to the molecular field of Weiss representing the exchange energy) as equivalent to the applied field which would have the same effect on the magnetisation as the magnetic anisotropy, and is obtained from $K = \frac{1}{2} J_s H_A$ analogous to equations (1.4).

1.1.4. <u>Domain Boundaries</u>

The interface between domains is normally of relatively small

width compared with the mean domain dimension and since the crystals of most ferromagnetic materials have cubic symmetry, preferred directions of magnetisation will tend to be $\langle 100 \rangle$ so that neighbouring domains whose directions of magnetisation are either nearly perpendicular or antiparallel i.e. 90° or 180° boundaries will be favoured. Bloch (1 6) first pointed out that the transition of the direction of magnetisation from one domain to the next must be as gradual as possible in order to minimise the exchange energy at any point in the crystal. The exchange force being a very short range force extends only over immediately neighbouring atoms and any antiparallel component of spin of the electrons contributing to the ferromagnetism adds to the energy of the system at that point. The exchange interaction thus has the tendency to make any change in direction as gradual as possible, that is to increase the width of the domain boundary, δ , i.e. the region in which the spins are substantially inclined to the direction of easy magnetisation.

The energy of the domain boundary is thus increased by an increase in exchange energy or anisotropy energy. However, whilst the boundary is also wider for an increase in exchange energy, an increase in anisotropy energy will reduce the width of the domain wall (8).

1.2. Permanent Magnetism

The change in apparent magnetisation (i.e. magnetisation or "demagnetisation") of ferromagnetic bodies can be achieved by two mechanisms. (A) By nucleation and movement of domain boundaries so that the body is partitioned into domains with different directions of magnetisation, which can change in number or some may grow at the expense of others. (B) By rotation of the directions of magnetisation within individual domains to effect a net change in overall magnetisation.

1.2.1. Wall Nucleation (17)

In order to nucleate a wall in a perfect crystal the applied field is required to reverse one or more electron spins. Each individual spin is maintained in a preferred direction by the anisotropy energy and aligned by the exchange interaction energy with its neighbours.

The latter energy density is very high, much higher than any anisotropy energy, and even at the crystal surface where the surrounding is incomplete an effective energy density much higher than the anisotropy energy must be expected. (Brown (18) pointed out that the energy for wall nucleation in a perfect crystal is thus higher than the anisotropy energy and that hence no wall will be nucleated, no matter what size the crystal may be. Instead, uniform rotation of the magnetisation when the energy density of the applied field exceeds the anisotropy energy density will occur.

Experiments by Deblois and Bean (19) on iron "whiskers", very high purity single crystals of iron, have shown coercivities approximately equal to the anisotropy field. This demonstrated experimentally the occurrence of demagnetisation by uniform rotation in relatively large perfect crystals. When imperfections occur in the crystal, the coupling energy between neighbours can be low, or even negative locally, since as already stated, this energy is highly sensitive to the distance between neighbouring atomic moments. In this case easy nucleation is possible, the wall having low energy at such sites. Also sharp edged inclusions can provide easy nucleation because of strong local demagnetising fields. Imperfections are distinguished as surface defects and internal defects. De Blois and Bean (19) found easy nucleation at the sharp edges of iron whiskers. Turner et al (20) observed preferred nucleation of walls at scratches in the electropolished surface of Permalloy wires.

1,2.2. Wail Propagation (17)

In a perfect crystal a wall is moved at zero force, to a first approximation. The energy needed to rotate spins at the leading sice is compensated by the energy gained at the rear side, and tne energy constant of the moving wall is constant. However, considering the discrete nature of the spins it must be expected that it makes some difference E in energy whether the centre of the wail is just at an atomic plane or just between two planes. This difference can be appreciable when the wall is thin and thus the angles between neighbouring spins in the wall are large. This situation occurs in crystals with large (crystal) anisotropy energies where the anisotropy constant K becomes comparable to the exchange energy parameter A defined by

$E^{\wedge} = A(1 - \cos y)$ where is tne energy per unit volume required to rotate a spin by an angle $ from the direction of a neighbouring spin. For K/A approaching unity the energy barriers approach K, and hence the intrinsic coercivity approaches HA (17,21).

When in fact, more realistically, the crystal contains imperfections including variations in internal stress or any effect which may reduce the local exchange or anisotropy energies **then** the wall can have low energy at these sites.

As previously explained, both exchange and anisotropy energy are involved in the energy of a wall such that a reduction in either will reduce tne total energy per unit surface of the wall and a wall moving into such localised regions will be pinned. An account of the earlier theories of pinning in which the energy of the wall itself is modified by internal stress variations and inclusions is given by Foselitz (8). Neel (22) further suggested that the magnetostatic energy associated with inclusions of non-magnetic or less magnetic material or regions of internal stress which locally can conceivably

modify the direction of magnetisation is reduced by the presence of domain walls and therefore pins them causing hysteresis and coercivity. For relatively low energy walls these dispersed field theories of Neel (22) provide a more satisfactory explanation, since the energy which impedes the movement of the domain boundaries is situated throughout the volume of the domains and not confined to the much smaller volume of the boundary walls as was the case for the earlier theories (23»2^,8).

It is evident from the forgoing that higher magnetic anisotropy not only makes rotational processes of magnetisation and demagnetisation more difficult by establishing strong directional preferences, but also wall nucleation is more difficult, and pinning more effective for two different but contributory reasons.

(A) The wall contains more energy and so a large energy difference is possible between a trapped and a free wall.

(B) Larger anisotropy energies reduce the width of the wall so that only small displacements of the wall are necessary to produce this energy difference, i.e. there is a large rate of energy change per unit displacement. Furthermore a domain wall is little influenced by a possible barrier to its movement if the barrier is small in comparison to the wall width so any reduction of the width by larger anisotropy energies will allow smaller defects to influence the pinning of the wall. Ultimately then almost any defect in the crystal lattice will restrain a narrow wall to some extent and a recent theoretical study (26) has clarified this point.

The very strongly crystal anisotropic ferromagnetic materials are thus likely to be natural permanent magnets. Currently the most powerful permanent magnets are of this type and include cobalt alloyed with the rare earth metals notably samarium and praseodymium. Table 11 includes a range of typical crystal anisotropy constants

from which it may be seen that the best materials have the highest uniaxial anisotropy energies.

The presence of crystal defects has opposing effects on nucleation and pinning of walls respectively. Defects make nucleation easier, but movement of these walls once formed, harder, so that magnetic hysteresis may be controlled in these very high anisotropy materials by either nucleation or pinning control, giving characteristically different hysteresis curves for small grains of such material. Fig 7 (26) and Fig 8 presents simplified schematic versions illustrating the essential differences between these two behaviours. It is found in practice that small grained material gives the best magnetic properties which may be connected with the fact that imperfections are less likely to be present the smaller the grain and also more nucleation events (one per grain) are necessary to reverse the magnetisation of the complete specimen.

The best permanent magnet materials with these very high values of crystal anisotropy are intermetallic compounds mainly of cobalt or manganese. These materials tend to lack mechanical strength and, particularly in the case of the rare- earth cobalt compounds, are expensive both in terms of raw material cost and processing. The maganese compounds with bismuth or aluminium are less expensive in terms of material costs, but still suffer (particularly MnBi) from corrosion or oxidation problems. Prior to the discoveries of these high crystal anisotropy materials, and for normal commercial needs, recourse has had, and may still have, to be made to materials and systems with lower anisotropies in which domain nucleation and pinning is much easier and therefore the natural hysteresis and coercivity are very much lower. Numerous carbon and alloy steels fall into this catagory which provided the bulk of permanent magnet products prior to about 1935* The coercivity in these materials

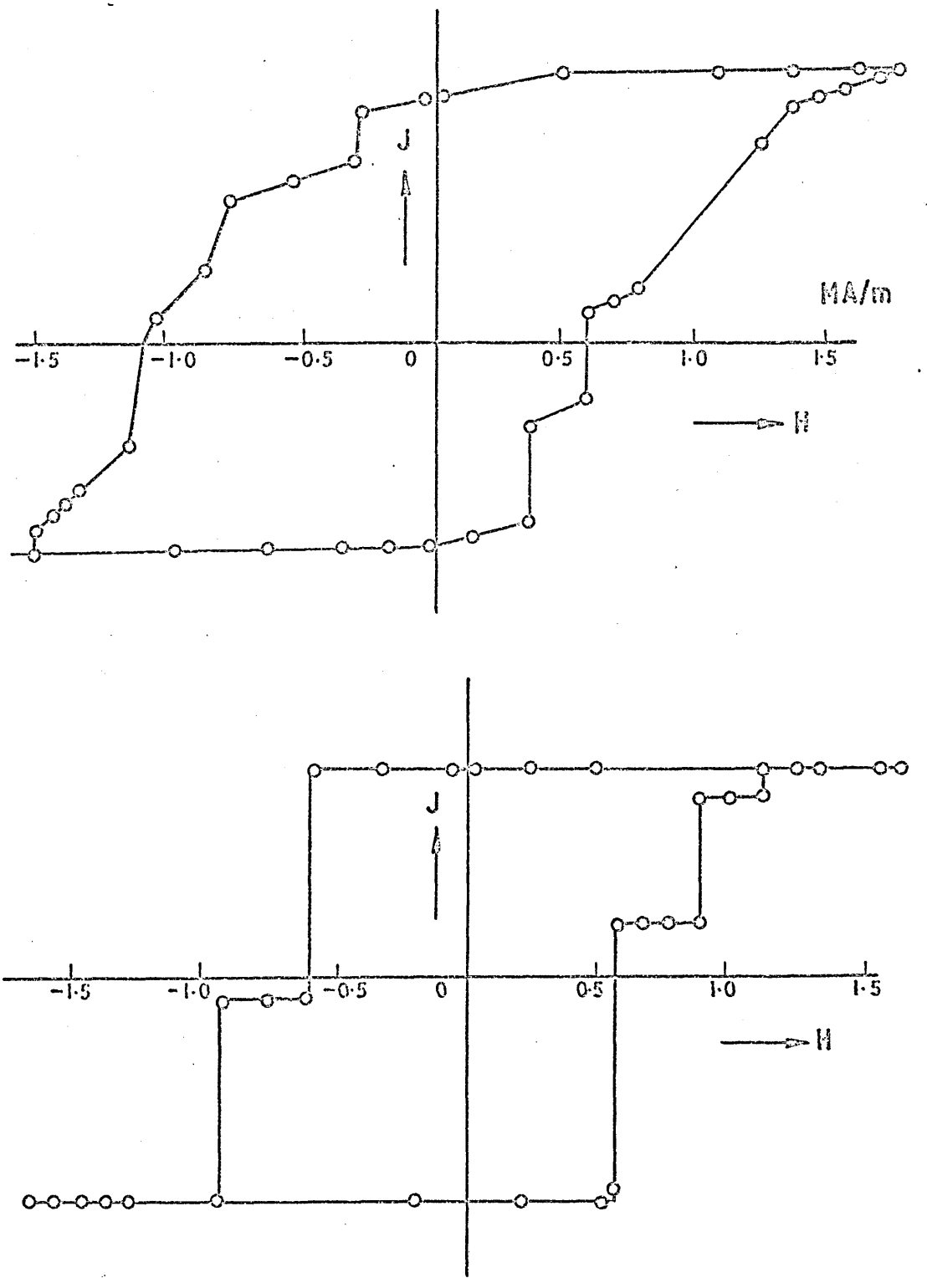

FIG. 7 MAGNETIC HYSTERESIS CURVES FOR $SmCo_5$ PARTICLES. AFTER ZIJLSTRA.[20]

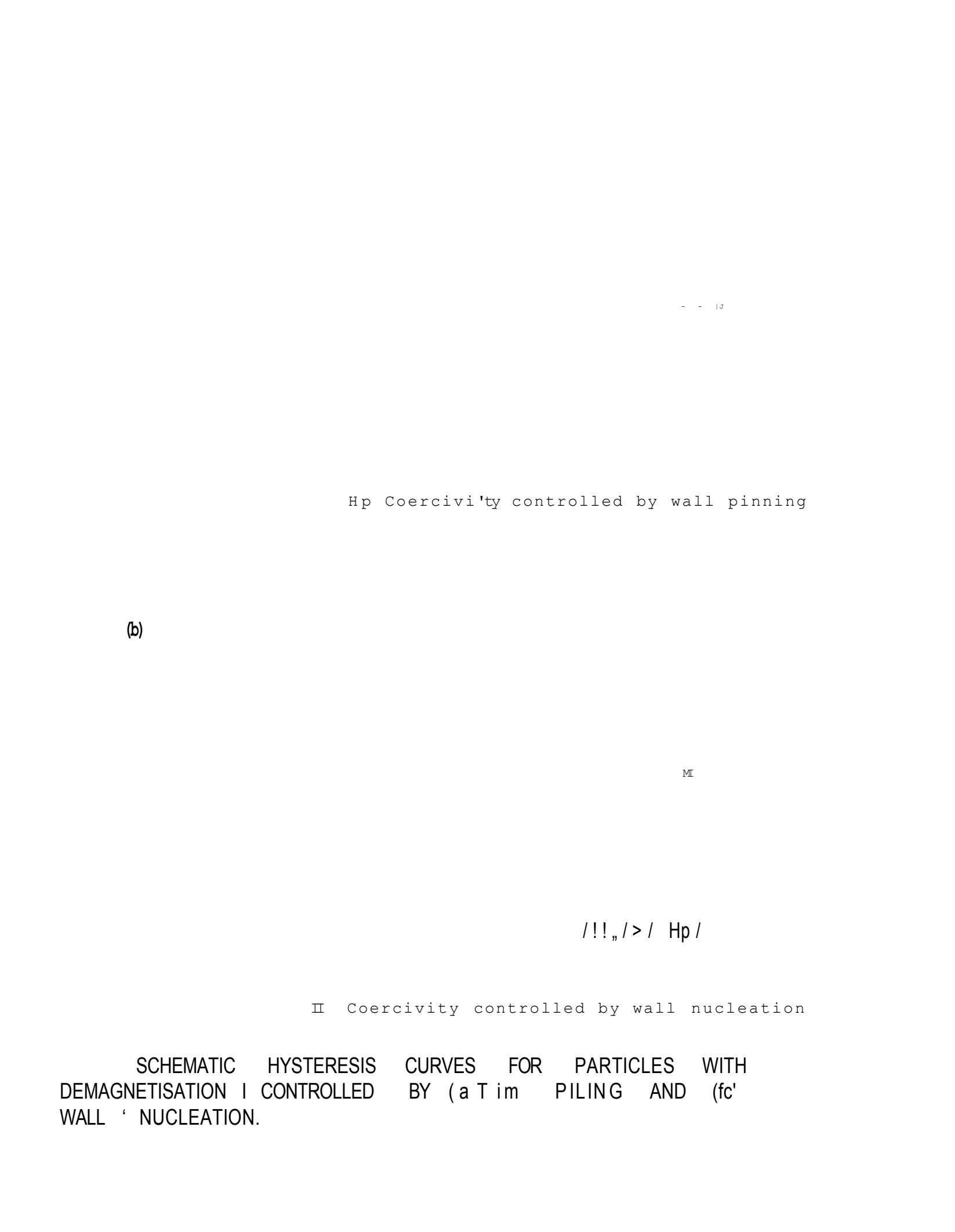

SCHEMATIC HYSTERESIS CURVES FOR PARTICLES WITH DEMAGNETISATION I CONTROLLED BY (a T im PILING AND (fc' WALL ‘ NUCLEATION.

relies on internal stress, inclusions and precipitates for wall pinning. Because of the relatively low combined crystal and stress anisotropy energy which can be developed in iron based alloys these mechanisms are limited to coercivities of the order of 20 kA/m with (BH) max levels of about 10 kj/m^ (27). Cobalt based precipitation alloys with iron and vanadium can have coercivities of about *ko* k.A/m and 25 ^J/m^x (BH) max. This can be compared with H„T of 1,500 kA/m (HcB ~ ^A/ra) at 1^0 kj/m^x (BH) max. for samarium and praseodymium cobalt alloys (**28**).

1.2.3. Fine particles

The problem of such relatively easy demagnetisation **of** materials with only moderate anisotropies, and hence less than adequate wall pinning, is overcome if the grains or particles **of** magnet materials are so small that they are of the same order of size or less than the width of a wall (29). In this case the magnetostatic energy of the particles may still be reduced by domain wall formations. However the energy of the wall would,, on this scale, be of the same order or more than the magnetostatic energy without the wall and therefore little is gained by its presence,so -that, in the absence of other mechanisms, demagnetisation will then only be achieved by rotation of the magnetisation of the single domain particles from the preferred axis, and the coercivity will then equate to the anisotropy field. The anisotropy constant still needs to be high, but not so high such that the domain wall thickness is reduced belov,' the smallest cross section of particle which can be conveniently produced.

The idea that such particles could be so small that they would not sub-divide into domains dates back to a paper of Ffenkel and Dorfraan (30) published in 1930. Until the experiments demonstra-ting the existence of single domain fine particle behaviour of Kittel

et al (31) with nickel particle suspensions in 1950, it was not clear that coercivities derived from fine particles could be attributed to single domain behaviour. The coercivity of fine particles over a range of materials with various crystal anisotropy energies is shown in Fig 9. (32) as a function of particle size. The fall in coercivity at very small particle sizes (< 10 nm), is due to thermal effects which on such small particles are strong enough to spontaneously demagnetise a previously saturated assembly of particles. Such particles are referred to as super-paramagnetic (33). In addition to crushing and grinding the more brittle solid alloys such as MnBi (34) and $SmCo_5$ (35) and then compacting and/or sintering to produce small particles or grains precipitation, metals and powders of more ductile metals such as iron and cobalt may be formed by chemical reduction of salts etc. of the metals (36), by electrolysis of salt solutions (37) followed by compaction or suspension in a non-magnetic solid matrix, or by precipitation from a solid solution alloy - the latter notably in the Aluminium-Cobalt system (38,39). Co and Fe suffer from their relatively low crystal anisotropy and further, the ferromagnetic constituent is diluted by the inclusion of a non-magnetic matrix material.

1.2.4. Shape Anisotropy in fine particles

The anisotropy data in table II which indicated the order of magnitude of various magnetic anisotropy mechanisms shows that there is at least one other mechanism which can compete with the crystal anisotropy of cobalt and iron. Shape anisotropy which, combined with the concept of particles of sub-critical domain size, is a highly useful alternative.

The theory of single domain particles was developed independ-

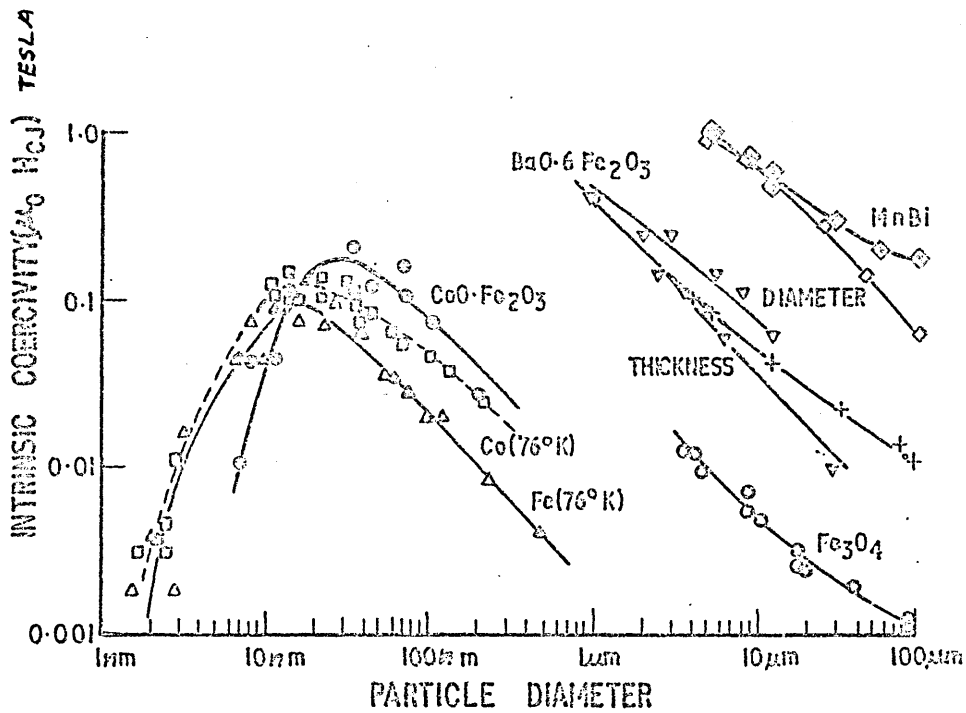

FIG. 9 VARIATION OF COERCIVITY WITH PARTICLE SIZE FOR PARTICLES DERIVING THEIR COERCIVITY PRINCIPALLY FROM CRYSTAL ANISOTROPY. LUBORSKY [32]

TABLE II

Anisotropy constants and saturation magnetisation of some ferromagnetic and ferrimagnetic substances.

Structure	Substance	Anisotropy Constants		Saturation magnetisation J_s (tesla) at 20°C
		K_1 (MJ/m^3)	K_2 (MJ/m^3)	
Cubic	Fe	.048	±.005	2.15
	Ni	-.005	-.002	0.60
Hexagonal	Co	0.45	0.015	1.78
	$BaO.6Fe_2O_3$	0.33		0.48
	Mn Bi	0.89	0.027	0.78
	Mn Al	1.0		0.62
	$Y Co_5$	5.5		1.06
	$Pr Co_5$	6.9-10.0		1.20
	$Sm Co_5$	8.1-11.2		0.96

Cubic Anisotropy	0.2-0.002	MJ/m^3
Hexagonal "	12 - 0.3	"
Shape(e/d=10) "	0.9	"
Stress (1500MN/m^3)	0.05	"
Directional order (Rolled 50Fe-50Ni)	0.02	"
Typical exchange energy coefficient (iron)	2,000	"

antly in England by Stoner and Wohlfarth (40) and also in France by Néel (36,41,42) in the period 1939-1948. It was first calculated by Poisson (43) that an ellipsoidal magnet is the right shape for the flux leakage from the surface exactly to balance the change in surface area by the taper towards the poles, and that this is true for ellipsoids of all dimensional ratios, whether extremely elongated to resemble a long wire, or a sphere, or the other extreme resembling a thin disc. The relationship in this case between the internal demagnetising field and the magnetisation of the ellipsoid is already given in equation (1.5). The demagnetising factor, N, can be found by an expression derived from that given by Maxwell (11), entirely in terms of the polar axial length, c , and the equatorial diameter, a , of the ellipsoid as

$$N = \frac{1}{m^2-1}\left[\frac{m}{\sqrt{m^2-1}}\cosh^{-1}m - 1\right] \quad \ldots\ldots\ldots (1.11)$$

where $m = c/a$

$$N = \frac{1}{m^2-1}\left[\frac{m}{\sqrt{m^2-1}}\log_e\left(m+\sqrt{m^2-1}\right) - 1\right] \quad \ldots\ldots\ldots (1.12)$$

N has the value of 1/3 for a sphere but is significantly lower even with the slightest elongation say m = 1.5, N = 0.233 and for m = 2, 0.173564; or m = 10, N = 0.0203.

To generalise it is well known that a uniformly magnetised ellipsoid with principal axes oriented along co-ordinate axes x_i ($i = 1,2,3$) and with magnetisation components J_i produces an energy per unit volume associated with the de-magnetising field

$$E_d = \frac{1}{2\mu_0}\left(N_1 J_1^2 + N_2 J_2^2 + N_3 J_3^2\right) \ldots\ldots (1.13)$$

where the N_i are the demagnetising factors for the three principal axes and depend only on the ratios of the three ellipsoid semi-axes, as exemplified by equations (1.11) and (1.12), and satisfy the relation

$$N_1 + N_2 + N_3 = 1 \quad \ldots\ldots\ldots\ldots (1.14)$$

The demagnetising factors are tabulated even for the case of three unequal axes (11,12).

For a single domain particle the magnetisation is, by definition, of constant magnitude but variable direction so that

$$E_d = \frac{1}{2\mu_o} J_s^2 (N_1 \alpha_1^2 + N_2 \alpha_2^2 + N_3 \alpha_3^2) \quad \ldots\ldots (1.15)$$

where α_i are the direction cosines with respect to the co-ordinate axes.

In a zero external field, stable equilibrium requires that J_s lie along the direction that minimises E_d, i.e. the longest axis corresponding to the smallest N_i say N_c so that $E_d = \frac{1}{2\mu_o} N_c J_s^2$ which is equation (1.5) substituted in equation (1.4). An external field can rotate J_s out of this direction. The behaviour of the general ellipsoid is complicated, and therefore the simpler prolate ellipsoid of revolution has usually been used, with long polar semi-axis, c, and short equatorial semi-axis, a, (the oblate ellipsoid of revolution is also easy to treat). The ellipsoid then has longitudal demagnetising factor N_c and transverse demagnetising factor N_a with $N_c + 2 N_a = 1$, and with $N_a > N_c$.

Rotation of J_s away from the polar axis (e.g. by means of an applied field) increases the demagnetising energy

$$E_d = \frac{J_s}{2\mu_o} \left[N_a \cos^2\theta + N_c \cos^2(90^\circ + \theta) \right] \quad \ldots\ldots (1.16)$$

$$E_d = \frac{J_s}{2\mu_o} \left[N_a (1 - \sin^2\theta) + N_c \sin^2\theta \right] \quad \ldots\ldots\ldots (1.17)$$

or neglecting terms independant of θ

$$E_d = \frac{J_s^2}{2\mu_o} (N_a - N_c) \sin^2\theta \quad \ldots\ldots\ldots (1.18)$$

which is the variable part of the demagnetising energy. This increasing to a maximum of $\frac{1}{2\mu_o} J_s^2 (N_a - N_c)$ as J_s is forced to rotate from the preferred direction through a 90° orientation to this direction. At some point the magnetisation will in general spontan-

eously jump to a position near to the 180° position - the preferred axis in the reverse direction.

The precise position at any time depends also on the actual direction and energy of the external field equal to equation (1.3) the total relevant energy being

$$E = \frac{J_s^2}{2\mu_o} (N_a - N_c) \sin^2 \theta - HJ_s \cos \phi \quad \ldots\ldots (1.19)$$

ϕ, being the angle between the magnetisation and field axis, can be replaced by $\alpha - \theta$, where α is the angle of orientation of the applied field with respect to the long axis of the particle. At any field the energy will always be a minimum i.e. at

$$\frac{dE}{d\theta} = \sin 2\theta + \frac{2\mu_o H \sin(\alpha - \theta)}{J_s (N_a - N_c)} = 0 \quad \ldots\ldots (1.20)$$

(when $\frac{d^2E}{d\theta^2}$ is positive).

This equation with two variables H and θ has been solved numerically (40) for a series of fixed values of α and presented in terms of the reduced magnetisation, resolved in the field direction

$$\frac{J}{J_s} = \cos \phi \quad \ldots\ldots (1.21)$$

and a reduced field $h = \frac{\mu_o H}{J_s (N_a - N_c)}$ $\ldots\ldots (1.22)$

These results are presented graphically in fig 10. from Stoner & Wohlfarth (40). These are reduced total hysteresis curves, which for an ellipsoid with its long axis in the field direction is a "square" loop with $h_c = 1$

$$\text{i.e.} \quad H_{CJ} = J_s (N_a - N_c) / \mu_o \quad \ldots\ldots (1.23)$$

for a very long particle $(N_a - N_c) \simeq \frac{1}{2}$ and therefore

$$H_{CJ} = \frac{J_s}{2\mu_o} \quad \ldots\ldots (1.24)$$

From equation (1.18) a shape anisotropy constant K_s can be defined analogous to equation (1.8) for crystal anisotropy

$$K_s = J_s^2 (N_a - N_c) / 2\mu_o \quad \ldots\ldots (1.25)$$

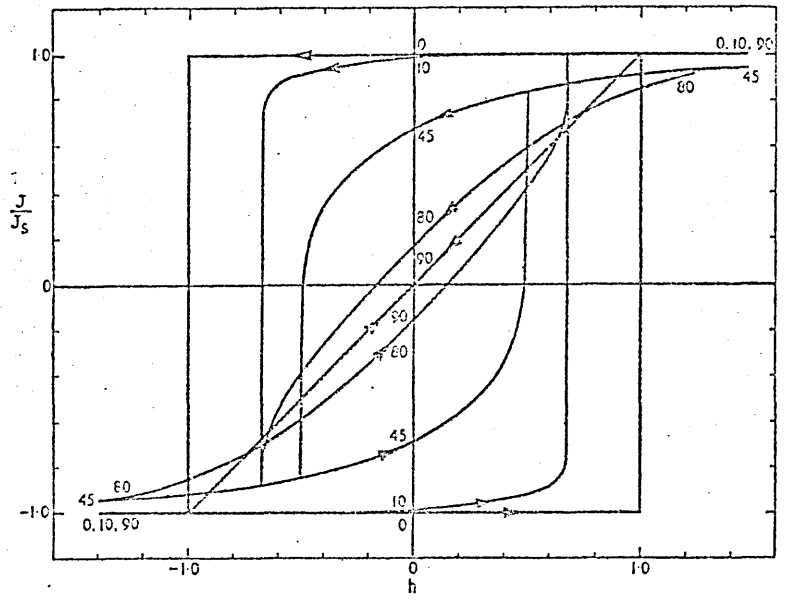

Fig 10. Theoretical hysteresis loops of assemblies of aligned single domain particles (40)

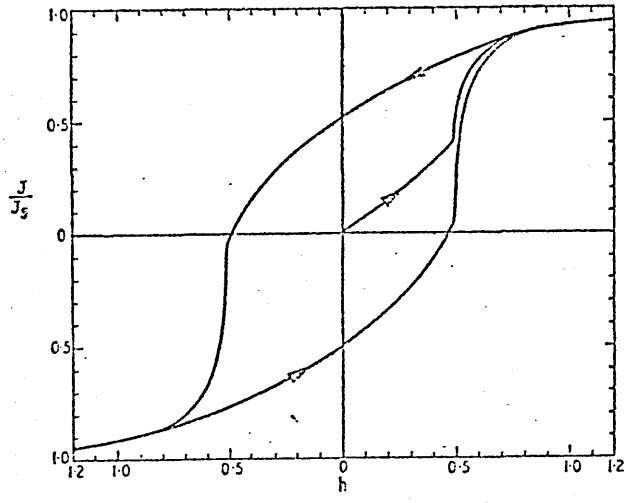

Fig 11. Theoretical hysteresis loop of an assembly of randomly aligned single domain particles. (40)

(K_s is the energy per unit volume of particles and for an assembly of aligned non-interacting particles making up a volume fraction p of a continuous specimen then $K'_s = pK_s = p J_s^2 (N_a - N_c) / 2\mu_o$ is the energy per unit volume of the specimen).

Carrying the analogy with crystal anisotropy further equation (1.10) suggests a shape anisotropy field $(H_A)_s$ also equal to the right hand side of equation (1.25) i.e. for a perfectly aligned particle $H_{CJ} = H_A$.

If the particle is aligned with its long axis transverse to the field then it may be seen from Fig 10. that there is no hysteresis, no spontaneous jump at any value of h, and a linear curve of $\frac{J}{J_s}$ against H of slope $\frac{\mu_o J}{J_s^2(N_a - N_c)}$ is calculated up to the anisotropy field H_A at saturation.

Stoner & Wohlfarth (40) also calculated the hysteresis curve for a non-interacting assembly of prolate ellipsoids orientated at random this is shown in Fig 11, and for this case

$$H_{CJ} = \frac{0.479}{\mu_o} (N_a - N_c) J_s \quad \ldots\ldots\ldots (1.26)$$

and

$$B_r = J_r = \tfrac{1}{2} J_s \quad \ldots\ldots\ldots\ldots (1.27)$$

1.2.5. Extension of fine particle theory to particles of any shape and magnetic anisotropies of any type.

Brown and Morrish (44, 45) have calculated that the above treatment of single domain behaviour (40) is not restricted to ellipsoids, so long as the particles are non-interacting and uniformly magnetised internally. Even if the particles are interconnected or full of holes or have edges or corners such as those on a cylinder or prism etc, values of N_i will exist for an equivalent ellipsoid of the same volume for any arbitrarily shaped particle.

Equation (1.20), derived for shape anisotropy energy is

analogous to crystal anisotropy equations, for example equation (1.8), so that a shape anisotropy constant, equation (1.27) can be defined. Reversing this analogy the shape anisotropy constant K_s can be replaced by a crystal anisotropy constant such as equation (1.8), or any other uniaxial magnetic anisotropy without any other modification of the theory. So that the shape theory of small particles applies to particles with any uniaxial or mixture of uniaxial magnetic anisotropies and is therefore a general theory of single domain demagnetisation.

1.2.6. Particle Interaction

A single domain ferromagnetic particle which is itself part of a body which also contains numerous other similar particles is not only affected by its own internal magnetic anisotropy but also by the field generated by the presence of the remaining particles. Néel (36,41) bypassed this problem for shape anisotropy by considering the system as a continuous ferromagnetic body containing cavities. If p is the volume fraction of ferromagnetic particles then (1-p) is the volume fraction of "cavities" which will have a magnetostatic energy per unit particle volume of

$$E_d = p\,(1-p)\frac{N}{2\mu_o} J_s^2 \quad \ldots\ldots\ldots \quad (1.28)$$

The anisotropy energy constant per unit volume of the system is then

$$K_s' = p\,\frac{(1-p)}{2\mu_o}\,(N_a - N_c)\,J_s^2 \quad \ldots\ldots \quad (1.29)$$

which is thus the generallised form of equation (1.25) for systems of particles.

However whilst this may be valid for anisotropic assemblies of particles whose magnetisation is parallel and uniform (46), a coercivity based on this energy is only valid if the magnetisation of all the particles remain uniform not only internally but also with

respect to each other during demagnetisation when

$$(H_{CJ})_p = (H_{CJ})_{p=o} \times (1 - p) \quad \ldots\ldots\ldots (1.30)$$

Shtrikman (47, 48) also derived equations (1.30) for an anisotropic random assembly of parallel infinite cylinders of arbitrary cross section reversing their magnetisation coherently (internally uniform) in a field parallel to the cylinders. He also derived equation (1.30) approximately for a similar model for which although each cylinder reverses coherently, neighbouring cylinders, here situated on a infinite square lattice, reverse their magnetisation equally but oppositely. Despite this supporting evidence for this model for particle interaction, Wohlfarth (49, 50) stresses that equation (1.30) may have only limited applicability and calculates (50) a more general formula

$$(H_{CJ})_p = (H_{CJ})_{p=o} - J_s (A_p - Bp^{5/3} + \ldots) \ldots\ldots (1.31)$$

where A, B, ... depend critically on the orientations and geometrical arrangement of the particles. This is an equation which is however less amenable to experimental test.

A slight modification to equation (1.29) will make it applicable to an assembly of ferromagnetic particles within a matrix which is itself more weakly ferromagnetic. If the particles have a saturation magnetic moment per unit volume of J_p and the matrix J_m then the spaces between the particles will be equivalent to cavities of a depth $J_p - J_m = \Delta J_s$ so that J_s must be replaced by ΔJ_s in equation (1.29) to give (49, 50)

$$K_s = p \left(\frac{1 - p}{2\mu_o}\right) (N_a - N_c) \ (\Delta J_s)^2 \quad \ldots\ldots\ldots 1.32)$$

These equations have since been more rigorously derived by Zijlstra (51) who also points out that the anisotropy energy is given by equation (1.32) whether the particles have larger or smaller magnetisation than the surrounding medium.

When crystal anisotropy is the cause of hysteresis then coercivity is expected to be largely independant of p and this view is largely supported by experiment, except where the particles begin to physically contact each other when slight reductions in coercivity are observed (52,53,54) presumably due to loss of single domain behaviour.

It is because crystal anisotropy is due to forces (spin-orbit coupling) which are internal to the particle, in contrast to shape anisotropy which is due to magnetostatic fields external to the particle, that crystal anisotropy is expected to be independent of p.

1.2.7. Incoherent reversal demagnetisation processes

Although previous equations in fine particle theory apply perfectly well in conditions of full magnetisation i.e. for measurements of anisotropy by rotation of the specimen in a strong magnetic field, it was rapidly realised soon after the formulation of the coherent reversal theory of single domain fine particles, that the levels of coercivity observed in practice for shape anisotropic systems fell short of the levels predicted.

A method was developed for making very thin, elongated iron particles with axial ratios from about 1 to well over 10 by electrodeposition on a mercury cathode (55). Measurements on aligned, dilute compacts of these particles showed that H_{CJ} increased with axial ratio, c/a, but did not exceed about 145 kA/m for c/a larger than 10 (56), which, according to equation (1.23) should be 800 kA/m. These results showed that the observed coercivity could certainly not be explained by crystal anisotropy, which by inspection of table II $\frac{2K}{J_s}$ = 45 kA/m, but neither was it as large as expected for shape anisotropy.

Frei, Shtrikman and Treves (57) and Jacobs and Bean (58) were both soon to show that there were, under certain circumstances

alternative mechanisms to the uniform rotation of magnetisation in the absence of domain walls. Frei et al obtained solutions of Brown's equations by the methods of micromagnetics (57,59) and give two new mechanisms of demagnetisation referred to as "buckling" and "curling". The deviations in magnetic moment within the particle at some point during demagnetisation are shown schematically in Fig 12. In buckling spin or magnetic moment deviation occurs only in one plane in a direction at right angles to the long axis. The deviation is a periodic function of displacement in the direction of the long axis. With the curling mechanism the magnetisation aquires a circumferential component that depends only on distance from the axis. This mechanism is particularly interesting since, unlike buckling in which the applied field must overcome anisotropy and exchange forces, however in the case of curling, for an infinitely long or cylindrical particle at least, the magnetisation aquires no extra magnetostatic forces because during reversal all new components of the magnetisation are circumferential, and the flux is therefore continuous. Half way through reversal by this method, the spins are all parallel to planes normal to the long axis and form closed circles of flux in all cross sections, In contrast, coherent rotation produces increases in anisotropy and magnetostatic forces but no exchange forces during reversal. A further conclusion that reversal by curling of highly elongated particles should be independant of the packing function may also be expected because no magnetostatic energy is involved (48) again this is in sharp contrast to coherent rotation theory.

The reversal mode considered by Jacobs and Bean (58) was suggested by the shape of the electrodeposited iron particles observed by electron microscopy. The particles were considered to be chains of spheres where rotation occurs by a fanning mechanism in

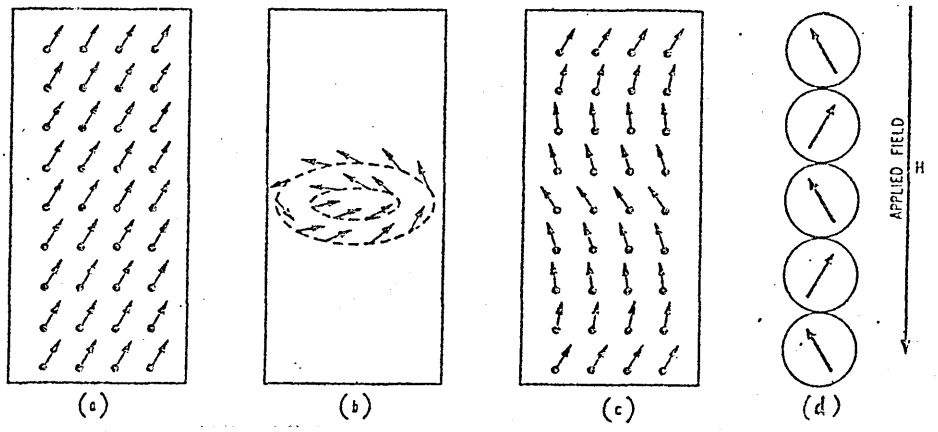

(a) Rotation in unison, (b) Curling, (c) buckling, (d) fanning

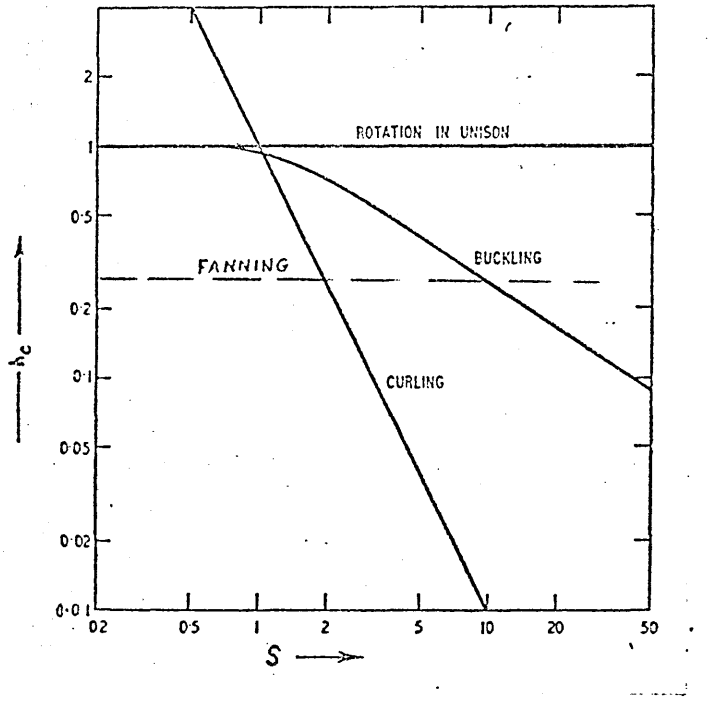

Fig 12. Calculated fields for nucleation of magnetisation reversal in infinite cylindrical particles (a,b and c) or chains of spheres (d) for various modes of reversal (40,57,58,)

The axial field is given by $H_{cr} = J_s h_{cj} / 2\mu_0$.

The particle diameter is given by $d = 2\mu_0^{\frac{1}{2}} \frac{S\ C^{\frac{1}{2}}}{J_s}$ where C is the exchange constant between two neighbouring spins.

which the magnetisation in successive spheres rotates in alternate directions. They also considered rotation in unison (symmetric fanning) in which the magnetisation of all the spheres is always parallel. Each sphere is assumed to be a single domain with no anisotropy of its own and within which the spins reverse coherently. Each sphere is treated as a magnetic dipole and overall anisotropy energy obtained by interaction between them. They showed that the energy barrier for reversal by the fanning mode is only one third of that for coherent rotation with the same particle system.

Fig 12 shows diagramatically the variation of H_{CJ} for the various modes for long particles as a function of the (reduced) diameter (57). Buckling is in practice not very important because it is found to give a lower coercivity than the other modes only over a very restricted range of diameter near to the maximum critical diameter for coherent rotation. The critical diameter for long iron or cobalt iron particles above which the curling mode is energetically more favourable is calculated to be about 17 nm which explaines why the coercive force found is lower than the maximum J_s, the value for uniform rotation. By contrast the particle size $\frac{J_s}{2\mu_o}$ at which actual domain walls can start to appear for materials of moderate crystal anisotropy such as iron or nickel is expected to be greater than the natural domain wall thickness which is about 10 - 50 nm. Information on not only the distribution of anisotropy and alignment of particle assemblies but also the mode of reversal of the particle magnetism may be obtained from the analysis of torque magnetometry measurements (60,13). If torque curves are measured for assemblies of fine particles, the measurements in very high fields can give information about particle alignment. For randomly aligned particles no torque curve has an amplitude which is characteristic of the distribution. Torque curves taken in a clockwise and anticlockwise direction in high fields are identical.

In fields of the order of half the anisotropy field there is a difference between such torque curves and the area between them is referred to as rotational hysteresis loss.

It has been shown (59,27,60,48) that the variation of rotational hysteresis loss with field differs for different modes of magnetisation reversal. Moreover, these curves also differ for random and aligned particles and this type of analysis permits some far reaching conclusions about the demagnetisation of fine particle systems.

Jacobs and Luborsky also find that the rotational hysteresis integral, $R = \int \frac{W_r}{J_s} \, d\left(\frac{1}{H}\right)$, where W_r is the rotational hysteresis loss, has a value of about 0.4 for random or aligned particles with coherent rotation of magnetisation, but a value of 1 or 1.5 for random and aligned particles respectively in which the magnetisation changes by fanning.

Shtrikman et al (57,59,60,48) have made similar calculations for curling and buckling in long cylindrical particles and found that the shape of the W_r -H curve and the value of R depends on the particle diameter.

1.3. Fine Particle permanent magnets from alloys

1.3.1. Alnico alloys, technological developments

The discovery of an alloy system, which it is now universally agreed, derives its permanent magnet properties from fine particle shape anisotropy, was made some years before the cause of the magnetic hysteresis was known. In 1931 Mishima in Japan discovered that an alloy of 58 percent Fe, 30 percent Ni and 12 percent Al had a coercivity of over 30 kA/m or about double that of the best magnet material, a magnet steel, previously available.

Work by Bradley and Taylor (61) and Bradley (62) established the broad metallurgical behaviour of the iron-nickel-aluminium alloys and showed that in the ternary diagram the alloys with interesting permanent magnet properties lay close to the line from Fe to Ni Al and centred around the composition corresponding to Fe_2 Ni Al. The Alnico permanent magnet alloys comprise a wide range of alloys based on Fe-Ni-Al with major additions of cobalt, copper and titanium and additions of niobium, silicon, sulphur and other elements.

Gould (63) lists the compositions and outlines manufacturing techniques for the Alnico alloys which are currently the most important commercial permanent magnet materials, principally because the metals from which they are made are relatively inexpensive and abundant in contrast to the best permanent magnet materials based on rare-earth-cobalt intermetallic alloys.

Among the possible additions allowed for in the Mishima patent (64) was 0.5 to 40% Cobalt. However the realisation of economically justifiable improvements in properties from additions of cobalt came from independent work in Germany (65) and in Sheffield (66).

Other additions such as titanium and niobium (which also neutralised the effects of impurity levels of carbon) and copper were also made resulting in a range of alloys with (BH) max of 10-16 kJ/m^3 and coercivities 54-60 kA/m (63). Optimum magnetic properties are obtained by cooling slowly from a temperature of about 1250°C followed by annealing or tempering for several hours in the region 550 - 600°C.

In 1938 Oliver and Sheddon (67) obtained slight improvements in the (BH) max and remanence of an alloy containing 12% cobalt and 6% copper by cooling in a magnetic field of 350 kA/m. The improvements were found when the alloy was tested in the same direction as the previously applied field and reduced properties when tested at right angles to this direction. This was quickly followed by the discovery

of a range of alloys containing 16 - 30% cobalt which responds so well to magnetic field treatment that energy products two or three times those of the isotropic properties could be obtained in the field treatment direction (68). The significant change is the very large increase in remenance B_r or J_r. Cooling in the absence of a field gives $\frac{J_r}{J_s}$ = 0.5 - 0.7 but with the field $\frac{J_r}{J_s}$ values of over 0.9 are achieved. This change is accompanied by squaring of the demagnetisation curve so that the fullness factor (BH) max/ $B_r H_{CB}$ increases from about 0.4 in the isotropic alloys to 0.6 or more for the best field cooled alloys.

Further improvements in the directional magnetic properties were achieved by making magnets with columnar grains and then field cooling in the direction of the long axis of the grains (69), giving values of J_r/J_s in this direction approaching 1 and up to a further 70% improvement in energy product.

Other developments have stemmed mainly from composition adjustments, notably substantial quantities of titanium (up to 8 wt.%) with a simultaneous increase of the cobalt content up to 35-40%, have achieved much higher coercivity and some improvement in (BH) max; however, at the expense of the remanence (70). Difficulties of achieving columnar growth due to the presence of both aluminium and titanium (71) were solved by small additions of sulphur or tellurium (72). These titanium bearing alloys require isothermal annealing in a magnetic field in contrast to the other alloys which are cooled from the high temperature conditions in the field.

Details of these materials are conveniently summarised by Gould (63) and a few representative BH demagnetisation curves are presented in Fig 13.

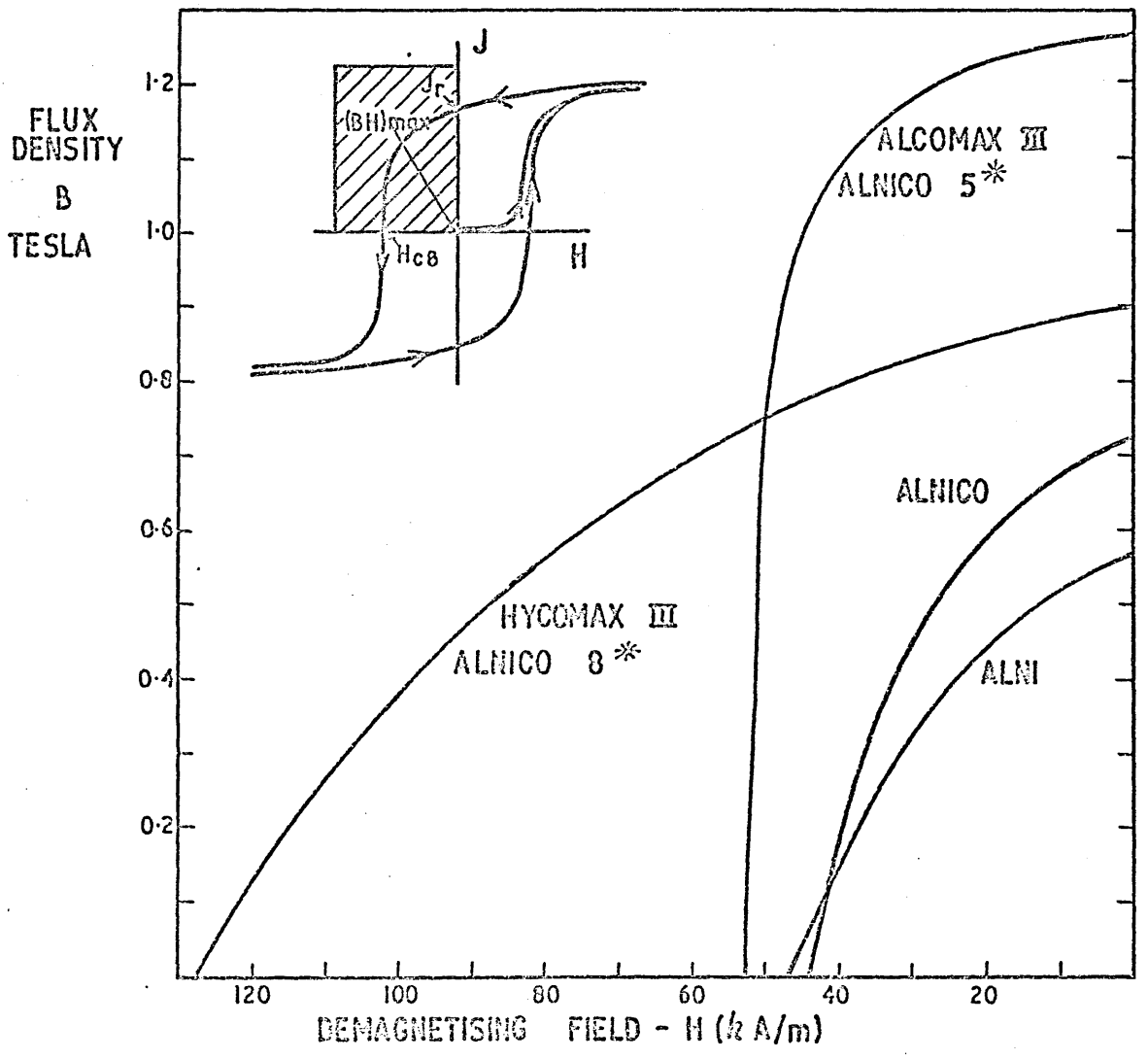

FIG. 13 TYPICAL DEMAGNETISATION CURVES FOR SOME COMMERCIAL ALLOY MAGNET MATERIALS OF THE ALNICO TYPE.
(* U.S.A. TRADE NAMES)

1.3.2. Alnico alloys - Fundamentals

It is well established that permanent magnet behaviour in the Fe-Ni-Al systems is connected with the breakdown of the high temperature b.c.c. phase structure into two finely dispersed b.c.c. phases at lower temperatures with very similar lattice parameters. Bradley and Taylor (61) first indicated the existence of a b.c.c. phase miscibility gap at low temperatures in an X-ray diffraction investigation of the constitution of slowly cooled alloys. The resulting diagram was radically different from earlier constructions (73) but confirmation of this miscibility gap transformation was established by subsequent investigations of optical (62,74) and electron optical (75-77) microstructures. Fig 14. is the isothermal sections at 750°C of the Fe-Ni-Al system according to Bradley (62) based on optical microscopy, which is essentially the same as the diagram originally proposed by Bradley & Taylor (61) based on X-ray diffraction data. Fig 15. shows part of the isothermal sections (62) at 850°C and 950°C and Fig 16. includes three vertical sections all close and parallel to the section joining the Fe corner with the composition Ni Al. These are probably pseudo-binary sections coincident with tie lines. A miscibility gap thus exists in the broad b.c.c. field that extends from α-Fe across to the intermetallic compound Ni Al as shown. These alloys consist, at high temperatures, of a single body - centred cubic phase that decomposes at lower temperature (less than 1000°C in general) into two b.c.c. phases of slightly different lattice parameter, one rich in iron (designated α) and one rich in Ni Al. The Ni Al phase, α', is ordered with the aluminium atoms on the centre sites of the b.c.c. cell.

Several investigators, notably Burgers and Snoek (78,79), Geisler (74) and de Vos (80,81) have also studied the structure and magnetic properties of alloys with compositions across the miscibility gap on the tie-line from Fe to Ni Al. Fig 17 shows the saturation

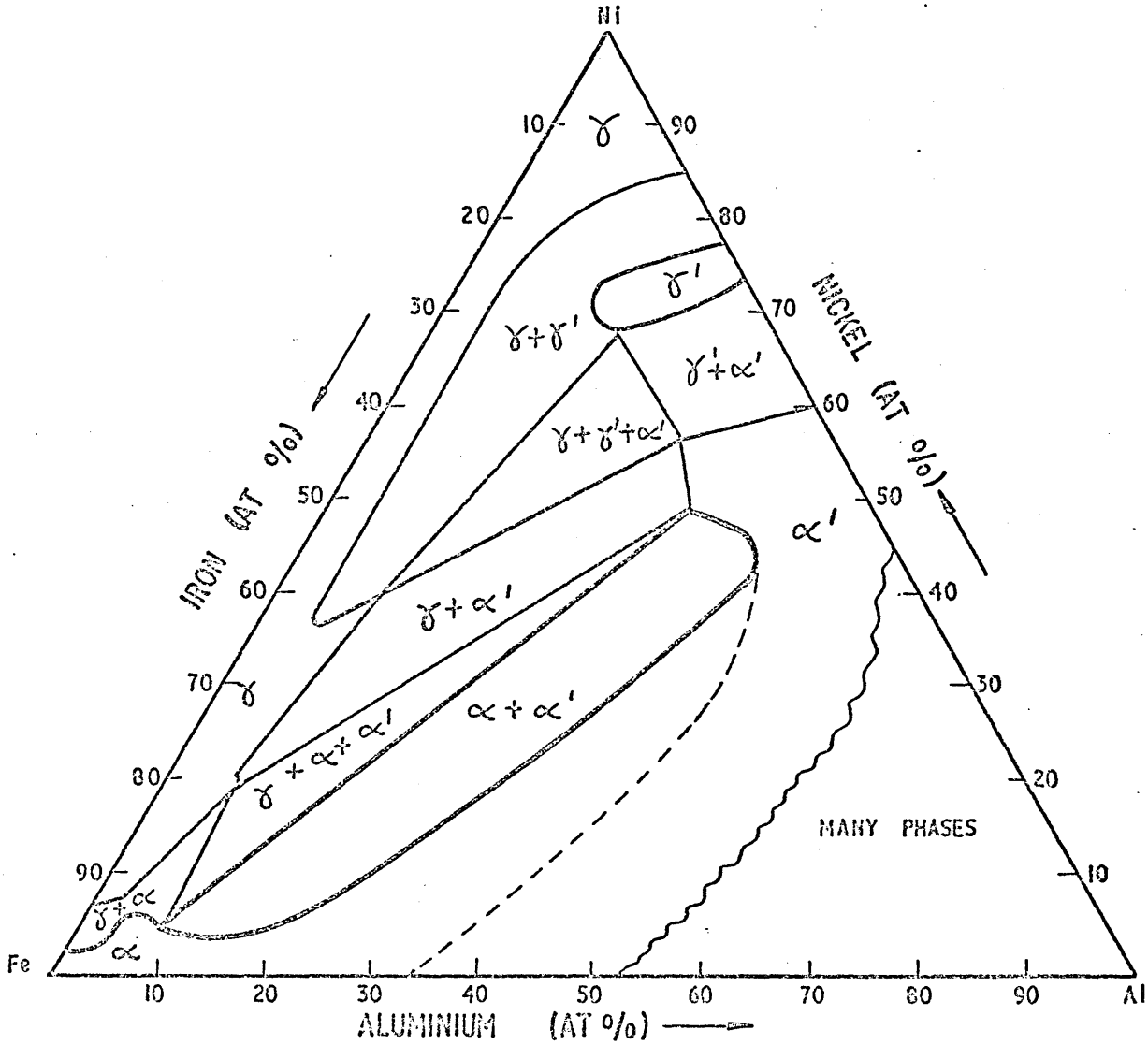

FIG. 14 ISOTHERMAL SECTION OF THE PHASE DIAGRAM FOR THE Fe-Ni-Al SYSTEM AT 750°C., BASED ON A MICROSCOPICAL STUDY BY BRADLEY[62] WITH CHANGE OF NOTATION.

α	b.c.c.	A 2 LATTICE
α'	b.c.c.	B 2 LATTICE
γ	f.c.c.	A 1 LATTICE
γ'	f.c.c.	$B i_2$ LATTICE

– – – – MAGNETIC BOUNDARY FROM THE WORK OF BRADLEY AND TAYLOR[61]

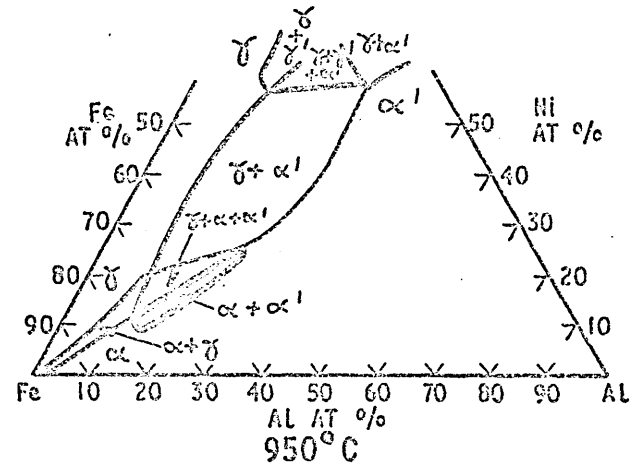

FIG. 15 ISOTHERMAL SECTIONS OF THE PHASE DIAGRAM FOR THE Fe-Ni-Al SYSTEM AT 950°C AND 850°C, BASED ON LIGHT MICROSCOPY BY BRADLEY (52)

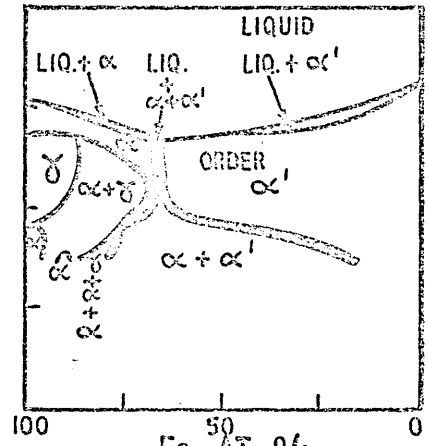

SECTION FROM THE IRON CORNER TO THE COMPOSITION NiAl.

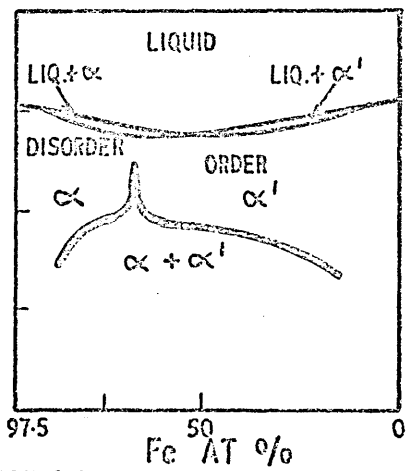

SECTION PARALLEL TO Fe-NiAL WITH EXCESS Al (+1·25 % Al -1·25 % Ni)

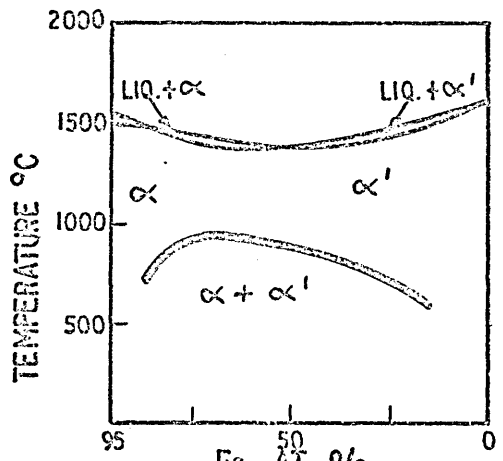

SECTION Fe-NiAL (+2·5 % Al - 2·5 % Ni)

FIG. 16 THREE VERTICAL SECTIONS OF THE Fe-Ni-Al TERNARY PHASE DIAGRAM SHOWING THE MISCIBILITY GAP BASED ON LIGHT MICROSCOPY BY BRADLEY (62)

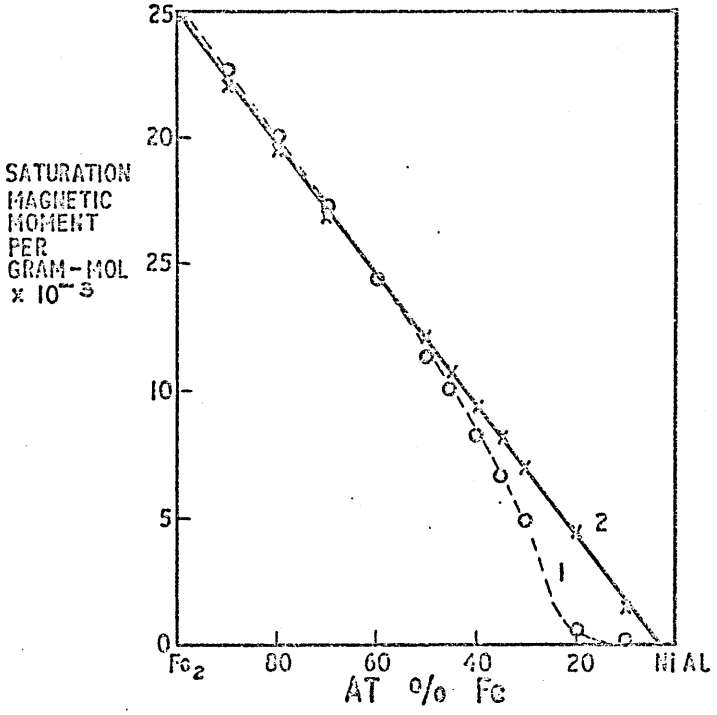

AFTER SNOEK (79)

FIG. 17 (a) MAGNETIC SATURATION AS A FUNCTION OF CONCENTRATION. IN Fe-Ni-Al.

CURVE 1: QUENCHED STATE.
CURVE 2: QUENCHED + ANNEALED AT 500° C.

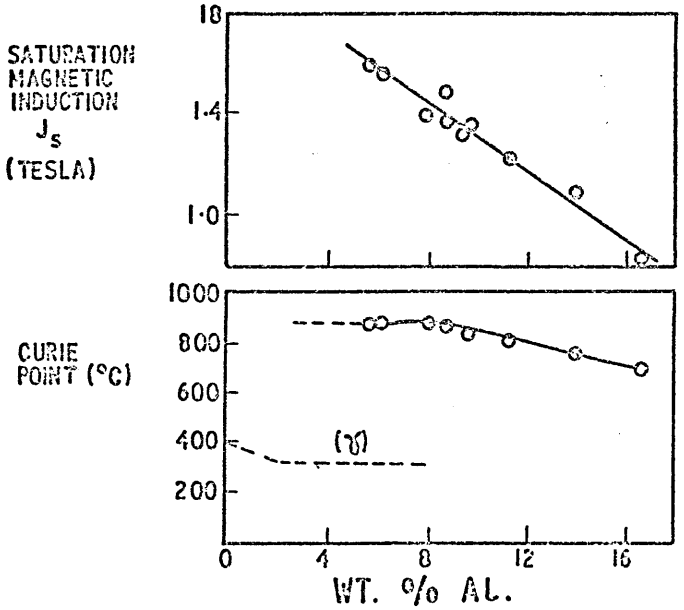

AFTER JELLINGHOUSE (139)

FIG. 17 (b) DEPENDENCE OF SATURATION AND CURIE POINT OF ALNICO 5 TYPE ALLOYS ON THE ALUMINIUM CONTENT (23 % Co, 15 % Ni, 3 % Cu, VARIABLE Fe AND Al).

magnetisation as a function of composition from Fe to Ni Al for various states of heat treatment of the alloys.

Oliver and Goldschmidt (82) extended the X-ray diffraction experiments to include an alloy with 24% Cobalt which responded to field heat treatment and showed that similar behaviour occurred, as summarised in Fig 18. They found evidence of segregation or particle separation into two b.c.c. phases, α and α' with very small differences in lattice sonstants, following either controlled cooling from high temperature or tempering of quenched samples. They observed that the lattice dimension of α appeared to change slightly according to the degree of tempering or rate of cooling. Other workers also confirm that the difference in lattice parameters of α and α' in some of the Alnicos is small, and the expected splitting of the main lines is difficult to detect by X-ray methods (74,83) and completely irresolvable by electron diffraction (75,84,85,86).

The morphology of the alloys in the optimum permanent magnet state consists of elongated particles of α , the iron rich phase, with orientations distributed preferentially in $\langle 100 \rangle$, first observed and deduced by Nesbitt and collaborators (75,87,88). This morphology consisting of fine ferromagnetic particles aligned in $\langle 100 \rangle$ in a matrix with an ordered b.c.c. lattice of very similar parameter, the particles having diameters of the order of 10 nm or more and 40 nm or more long, has been confirmed and investigated in numerous papers (89,90,91,52,92,77,93,81,80,85,94,95,84). Together with fine particle theory, this provides a widely acceptable explanation, not only of the magnetic properties of the magnetically isotropic Fe-Ni-Al and Fe-Ni-Al-Co-(Cu) alloys with hysteresis curves characterised by Fig 11, but also of the alloys which can be made to exhibit anisotropic magnetic properties by cooling or holding at a temperature in the

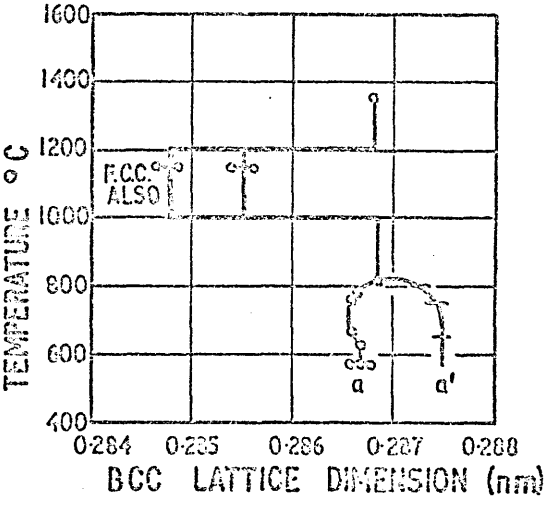

FIG. 18. CHANGES IN LATTICE DIMENSIONS OF b.c.c. PHASES DURING SLOW COOLING OF AN ALNICO ALLOY. AFTER D.A. OLIVER AND H.J. GOLDSCHMIDT.[82]

presence of an applied magnetic field, and the enhanced effect if the applied field is directed in the long axis of columnar grains of the material.

This behaviour can also be explained by the preferred $\langle 100 \rangle$ orientations of the ferromagnetic particles. Field treatment causes the development of anisotropic properties in those alloys with sufficient cobalt content to raise the Curie point into or above the 800 - 850°C temperature range in which the α and α' phases separate. In this case particles are encouraged to form preferentially in the nearest $\langle 100 \rangle$ to the field axis. The extra improvement in columnar grain alloys is due to the fact that columnar grains also grow from the melt in a $\langle 100 \rangle$ so that the field axis coincides with a $\langle 100 \rangle$ in these alloys, wereas in random grain alloys the angle between the field axis and the nearest $\langle 100 \rangle$ can vary in any given grain between 0° and 54°. The best magnetic results have been achieved from single crystals given $\langle 100 \rangle$ field heat treatment and tested in the same direction (80).

Both the electron microscopy investigations previously referred to, together with magnetic torque experiments (87,88,76) confirm that the ferromagnetic particles are distributed in $\langle 100 \rangle$, and respond in the manner expected when heat treated in a suitable field.

Other investigators (69) again using torque magnetometry with columnar discs of Alnico 5 (25% Co, 3% Cu, anisotropic type) believed that the particle alignment after magnetic heat treatment was greater than that allowed by strict alignment with the nearest $\langle 100 \rangle$, but that tempering reduced this effect.

Clegg and McCaig (96) deduced from magnetisation temperature curves obtained with the Sucksmith balance that, for Alnico 5 in the

optimum state, the Curie point of one phase is about 850°C while that of the other is below room temperature. If the alloy is not fully heat treated or is exposed to a temperature above 600°C the less magnetic phase may have a Curie point between room temperature and 450°C. In this state at temperatures below the lower Curie point, when both phases are ferromagnetic the coercivity is low, but it rises when the temperature is increased above the lower Curie point. This sort of effect may be expected for a system with magnetic anisotropy energy described by, for example, equation (1.32). It was further found that if, after exposure to temperatures above 600°C the second Curie point disappears, and provided the alloy has not been too long at a high temperature the coercivity is restored. This behaviour suggests that the composition of the particles changes rather easily by diffusion without much affecting their morphology, The deductions from this work have been amply confirmed by later workers making similar coercivity temperature measurements in conjunction with X-ray diffraction exploration of both lattice changes and interparticle spacing (83), and from Mössbauer spectra in which some Fe atoms in the alloys studied are shown to be in paramagnetic surroundings when tempered to the magnetically optimum state, suggesting a non-ferromagnetic matrix (77,84).

Microstructural investigations of the high titanim alloys indicates that the phase structure is essentially the same, however the particles are even finer, more elongated and possibly of greater structural perfection (80). Paine and Luborsky (98) investigated the question of imperfections and showed that the variation of coercivity and J_r/J_s with angle of the columnar axis in columnar alloys (except those with the highest titanim content) may be represented by models of the magnetisation of interacting permanent magnet particles

(represented in the model by pivoted magnets) with intermittent "cross-ties" or junctions between rows of particles. The behaviour of a high titanim alloy was consistent with the model without "cross-ties". The phase compositions of an alloy containing 34 wt% Cobalt and 5 wt% titanium were investigated by subjecting a combined group of extraction replicas of etched surfaces to electron-probe micro-analysis (99). The results of the investigation was that the precipitate was thought to consist of 42% Co and 50% Fe, and the matrix 30 Wt% Co, about 12 wt% Fe and 38 wt% Ni with the majority of the Al and Ti in the matrix.

Alloys containing substantial amount of cobalt are not in their equilibrium phase state after optimal heat treatment. Sufficiently slow cooling from high temperatures causes precipitation of an f.c.c. phase which, unless avoided can cause considerable spoiling of the magnetic properties. Additions, notably silicon, titanium, niobium or tantalum may be made to render the f.c.c. phase less stable.

Various investigators have nevertheless indicated the presence of this and other phases in the optimally heat treated state (84,70,73,82).

Detailed X-ray diffraction studies by several Russian investigators (94,100,101) have shown that in the optimum magnetic state, the α and α' phases may be slightly tetragonal, especially the high coercivity alloys containing substantial quantities of titanium. It is suggested that the strain anisotropy introduced by this tetragonality may contribute significantly to the coercivity of these alloys.

1.3.3. Other fine particle permanent magnet alloys

The Alnico alloys are certainly the most familiar and

commercially exploited alloys which owe their magnet properties to fine particle shape anisotropy. However alloys in other systems, such as Cu-Ni-Fe ("Cunife") (102), Cu-Ni-Co ("Cunico") (102), and the recently discovered alloys in the Fe-Cr-Co systems (103,104,105, 106,107) are believed to be in this category. So also are the dilute alloys in the Cu-Co (108,109,110) Au-Ni, Au-Co systems and Brass-iron and stainless steel wires (111, 50) in which the ferromagnetic precipitate is produced by heat treatment (sometimes combined with mechanical treatment) from a high temperature homogeneous solid solution. In all these dilute systems and in Cn-Ni-Fe and Cn-Ni-Co, magnetic particle shape anisotropy is achieved by mechanical treatment. However in the Cu-Co system shape anisotropy is also achieved by field heat treatment. In all of these systems however, either because of the low concentration of ferromagnetic component in the alloy or lower coercivity generally, the magnetic properties of the alloys are considerably inferior to many in the Alnico range.

Only in the Fe-Cr-Co alloys investigated by Kaneko et al, are properties approaching those of Alnico 5 achieved by field heat treatment (Fig 13).

1.3.4. Fe-Cr-Co Alloys

Kaneko et al realised that the Fe-Cr system, in which there is a miscibility gap below about 600°C where the b.c.c. phase decomposes into two isomorphous phases α and α' rich in iron and chromium respectively (112, 113), is analogous to the Fe-Ni-Al system with (Ni-Al) replaced by Cr. Prior to 1957 it had been widely held that the "495°C enbrittlement" common in ferritic Fe-Cr steels was always in some way directly connected with the formation of sigma phase which preferentially occurs on slow cooling over the same range

of compositions. However Williams and Paxton (112, 113) on the basis of detailed investigations including resistivity, hardness, saturation magnetisation, Curie point and X-ray diffraction concluded that a metastable $\alpha + \alpha'$ miscibility gap was present at sufficiently low temperatures so that sigma formation did not occur within the relatively short time required for decomposition into $\alpha + \alpha'$ phases. The α phase apparently consisted of particles of the order of 20 nm diameter depending on temperature, which are at all times completely coherent and strained to a common lattice parameter, that of the unaged solid solution. Chemical leaching out of α particles from the alloy showed them to have a high Fe content whereas the residue contained mainly Cr.

Electron microscopy of both extraction replicas and thin foils confirmed the general size, and that the particles were essentially spherical, contrast in TEM (transmission electron microscopy) was achieved only in extinction contours. A miscibility gap very similar to the one given by Williams and Paxton by direct studies of alloys as given in Fig 19 has since been calculated from thermodynamic data (114, 115). Mössbauer analysis confirms the presence of two phases inside the miscibility gap, one paramagnetic and the other ferromagnetic and rich in iron (116, 117). Both X-ray diffraction and Mössbauer effect studies show the absence of both sigma phase and any sign of an ordered phase within the miscibility gap (112, 113, 116, 117).

Kaneko et al (103) showed that by introducing 23 wt% Co cobalt into an alloy also containing 31 wt% Cr, and further applying an isothermal field heat treatment at 640°C and tempering at a slightly lower temperature, magnetic properties similar to those of Alnico 5 can be obtained. This demonstrated the presence of aligned elongated

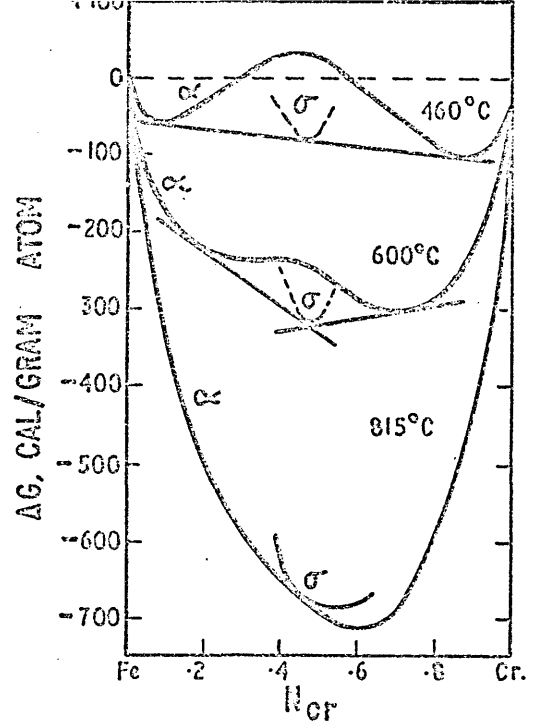

FIG. 19(a) FREE ENERGIES OF FORMATION OF THE α AND σ PHASES IN THE SYSTEM IRON-CHROMIUM AT THREE TEMPERATURES. FROM THERMODYNAMIC DATA. (114)

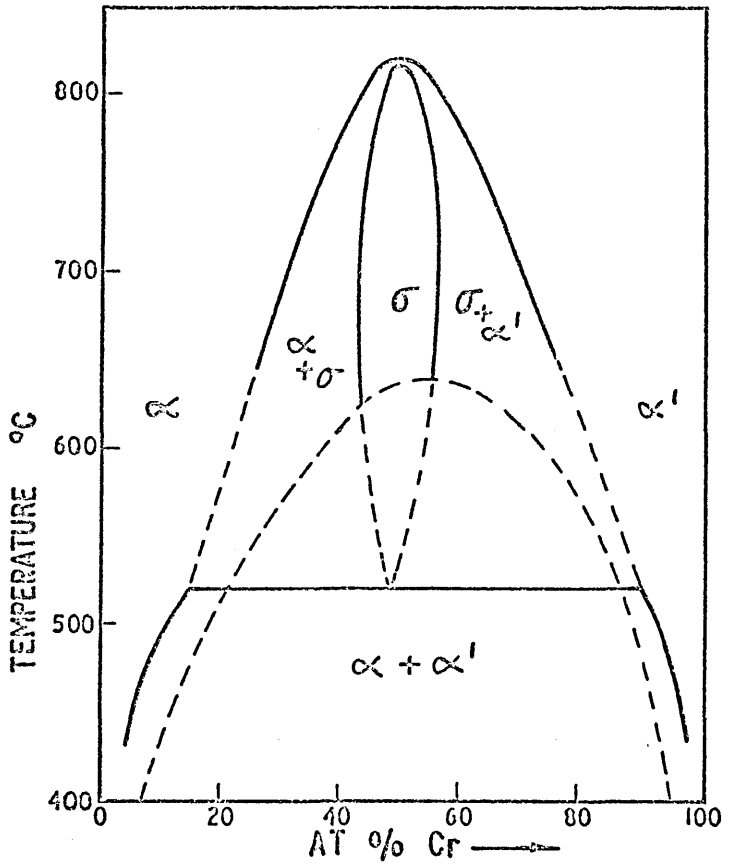

FIG. 19 (b) REVISED LOW-TEMPERATURE PHASE DIAGRAM OF THE IRON-CHROMIUM SYSTEM. DATA α+α' (113, 116, 117) σ FIELD (113) THERMODYNAMICS PLUS HIGH TEMPERATURE DATA. (115, 114)

particles in these alloys and was confirmed by TEM. Some further improvement in magnetic properties were demonstrated by Mo (103) and Si (104) additions. Part of the chromium may also be replaced by vanadium without loss of magnetic properties (107). The introduction of small amounts of Nb and Al to the ternary alloys allow the cobalt content to be reduced to 15 wt% maintaining similar magnetic properties (106).

An f.c.c. phase may also be present in these alloys as shown in the vertical sections in Fig 20, however the presence of the Nb and Al also allows cooling in a magnetic field analogous to the heat treatment for Alnico 5.

All the Fe-Cr-Co appear to be ductile in the quenched state in contrast to the Alnicos which are brittle unless transformed partially to the f.c.c. structure which is however difficult to remove afterwards.

1.4. Mechanism for the formation of shape anisotropic fine particle structures in permanent magnet alloys

Prior to the work establishing fine particle shape anisotropy theory it was supposed (61) that when heat treated to the optimum permanent magnet state, the Alnico alloys consisted of a structure in a state of "pre-precipitation" with a lattice parameter intermediate between that of the solid solution and those of the $\alpha + \alpha'$ phases at equilibrium, thus creating a highly heterogeneous structure with a large internal strain. It was further supposed that the internal strain was sufficient to account for the coercivity. The work of Nesbitt (118) showed however that the magnetostriction of some of the Alloys is zero when the coercivity is 32 kA/m or more.

Subsequent to the realisation that fine elongated particles

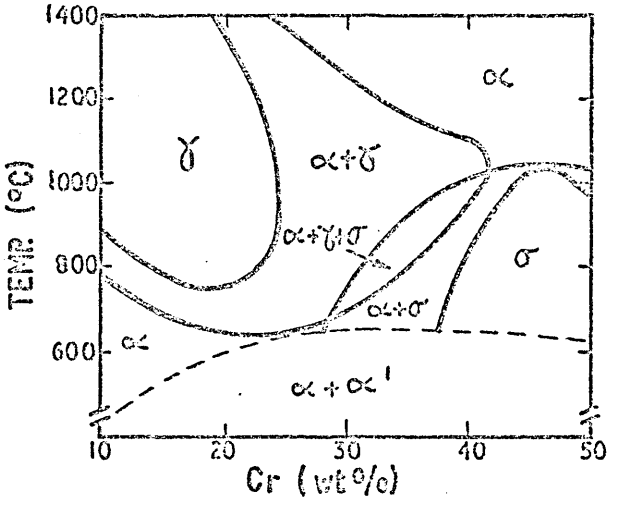

FIG. 20 (a) VERTICAL SECTION OF Fe-Cr-Co SYSTEM AT 15 wt. % Co.

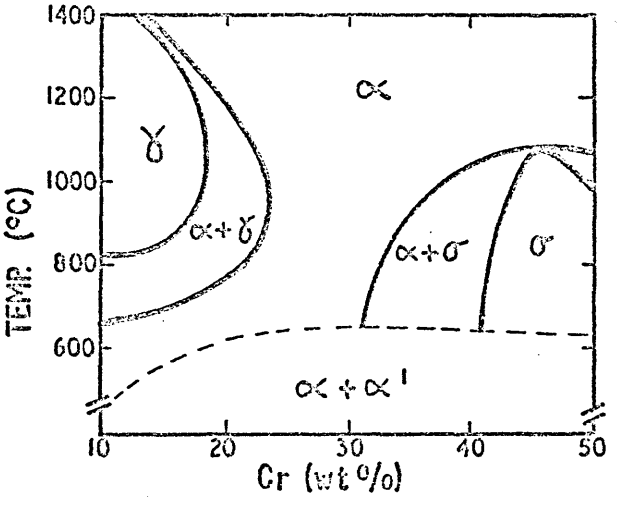

FIG. 20 (b) VERTICAL SECTION OF Fe-Cr-Co Nb-AL SYSTEM AT 15 wt.% Co, 1wt.% Nb AND 1wt.% Al. BASED ON EXPERIMENTAL WORK OF KENEKOETAL.[106]

are sufficient requirement for coercivities of these levels, discussion of the kinetics of formation of such particles was made on the basis of nucleation and growth (119, 120, 121, 51). A special requirement for good permanent magnets is that the particles should be distributed homogeneously implying the possibility of homogeneous nucleation.

1.4.1. Spinodal Decomposition

Daniel & Lipson (122) interpreted observations, by Bradley (123) in Cu-Ni-Fe alloys, and by Bergers and Snoek (78) in Fe-Ni-Al alloys of "side-bands" on X-ray diffraction lines, as due to modulations or a wave-like periodicity of composition within the alloys on a scale of the order of 5 - 15 nm.

The deduction was made by interpretation of the side bands by analogy with radio frequency theory (hence the term "side-band") where the superposition (modulation) of a larger wavelength signal on the carrier wave produces side-bands round the normal frequency), and the numerous observations of such structures by electron microscopy in Fe-Ni-Al and Alnico have already been reviewed, and similar X-ray diffraction observations have also been made in the Cu-Ni-Fe (124,125,126) and Cu-Ni-Co (127) systems, and the persistence of the side-bands to the earliest ageing times indicates that this modulated structure exists at the earliest stages of decomposition even in the quenched state.

Hillert (128) first pointed out that there could be a thermodynamic reason for the formation of modulated structures inside the miscibility gap. He derived an equation which was capable of explaining the main characteristics of the formation and morphology of modulated structures which answered the two criticisms made by

Guinier (129) of the modulation interpretation of side bands; the diffuseness of the side-bands being due to a spectrum of wavelengths and provision of a mechanism of wavelength growth by the theory. Hillert's model was based on compositional variations in one dimension only, and a more flexible three dimensional continuum model was subsequently developed by Cahn and his associates (130-136). In Cahn's theory, which is a theory of spinodal decomposition inside the miscibility gap, in addition to the free energy of the homogenous phase Cahn introduces other terms, an interfacial energy term, a term for the effect of coherency strains and included the effects of external fields such as stress and magnetic fields.

If initially only the interfacial energy term is considered then the total free energy

$$G_T = A_c \int \left[G + K \left(\frac{dc}{dx} \right)^2 \right] dx \quad \ldots\ldots\ldots \quad (1.33)$$

Where A_c is the cross sectional area of the solid, G the free energy of the homogeneous phase and $K \left(\frac{dc}{dx} \right)^2$ is the interfacial energy term representing the surface energy differences between planes of atoms of different composition; K is a constant - the gradient energy coefficient.

Free energy is related to the interdiffusion coefficient by

$$D = \frac{M}{N_v} \frac{d^2 G}{dx^2} \quad \ldots\ldots\ldots\ldots \quad (1.34)$$

where M is the mobility, N_v the number of atoms per unit volume and x represents displacement. Using equation (1.34) and the minimum value of the integral, equation (1.33), Fick's second law of diffusion is obtained but with an extra term (other non-linear terms of higher order are ignored)

$$\frac{\partial c}{\partial t} = \tilde{D} \frac{d^2 c}{dx^2} - 2 \frac{K M}{N_v} \frac{d^4 c}{dx^4} \quad \ldots\ldots \quad (1.35)$$

where c is composition and t is time.

If the strain due to composition differences are taken into account then the equation is further modified.

$$\frac{\partial c}{\partial t} = \left(\tilde{D} + 2\eta^2 Y \frac{M}{N_v}\right) \frac{d^2c}{dx^2} - 2\frac{K M}{N_v} \frac{d^4c}{dx^4} \quad \ldots\ldots (1.36)$$

η is a function of the change of lattice parameter with composition and Y a function of the elastic constants which in general vary with crystallographic direction.

The solution of equation (1.36) assuming K, η, Y, M and $\frac{d^2G}{dx^2}$ (and therefore D) are constant is

$$c - c_0 = A e^{-Dt/r^2} \cdot e^{-\eta^2 Y t/r^2} \cdot e^{-2Kt} \cdot \cos\left(\frac{x}{r}\right)$$

$$= A e^{-\left(\frac{\tilde{D}}{r^2} + \frac{\eta^2 Y}{r^2} + 2K\right)t} \cdot \cos\left(\frac{x}{r}\right) \quad \ldots\ldots\ldots (1.37)$$

where C_o is the composition of the initial homogenous solid solution.

The variation of composition is made up of two factors, one depending on distance, Cos ($\frac{x}{r}$), which means that the fluctuations are periodic and sinusoidal. However a summation of any number of such terms as given by the right hand side of equation (1.37) with different values of r is also a solution of equation (1.36) so that the fluctuations may be periodic but not necessarily strictly sinusoidal, and x can represent different directions in different terms.

The other factor, e^{-Rt} indicates that R must be negative if the fluctuations are not to decay. $\eta^2 Y/r^2$ and K are always positive so that $D = \frac{M}{N_v} \frac{d^2G}{dx^2}$ must be negative and relatively large. By definition $\frac{d^2G}{dx^2}$ is negative inside the spinodal within the region of the points of inflexion in the variations of G with composition, corresponding to a miscibility gap situation (Fig 21).

From the known likely values of K it is only significantly large when the wavelength ($2\pi r$) of fluctuations is greater than about 10 nm, and this then explains the scale of such fluctuations in real systems.

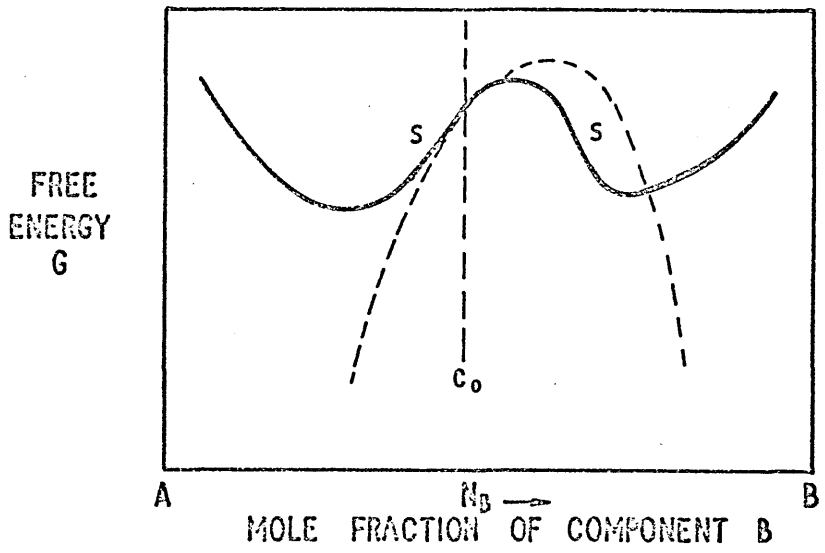

FIG. 21. THE ASSUMPTION THAT $\left(\frac{\partial^2 G}{\partial C^2}\right)$ IS INDEPENDENT OF COMPOSITION IS EQUIVALENT TO FITTING THE FREE-ENERGY FUNCTION (FULL CURVE) TO A PARABOLA (DASHED CURVE).

$\eta^2 Y$ is a sensitive function of crystallographic orientation so that in practice only fluctuations oriented in certain crystallographic directions may survive. $\eta^2 Y$

Perhaps the most serious problem in the solution of equation (1.36) is the assumption of constant $\frac{d^2G}{dx^2}$ to the free energy composition curve as shown in Fig 21. It is expected then that equation (1.37) is only applicable at the very early stages of decomposition. However this is sufficient to fix the wavelength of composition fluctuations, i.e. the morphology, which can then change only relatively slowly with time.

Cahn (132,130,131) showed that, for b.c.c. structures, composition fluctuations will have a specific wavelength (equivalent to the separation between particles) controlled by the anisotropy in elastic energy in the crystal axes so that the peak of composition fluctuations would tend to lie along $\langle 100 \rangle$, which in three dimensions will be equivalent to diffuse particles arranged in an infinite cubic array of spacing of perhaps 20 nm.

If the composition is ferro-magnetic at the temperature at which fluctuations commence then magnetostatic energy of the possible fluctuations can effect the morphology (133).

Re-writing equation (1.37) as

$$C - C_o = Z \cos \beta x \quad \ldots\ldots\ldots (1.38)$$

where $z = A e^{-Rt}$ and $\beta = \frac{1}{r}$ and if the specimen is magnetised in the x direction. Because magnetisation is composition dependent i.e.

$$J_s = J_o + (C-C_o) \frac{\partial J_s}{\partial c} + \tfrac{1}{2} (C-C_o)^2 \frac{\partial^2 J_s}{\partial c^2} + \ldots\ldots (1.39)$$

which is a Taylor's series expansion of $J_s(C)$, where J_o is the mean J_s.

Taking the first two terms only is equivalent to assuming a

linear relation between J_s and c so that

$$J_s = J_0 + Z \left(\frac{\partial J_s}{\partial c}\right) \cos \beta x \quad \ldots\ldots\ldots (1.40)$$

J_s fluctuates sinusoidally, however at all points along x Maxwell's equations require that the flux density B is constant, as $B = \mu_0 H + J_s$ then

$$H_{(x)} = -\mu_0 Z \left(\frac{\partial J_s}{\partial c}\right) \cos \beta x \quad \ldots\ldots\ldots (1.41)$$

The magnetostatic energy per unit volume associated with this field is

$$E_x = -\tfrac{1}{2} \int (H_{(x)} J_s) \, dx$$

$$= \tfrac{1}{2} \int \left[-\mu_0 J_s Z \left(\frac{\partial J_s}{\partial c}\right) \cos \beta x - \mu_0 Z^2 \left(\frac{\partial J_s}{\partial c}\right)^2 \cos^2 \beta x\right] dx$$

The integral of the first term in the square bracket over $n \longrightarrow \infty$ cycles is zero and for $\cos^2 \beta x$ is $\tfrac{1}{2}$ (when $\beta x = 2\pi$, $\int_0^{2\pi} \cos^2 \beta x \, . \, dx = \pi$)

therefore

$$E_x = \frac{\mu_0}{4} Z^2 \left(\frac{\partial J_s}{\partial c}\right)^2 \quad \ldots\ldots\ldots (1.42)$$

from equation (1.40) $J_s \max - J_s \min = \Delta J_s = 2 \left(Z \frac{\partial J_s}{\partial c}\right)$

$$E_x = \frac{\mu_0}{8} (\Delta J_s)^2 \quad \ldots\ldots\ldots\ldots (1.43)$$

If this magnetostatic energy is included in the decomposition equation (equation (1.36)

$$\frac{\partial c}{\partial t} = \left(\tilde{D} + \left[2\eta^2 \gamma + E_x\right] \frac{M}{N_V}\right) \frac{\partial^2 c}{\partial x^2} + 2K \frac{M}{N_V} \frac{\partial^4 c}{\partial x^4} \quad \ldots\ldots\ldots (1.44)$$

then this will lead to an extra exponential factor in the solution $e^{\left(\frac{E_x}{2I^2}\right)t}$.

Application of a strong magnetic field in the x direction during ageing thus suppresses planes of fluctuation in this direction, but not in perpendicular directions where the component of J_s is zero. Taking into account the crystallographic factor $\eta^2 \gamma$, which will generally allow decomposition (in most cubic systems) in only the three $\langle 100 \rangle$, the morphology should consist of diffuse rod-like particles in the nearest $\langle 100 \rangle$ to the direction of the applied field.

At the early stages of decomposition, where these equations apply, the composition of the particles and matrix is likely to be far from the equilibrium composition of the two phases. This is radically different from the classical nucleation and growth model, where the particles start off small in size but with a composition corresponding to the equilibrium phase. The difference is indicated schematically in Fig 22.

Cahn has shown, by consideration of additional non-linear terms in equation (1.35), that at later times the morphology will be essentially the same except that the compositions of particles and matrix will approach their equilibrium values. (Hillert's (1.28) earlier one dimensional decomposition model also predicts this condition).

Furthermore, dependant on the relative equilibrium proportion of the two final phases, spinodal decomposition can lead to either discrete particles or more intermixed phases (132,131) and both the Cahn (131) and Hillert (128) theories indicate that particles characteristic of "zones" may also be formed by spinodal decomposition near to the extremes of the spinodal range of compositions.

Estimates of the best possible time constants R in e^{-Rt} in equation (1.37) from diffusion coefficients (129) are several milliseconds for a solid near its melting point up to perhaps a few seconds for miscibility gaps which are well below the melting point. Thus, in only the first few seconds the morphology is fully determined and suppression of the reaction altogether may be extremely difficult.

1.4.2. Studies of early stages of decomposition in fine particle magnet alloys.

By electron microscopy in both the Cu-Ni-Fe system (125) and Cu-Ni-Co (127) (both based on f.c.c. structures), it was found that

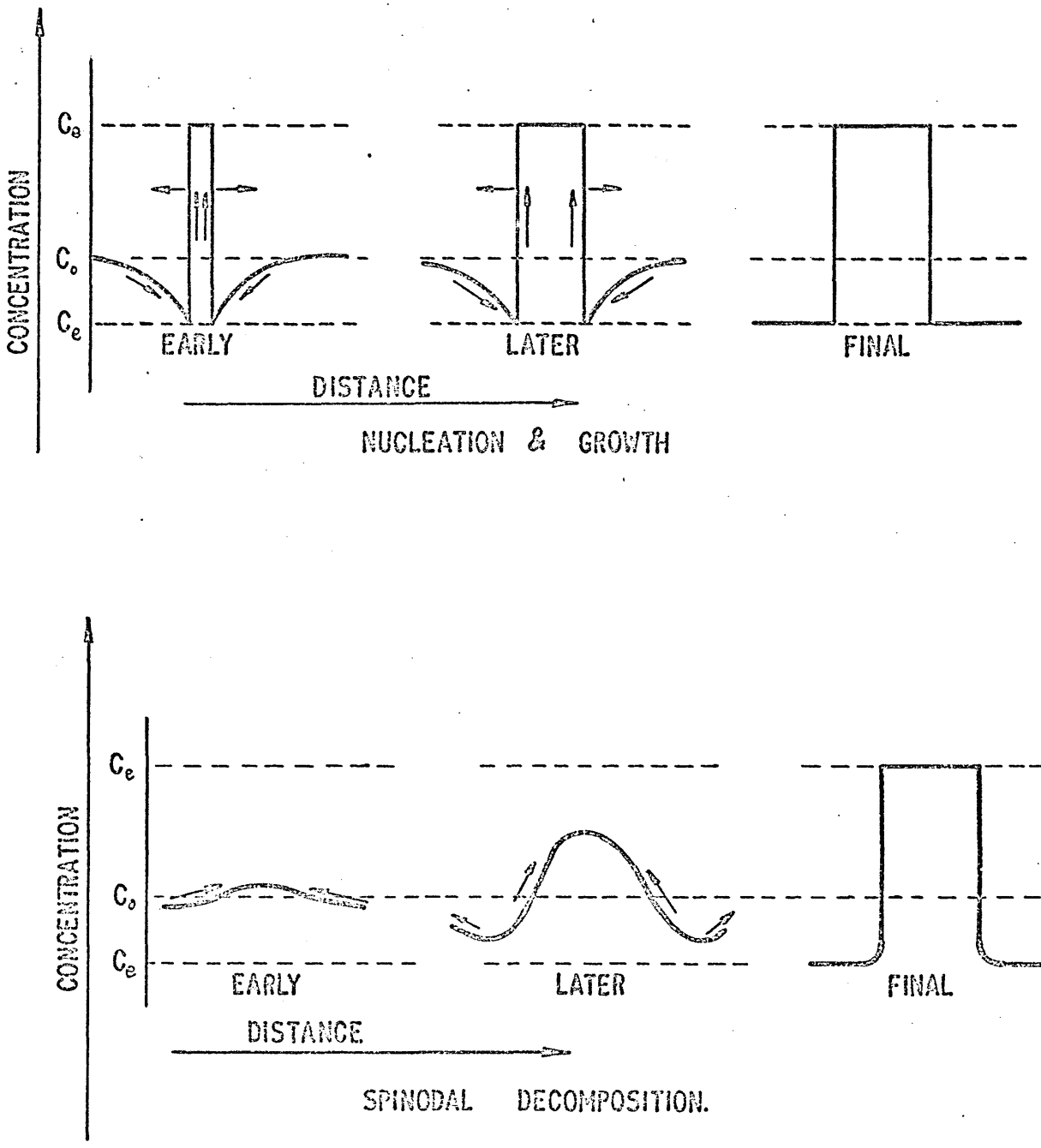

FIG. 22 SCHEMATIC EVOLUTION OF CONCENTRATION PROFILES TO ILLUSTRATE THE DIFFERENCE BETWEEN NUCLEATION & GROWTH AND THE SPINODAL MECHANISM.

decomposition could not be suppressed completely, even by vigorous quenching, and this is common with other systems believed to undergo spinodal decomposition (131).

The electron microscopy studies made by De Vos (80, 81) of Fe-Ni-Al and Alnico alloys also indicated that decomposition could not be completely suppressed. He concluded that the decomposition was in accordance with Cahn's theory.

Several papers by Russian workers provided useful confirmations of this view (94, 137), and others based on microscopy and in one case (137) using torque magnetometry of single crystal discs of Alnico alloys. They found that α and α' were slightly tetragonal with increasing difference in tetragonality between α and α' with increasing titanium content. It was supposed that the increasing elastic energy was responsible, via the spinodal decomposition mechanism, for the observed elongation and increased perfection of the particles. Measured coercivity as a fraction of the magnetic anisotropy field also increased with the titanium content of the alloys.

Other Russian workers using X-ray diffraction techniques on Alnico alloys (138,77,101) interpret their findings in some alloys as evidence for the formation of spherical zones, prior to the formation of a periodic structure. In other alloys the periodic structure is believed to form directly (101) but randomly with evolution of an anisotropic structure later in ageing. Body-centred-tetragonality of α and α' were also evident in this latter work.

The relatively low coercivity and hysteresis of Alnico alloys which were heat treated but not tempered, was attributed to the presence of a ferromagnetic matrix by Clegg and McCaig (96,139), and further demonstration of reversibility of coercivity with tempering confirmed by other workers (70,83,80), implies that both particles and matrix are not necessarily at their equilibrium compositions and that

adjustments are easily made by diffusion between pre-existing particles and matrix rather than growth of the particle phase which would tend not to be reversible.

Mössbauer spectra of Alnico alloys (97,84) also indicate that iron atoms change from a paramagnetic to a ferromagnetic condition during tempering (i.e. transfer to the ferromagnetic phase).

Attempts have been made to measure J_s for the particle composition at various stages of heat treatment using the fine particle coherent rotation formula for coercivity (equation includes(1-p) to account for particle interaction)(75,85,140).

Nesbitt and Williams (120) and others (75,140) found, by interrupted heat treatment of Alnico 5, that the necessary magnetic anisotropy for normal magnetic properties was established at the earliest part of ageing in a magnetic field. Some of these results are presented in figures 23 and 24. The Mössbauer spectra of Fe-Cr alloys (116,117) can separate regions inside the miscibility gap at the higher temperatures (540°C) which apparently decompose by nucleation and growth. For high Fe alloys (117), the precipitate which appears is paramagnetic from the beginning of decomposition, whereas when ageing the same alloy at 470°C decomposition is much slower with no paramagnetic composition even after 1050 hr., which is interpreted as spinodal decomposition. (The essential difference between nucleation and growth and spinodal decomposition is used here; that is, a nucleus has the equilibrium phase composition, whereas spinodal fluctuations start with small deviations of composition and progress towards equilibrium composition as indicated in Fig 22). A Fe - 60wt% Cr alloy also decomposes spinodally (116), and again relatively long times confirm a rate of composition change as predicted by Hillert's theory (128). Fe-Cr compositions in the range 12 to 30 atomic % Cr decomposed via nucleation and growth. Imai et al (141) showed that during ageing of a 74% Cr alloy the Curie point at -90°C splits into

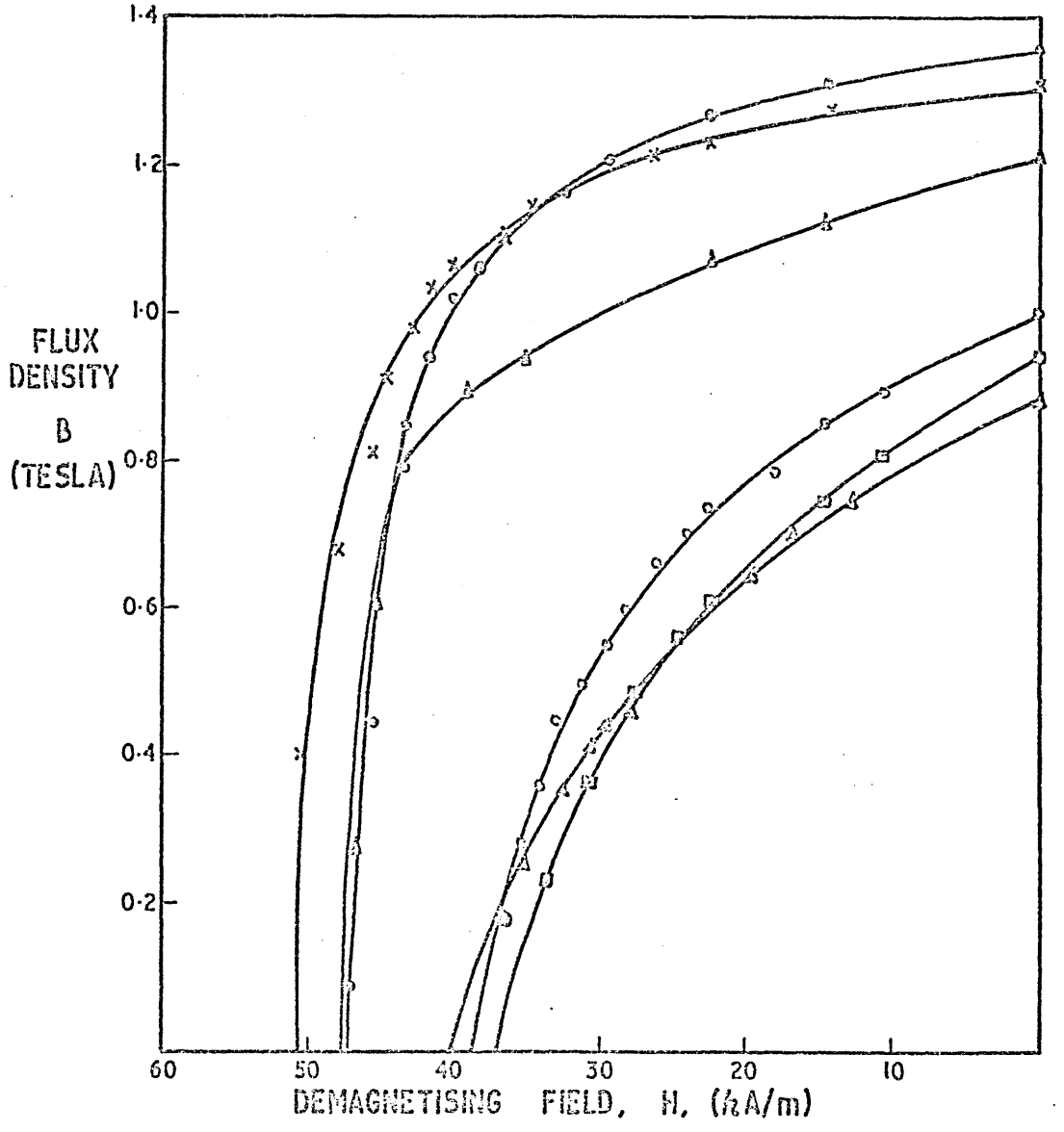

FIG. 23 DEMAGNETISATION CURVES FOR SAMPLES OF ALNICO 5 AFTER COOLING AT 1·5°C PER SECOND AND THEN AGEING FOR 15 HOURS AT 600°C – AFTER NESBITT AND WILLIAMS [120]

x – MAGNETIC FIELD ALWAYS ON DURING COOLING.
o – " " ON FROM 890°C TO 790°C
Δ – " " " " 840°C TO 790°C
o – " " " " 790°C TO 590°C
□ – " " " " 760°C TO 590°C
Δ – NO MAGNETIC FIELD DURING COOLING.

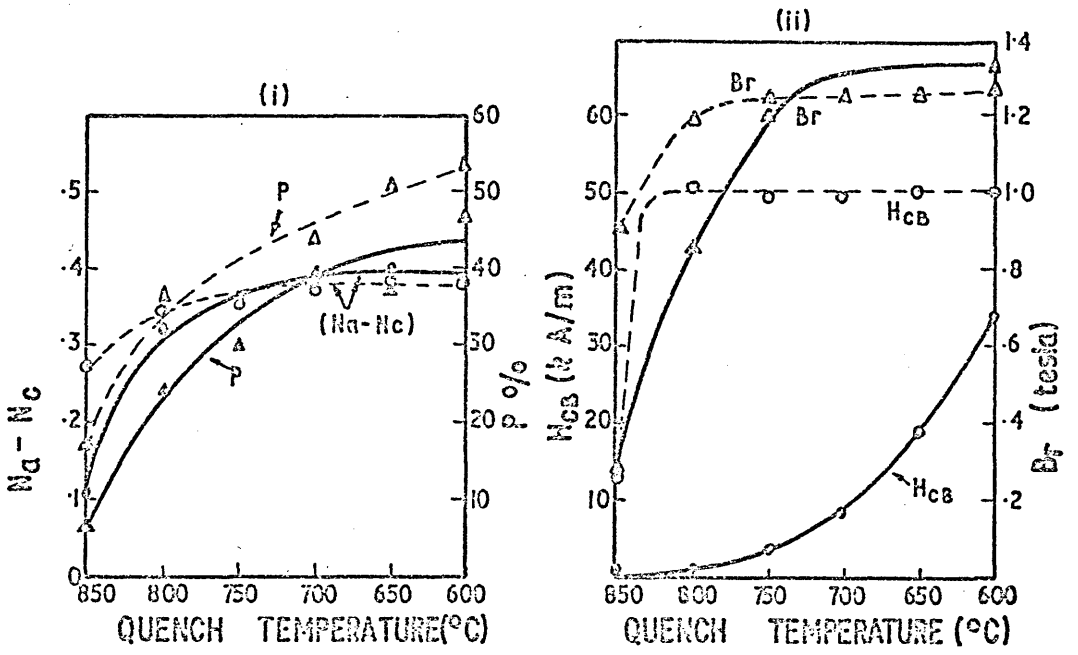

FIG. 24(a) VARIATION OF BOTH STRUCTURAL PARAMETERS OF α' PARTICLES AND MAGNETIC PROPERTIES OF ALNICO 5 AFTER COOLING AT 0·5°C/sec IN A 318 k A/m FIELD INTERRUPTED BY QUENCHING AT THE GIVEN TEMPERATURES. DASHED LINES ARE AFTER A FURTHER TEMPER OF ONE HOUR AT 640°C AND 4 HOURS AT 520°C. (140)

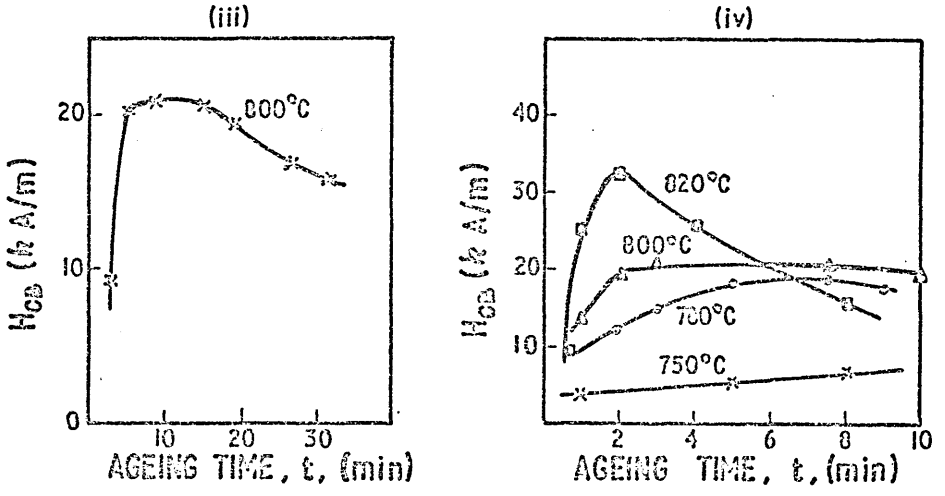

FIG. 24 (b) COERCIVITY OF ALNICO ISOTHERMALLY AGED. (iii) MEASURED AT THE AGEING TEMPERATURE DURING AGEING (iv) MEASURED AT R.T. AFTER TEMPERING AT 585°C. (70)

two, the separation between them increasing with ageing time, one continuously increasing above -90°C, the other decreasing below this temperature.

1.4.3. Particle coarsening

In a system of particles of a phase in the matrix of another phase, the total surface of the particle decreases if their number is reduced, simultaneously keeping their volume fraction constant (approx.), The corresponding decrease of the total interfacial energy represents the driving force for the coarsening of particles.

The theoretical relationship between mean particle radius r and the time of coarsening t, has been shown (142,143) to be of the form

$$r^3 - r_o^3 = kt \quad \ldots\ldots\ldots\ldots (1.45)$$

where r_o is the particle radius at the beginning of coarsening and k is the rate constant. The original theory, which was derived for spherical liquid particles has been shown to apply generally to solid particles of arbitrary shape (144,145,146).

At long times r_o is small compared with r so that

$$r \gg r_o \quad r = (k't)^{1/3} \quad \ldots\ldots (1.46)$$

Studying spinodally decomposed alloys in the Cu-Ni-Fe system, Butler and Thomas (125) found that the law was obeyed, even for the coarsening of highly elongated periodic particles. It is apparently obeyed in Cu-Fe (110) and for many other systems (146-154) some of which may also have originated by spinodal decomposition and others by nucleation.

A similar equation to (1.45) governs the rate of decrease of solute content of the matrix which apparently occurs simultaneously with the coarsening of the particles in solid systems (146,149) i.e.

there is a change in the solubility of the solute with size of particles in accordance with

$$\left(\frac{1}{C-C_e}\right)^3 + \left(\frac{1}{C_o-C_e}\right)^3 = kt \quad \ldots\ldots\ldots (1.47)$$

where C_e is the equilibrium matrix solute concentration, C_o is the concentration at the start of coarsening, and C the concentration at time t.

For long ageing times

$$(C_o-C_e) \gg (C-C_e) \text{ and } (C-C_e) = (kt)^{-1/3} \quad \ldots\ldots (1.48)$$

and this relationship is also seen to apply in a number of alloy systems (146,148,149,154).

1.4.4. Particle coarsening in a magnetic field

Zijlstra, (51) assumed as an initial condition, a uniform distribution of very small particles of equilibrium composition (i.e. homogeneous nucleation) which may then simultaneously coarsen and also elongate in the direction of an applied field to reduce simultaneously both interfacial and magnetostatic energies respectively. Numerical solution of two simultaneous differential equations, one for each driving force, gave two equations ; one for coarsening and the other for change in magnetic anisotropy due to the particle elongation.

The numerical derivation was restricted to large elongations so that the two equations again only apply to long ageing times.

They are for K_s approaching $(K_s)_\infty$

$$V = V_o t \quad \ldots\ldots\ldots (1.49)$$

$$K_s = (K_s)_\infty - At^{-1/3} \quad \ldots\ldots (1.50)$$

Where K_s is the measured particle shape anisotropy; $(K_s)_\infty$ is the value at infinite time; V is the particle volume, V_o is the volume at the start of coarsening; t is the time and A is a constant.

Zijlstra (52,121) obtained values of K_s with ageing at various temperatures and times from both single crystal and polycrystalline samples of Alnico 5, previously quenched from a higher temperature. These results seem to fit a $t^{-1/3}$ relationship at long ageing times, and are shown in Figs 25 and 26.

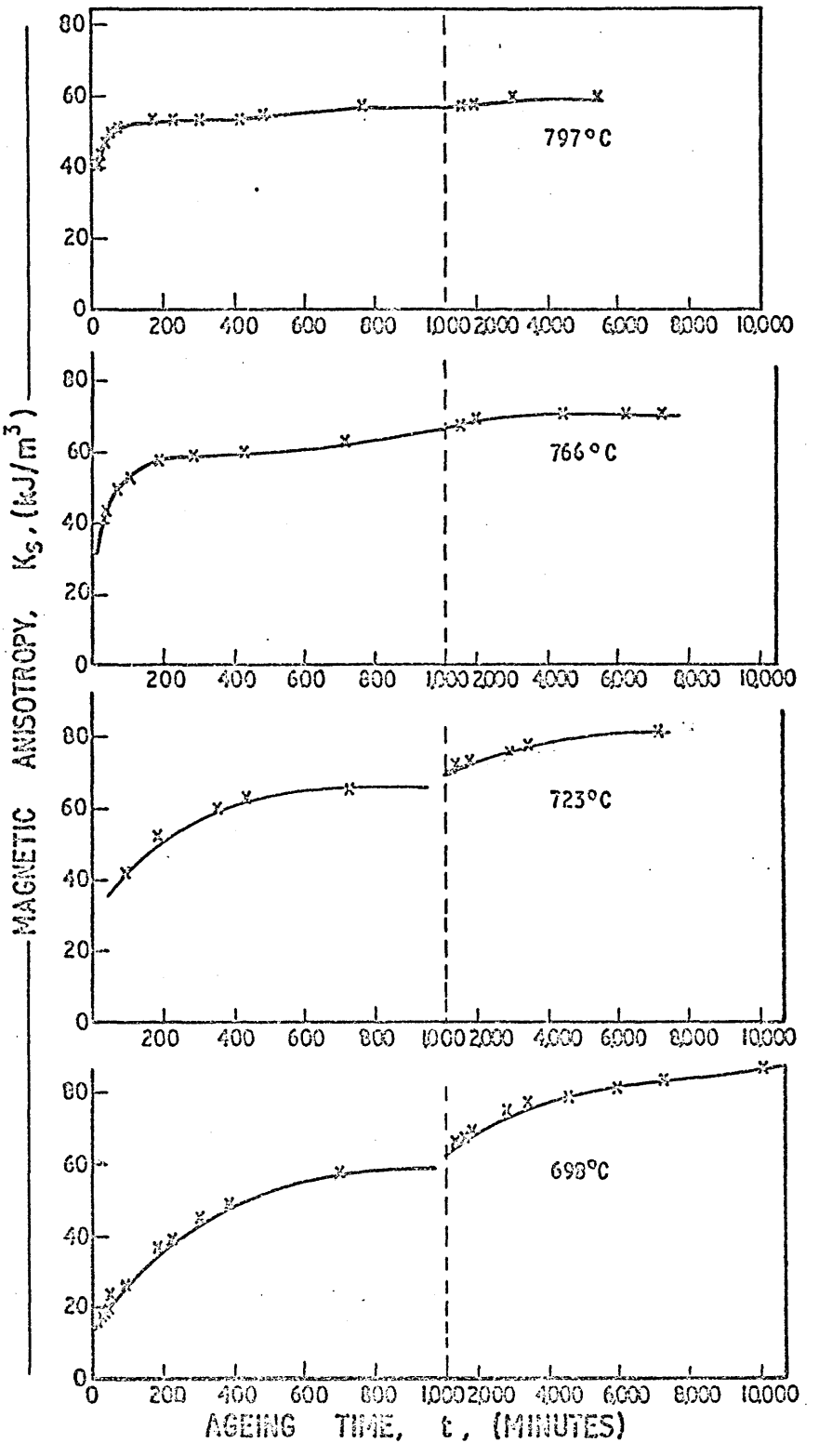

FIG. 25 ZIJLSTRA'S[51] MAGNETIC ANISOTROPY RESULTS FOR POLYCRYSTALLINE SAMPLES OF ALNICO 5 AGED FOR VARIOUS TIMES AT THE GIVEN TEMPERATURES IN A MAGNETIC FIELD. - ANISOTROPY MEASURED AT THE AGEING TEMPERATURE.

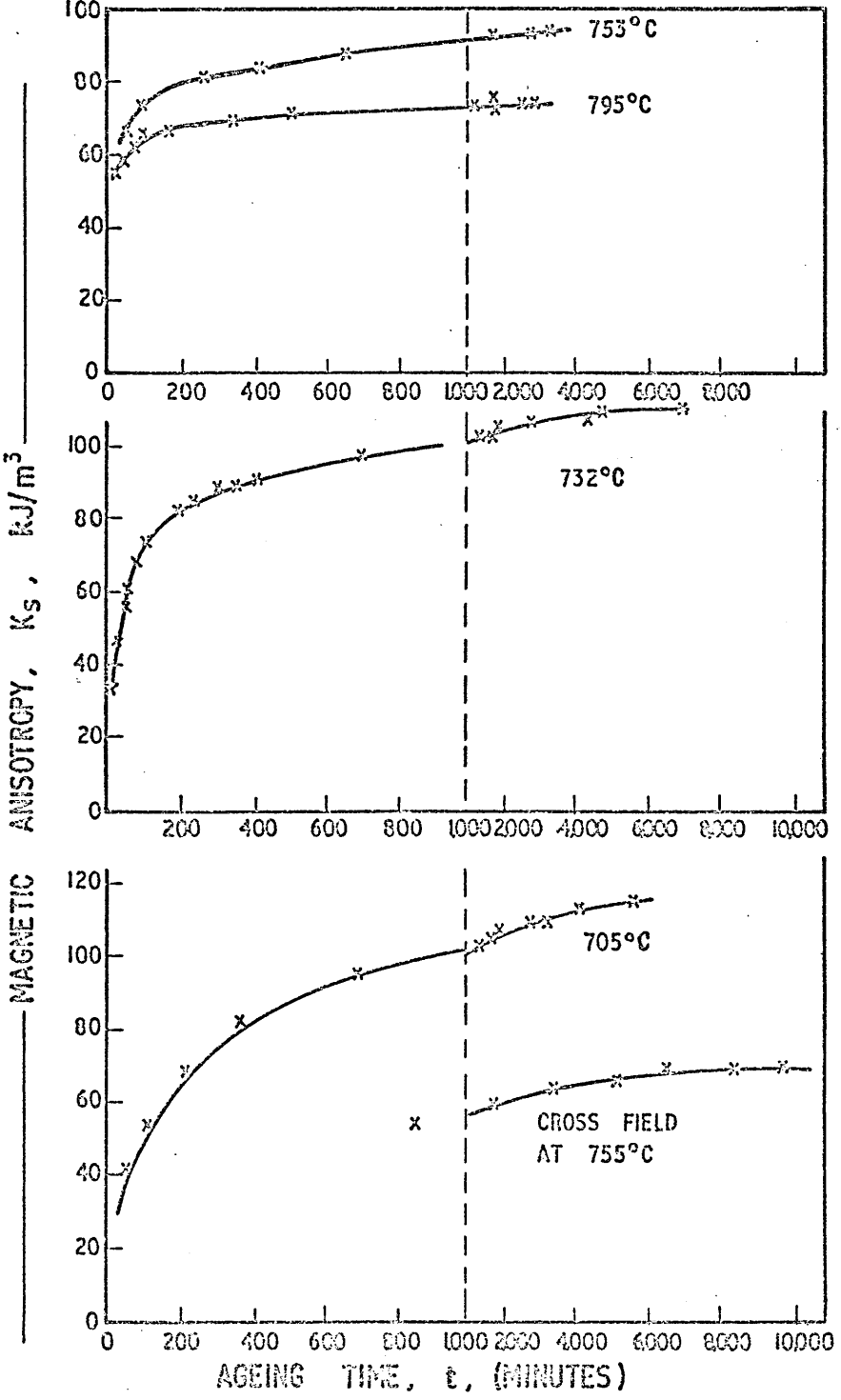

FIG. 26. ZIJLSTRA'S [51] MAGNETIC ANISOTROPY RESULTS FOR SINGLE CRYSTAL SAMPLES OF ALNICO 5 AGED FOR VARIOUS TIMES AT THE INDICATED TEMPERATURES IN A MAGNETIC FIELD. ANISOTROPY MEASURED AT THE AGEING TEMPERATURE.

CHAPTER 2.

Experimental Procedure

2.1. Preparation of the alloys

2.1.1. Fe-Ni-Al-Co Alloy

An Fe-Ni-Al-Co (four component) alloy was prepared similar in composition to Alnico 5 or Alcomax 111 except that no minor elements such as copper etc. were added. The alloy was melted from electrolytic iron of 99.9% purity, Inco (mond) nickel pellets (99.9% purity), electrolytic cobalt (99.8% purity) and aluminium of 99.5% purity. The main impurity elements in the aluminium were however iron and nickel constituting approximately 0.4%. The alloy was melted under argon in a sillimanite crucible using a 13.5 kg capacity induction furnace, and cast into shell moulds. Two sizes of samples were made approximately 15 mm long by 16 mm diameter cylinders, and rod samples 3.5 to 4 mm diameter and 25 mm long, both types being incorporated within the same mould. The composition of the alloy expressed both in weight percent and atomic percent is given in table 111. This alloy will henceforth be referred to as alloy Al.

2.1.2. Fe-Cr-Co Alloy

A Fe-Cr-Co alloy was prepared by melting and casting from high purity metals of at least 99.9% purity. The metals were melted in vacuum using a magnesite crucible and a 13.5 kg capacity induction furnace. The alloy was cast under a low pressure of argon into a precast investment mould. The castings were in the form of rods of three different diameters, approximately 12 mm, 4.4 mm and 3.5 mm diameter and various lengths up to 130 mm, all were incorporated in the same mould. Table 111 gives the composition of the alloy in both weight and atomic percent and henceforth is referred to as alloy Cl.

TABLE III

CHEMICAL COMPOSITION OF ALLOYS A1 and C1

Alloy		COMPOSITION Fe	Al	Ni	Cr	Co	C	N
Fe-Al Ni-Co (A1)	Wt.%	53.0	8.20	15.70		23.10		
	At.%	49.6	15.9	14.0		20.5		
Fe-Cr -Co (C1)	Wt.%	45.85			30.80	23.30	.022	.019
	At.%	45,4			32.75	21.85	(.0010)	(.00075)

TABLE IV

CHEMICAL COMPOSITION OF ALLOYS C2 and C3

Alloy		Composition Fe	Cr	Co	Si	C	N
Fe Cr Co - C2	Wt.%	46.3	31.0	22.4	0.22	0.0009	0.075
- C3	Wt.%	48.4	29.2	22.1	0.21	0.019	0.047

2.1.3. Other Alloys

Other Fe-Cr-Co alloys of similar composition were also made using the same technique as for alloy A1; that is melting under argon rather than vacuum. However the lack of purity, particularly in terms of nitrogen content, of the resulting alloys was such that only a very low coercivity could be obtained. This was demonstrated to be the cause by subsequent annealing of samples in hydrogen or argon at high temperatures, which reduced the nitrogen and led to a much better level of coercivity after optimum heat treatment, although not up to the level of alloy C1 and the levels also obtained by Keneko et al (103) in the original work on these alloys. The compositions of two of these argon melted alloys, alloys C2 and C3, are given in table 1V.

Though some interesting TEM observations were made, in view of the complications with impurities, no other work was done on these alloys.

Thus the work was concentrated mainly on the alloys C1 and A1 although a considerable amount of other work, in particular on commercial Alcomax 111, and also some other Alnico grades, was conducted. It is considered more convenient to describe some of the details of sample preparation of these alloys in later sections, however all such samples were melted and cast under normal commercial conditions using induction furnaces and shell or stack moulding and nominal composition of these alloys are given in table V.

2.2. Sample Preparation

Alloy A1 and the Alnico alloys generally are brittle and the conventional method of manufacture is from castings. Both alloys A1 and C1 were cast into convenient sizes for the subsequent planned investigations so that then only surface grinding and centreless

TABLE V

Nominal Chemical Compositions of Commercial Alnico Alloys.
(mainly British Trade names)

Alloy	Composition (Wt.%)						
	Al	Ni	Co	Cu	Nb	Ti	Fe
Alni	12.5	26.0		4.0			BALANCE
Alnico	9.5	17.0	12.0	5.0			
Alcomax III	8.0	13.5	24.5	3.0	0.6		
Alnico 5*	8.0	14.0	24.0	3.0			
Hycomax III	7.0	15.0	34.0	4.0		6.3	
Alnico 8*	7.0	15.0	35.0	4.0		5.0	

* - U.S.A. Trade names.

.....

grinding of the cylindrical surfaces were usually necessary to produce accurately dimensioned specimens. (Samples of Alloy C2 were prepared from a graphite mould. This was hot swaged and then rolled at 1100°C to 13 mm diameter rod). Where necessary and certainly in the case of the rods for TEM, torque magnetometry and for alloy C1, generally, which was all in the form of relatively long bars, samples of an appropriate length or thickness for testing were prepared by slitting using normal laboratory slitting facilities with ceramic slitting wheels. In the case of alloy C1, rods could be reduced in diameter by turning when in the solution treated condition, so that rods for TEM which needed to be 3.1 mm diameter were sometimes turned down. In other cases and particularly for alloy A1 and the Alnico alloys generally, the correct diameter bar was produced by centreless grinding.

Some allowance was always made so that all samples were ground on all surface after heat treatment was complete and prior to any measurements or tests which were subsequently undertaken.

2.3. Heat Treatment

2.3.1. Continuous cooling in a magnetic field

Prior to any fundamental experimental work on alloys A1 and C1, a heat treatment survey of both alloys was performed, employing the usual heat treatment techniques with variations of certain parameters i.e. temperatures, times and cooling rates, in order to determine the optimum technological magnetic properties for comparative assessment with results for similar alloys as given in the literature. As alloy A1 is basically an Alnico 5 alloy these initial trials were conducted using methods traditionally used for this kind of alloy. Cylindrical samples of A1 were held at 1250°C for 30 mins and then allowed to cool at various rates between 10 and 70°C min. in a magnetic

field of approximately 300 kA/m in the direction of the cylindrical axis of the sample. Magnetic properties were subsequently measured after tempering (in the absence of a field) for 48 hours at 590°C followed by a further 48 hours at 560°C in the same direction. The furnaces used here were electric nichrome wire resistance furnaces, and temperature control was effected using thermocouples and on/off electromechanical controllers, accurate to ± 5°C.

2.3.2. Solution treatment

Solution treatment was performed on all samples prior to any subsequent isothermal ageing treatments in order to obtain and retain a single phase b.c.c. microstructure. This involved holding at an appropriate temperature for the alloy and then generally quenching into iced brine. The Fe-Cr-Co alloys were held at 1400°C (103) in an argon atmosphere for 1 hour, and the Fe-Ni-Al-Co alloy Al and the other Alnico alloys held at 1260°C in argon for 30 minutes.

The only deviations from this procedure were made for some of the Al samples which were subsequently to be sectioned for TEM. Some difficulties were experienced with some of the samples from alloy Al which were brine quenched. Because of their extreme brittleness thin foils could not be prepared without fracturing the discs. It was found however by TEM and magnetic tests that there was no observable difference if the discs were, in these instances, oil quenched from 1260°C, and the brittleness was reduced sufficiently for foils to be successfully prepared.

The furnace used for all solution treatments was an electric resistance furnace using silicon carbide rods as heating elements and argon was inserted via a ceramic tube through the side wall of the furnace. Temperature control was effected using thermocouples and electromechanical on/off controllers with a chart recorder, and the system was accurate to ± 5°C.

2.3.3. Initial heat treatment survey of alloy C1

Following the work of Keneko et al (103), in which it was established that for Fe-Cr-Co alloys optimum magnetic characteristics were obtained by isothermal ageing in a magnetic field after solution treatment (section 3.3.2.), a series of samples were isothermally aged at various temperatures and times using a specially constructed permanent magnet jig, details of which are given in Fig 27. Here use is made of the fact that the range of ageing and tempering temperatures for Fe-Cr-Co alloys which is 670°C - 530°C is also within the tempering range of Alnico 5 alloys. Although exposure of Alnico 5 to temperatures in the range 600-670°C reduces the room temperature magnetic properties it has been previously shown by several investigations (70,83,80) that with exposure to temperatures even as high as 750°C, although room temperature magnetic properties were reduced, these magnetic properties could be restored to near their original level by further tempering in the range 600-530°C. The isothermal ageing and tempering cycle used for the Fe-Cr-Co alloys were thus found to be such that any detrimental effects at the higher temperatures were offset by the later tempering stages if both ageing and tempering were done in the jig, in which the magnetic flux required for alignment during ageing was provided by blocks of columnar Alcomax III ("Columax") with a remanence, J_r, of 1.35 tesla. If samples of Fe-Cr-Co were required in the aged-only condition or at some intermediate temper then tempering of the jig through the same cycle of tempers was preferred without the Fe-Cr-Co sample in order to restore the magnetic properties of the columnar blocks to their original magnetic properties. The tempering stages used, after the ageing which was in the range 600-670°C, were as follows

2 hours at 600°C
4 hours at 580°C
16 hours at 560°C

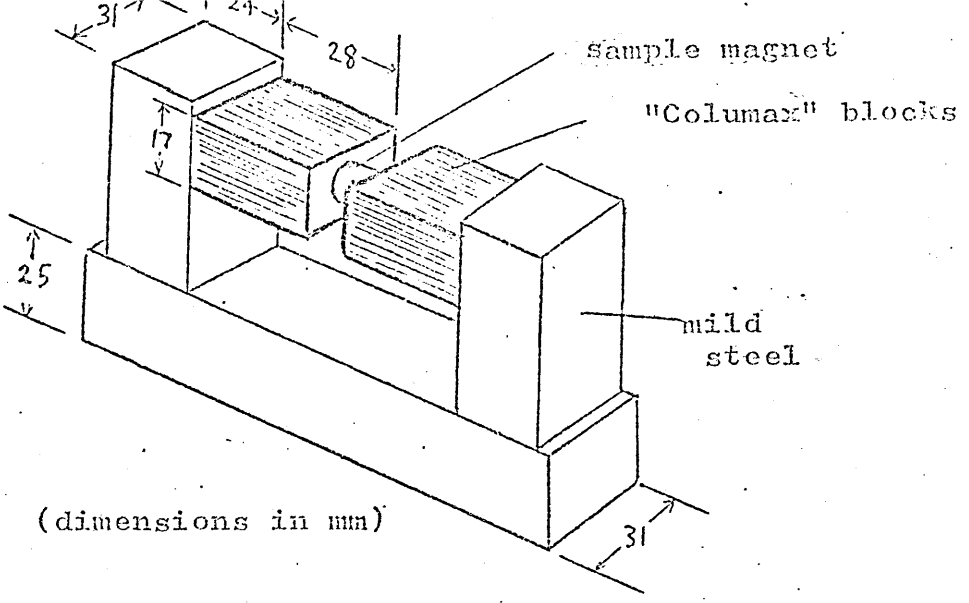

Fig. 27. Permanent magnet jig for heat treatment of FeCrCo magnets.

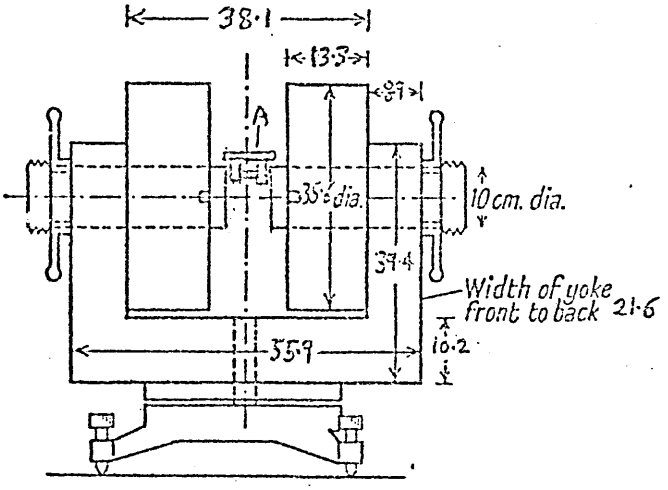

(dimensions in cm)

Fig. 28. Schematic diagram of electromagnet used for experiments with permanent magnet samples and discs.

The procedure for insertion of the sample for heat treatment in the permanent magnet jig was first to assemble the magnets sample and mild steel blocks as in Fig 27 so that a complete magnetic circuit is obtained with, ideally, no gaps. In order to minimise gap losses all contact surfaces were ground and/or linished prior to assembly. The assembly was then magnetised in a large electromagnet which, operating at 250 volts and 18 amps in the coil windings, delivers 1670 kA/m in a gap of 22 mm width and diameter of 100 mm this being the diameter of the pole pieces of the electromagnet. The design of the electromagnet is the same as that of Sucksmith (155,8). Further details are given in Fig 28. The permanent magnet jig was magnetised with the jig inserted in the gap as shown in Fig 28 at A, with the pole piece ends screwed up into contact with the jig so that there was no obvious gaps in the magnetic circuit.

Pre-magnetisation of the assembled jig with the sample of Fe-Cr-Co alloy was found necessary after a series of preliminary experiments which showed that optimum magnetic properties of Fe-Cr-Co alloys were obtained in this way. In fact, these properties were slightly better than those obtained by the other methods of isothermal heat treatment described in the next section, which is why the initial heat treatment survey of the technological magnetic properties of alloy C1 was conducted using the permanent magnet jig.

Control of the temperature of the resistance wound (nichrome) electric furnace used to hold the jig assembly was achieved using a thermocouple in the furnace connected to an electromechanical on/off controller plus a chart recorder. The system was seen to control to $\pm$ 2°C at the set temperature. The temperature of the jig assembly itself containing the magnet was measured using a chromel-alumal thermocouple with the bare junction resting on top of the jig. The

thermocouple was connected to a chart recorder so that the time and temperature range at the control temperature could be carefully monitored. Each heat treatment began by loading the pre-magnetised jig into the furnace which was already at the ageing temperature. The jig was placed in the furnace onto a 1 cm thick heat resisting steel tray which was also at the ageing temperature. A typical chart record of the temperature as measured by the thermocouple on the sample is shown in Fig 29 from which it may be seen that the assembly takes approximately 16.7 minutes to reach 650°C ± 3°C which is the control temperature.

Prior to use in the jig the Columax permanent magnet blocks had magnetic characteristics of remanence (J_r) 1.35 ± .02 tesla, energy product ((BH) max) of 61 ± 2 kJ/m^3, and coercivity(H_{CB}) of 61 ± 2 kA/m. Frequent tests were made on the blocks after use in the jig, and, after using in up to 10 cycles of ageing and tempering, losses in magnetic properties were such that no less than 1.32 tesla J_r, 58 kJ/m^3 (BH) max and 57 kA/m H_{CB} was ever obtained. No two magnet blocks were used for more than 10 heat treatment cycles however. Other workers have also used this method of heat treatment for similar Fe-Cr-Co alloys with equal success (156), however because of the relative slow heating to the ageing temperature, as demonstrated in Fig 29, and slow cooling to the tempering temperatures it is not a precisely reproducible method.

2.3.4. Isothermal ageing using the salt bath

Isothermal magnetic ageing of samples (apart from the initial survey described in the previous section) of all alloys was done in a magnetic field of approximately 250 kA/m using a salt bath. The salt is 50% potassium chloride and 50% sodium carbonate with a useful temperature range from approximately 630°C to over 900°C.

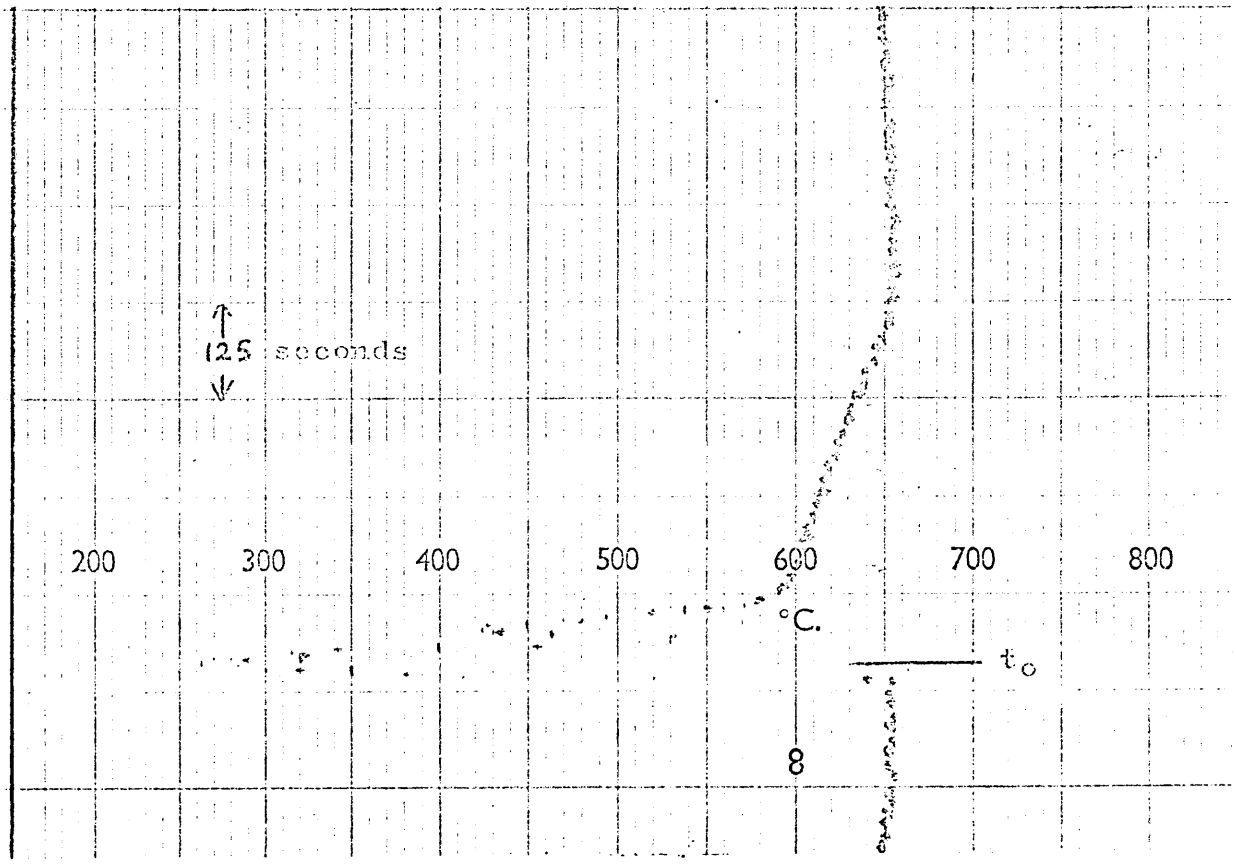

Fig 29. Temperature record from permanent magnet jig after placing into the furnace onto a heat resistant tray (furnace and tray initially at 650°C) at time t_o

A diagram giving further details of the salt bath and electromagnet, plus the power supplies for both the magnetic field and heating the salt bath is given in Fig 30. Samples which required ageing with the field in the long axis of the sample were lowered using nickel tongues into the salt at the appropriate temperature, onto a protruding shelf just below the central axis of the electromagnet poles. The shelf was welded horizontally onto the inside of the mild steel box which contained the salt and was situated inside the gap between the poles of the electromagnet. The field was then switched on with the sample still being held by the tongues, and, so long as the cylindrical magnets had their axes in the direction of the applied field and the length of the sample was greater than the diameter, it was found that the field itself effectively held the sample in this position and the tongues could then be removed.

Calibration of the field in the region just above the shelf, with the current supplied to the electromagnet from a D.C. source, was initially done at room temperature both before salt was added and melted, and was also checked at regular periods by allowing the salt to freeze and cool to room temperature with a vertical copper rod resting on the shelf. When cold this could then be withdrawn allowing measurements to be made. Magnetic field measurements were made in this case using a hall probe and gaussmeter which was calibrated up to field of 796 kA/m using a standard permanent magnet which had itself been checked using a Hysteresigraph of the type described by Scoles (157) with a standard inductor previously calibrated by the Permanent Magnet Association.

It was found that the direction and strength of the field was effectively constant within the circular volume within 40 mm radius from the central axis of the poles and above the shelf.

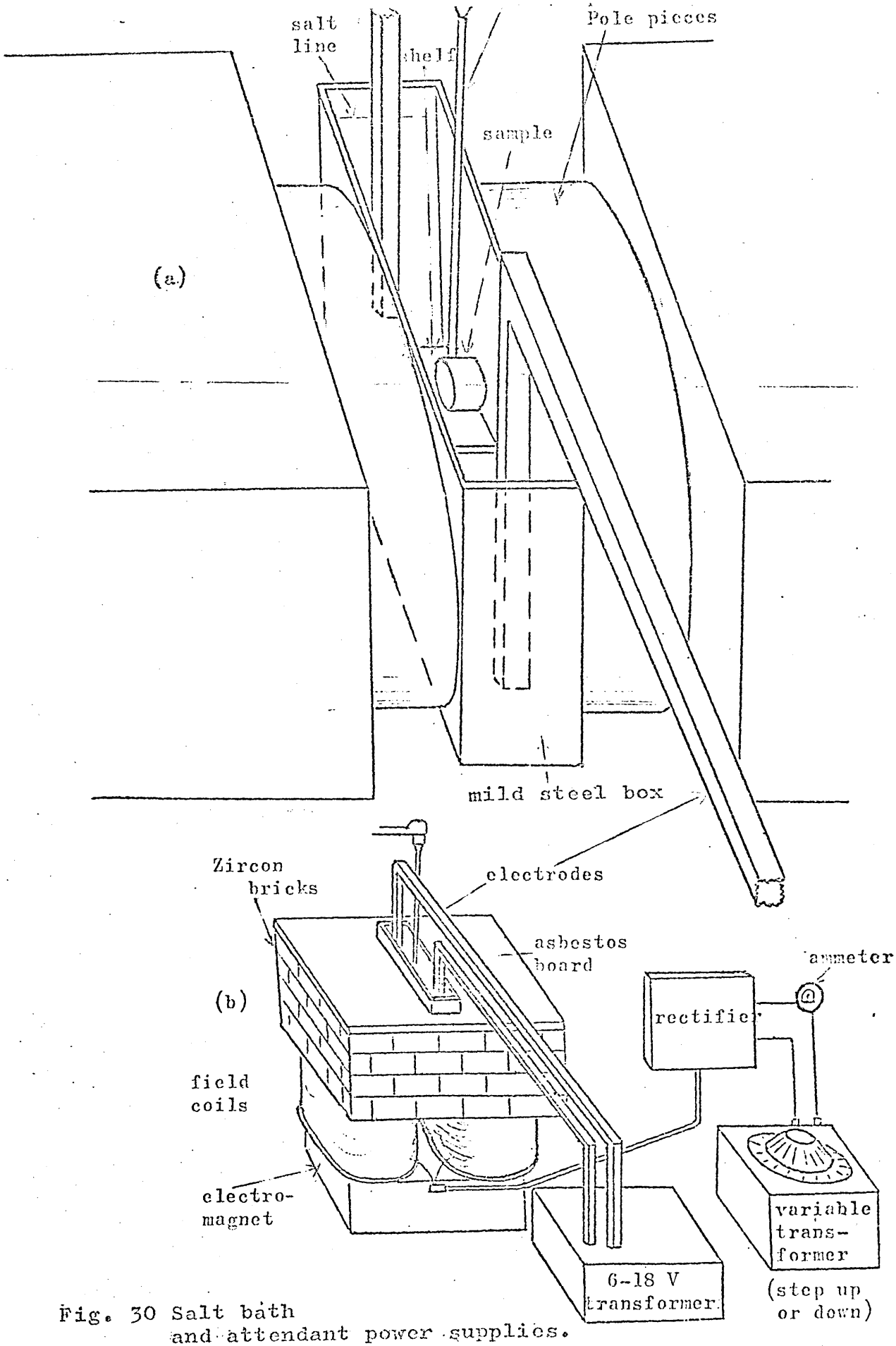

Fig. 30 Salt bath and attendant power supplies.

The temperature, as measured with a flexible mineral insulated base metal thermocouple, was constant within ± 1°C within the same volume of the bath once steady temperature control was achieved for all temperature levels from 630 to 850°C. All samples which were aged in this bath were always located well inside this region. For samples for which the applied field during ageing was required to be applied radially i.e. parallel to a diameter of the bar sample a mild steel suspension jig was constructed and used, in which the sample was securely gripped and as a further precaution secured into place using 32 SWG nichrome wire. The jig is shown diagramatically in Fig 31 with a sample in position and suspended in the salt bath. The jig is made from strip which is long enough to be bent so that the other ends of the strip come over the top of the electromagnet enabling an accurate clamping of the sample in the field to ensure that the direction of the field coincides with a radial direction of the rod sample. The length of the vertical arms of the jig are such that the sample is suspended at the central axis of the field in the gap of the electromagnet.

Initial measurements of the time for samples to heat up to the control temperature of the salt were made using a mineral insulated base metal thermocouple connected to a chart recorder. The chart showed that, by immersion of the thermocouple, on its own, into the salt at 650°C, this temperature was achieved after 30-60 secs. On immersion, a 4 mm diameter, 25 mm long sample of magnet alloy, with the thermocouple attached, reached this temperature in approximately the same time and so did the thermocouple attached to the suspension jig. The jig plus sample plus thermocouple took 1 min. 46 secs. to reach 650°C. Temperature control was achieved using a chromel alumel thermocouple inside a sealed silica sheath with the end of the

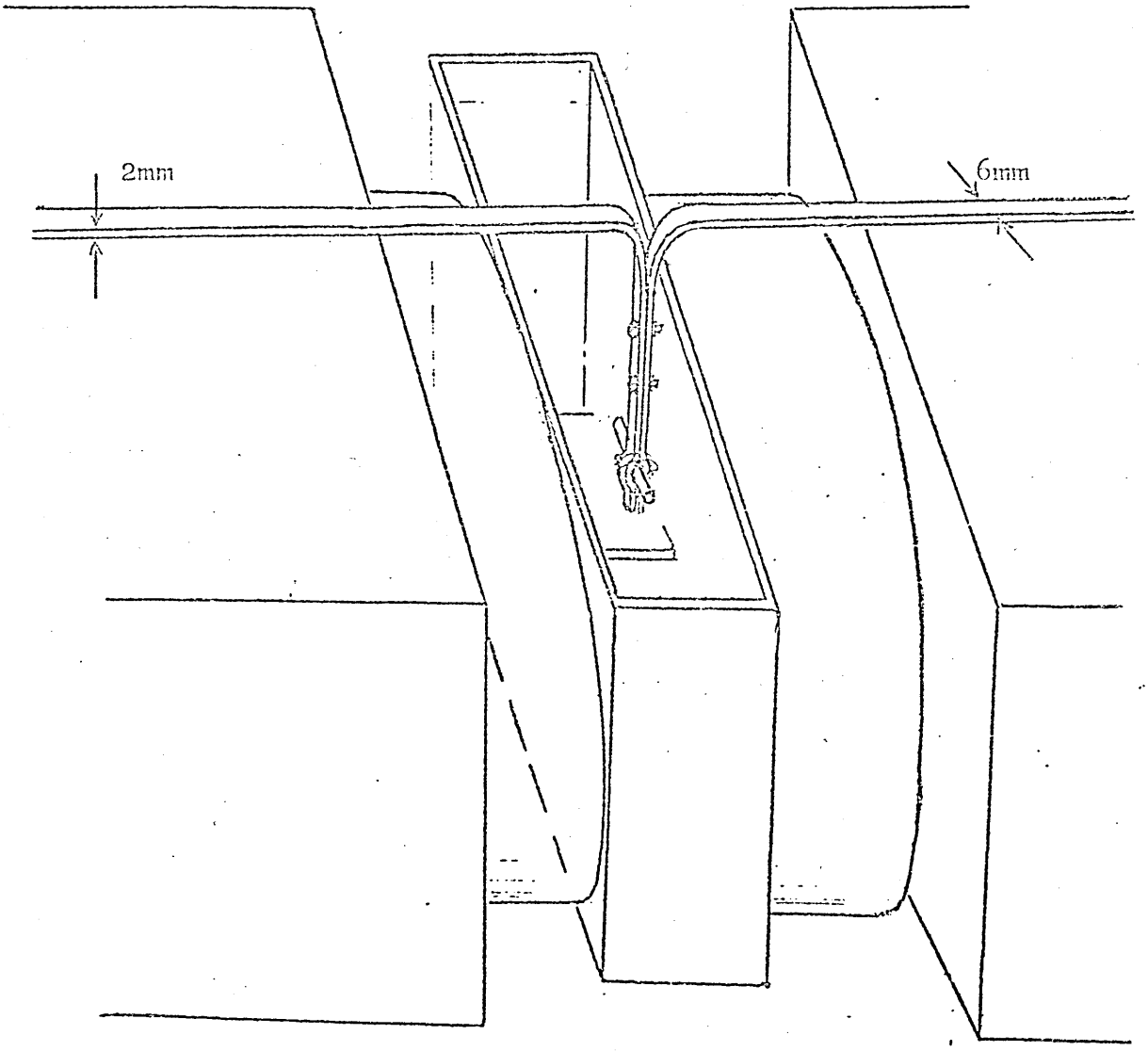

Fig. 31. Steel strip jig for holding rod specimens with their long axis at right angles to direction of applied field during salt bath heat treatment.

thermocouple in the centre of the gap between the pole pieces but slightly displaced (about 1 cm) horizontally from the central axis, just above the shelf (see Fig 30), so that with a sample in position at the central axis during ageing the thermocouple was as close as practicable to it. The silica sheath actually housed two thermocouples one of which was connected to a chart recorder and the other to an Ether "mini" proportional controller. This instrument has an adjustable timer for the selection of timed supplies of power within a small temperature band with direct on/off control outside the band. This instrument proved to be ideal for control of the furnace once the bath and associated equipment had attained a steady state heat loss at a particular ageing temperature. This was achieved after 1-2 hours of holding at the control temperature after starting up from cold with the heat resistant (zircon) brick surround in position as shown in Fig 30 (b). By adjustment of the time band on the instrument, temperature was well within a $\pm$ 2°C range of the set temperature. Cooling after ageing was done by quenching into iced brine in the case of alloy C1 and into iced brine or oil for alloy A1 and the Alnico alloys. Only those A1 and Alnico samples from which thin foils were subsequently to be prepared for TEM were oil quenched since water or brine quenched samples usually broke up in preparation. It was found in comparisons of the few brine and water quenched foils which did survive, that the same microstructure was produced irrespective of which of these quenching methods were used.

It was also definitely found necessary to quench all samples which were subsequently to be magnetically tested. The magnetic results if tested at this point, particularly the coercivity, markedly increased if the samples were allowed to cool in air after ageing. This was ascribed to a tempering effect taking place during cooling.

2.3.5. Tempering

Any other tempering was carried out using an electric nichrome wire resistance would furnace. Thermocouples (base metal) inside the furnace were connected externally to an electromechanical on/off controller and a chart recorder respectively. Temperature was found to be accurate to $\pm 3^{o}C$.

Cooling after tempering was in air unless otherwise specified in later sections.

2.4. Apparatus and techniques

2.4.1. Torque Magnetometry

A sensitive torque magnetometer was built which used specimens in the form of circular discs about 4 mm in diameter and 0.4 to 0.7 mm thick. The thicker discs were prepared where only very small anisotropy torques were expected. The discs were slit from centreless ground bars using a "Polaron" slitter which is essentially a lathe with a rotating ceramic slitting wheel. The disc faces were ground parallel using 600 and 800 grade emery papers and a jig to hold the disc as shown in Fig 32. The mass of the discs was measured using a chemical balance accurate to $\pm 5\mu g$ for sample weights in the range 0.02 to 0.07 g. The diameter and thickness of the discs were also measured to three significant digits using a micrometer.

A diagram of the magnetometer is given in Fig 33. The specimen is suspended from a torsion wire between the poles of an electromagnet. The electromagnet is of the type used by Sucksmith (155) as shown in Fig 28. The gap between the poles was fixed at 22 mm and a calibration was made of D.C. current in the windings of the coils against field strength in the gap. The calibration curve is given in Fig 34. Field strength was measured using a hall probe connected to a hysteresigraph to be described in section 2.4.2.

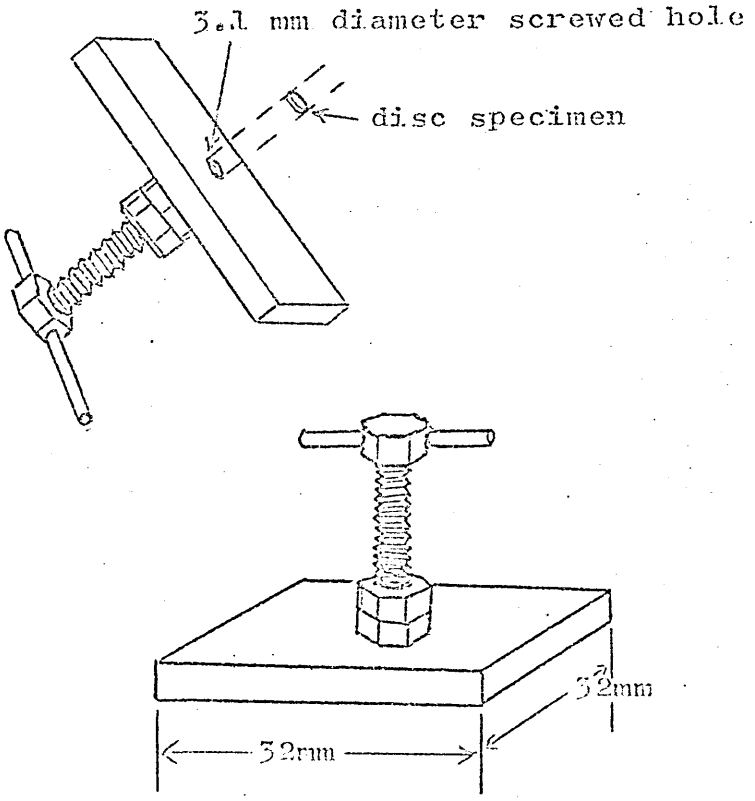

Fig. 32. jig used for grinding thin disc specimens on 600-800 grit paper.

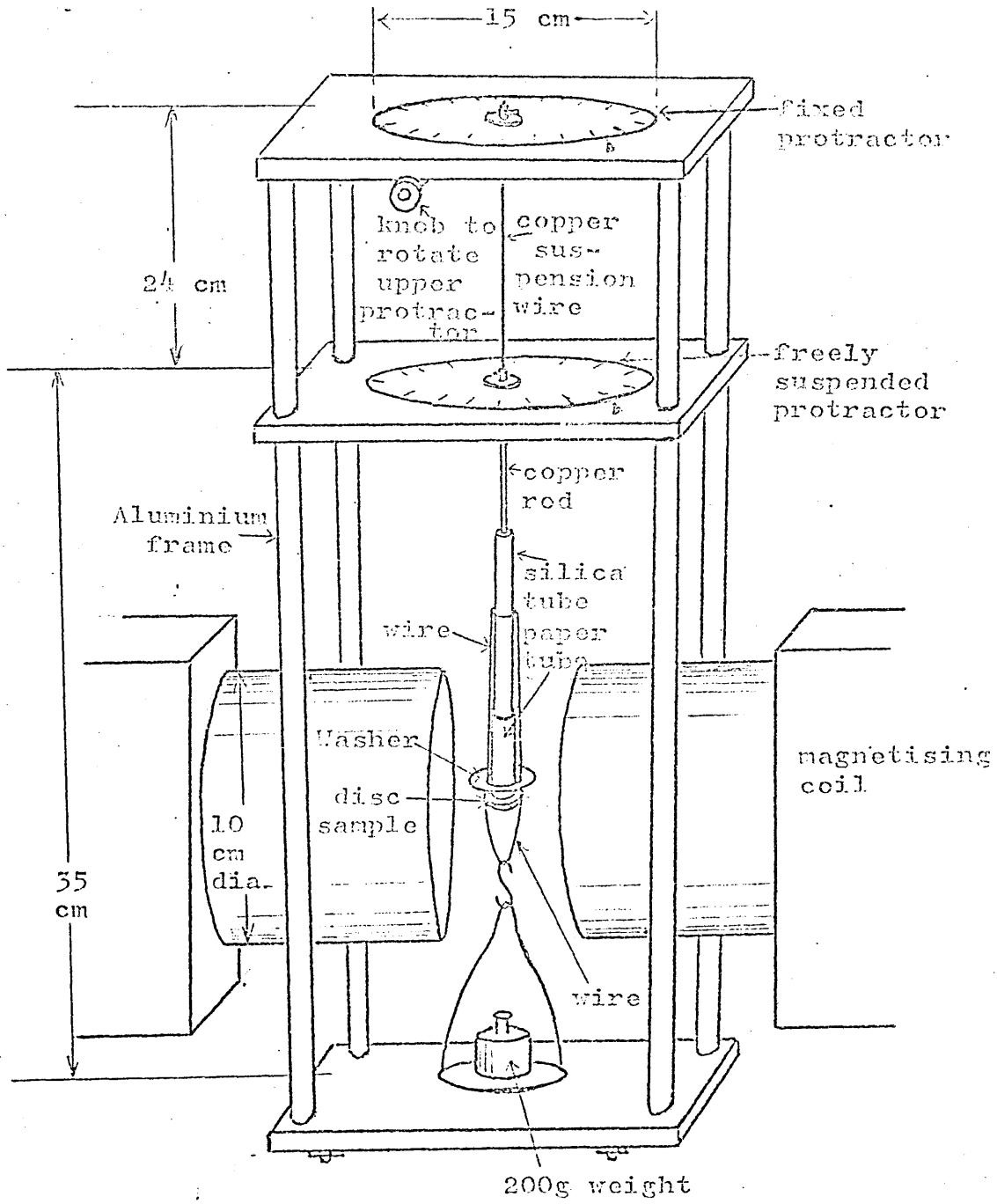

Fig. 33. sketch of torque magnetometer with disc sample in position ready for torque curve determination.

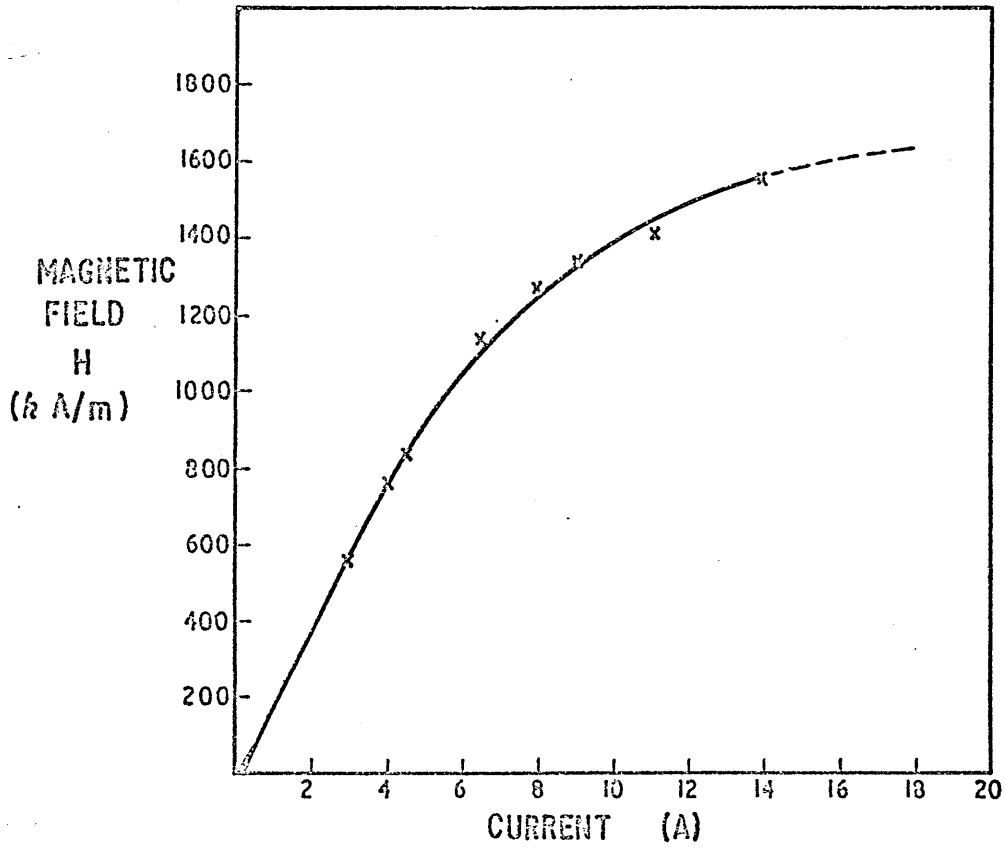

FIG. 34 CURRENT v. GAP FIELD STRENGTH FOR SUCKSMITH TYPE ELECTRO MAGNET USED FOR TORQUE MAGNETOMETRY VALUES ARE FOR A 22 mm POLE GAP USING CONICAL POLE PIECES.

The frame holding the magnetometer is aluminium. The top of the torsion wire which was 0.3 mm copper wire, 140 mm long, was soldered to a short 1 mm dia. rod which was secured to the centre of a disc shaped 14 cm diameter perspex protractor, with a small chuck which is part of a brass fixture in the centre of the protractor as shown in the section given in Fig 35. The protractor itself is located in the top plate of the aluminium frame and centrally supported by a nylon bearing in which the circular bottom part of the brass fixture sits, allowing the protractor to rotate about its centre. The edge of the circular protractor is marked off in one degree intervals through the full 360^{o} circumference, and could be aligned with a reference mark on the top plate near to the protractor edge. On the short 1 mm diameter rod just underneath the top plate is a cog which, by means of another screw cog and short brass rod, is connected to a knob at the front of the top plate. This knob then enabled the protractor to be turned to any required position.

There is sufficient frictional resistance in the gearing to effectively hold the angular position of this top protractor once set.

The bottom end of the torsion wire which is approximately 13 cm long is also soldered to a 1 mm diameter copper rod which is centrally located by means of a grub screw into the central brass fixture holding an identical protractor. However this protractor does not make any contact with the lower plate on the aluminium frame but is entirely supported by the torsion wire. The vertical position of the protractor is adjusted so that it is only just above the lower plate which also has a reference mark coinciding with the edge of the protractor to enable angular readings to be taken.

A 1 mm diameter non-ferromagnetic steel rod was located centrally by means of a grub screw in the base of the brass fixture in the centre of the lower protractor. The bottom part of this rod

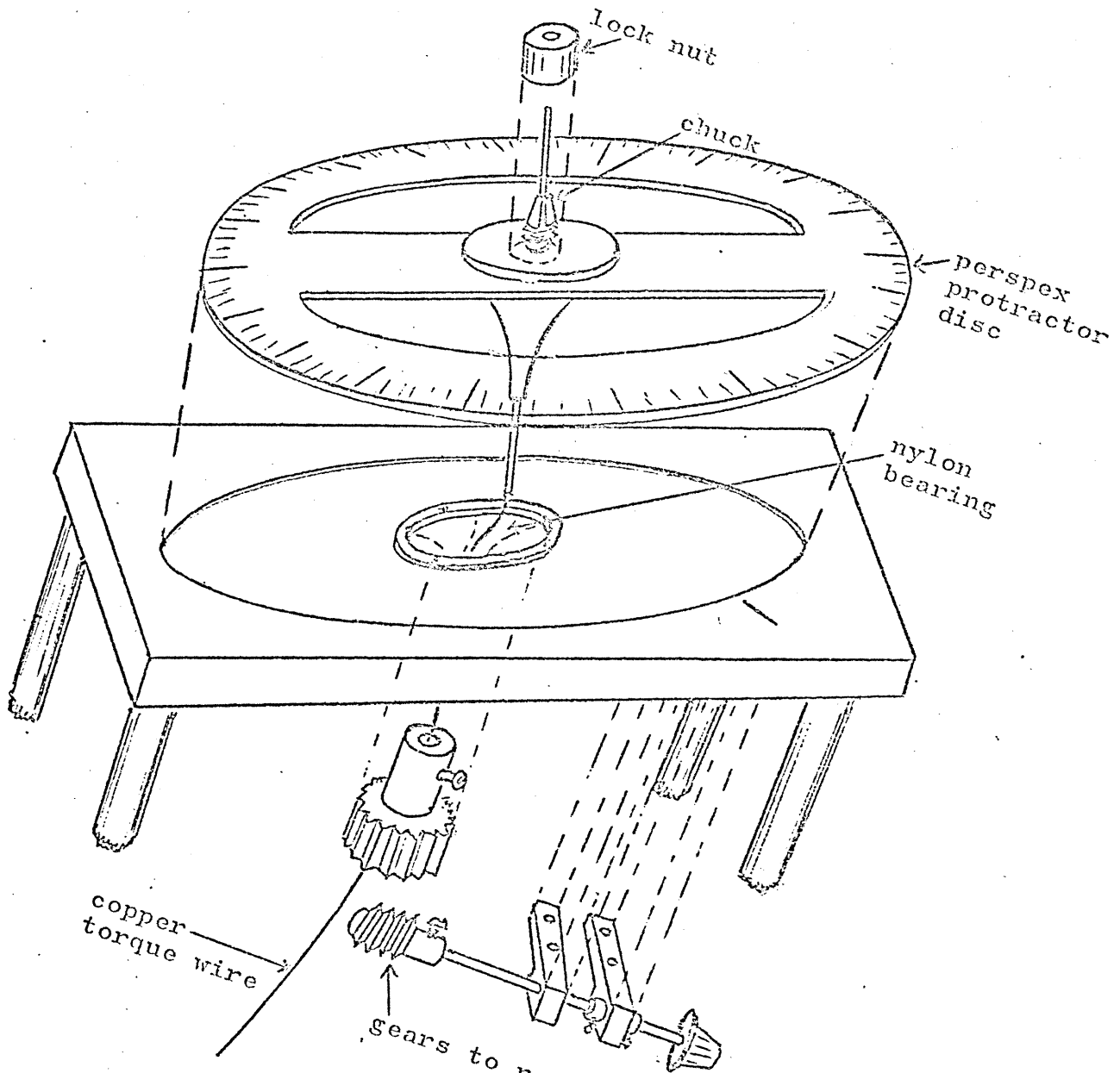

Fig. 35. Constructional details of top protractor assembly of torque magnetometer.

hanging through a hole in the plate is inserted into a silica tube which is fixed into position using high temperature vacuum wax. The disc specimen is attached to the bottom of the silica tube by first fixing the sample to the bottom of a paper tube using the high temperature wax and then sliding the paper tube over the silica tube until the disc sample rests on the smooth base of the silica tube. In this way the disc was fixed horizontally but could easily be removed by melting the wax.

To provide a stabilising effect it was found necessary to suspend a brass pan holding a 200 g weight below the specimen. The pan was attached by thin copper wires to the silica tube above the paper tube, again by high temperature wax. The wires provided additional support for the paper tube and specimen, ensuring that they did not rotate during testing.

The aluminium frame was supported on three adjustable screws under the base plate so that the vertical position of the sample and the level of the frame could be adjusted. A spirit level was used to ensure the frame was perfectly level. Prior to testing, checks and adjustments were made so that the sample disc was at the central axis of the poles and equidistant from them. In practice once the instrument was correctly set up, there was little necessity for any such adjustments after changing the sample. Fig 36 shows the torque curve for a polycrystalline disc of 2.5% silicon iron. In fact the disc was composed of only a few grains so that the characteristic biaxial torque curve for silicon iron was obtained. Calibration of the magnetometer was made by removing all but the torsion wire which was left fixed into the top protractor. A 2.8554 cm diameter thick metal disc of 58.984 g was fixed onto the 1 mm diameter copper rod at the bottom of the torsion wire into a hole drilled

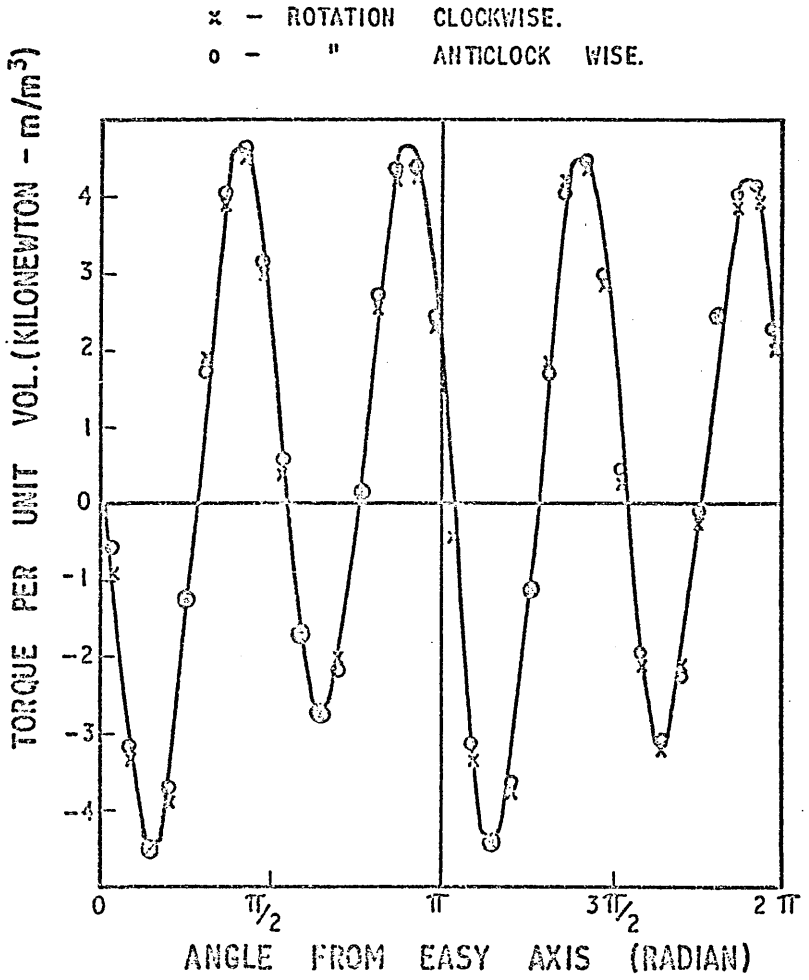

FIG. 36. TORQUE CURVE FOR A POLYCRYSTALLINE DISC OF 2·5 % SILICON IRON (LARGE GRAIN SIZE).

into the central axis of the disc. The rod was a tight fit and no additional means of securing was found to be necessary. The magnetometer set up for calibration is shown diagramatically in Fig 37.

The disc was made to oscillate in torsion about its central axis by a sudden rotation of the top protractor. A time was measured for up to 60 such oscillations which was repeated several times. The time T per oscillation was 1.095 C $\pm$ .002 sec.

A torsional constant was calculated using the mass M and radius R of the disc from the formula (13)

$$C = \frac{2\pi^2 MR^2}{T^2} \quad \ldots\ldots\ldots (3.1)$$

which was subsequently used to determine the anisotropy energy of the disc samples. This constant was determined as $1.9876 \times 10^{-4} \pm 7 \times 10^{-7}$ newton metre per radian.

The torque per unit volume on the crystal of a test sample is given by

$$L = \frac{C\phi}{V} \quad \ldots\ldots\ldots\ldots (3.2)$$

where ϕ is the angle in radians from the preferred axis and V the volume of the test sample.

For uniaxial anisotropy

$$L = \frac{dE}{d\phi} = -K \sin 2\theta \quad \ldots\ldots (3.3)$$

so that the maximum minus the minimum torque is twice the anisotropy constant.

Rotations of the sample through the preferred axis involves large changes in torque so that relatively large rotations of the top of the torsion wire produce small rotations of the protractor fixed to the bottom of the wire. With the field at right angles to the preferred axis, however, the bottom protractor rotates through large angles for only small changes in angle of the top protractor

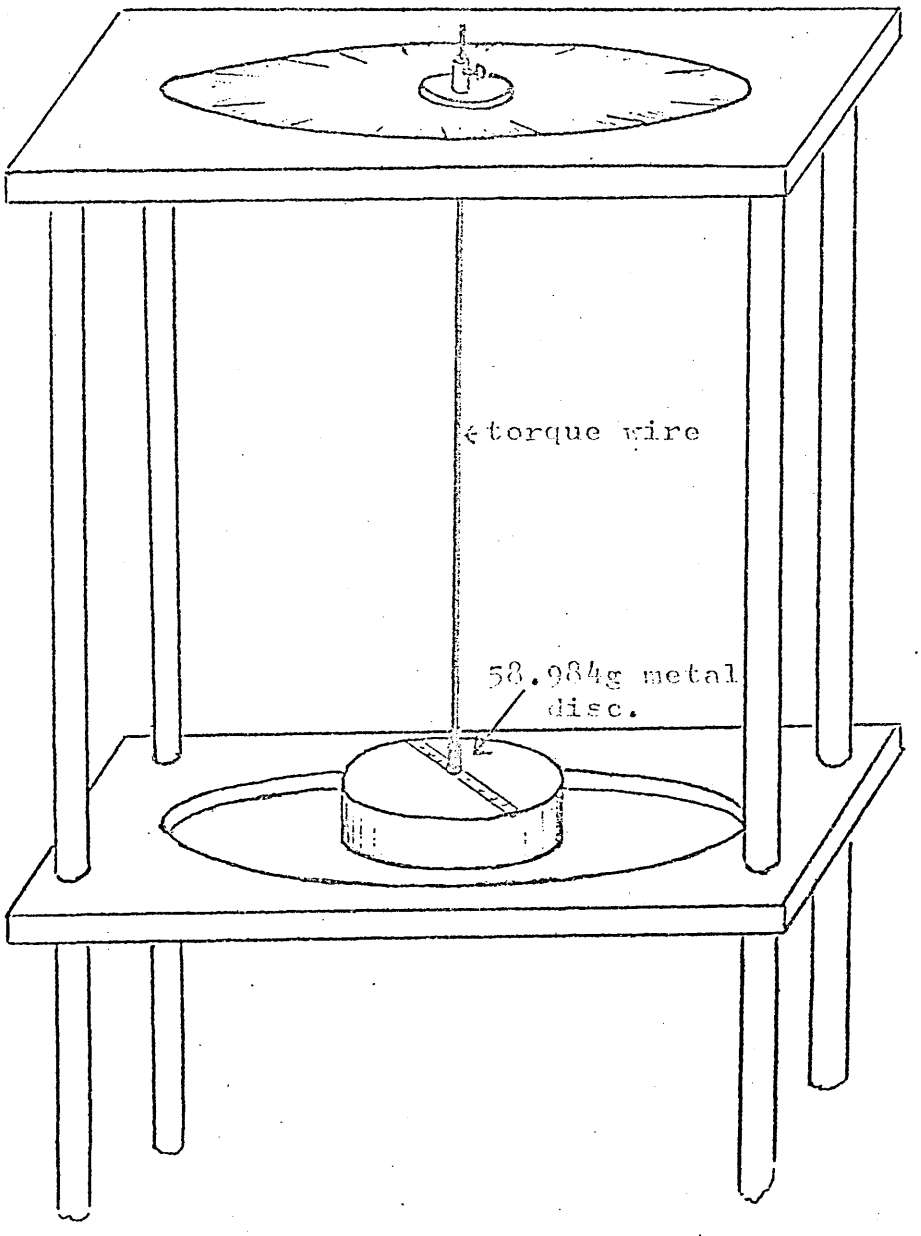

Fig. 37. The top half of the torque magnetometer set up for determination of the characteristic frequency of oscillation in torsion of the torque wire.

and it was found that, depending on the amount of anisotropy and the volume of the disc, if these were relatively large then the rotation through the "hard" direction was too rapid and difficult to measure. In these instances rather than disturbing the suspension system, the volume of the disc was reduced by linishing with 600 and 800 emery papers using the disc grinding jig as in Fig 35.

The procedure used, before taking readings, was first to switch on the field and after ensuring that this was at the correct value and the disc specimen located correctly, to rotate the disc carefully and slowly through at least 360^{o} to ensure that the specimen stayed in the same position and that the effects of any pre-magnetised state were eliminated before taking reading to be used for plotting the torque curve.

The level of field for most of the remainder of the torque plots was established in the first place by determining torque curves for various levels of field of a sample of alloy C1, which had been previously heat treated in a magnetic field applied diametrically and tempered to give optimum technological magnetic characteristics. At each level of field a torque curve was determined for both a clockwise rotation of the sample and an anticlockwise one. It was found that for fields of 438 kA/m and above (up to 764 kA/m) both clockwise and anticlockwise curves at each level of field were identical and the anisotropy energy constant measured for the curves were the same within $\pm$ .33% for fields of 637 kA/m and above. The standard level of field strength was therefore taken as 637 kA/m and unless otherwise specified, all curves were determined at this level. For fields of 239 kA/m and less the clockwise and anticlockwise torque curves were distorted and displaced both in angular position and values of torque i.e. there was rotational hysteresis loss. An example of this is given in Fig 38.

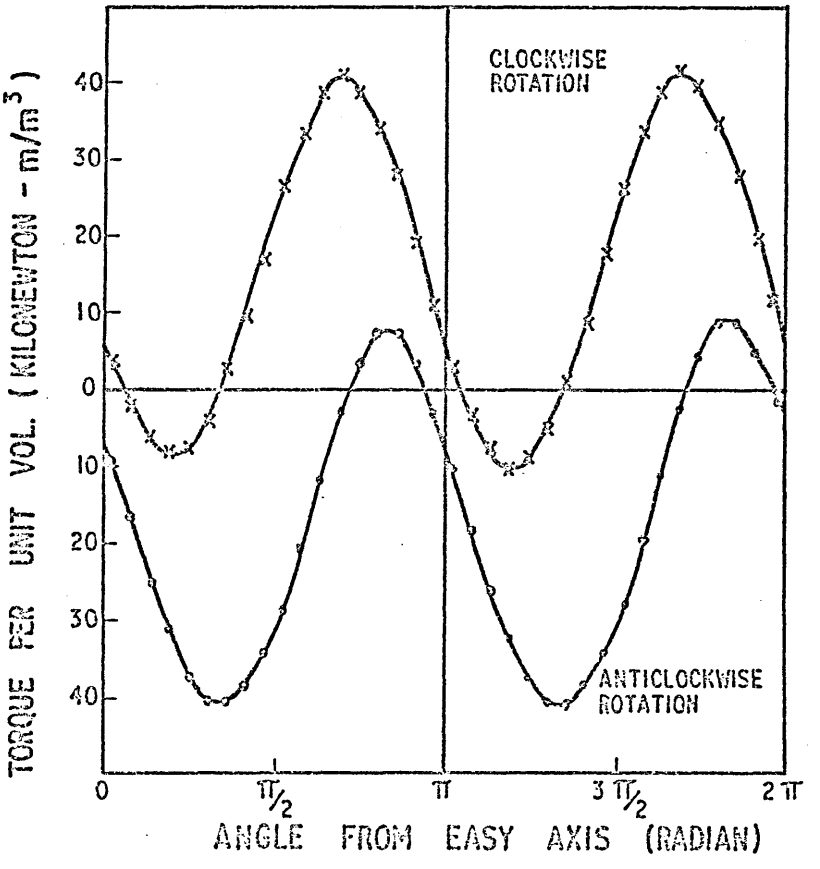

FIG. 38 TORQUE CURVES FOR DISC OF ALLOY C1 OPTIMALLY HEAT TREATED AND TEMPERED. TESTED IN AN EXTERNAL FIELD OF 119 kA/m, SHOWING ROTATIONAL HYSTERESIS.

For all torque curves, points were determined at 10° intervals through a full 360° with at least one repeat point to establish the repeatability of the curve. Without exception the repeat point always agreed to $\pm$ 1° with the original angular value.

Torque curves for any of the sample discs were determined twice, once clockwise and the other anticlockwise, A few were also repeated again. The accuracy of the maximum torque angle was estimated in all cases to be within $\pm$ 1°. The anisotropy constant were calculated from the maximum torque angle, the mass of the disc, the known density of the alloy and the torsional constant of the wire.

2.4.2. Magnetic Properties using a recording Hysteresigraph

A recording hysteresigraph as described by Scoles (157) was used to determine remanence Br or Jr, coercivity H_{CB}, and intrinsic coercivity H_{CJ}, and maximum energy product, (BH) max. The instrument provides magnetising fields of the order of 1600 kA/m using an electromagnet similar to that in Fig 28. Applied field (H) is measured by a hall probe, and flux density (B) or magnetisation (J) by an air flux compensated search coil. The search coil was standardised using an inductor in the same circuit. This was calibrated using the fields of permanent magnet yokes initially checked by comparison with the standard inductor and extraction of a coil of known area and turns from the permanent field. The pole faces, in contact with the sample during testing, were regularly cleaned with emery paper and parallel with the surfaces of the test specimen so that the best possible contact could be made.

The magnetic properties are recorded as a demagnetisation curve, magnetisation curve, or full hysteresis loop on an X-Y recorder. The demagnetising field was generally applied gradually by a capacitor

discharge circuit. Magnetic characteristics were reproducible to better than ± 3% except for J_r when H_c is less than 30 kA/m.

In these latter cases i.e. where J is a rapidly changing function of H near H = 0, then the reluctance of the magnetic circuit formed by the test piece and the yoke of the electromagnet have a small but significant effect. The hysteresis loop for the test sample is in effect sheared slightly by the small demagnetising fields introduced by small gaps which exist at various junctions between the pieces of iron, steel and test alloy making up the circuit and also the magnetic permeability of the materials making up the yoke itself. Under these conditions the applied field

$$H' = H + \frac{N_x J}{\mu_o} \quad \ldots\ldots\ldots (2.4)$$

where H is the effective field acting on the specimen and J is the intensity of magnetisation in it. N_x is the demagnetising factor for the magnetic circuit. When the permeability (B/H) of the specimen is high, which it certainly is for ferromagnetic materials near H = 0, and N_x is not too small, then for sufficiently small H', H will be small compared with $N_x J$ and $H' = N_x J$ approximately, giving a linear relation between H' and J representing the angle of shear. This angle was measured by plotting the magnetisation with increasing H' for several samples of mild steel silicon iron and also quenched samples of alloy A1 which had a coercivity which was so small (< 80 A/m) as to not be measurable at the normal working sensitivity of the instrument. By taking the tangent to these magnetisation curves gives the relationship $H' = N_x J$, and the slope is N_x/μ_o. For all these materials N_x/μ_o was found to be 0.50 ± 0.10 or a shear of H = 2.0 ± 0.4 kA/m at 1 tesla. J_r for all tests with H_c less than 30 was determined by projecting a straight line from (J,H) = (0.0), point A through the point for H = 2 kA/m, J = 1 tesla, point B in

the first quadrant of the demagnetisation curve as shown in Fig 39. For tests with $H_c > 30$ kA/m, projections of this kind gave increases of remanance of less than 0.4% compared with the value given by the intersection with the vertical axis. That is for all the tests performed in the investigation the demagnetisation curves were sufficiently "square", as long as $H_c > 30$ kA/m, for this correction to be ignored since it was in most cases indistinguishable from the uncorrected value and in all cases less than the overall experimental reproducibility.

From the variation in reproducibility of N_{x/μ_o} the order of accuracy for remanance values for samples over a range of H_c values could be determined from the actual test curve. The range of accuracy to be expected from the J_r values as a function of H_c is plotted in Fig 39.

During the course of this work the hysteresigraph was used as part of an international investigation of testing methods for permanent magnets. Samples of a wide range of permanent magnet materials including Alnico types were tested and the results compared with 27 other test units in laboratories throughout Europe. The results of this survey were presented at the third European Conference on hard magnetic materials in Amsterdam in 1974 (158). Of the twelve Alnico type magnets tested in this survey remanences were within the range - 0.87% to $^{+}$ 1.22% of the means of the 27 other test units. Coercivity values were + 0.75% to + 3.28% of the overall means, and (BH) max values at -1.5% to + 7.06% of the mean. The remanance values were all within $\pm$ 1 standard deviation, coercivities within 0 + 3 standard deviation and (BH) max values within -1 to + 2 standard deviations of the mean of the results of these 27 test units (158).

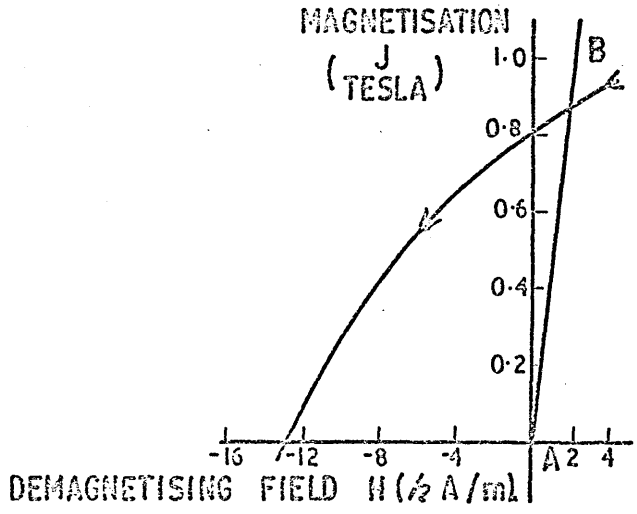

FIG. 39 (a) DEMAGNETISATION CURVE OF ALLOY A1 SAMPLE AGED 15 MIN. AT 800°C (WITHOUT A FIELD) AND TEMPERED FOR 6 HOURS AT 600°C. LINE A B REPRESENTS THE SHEAR PRODUCED BY THE RELUCTANCE OF THE MAGNETIC TEST CIRCUIT.

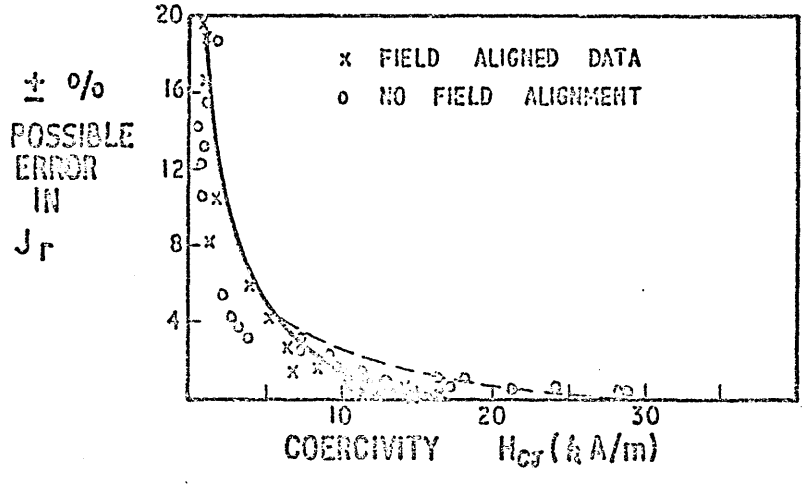

FIG. 39 (b) ACCURACY OF REMANENCE MEASUREMENTS AS A FUNCTION OF MEASURED COERCIVITY USING HYSTERESIGRAPH.

Comparative values of saturation magnetisation could also be obtained using the hysteresigraph by plotting the magnetisation curves for increasing applied field. The magnetisation curve usually became almost horizontal and linear before 800 kA/m. The tangent of this was projected back to H = 0 which was taken as the spontaneous saturation magnetisation J_s. Although used for some relatively large samples, this was not the basic method used for determination of J_s which is to be described in the next section.

2.4.3. Saturation Magnetisation measurements

The saturation magnetisation was also measured as a specific saturation at room temperature, in a magnetic field of about 1150 kA/m, provided by a large permanent magnet. The intensity of magnetisation was determined from the deflection on a "Norma" fluxmeter as the sample was pulled out of the magnetising field through a special search coil as described by Klitzing (159) and critically assessed by McCaig (156). The equipment was calibrated by appropriately sized pieces of pure nickel ("Inco" nickel), and the test samples were the small discs used for torque magnetometry and other slightly larger test samples. Appropriately sized samples of nickel were used for calibration so that the same scale setting was used for test samples. The measurements were reproduceable to better than 2%.

2.4.4. Electron Microscopy (TEM)

Thin foils were prepared from 3.05 diameter discs from the same bars from which the torque magnetometry discs were prepared. The TEM discs were thinned mechanically, using the same techniques and a similar holding jig (Fig 32) as for the torque discs, to 200 - 400 μm followed by "dishing" for from 15 to 120 seconds on

each face in a solution of 10% perchloric acid in methanol electrolytically at 17 volts. Further metal dissolution was made more slowly by electrolytic polishing in the same solution at 4.8 - 4.3 volts for 60 seconds on one face. This was then repeated on the other face after reversing the disc, and then reversed and repeated again. This procedure was continued until perforation occurred. This event was observed using a microscope focussed on the face of the disc through the glass wall of the vessel holding the acid solution, and the power to the electrodes in the solution was switched off as soon as the foil was perforated.

The dishing operation time of 15 seconds applies to discs 200 μm thick and up to 120 seconds for 400 μm discs. Sometimes the larger thickness discs were necessary with the Al and Alnico alloys because of their characteristic brittleness, and the above procedure was developed to minimise the number of foils which fractured before or at the point of perforation at the centre of the disc. Even so it was found necessary to quench some of the Al samples into oil from the ageing temperature and even then approximately two thirds of thin foils attempted in the alloys broke during preparation and, together with others which did not have a sufficiently thin area of foil surface, were unsuitable for subsequent TEM. Much less trouble was experienced with the Cl and other Fe-Cr-Co alloys which did not fracture, which is consistent with the known better ductility and lower hardness of these alloys.

The precise voltage required for the final thinning operation for these alloys was arrived at by determination of the e.m.f. current characteristics of the system as given in Fig 40.

Examination of the foils was made using a JEM 6A electron microscope at 100 KV.

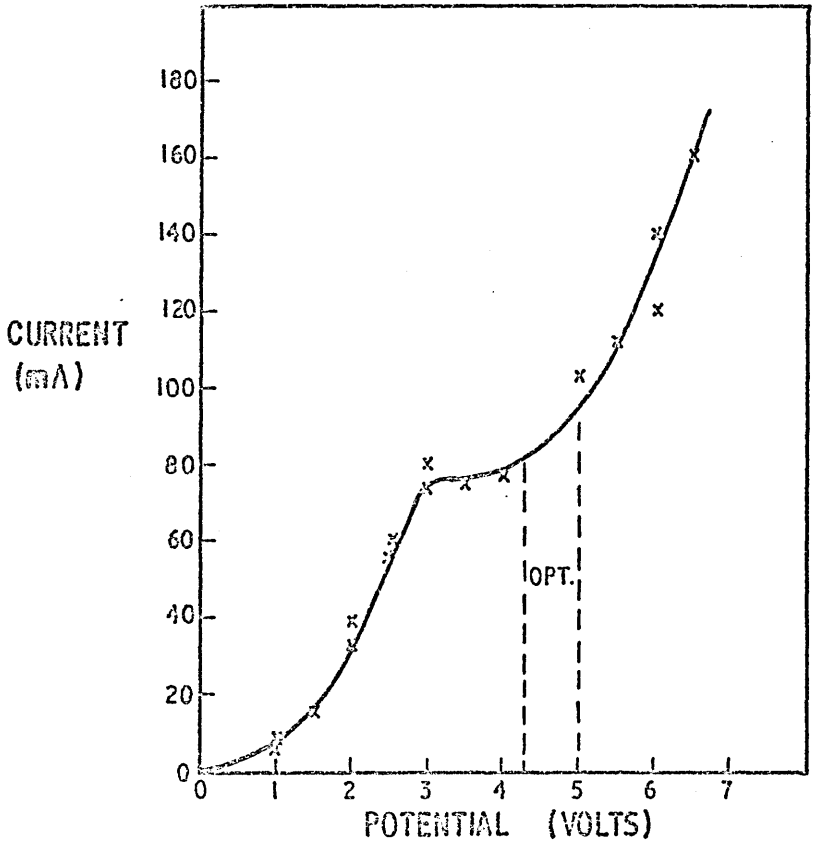

FIG. 40 ELECTROCHEMICAL POLARISATION CURVE FOR ALLOY Al DISCS IN A 10% CHROMATE SOLUTION IN METHANOL, USED TO DETERMINE THE CORRECT CONDITIONS FOR POLISHING FOR SUBSEQUENT TRANSMISSION ELECTRON MICROSCOPY.

2.4.6. Hardness and microhardness tests

Hardness tests were made using a "Firth Hardometer" with a 120 Kg load and a 2 mm ball indentor.

Microhardness tests were made using a Vickers M12a microhardness tester which incorporated a M12 bench microscope with a pneumatically operated indentor unit with a diamond indentor. The load used for Microhardness testing was 100 g. Both instruments were checked with calibrated hardness blocks before and after testing.

TABLE VI

Technological Magnetic Properties for alloy A1.

(a) After cooling in a magnetic field of 300- kA/m from 1250° to 550°C, and,

(b) plus 24 hours at 590°C and then 24 hours at 560°C.

Cooling rate (°C/Min)	Remenence J_r (tesla)	Coercivity H_{cB} (kA/m)		Max. energy. $(BH)max$ (kJ/m^3)
(a)				
A-14.0	1.280	25.9		14.7
B-17.5	1.320	27.5		18.5
C-21.2	1.330	27.2		19.1
D-25.0	1.285	28.0		15.5
E-28.0	1.350	29.9		22.3
F-31.8	1.360	29.1		21.5
G-41.2	1.340	28.3		20.5
H-50.0	1.380	26.3		21.1
J-58.3	1.310	23.1		17.1
K-70.0	1.380	22.3		17.9
(b)				
		H_{cB}	H_{cJ}	
A-14.0	1.125	42.6	43.4	20.3
B-17.5	1.170	43.0	43.4	23.9
C-21.2	1.160	45.0	46.6	25.5
D-25.0	1.170	48.4	48.9	25.5
E-28.0	1.230	45.8	47.4	26.7
F-31.8	1.210	50.1	51.6	31.4
G-41.2	1.215	52.5	53.3	31.8
H-50.0	1.235	53.3	53.7	33.4
J-58.3	1.190	51.1	51.3	26.4
K-70.0	1.250	50.9	51.3	29.8

.....

CHAPTER 3.

Results

3.1. Heat treatment survey of alloys A1, C1 and C2

3.1.1. Alloy A1

The magnetic test results of the heat treatment survey of alloy A1 which was conducted using the normal production methods for Alnico 5 (Alcomax 111) is presented in table V1 for cooling rates in the range 14 to 70°C/min. in a 300 kA/m magnetic field. The magnetic properties after tempering are also given in Fig 41. It can be seen that the magnetic properties vary only slowly with cooling rate, in common with commercial Alnico 5, with a broad maximum between 30-60°C/min. The best magnetic properties for alloy A1 were for a cooling rate of 50°C/min giving remanence J_r= 1.235 tesla, coercivity, H_{CJ}= 53.7 kA/m and (BH) max = 33.6 kJ/m^3 .This compares with typical magnetic characteristics for Alcomax 111 or Alnico 5 of J_r= 1.26 tesla, H_{CJ}= 55 kA/m and (BH) max= 43 kJ/m^3 for a cooling rate of the order of 20°C/min (plus tempering). The values of J_s quoted in table V1 were, like the rest of the results on this table determined using the Hysteresigraph.

The ten alloy A1 samples were subsequently re-solution treated and then cooled at 50°C/min in the magnetic field. The saturation magnetisation determined for the samples, again using the hysteresigraph were all within ± 1.23% of 1.509 tesla. This is confirmation of the homogeneity of composition of the test samples of this alloy, and indeed subsequent groups of saturation magnetisation tests also have consistently reinforced this conclusion.

3.1.2. Alloy C1

A group of eight samples of alloy C1 were solution treated and then tested using the hysteresigraph. The saturation magnetisation of the group was 1.23 ± 0.005 (i.e. all within 1%), indicating that this alloy is also homogeneous in terms of composition. This

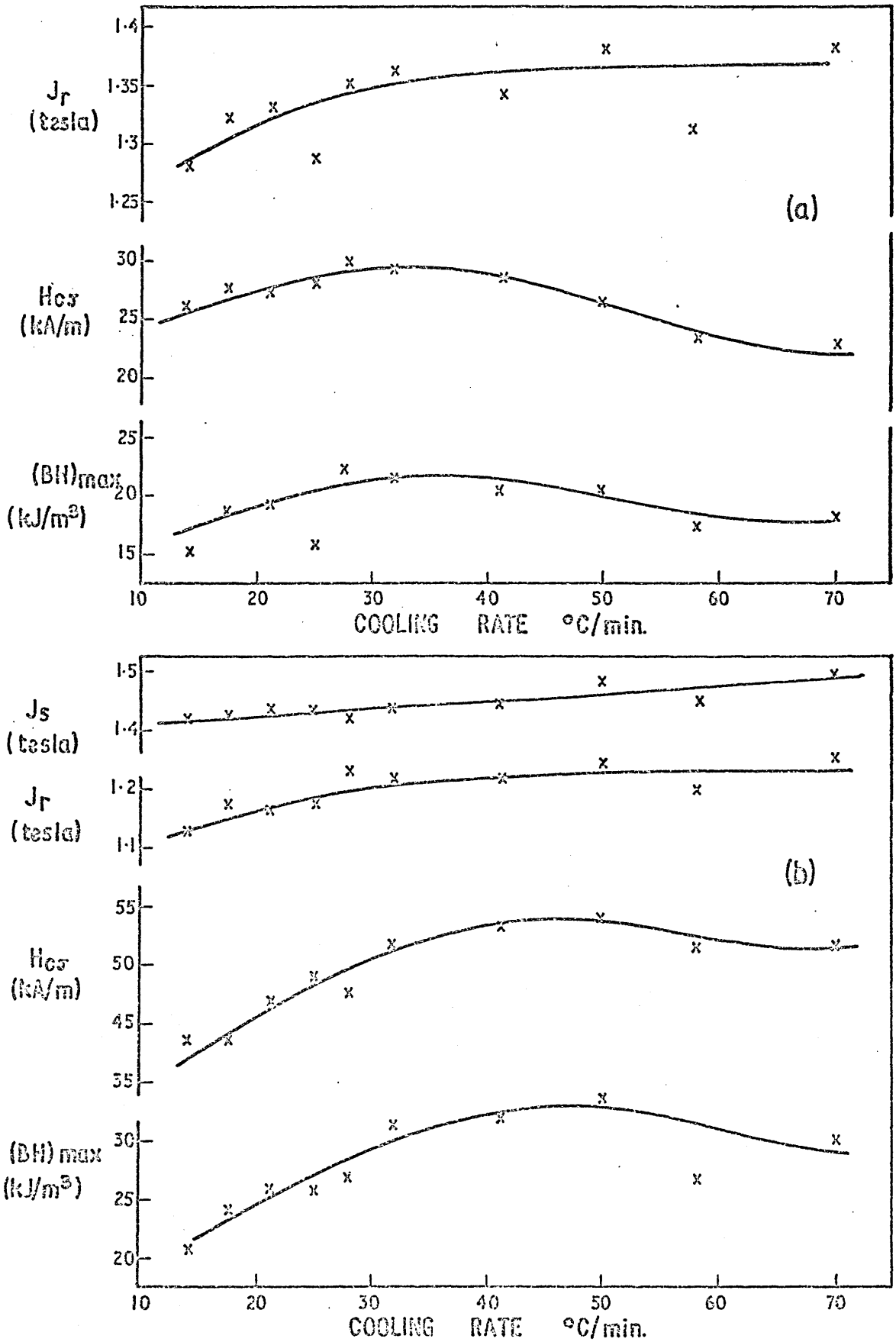

FIG. 41. ALLOY AI - MAGNETIC PROPERTIES (a) AFTER COOLING IN A MAGNETIC FIELD FROM 1250 TO 550°C, AND (b) FOLLOWED BY A TEMPER OF 24 HOURS AT 590° C PLUS 24 HOURS AT 560°C.

conclusion was supported by other groups of samples which were also subsequently tested in the solution treated condition and showed a similar stability of saturation magnetisation in this state. The coercivity in this state was always within the range 0-0.4 kA/m.

This group of eight samples were heat treated using the magnetic jig and heat treatment cycles similar to those used by Keneko et al (103). An isothermal ageing heat treatment in the temperature range 630-660°C for 15-60 min. was followed by the three stage temper as given in section 2.3.3. The magnetic characteristics of this series of samples, which were obtained using the hysteresigraph, are presented in table V11 and Fig 42.

The best results are given by the identical ageing treatment to that found for Keneko's alloys i.e. 30 min. at 650°C, and for alloy C1, are remanence J_r = 1.18 tesla, coercivity, H_{CJ}= 62.5 kA/m and (BH) max = 36.8 kJ/m^3. Both alloys A1 and C1 therefore appear to be analogous to Alnico 5 in terms of magnetic properties.

3.1.3. Alloy C2

Some magnetic results together with other information on microstructure and nitrogen content is presented in Table V111, after various heat treatments sufficient to show that the magnetic properties of Fe-Cr-Co alloys are adversly affected by high nitrogen contents.

3.2. Magnetic characteristics of isothermally aged specimens

3.2.1. Alcomax 111

Table 1X presents the magnetic properties obtained after ageing without a magnetic field for times from 0-15 min. at 800°C, followed by tempering from 0-7 hours at 600°C. The samples were initially aged and then tested. The specimens were then tempered

TABLE VII

Technological Magnetic properties for alloy C1

Aged in the jig followed by tempering for 2 hours at 600°C, plus 4 hours at 580°C plus 16 hours at 560°.

No.	Ageing temperature (°C)	Ageing Time (Min.)	Remenence J_r (tesla)	Coercivity H_{cJ} (kA/m)	Max. Energy (BH) max. (kJ/m^3)	Hardness (HB120)
2-0	630	30	0.350	0.50	0.0	444
3-0	640	30	1.260	32.6	23.1	477
7-0	650	15	1.190	54.8	29.8	444
4-0	650	30	1.180	62.5	36.8	461
6-0	650	60	1.140	53.4	34.7	460
5-0	660	30	1.130	65.3	33.4	444

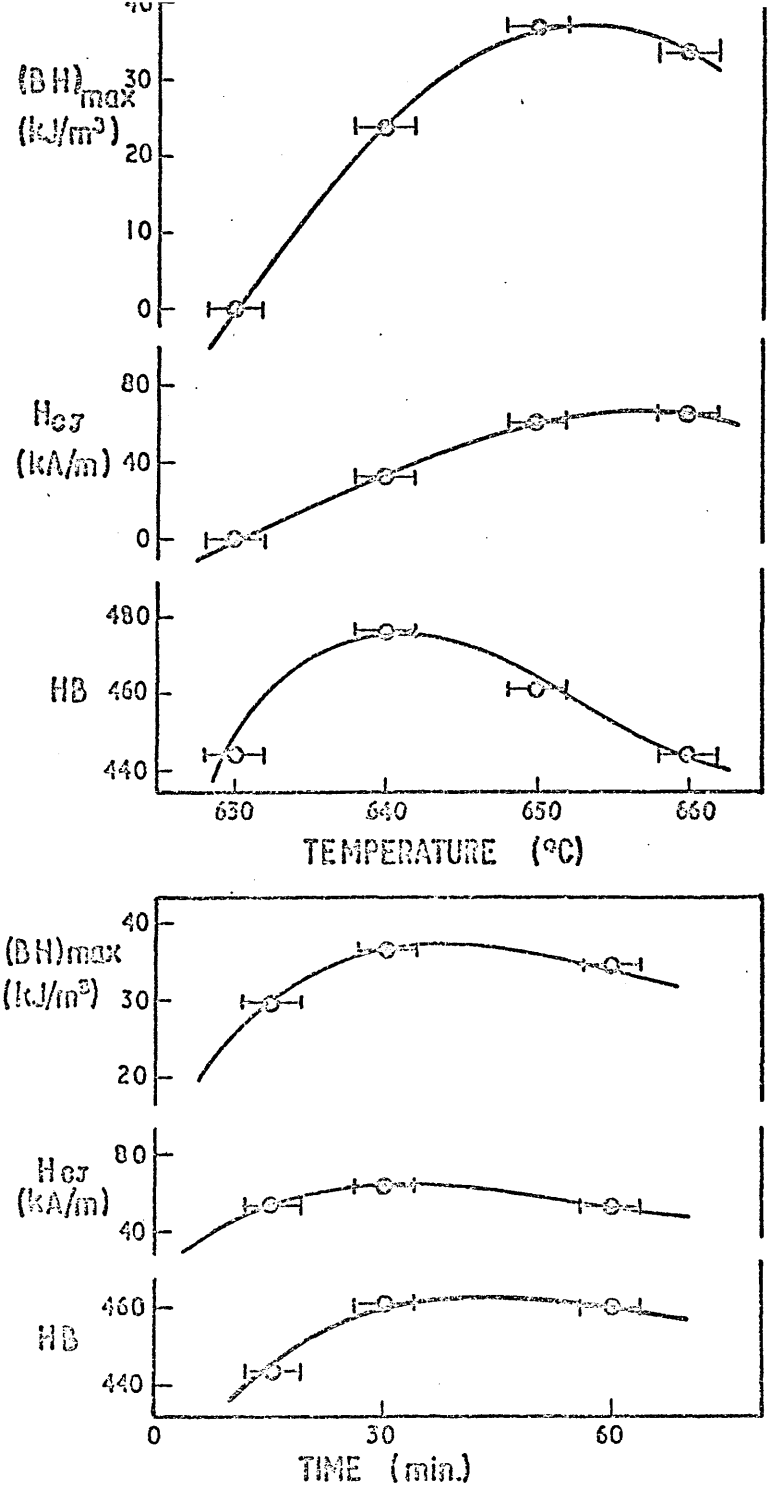

FIG. 42 ALLOY CI - MAGNETIC PROPERTIES AFTER (a) 30 MIN. AGEING IN A MAGNETIC FIELD AT SPECIFIC TEMPERATURES AND (b) AGEING IN A FIELD AT 650°C FOR VARIOUS TIMES, BOTH FOLLOWED BY TEMPERING OF 2 hrs. AT 600°C PLUS 4 hrs. AT 580°C PLUS 16 hrs. AT 560°C.

TABLE VIII

Alloy C2. Variation of magnetic properties notrogen content and microstructure with heat treatment.

Pre-heat treatment and Solution Treatment	Nitrogen content %	Micro Structure
A. as-rolled	0.075	2 phase ($\alpha+\gamma$)
B. 1 hour 1350°C in air-quenched into brine.	0.075	2 phase ($\alpha+\gamma$)
C. 3 hours 1350°C in argon-quenched into brine	0.048	single phase
D. 2 hours 1350°C in hydrogen-quenched into brine		
E. (i) in hydrogen (a) heated to 1310°C in period of 3 hours (b) held at 1310°C for 35 mins. (c) Slow cool to 400°C in period of 3 hours plus (ii) 1 hour 1350°C in argon-quenched into iced brine	0.057	Single phase

Ageing (in magnetic field of 240kA/m)	Tempering (No field)
Y. 30 min. 650°C	2 hrs. 600°C
Z. " "	2 hrs. 600°C plus 4 hrs. 580°C

Pre-heat treatment and solution treatment	Ageing and Tempering	J_s (tesla)	J_r (tesla)	H_{cB} kA/m	(BH)Max kJ/m³
B	Z		0.800	43.8	15.1
C	Z		1.150	47.0	25.5
D	Z		1.060	29.4	15.1
E	Y	1.33	1.060	54.1	26.7
E	Z	1.36	1.100	53.7	28.7

TABLE IX

Magnetic properties of Alcomax III after isothermal ageing (in the absence of a magnetic field) at 800°C and tempered at 600°C

No.	Isothermal ageing time (min.)	Time of temper (min.)	J_s (tesla)	J_r (tesla)	H_{cJ}(kA/m)	$\frac{J_r}{J_s}$
0X	0	0		0.280	0.4	
		2		0.200	0.5	
		12	~1.4	0.300	0.8	.21
		30	~1.4	0.240	0.7	.17
		60	~1.4	0.180	0.5	.13
		120	~1.4	0.090	0.5	.06
		180	1.38	0.065	0.6	.05
2X	2	0		0.270	0.6	
		2		0.300	0.8	
		12	~1.4	0.300	1.2	.21
		30	~1.4	0.310	1.6	.22
		60	~1.4	0.290	1.9	.21
		120	1.36	0.320	2.6	.24
		180	1.35	0.255	2.6	.19
		300	~1.3	0.255	4.0	.20
		420	~1.3	0.330	3.8	.25
5X	5	0		0.280	0.7	
		2		0.410	0.9	
		12	1.4	0.350	1.2	.25
		30	1.4	0.370	1.4	.26
		60	1.4	0.380	1.9	.27
		120	1.36	0.335	2.3	.25
		180	1.35	0.310	2.6	.23
		300	1.3		5.2	
		420	1.3		6.1	
10X	10	0		0.405	1.0	
		2		0.465	1.3	
		12	1.4	0.520	2.3	.37
		30	1.4	0.545	2.7	.39
		60	1.4	0.540	3.3	.39
		120	1.36	0.555	4.2	.41
		180	1.35	0.525	4.6	.39

TABLE IX (Cont.)

No.	Isothermal ageing time (min.)	Time of temper (min.)	J_s (tesla)	J_r	H_{cJ} (kA/m)	$\frac{J_r}{J_s}$
10X	10	300	1.3	0.500	6.3	.39
		420	1.3	0.455	7.5	.35
15X	15	0		0.550	1.4	
		2		0.600	1.8	
		12	1.4	0.580	2.5	.41
		30	1.4	0.635	3.7	.45
		60	1.4	0.630	4.5	.45
		120	1.35	0.720	6.0	.53
		180	1.32	0.715	7.2	.54
		300	1.3	0.740	9.2	.57
		420	1.3	0.755	10.7	.58

for times from 0-407 hours at 600°C. following the same procedure as in section 4.2.1. Table X presents the results for ageing without applied magnetic field and Table Xl gives the magnetic characteristics for the specimens which were aged in the field. Table Xll gives some supplemental results for other samples of Al which in addition to an isothermal ageing treatment of 10 min. at 800°C were allowed to cool at various rates in the salt bath with the magnetic field switched on (one sample however, specimen A, was cooled after removal from the bath in a 320 kA/m field at approximately 80°C/min.) and subsequently tempered at 600°C.

3.2.2. Alloy Cl

Isothermal ageing of specimens in the range 630-682°C was conducted for times of 9 up to 120 minutes. The magnetic results after testing these samples on the hysteresigraph are presented in Table Xlll.

Several of these samples were ground into a cuboid shape from their original cylindrical shape, in order to obtain hysteresis curves in a direction perpendicular to that of the applied field direction during ageing. Comparison of these hysteresis curves for the preferred and perpendicular directions enabled an anisotropy energy to be calculated. This was taken as the mean area between the two hysteresis loops, calculated using a machine method based on Simpson's Rule. The total hysteresis energy was similarly calculated from the area inside the hysteresis loop of the preferred direction. The results are given in Table XlV and examples of such hysteresis loops are given in Fig 43 . for both the Cl alloy and alloy Al.

TABLE X

Alloy A1 - Magnetic properties after isothermal ageing (in the absence of a magnetic field) at 800°C followed by tempering at 600°C

No.	Isothermal ageing time (min.)	Duration of temper at 600°C (hrs.)	J_s (tesla)	J_r (tesla)	H_{cJ} (kA/m)	$\frac{J_r}{J_s}$
ON	0	0	1.56		0.1	
		2	1.52	0.210	0.7	0.14
		4	1.50	0.160	0.5	0.11
		6	1.51	0.200	0.6	0.13
		9	1.50	0.190	0.6	0.13
		12	1.52	0.170	0.7	0.11
		15	1.52	0.170	0.6	0.11
		21	1.52	0.200	0.9	0.13
		37	1.51	0.210	1.2	0.14
		77	1.50	0.230	1.7	0.15
		149	1.51	0.335	2.8	0.22
		263		0.285	3.2	
		407		0.340	4.4	
2N	2	0	1.57	0.240	0.5	0.15
		2	1.53	0.360	2.4	0.24
		4	1.53	0.360	2.8	0.24
		6	1.52	0.400	3.3	0.26
		9	1.53	0.385	3.7	0.25
		12	1.52	0.390	4.1	0.26
		15	1.52	0.365	4.6	0.24
		21	1.50	0.400	5.2	0.27
		37	1.47	0.400	5.9	0.27
		77	1.47	0.425	6.8	0.29
		149	1.42	0.445	7.6	0.31
		263	1.43	0.445	7.8	0.31
		407	1.42	0.460	8.4	0.32
5N	5	0	1.57	0.230	1.0	0.15
		2	1.52	0.580	7.5	0.38
		4	1.52	0.640	9.4	0.42
		6	1.52	0.665	10.5	0.44
		9	1.53	0.690	11.1	0.45
		12	1.52	0.720	12.5	0.47
		15	1.52	0.695	11.9	0.46
		21	1.50	0.780	13.5	0.52
		37	1.48	0.800	15.0	0.54
		77	1.48	0.810	16.5	0.55
		149	1.42	0.795	19.1	0.56
		263	1.42	0.795	19.4	0.56
		407	1.42	0.775	19.1	0.55

Cont.....

TABLE X (Cont.)

No.	Isothermal ageing time (min.)	Duration of temper at 600°C (hrs.)	J_s (tesla)	J_r (tesla)	H_{cJ}(kA/m)	$\frac{J_r}{J_s}$
10N	10	0	1.57	0.500	1.8	0.32
		2	1.52	0.700	7.1	0.46
		4	1.51	0.845	10.0	0.56
		6	1.50	0.880	12.9	0.59
		9	1.50	0.880	16.2	0.59
		12	1.51	0.880	17.2	0.58
		15	1.49	0.865	17.2	0.58
		21	1.48	0.880	18.7	0.59
		37	1.46	0.860	21.3	0.59
		77	1.47	0.850	24.4	0.58
		149	1.41	0.845	28.3	0.60
		263	1.42	0.825	29.0	0.58
		407	1.41	0.820	29.0	0.58

TABLE XI

Alloy AI - Magnetic properties after isothermal ageing in a 240 kA/m magnetic field at 800°C - followed by tempering at 600°C

No.	Isothermal ageing time (mins.)	Duration of temper at 600°C (hours)	J_s (tesla)	J_r (tesla)	H_{cJ}(kA/m)	$\frac{J_r}{J_s}$
2F	2	0	1.55	0.200	0.1	0.13
		2	1.49	0.620	0.9	0.42
		4	1.49	0.480	0.8	0.32
		6	1.50	0.610	0.9	0.41
		9	1.50	0.540	1.0	0.36
		12	1.50	0.260	0.3	0.17
		15	1.48	0.400	1.0	0.27
		21	1.47	0.850	1.2	0.58
		37	1.47	0.445	1.2	0.30
		77	1.46	0.670	2.1	0.46
		149	1.41	0.650	2.4	0.46
		263	1.41	0.605	3.0	0.43
		407	1.41	0.690	3.8	0.49
5F	5	0	1.55	0.200	0.4	0.13
		2	1.49	1.010	4.0	0.68
		4	1.49	1.055	5.3	0.71
		6	1.50	1.155	6.6	0.77
		9	1.48	1.185	8.0	0.80
		12	1.48	1.260	7.7	0.85
		15	1.48	1.265	8.7	0.86
		21	1.46	1.295	11.8	0.89
		37		1.270	13.5	
		77	1.46	1.235	16.2	0.85
		149	1.41	1.230	17.4	0.87
		263	1.41	1.175	18.3	0.83
		407	1.42	1.140	17.9	0.80

TABLE XI (Cont.)

No.	Isothermal ageing time (min.)	Duration of temper at 600° C (Hours)	J_s (tesla)	J_r (tesla)	H_{cJ}(kA/m)	$\frac{J_r}{J_s}$
10F	10	0	1.55	0.700	1.1	0.45
		2	1.44	1.320	8.3	0.89
		4	1.49	1.380	11.5	0.91
		6	1.50	1.380	12.3	0.92
		9	1.49	1.365	16.6	0.92
		12	1.48	1.360	15.9	0.92
		15	1.48	1.340	17.5	0.91
		21	1.46	1.300	19.9	0.89
		37		1.310	22.0	
		77	1.44	1.275	24.5	0.89
		149	1.41	1.215	26.3	0.86
		263	1.41	1.220	26.5	0.87
		407	1.41	1.165	25.5	0.83
15F	15	0	1.55	1.040	1.4	0.67
		2	1.49	1.345	6.8	0.90
		4	1.49	1.350	10.4	0.91
		6	1.50	1.365	14.2	0.91
		9	1.50	1.340	15.0	0.89
		12	1.48	1.325	17.2	0.90
		15	1.48	1.330	19.5	0.90
		21	1.47	1.320	21.1	0.90
		37	1.46	1.300	23.9	0.89
		77	1.46	1.270	26.1	0.87
		149	1.41	1.235	28.0	0.88
		263	1.41	1.205	28.8	0.86
		407	1.41	1.200	28.3	0.85
	15	0	1.51	0.950	1.2	0.63
		0	1.51	1.160	1.3	0.77
		0	1.52	0.960	1.4	0.63
	30	0	1.52	1.150	1.9	0.76
	45	0	1.51	0.850	2.1	0.56

TABLE XII

Alloy AI - Magnetic properties after isothermal heat treatment for 10 mins. in a 240 kA/m field at 800°C followed by various cooling rates in the field and subsequent temper at 600°C

P. Cooled from 800°C in a 240 kA/m magnetic field at approximately 80°C/min.

Duration of temper at 600°C Hours	J_s (tesla)	J_r (tesla)	H_{cJ} (kA/m)	$\frac{J_r}{J_s}$
0	1.51	1.210	2.8	0.80
16	1.45	1.280	15.1	0.88
152	1.43	1.230	20.3	0.86

Q. Cooled from 800-750°C at 45°C/min. and 750-650°C at 9°C/min in a 240 kA/m field.

0	1.51	1.380	7.2	0.91
16	1.45	1.310	20.3	0.90
152	1.43	1.275	21.0	0.89

R. Cooled from 800-750°C at 45°C/min. and 750-620°C/min in a 240 kA/m field.

0	1.49	1.360	6.8	0.91
16	1.43	1.290	19.1	0.90
152	1.42	1.240	19.2	0.87

S. Cooled from 800-700°C at 19°C/min. and 700-620°C at 8°C/min in a 240 kA/m field.

0	1.46	1.165	7.7	0.80
16	1.42	1.200	20.3	0.85
152	1.39	1.150	22.3	0.83

TABLE XIII

Alloy C1 - Magnetic properties after isothermal ageing in a magnetic field in the range 630-682°C

No.	Ageing Temp. (°C)	Ageing Time (min.)	J_s (tesla)	J_r (tesla)	H_{cJ}(kA/m)	$\frac{J_r}{J_s}$	J_s(Klitzing method) (tesla)
8-0	630	30	1.300	0.530	2.0	0.41	
3-1	640	21	1.300	1.045	1.9	0.80	
2-5	650	9	1.280	1.040	3.5	0.81	1.265
2-4	"	15	1.270	0.995	5.3	0.78	
3-8	"	21	1.300	0.960	2.4	0.74	
2-3	"	30	1.265	1.045	9.3	0.82	1.253
3-4	"	45	1.300	1.150	7.6	0.89	
2-6	"	60	1.250	1.010	12.3	0.81	1.235
4-4	652	9	1.290	0.520	2.5	0.40	1.252
4-7	"	12	1.300	1.185	3.3	0.91	
4-3	"	15	1.290	1.140	6.5	0.88	1.273
4-2	"	30	1.280	1.150	10.9	0.90	
4-8	657	12	1.290	1.115	5.2	0.86	1.270
4-9	"	18	1.260	1.130	6.1	0.90	
4-5	"	21	1.290	1.165	7.1	0.90	1.267
4-1	"	30	1.260	1.070	8.4	0.85	
3-2	660	21	1.280	1.130	8.0	0.88	1.258
3-5	"	45	1.270	1.135	12.0	0.89	1.262
3-9	"	120	1.160	0.790	12.5	0.68	
3-3	670	21	1.160	0.205	3.3	0.18	
4-6	682	12	1.270	0.585	3.5	0.46	
As quenched.							1.236

TABLE XIV

Alloy C1 Anisotropy and hysteresis energy variation with isothermal heat treatment , derived from J ~ H curves.

No.	Ageing time (Min.)	Ageing temperature(^{o}C)	H_{cJ} (kA/m)	Total anisotropy energy(kJ/m^3)	Total Hysteresis energy (kJ/m^3)
2.5	9	650	3.5	10.33	18.45
4.4	9	652	2.5	5.11	14.71
4.8	12	657	5.2	12.10	25.51
4.3	15	652	6.5	14.65	31.61
4.5	21	657	7.1	17.68	37.79
2.3	30	650	9.3	18.1	43.42
3.2	45	660	12.0	14.83	58.74
2.6	60	650	12.3	6.75	61.49

.....

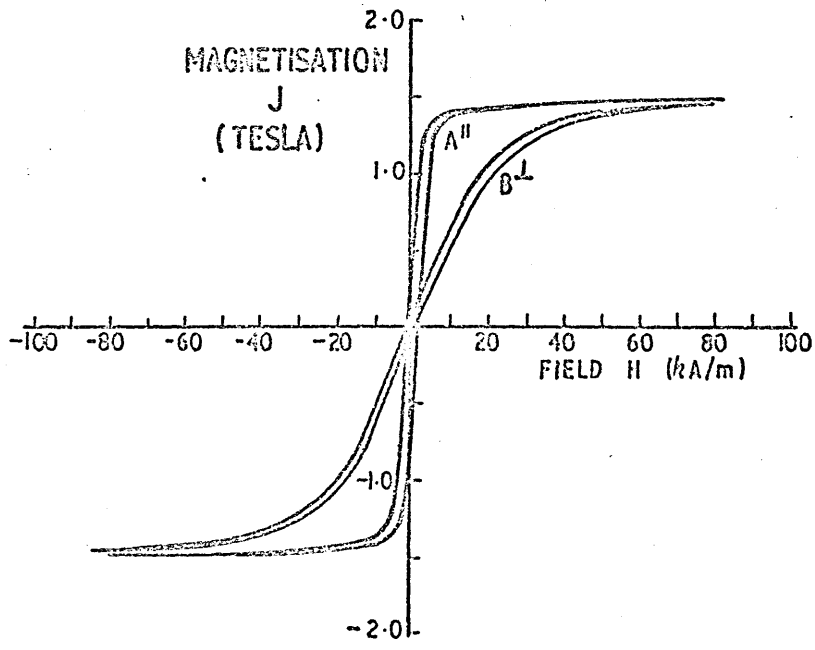

FIG. 43 (a) HYSTERESIS LOOPS FOR Fe-Ni-Al-Co ALLOY A1 AFTER ISOTHERMAL AGEING IN A MAGNETIC FIELD AT 800° C FOR 15 MINUTES. A – PARALLEL TO AGEING FIELD.
B – PERPENDICULAR TO AGEING FIELD.

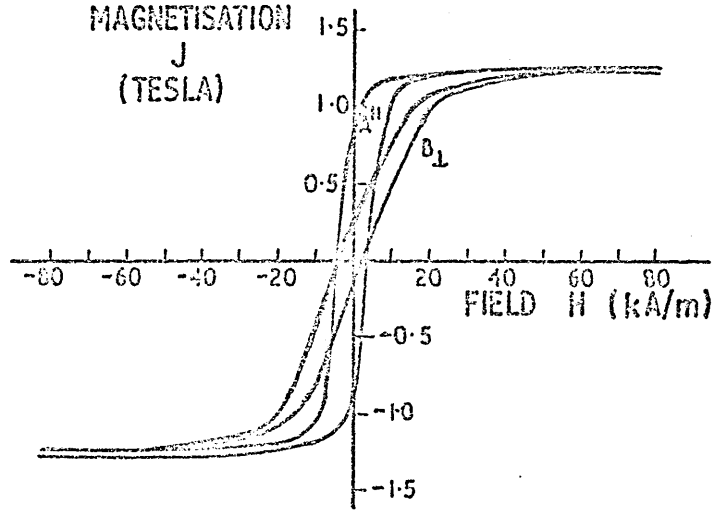

FIG. 43 (b) HYSTERESIS LOOPS FOR Fe-Cr-Co ALLOY C1 AFTER ISOTHERMAL AGEING IN A MAGNETIC FIELD AT 650°C FOR 9 MINUTES. A – PARALLEL TO THE APPLIED FIELD.
B – PERPENDICULAR TO THE APPLIED FIELD.

3.3. Torque Magnetometry and Saturation Magnetisation by the Klitzing method (159, 156)

Examples of some of the torque curves obtained are presented in Fig 44 for both alloys A1 and C1 in which zero angle is taken as the preferred direction.

3.3.1. Alcomax 111

The values of anisotropy obtained from the torque curves of the isothermally aged Alcomax 111 samples are given in Table XV. The ageing temperature performed ranged from 650 up to 800°C and for times of from 1 to 60 minutes.

Also included in this table are the magnetic anisotropy results of samples which were first aged for 5 minutes at 750°C, removed from the salt bath and quenched, and then rotated in the holding jig so that when placed back in the salt bath the applied magnetic field was perpendicular to its original direction, but still radial with respect to the sample bar so that when cut into discs the two perpendicular directions were both in the plane of the disc. These samples were given a further 5 or 15 minutes at 750°C in this perpendicular field prior to re-quenching. The magnetic anisotropy results from other samples are also included here which were aged at 750°C in the field for 5 minutes and then the field was switched off for from 5 to 55 minutes prior to removal and quenching. Saturation magnetisation values for the same series of discs was measured by the Klitzing method and included in Table XV.

3.3.2. Alloy A1

Torque magnetometry of disc sections from samples of Alloy A1 isothermally aged at both 800°C and 750°C for from 1 to 60 minutes

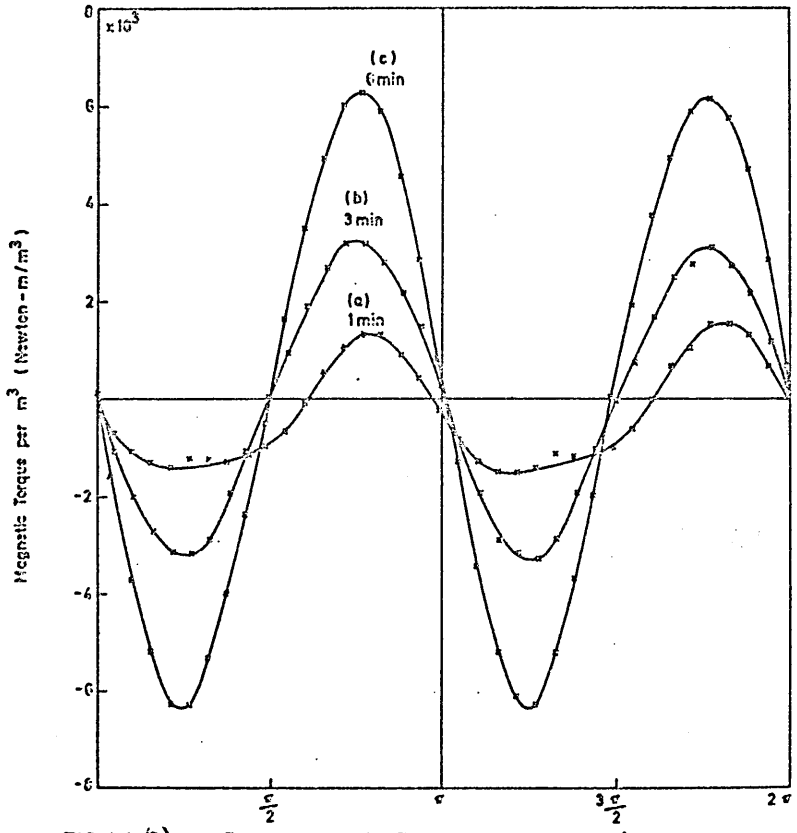

FIG. 4.4(a) Torque curves for Fe Cr Co alloy C1 after isothermal ageing at 650°C in a magnetic field for (a) 1min, (b) 3min, (c) 6min.

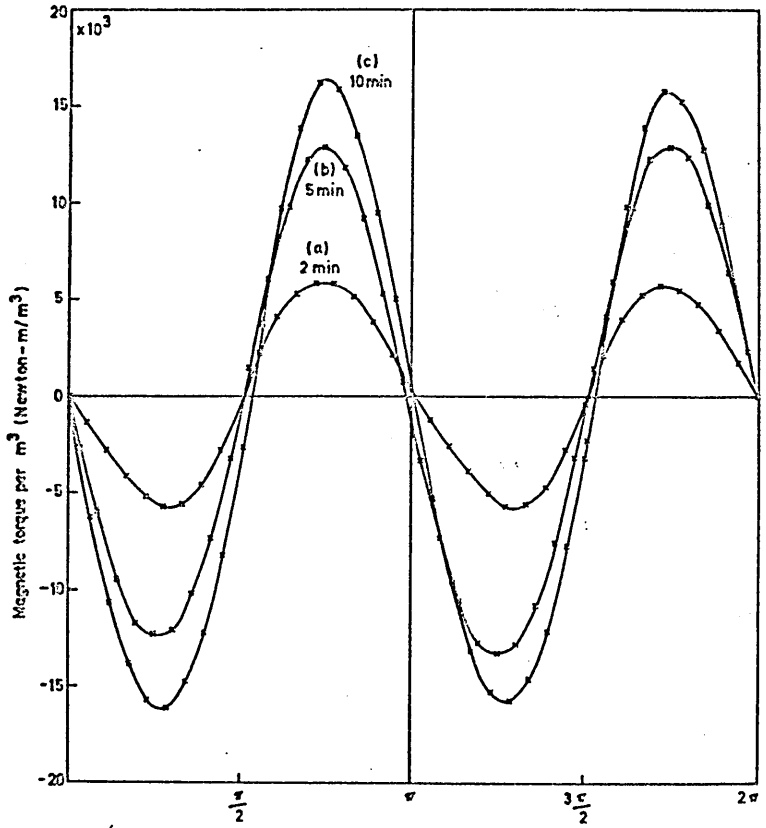

FIG. 4.4(b) Torque curves for Fe Ni Al Co alloy A1 after isothermal ageing at 600°C in a magnetic field for (a) 2min, (b) 5min, (c) 10min.

TABLE XV

Alcomax III - Isothermally aged in a magnetic field - at 650-800°C for 1-120 minutes - anisotropy measurements by torque magnetometry and saturation magnetisation by Klitzing method.

Isothermal Ageing Temperature (°C)	Duration of ageing (Min.)	Anisotropy (kJ/m^3)	Saturation Magnetisation (tesla)
800	1	6.05	1.439
	2	8.08	1.437
	5	7.35	1.484
	10		1.423
	20		1.385
	41	7.86	1.363
750	2	5.74	1.436
	5	13.09	1.432
	10	12.42	1.447
	20	9.94	1.479
	40		1.427
	60	10.23	1.413
	120		1.383
750	5+5 (FP)	2.12	
	5+15(FP)	6.92	
	5+5 (NF)	13.15	
	5+15(NF)	9.13	
	5+35(NF)	11.86	
	5+55(NF)	13.32	
700	3	2.07	1.456
	5	2.23	1.431
	10	4.54	1.428
	20	6.91	1.436
	40	6.49	1.408
	60	10.49	1.421
	120		1.362
650	5	1.37	1.448
	10	1.77	1.446
	20	2.02	1.445
	40	2.18	1.442

TABLE XV

Isothermal ageing temperature (°C)	Duration of ageing (Min.)	Anisotropy (kJ/m^3)	Saturation Magnetisation (tesla)
650	60	2.52	1.406
	120		1.401

(FP) in a magnetic field perpendicular to the original one.
(NF) without a magnetic field.

.....

gave torque curves such as those in Fig 44 (a) from which the magnetic anisotropy results in Table XVl were derived. Again saturation magnetisation values for the discs were obtained and included in the table.

3.3.3. Alloy Cl

Table XVll lists the anisotropy values from the torque curves from discs which had previously been isothermally annealed as bars in the magnetic field for times from 1 - 60 min. at temperatures in the range 610 - 684°C.

This table also includes results from samples which had been exposed, after 3 minutes at 650°C to extra ageing treatments of 5-12 min. at 650°C in a perpendicular field at the same temperature in the same way as for the Alnico 5 samples in section 3.3.1. and also extra ageing times of from 7 to 27 minutes at the same and higher temperatures in the absence of the field after an initial 3 minutes in the field at 650°C. Saturation magnetisation for these discs are also included in Table XVll.

Table XVlll gives the anisotropy and rotational hysteresis loss for various values of applied field for a disc sample of Alloy Cl which had previously been aged in the magnetic jig at 650°C for 30 minutes and then tempered as given in section 2.3.3. The magnetic properties should therefore correspond to the optimally heat treated state as given in Fig 42. The specimen was demagnetised in an AC-field prior to each W_r determination.

The rotational hysteresis loss, W_r, was taken as half the area between the clockwise and anticlockwise torque curves, measured by taking the mean of the separations of equivalent points at 10° intervals on the two curves for the full 360° range multiplied by π .

TABLE XVI

Alloy A1 - isothermally aged in a field at 750-800°C for 1-60 minutes - magnetic anisotropy is measured by torque magnetometer and saturation magnetisation by Klitzing method.

Isothermal ageing temperature (°C)	Duration of ageing (min.)	Anisotropy (kJ/m^3)	Saturation Magnetisation (tesla)
800	1	8.92	
	2	5.73	1.532
	5	12.92	1.536
	10		1.524
	10	16.06	1.527
	15	16.12	1.509
750	2	4.77	1.440
	5	10.50	1.457
	10	12.56	1.403
	20	17.55	1.381
	40		1.384
	60	16.64	1.371

TABLE XVII

Alloy CI isothothermally aged in a magnetic field at 610-684°C for 1-60 minutes-magnetic anisotropy as measured by torque magnetmeter and saturation magnetisation by Klitzing method.

Isothermal Ageing temperature	Duration of ageing (Min.)	Anisotropy (kJ/m^3)	Saturation Magnetisation (tesla)
675	1	1.05	1.121
	2	1.32	1.092
	5	0.19	0.036
	10		0.633
	20	2.38	0.293
650	1	1.51	1.250
	2	2.02	1.265
	3	3.35	
	3		1.263
	6	6.30	1.266
	9	7.39	1.224
	15	8.79	1.257
	30		1.278
	60	10.69	1.235
650	3 + 5 (FP)	2.87	1.063
	3 + 12(FP)	8.72	1.011
	3 + 7 (NF)	6.27	1.214
	3 + 12(NF)	6.21	1.206
	3 + 27(NF)	7.32	1.189
650	3 + 5 at 684°C (NF)	6.88	0.976
	3 + 9 at 684°C (NF)	5.71	0.842
	3 + 16at 684°C (NF)	4.34	0.708
630	2	2.24	1.275
	2		1.254
	5	2.44	1.289
	5	2.48	1.280
	10	8.43	1.256

TABLE XVII

Isothermal ageing temperature	Duration of ageing (Min.)	Anisotropy (kJ/m^3)	Saturation Magnetisation (tesla)
630	20	9.26	1.206
	40	12.91	1.192
	60	10.49	1.251
610	2	2.46	1.217
	5	2.45	1.277
	10	4.64	1.291
	20	9.61	1.253
	40	8.48	1.264
	60		1.244
As quenched.			1.242
" "			1.244

.....

TABLE XVIII

Rotatonal hysteresis losses at indicated magnetic fields for Alloy C1 aged at 650°C for 30 mins. in a magnetic field and tempered 2 hours at 600°C, 4 hours at 580°C and 16 hours at 560°C

Magnetic Field		Rotational Hysteresis loss	$1/H_i$
External	Internal		$(A/m)^{-1} \times 10^6$
H_e (kA/m)	H_i (kA/m)	W_r (kJ/m^3)	
63.66	49.74	47.35	20.11
87.54	61.67	94.63	16.22
119.37	68.44	100.75	14.61
167.11	100.27	52.61	9.97
238.73	168.31	14.73	5.94
437.68	364.62	0	2.74
636.62	563.41	0	1.78
763.94	690.73	0	1.448

Fig 38. shows examples of some of the torque curves at reduced field for which rotational hysteresis was present.

3.4. Optical and Electron Microscopy

Fig 45. is an example of the typical optical microstructure for a sample of Alloy A1 solution treated and aged in a magnetic field. The microstructure for this alloy, alloy C1 and the Alnico alloys appears single phase when given optimal magnetic heat treatment.

The grains size for alloy A1 was typically 0.15 - 0.25 mm and the grain size for alloy C1 and other Alnico samples were also within this range. This means that the number of grains within a typical disc used for torque magnetometry was probably in the range 650 - 1100.

A series of micrographs illustrating the kind of microstructurness and diffraction patterns obtained by electron microscopy (TEM) for both alloys C1 and A1 and some of the commercial Alnico alloys are included. A full list of these plates, including electron photomicrographs for various ageing treatments of alloys A1 and C1 is included in the list of figures (see contents).

3.5. Hardness tests

The results of some hardness tests performed on Alloy C1 are included in table V11 and microhardness values for the same alloy after ageing for various times at 650°C are presented in Fig 46.

Fig* ^5 Alloy A1 opticel micrograph X120

Polished to 1 m diamond finish and then etched in an alcoholic solution containing 10% HCl and *2%* Br.

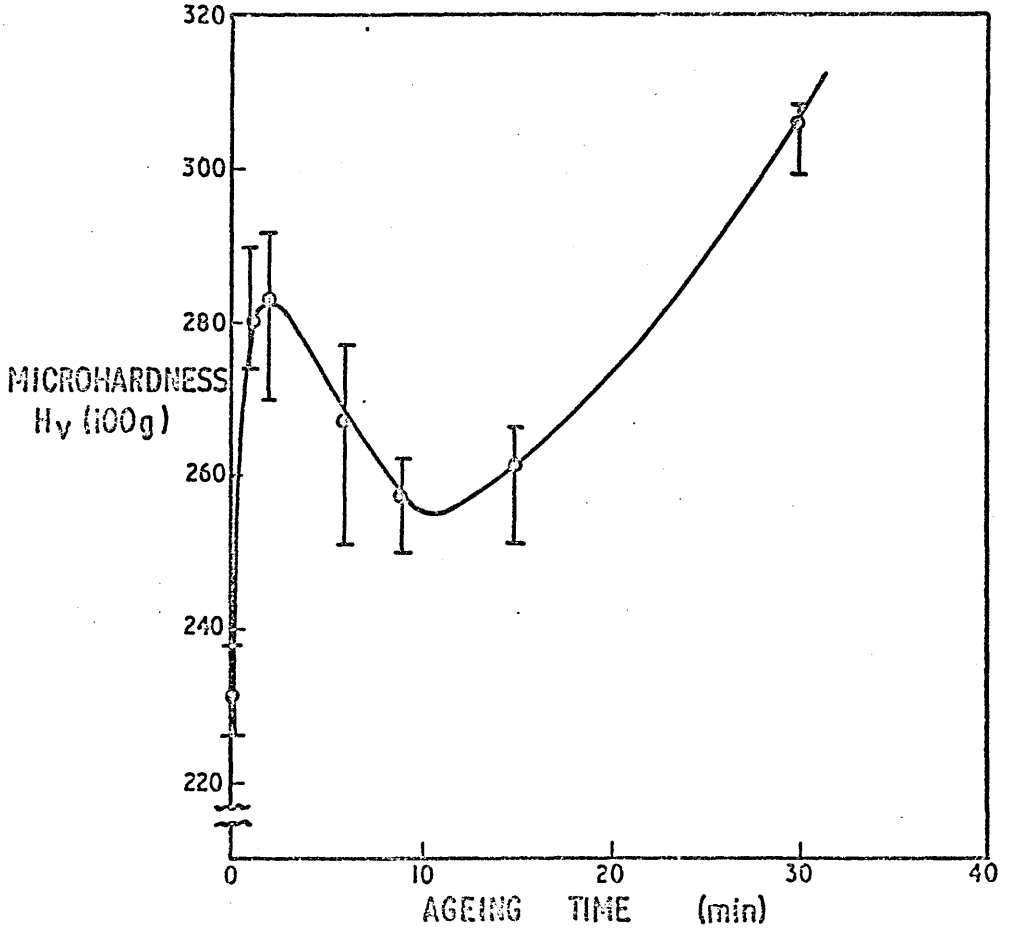

FIG. 46. DEPENDENCE OF MICROHARDNESS ON AGEING TIME FOR ALLOY C1 ISOTHERMALLY AGED AT 650°C IN A MAGNETIC FIELD.

CHAPTER 4.

THEORY - 1

Objectives and relevant calculations

4.1. Possible mechanisms of transformation and alignment in fine particle magnet alloys.

One of the main preoccupations and goals of this work is to provide evidence to decide on the mechanism of decomposition or transformation of the Alnico and Fe-Cr-Co alloys which produce the necessary homogeneous dispersion of fine particles of the ferromagnetic phase, and to distinguish at what stage the magnetic field alignment of these particles occurs.

Two alternative mechanisms of decomposition from a super-saturated solid solution which can give the necessary homogeneous dispersion of such particles are homogeneous nucleation and spinodal decomposition.

The homogeneous nucleation of a particle depends on the chance occurrence, through diffusional exchanges of atoms within the lattice, of a sufficiently large cluster of atoms, so that it may grow spontaneously. Because of this variation in the time required to produce an individual nucleus, then at some later time, say an order of magnitude longer than the incubation period, the microstructure can be expected to consist of particles with a wide range of different sizes, the amount of growth in each case depending on the time of the individual nucleation events. This distribution of particle sizes is contrary to what is observed from Alnico and Fe-Cr-Co under the electron microscope, and also to the requirements for fine particle permanent magnets which can have optimum coercivity only for a particular narrow range of particle sizes. The coercivity of fine particles is limited by superparamagnetic effects below about

10 nm (34) diameter and incoherent reversal mechanisms above approximately the same size (58) (Fig 47). This sharp peaking of coercivity with the particle size requires, then, a very narrow distribution of sizes within an assembly of particles. This condition is met as a natural consequence of spinodal decomposition, although homogeneous nucleation with some growth and coarsening (even though the size distributions of assemblies of such particles is expected to widen during coarsening up to some stable size range (148)) cannot be ruled out.

Alignment of the long axis with the applied field may occur, either, during the early stages of decomposition or during coarsening. If spinodal decomposition occurs then Cahn (133) has described how decomposition in a magnetic field will automatically lead to highly elongated particles, aligned with the nearest $\langle 100 \rangle$ to the field direction, so long as the ageing temperature is such that the variation of magnetisation with composition is large - i.e. near to (but not above) the Curie point (133) as outlined in section 1.4.1. In this case highly elongated particles will be produced instantaneously throughout the crystal, with a mean initial composition only slightly different from that of the original solid solution. The composition of particles and matrix would then progressively change by diffusion until they reached their equilibrium compositions at the transformation temperature used (Fig 22).

Homogeneous precipitation of initially elongated $\langle 100 \rangle$ particles can also be envisaged, and would presumably proceed according to the usual kinetics for precipitation governed by a Johnson-Mehl type equation (160, 161,162,163) i.e.

$$p = 1 - \exp(-At^m) \quad \ldots\ldots\ldots (4.1)$$

where p is the fraction transformed, t is time of ageing, and A and m are constants, the value of m being between 3 and 4 (161).

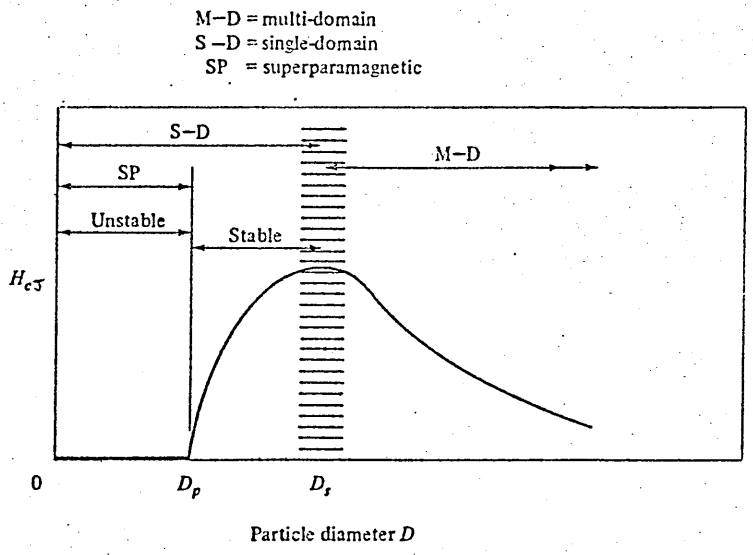

Fig. 4-7 Variation of intrinsic coercivity H_{cJ} with particle diameter D (schematic).

It is perhaps more likely however, as the lattice parameters of the two phases are so similar in most Alnicos and the Fe-Cr-Co alloys, that, if the ferromagnetic phase is homogeneously nucleated, it will not be well elongated initially and elongation in the nearest <100> simultaneously with particle growth or coarsening will then occur. This is the mechanism of alignment of such particles first envisaged by Néel (42) and developed into a "testable" theory by Zijlstra (51). However, directional elongation by this method is not necessarily confined to particles which originated by homogeneous nucleation since the spinodal decomposition mechanism is quite capable of producing particles which are indistinguishable from those occuring by the nucleation mechanism in terms of both composition profile through the particle (135,128,130,131) and the shape of such particles (132,130,131).

The questions which may then be asked are -

(a) Does the fine particle microstructure which is responsible for permanent magnetism in the Alnico and Fe-Cr-Co alloys originate by homogeneous nucleation or by spinodal decomposition, and,

(b) Is collective particle alignment in these systems achieved at the original decomposition stage or at some later stage i.e. during growth or coarsening of the particles.

4.2. Available test techniques

Ideally, a test should be chosen which apart from providing evidence to help decide on these two questions (at the end of section 4.1) it should also be based on the minimum of theory, which should be as sound and basic as possible, with no alternative theoretical interpretation.

An impressive test of this kind is mentioned in the last chapter; that of Mössbauer Effect Spectroscopy performed on alloys in the iron-chromium system (116,117) and to a limited extent on Alnico alloys (97,84). An important fact about this technique is that it is capable of detecting Fe atoms which are in paramagnetic surroundings and with some further interpretive effort can give information on the composition of individual phases at any time within an alloy via the magnetic condition of the Fe atoms within the phase. This method then, if applied to the early stages of decomposition in Alnico and Fe-Cr-Co, seems capable in principle of providing a convincing answer to (a) in section 4.1, relying only on the basic theory behind the Mössbauer effect, i.e. sound nuclear quantum theory without necessarily relying in any way on the mathematical details of precipitation or decomposition theory. The method can test whether the first product of decomposition has a radically different composition or whether it has a composition which only gradually changes from that of its parent phase. That is, the method is capable of distinguishing classical nucleation from spinodal decomposition independant of any mathematical model for these processes, recognising only their basic conceptual difference as originally categorised by Gibbs (164), (essentially the conceptual difference is as shown in Fig 22) and the starting point for all the theories. Mössbauer Effect Spectroscopy must then be regarded as perhaps the most powerful method for differentiation of these two mechanisms of decomposition and powerful confirmation of the relevant mechanism in Fe-Cr-Co and Alnico alloys may be expected to follow from use of this method in the early stages of ageing of these alloys as already performed in the Fe-Cr system (116,117).

Further use of X-ray diffraction effects based on satellite

reflections or side-band effects has also been used in a more intensive way in recent years, particularly 000 scattering i.e. low angle scattering intensity, which can be predicted for the early stages in the Cahn (130,131) theory of spinodal decomposition.

Observations of this kind have been made in various alloy and glass systems (131) which provides some support for spinodal decomposition in these systems in accordance with the theoretical description of Cahn. However the great drawback with this method, compared with the Mössbauer technique for example, is that interpretation of these X-ray diffraction effects are heavilly dependent on details of the theory of the mechanism which the method is being used to investigate. This point is emphasised by more recent theoretical work on spinodal decomposition which predicts somewhat different low angle scattering intensities from the original theory (165,166). Thus whilst this method may be useful in deciding the details of spinodal theory, once this theory is assumed, the fact that interpretation is so sensitive to variations within the theory, allows the possibility that some non-spinodal decomposition theory may also fit the behaviour observed since the presence of low angle scattering does not automatically imply spinodal decomposition. It can arise, for instance, from particle growth and coarsening effects (167). Also the inference of spinodal decomposition on the basis of straightforward observations of diffraction effects or electron microscopy for that matter, of a periodic structure is not valid since it is entirely possible that a nucleation and growth reaction could also yield a periodic structure due, for example, to elastic energy (147).

Other measurements that can be used to follow alloy transformations such as electrical resistance, dilation are also less capable of distinguishing the mode of transformation because of the complexity

of interaction of the various factors which may effect the measurements, again placing a strong dependance on the interpretive model chosen by the researcher.

Static magnetic test methods, such as saturation magnetisation—temperature measurements, have a more direct and unambiguous connection with the atomic constituents of an alloy so that in principle, and in practice in many alloys which have a ferromagnetic constituent, such measurements can pinpoint the presence of new phases and provide information on the kinetics of the reactions taking place principally by the appearance or changes in temperature of Curie points. For Alnico or Fe-Cr-Co the Curie points can be expected to be high i.e. of the same order as the ageing temperature for transformation, so that any changes of this kind would be completely "swamped" by changes engendered by the subsequent attempt at measurement. Other magnetic measurements such as coercivity, remanence, susceptibility and rotational hysteresis for example can be performed; however these are, in general, dependent on the mechanism of magnetic reversal for which, as outlined in Chapter 1, there are several possibilities and it is by no means clear in which circumstances a given mechanism or mechanisms apply.

4.3. Magnetic anisotropy due to particle shape - Testing considerations

The measurement of magnetic anisotropy is thought to be the most suitable magnetic method for the analysis of transformation in Alnico and Fe-Cr-Co, in order to follow changes brought about by variations in composition or particle shape, since, by the method of torque magnetometry, measurements are made only with the specimen fully magnetised and so reversal mechanisms are not involved. Also the accuracy of the formula for magnetic anisotropy, when particle

shape is taken to be the only source of anisotropy, and therefore is based on equation (1.32) i.e.

$$K_s \propto \frac{p\,(1-p)}{2\mu_o} \quad (N_a - N_c) \quad (\Delta J_s)^2 \quad \ldots\ldots\ldots (4.2)$$

is not in dispute. It is necessary of course to align or partially align, in some known and predictable manner, the particles which are produced during ageing so that the resulting anisotropy may be measured afterwards.

It may be assumed for instance that an applied field during ageing of a polycrystalline sample will, by some means, cause the particles to make their long axis the nearest $\langle 100 \rangle$ to the direction of the applied field in each grain (or possibly some angle between this $\langle 100 \rangle$ and the applied field direction, dependent on the strength of the field). The resulting overall magnetic anisotropy will be a combined effect of all the particles.

Considering first the anisotropy energy E due to a single particle, then as given already in equation (1.8) $E = K_s \sin^2\theta$ where K_s has the value given by equation (1.32) or the right hand side of equation (4.2) and θ is the angle between the direction of the applied field and that of the long axis of the particle. This applies for two particles separately, but if it is necessary to know the magnetic anisotropy for a combined system of two particles together, with their long axes at some angle, α , to each other, if it is initially assumed that their combined effect is equivalent to a new uniaxial anisotropy of the type $E = K_s \sin^2\theta$, then

$$K \sin^2\theta = K_1 \sin^2(\theta + \phi) + K_2 \sin^2(\theta + \phi_2) \ldots\ldots (4.3)$$

where $\phi_1 + \phi_2 = \alpha$, ϕ_1 and ϕ_2 being angles of deviation of the K_i from $\theta = 0$ as shown in Fig 48 (a).

By factorisation of the two terms on the right of equation (4.3) and discarding terms independant of θ, the right hand side

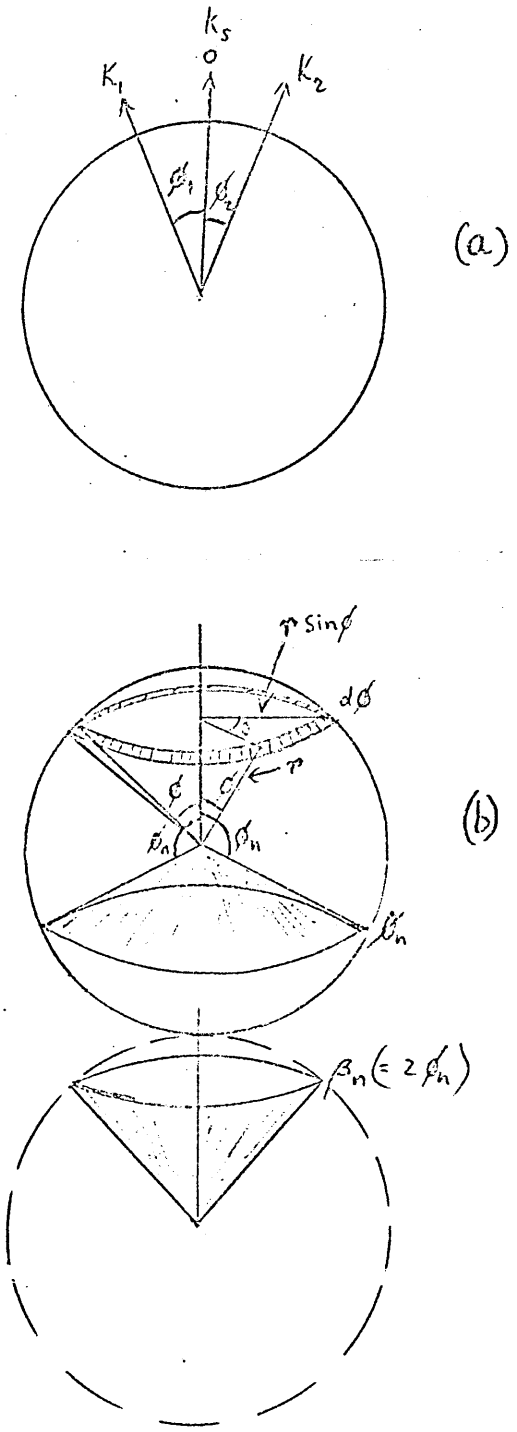

Fig 48 (a) Angles of deviation of individual anisotropy constants K_i from reference direction. (b) Integration over the solid angle defining the range of orientations of the long axes of the shape anisotropic particles and their effective anisotropy energy.

of equation (4.3) becomes -

$$(K_1 \cos 2\phi_1 + K_2 \cos 2\phi_2) \sin^2\theta + \tfrac{1}{2}(K_1 \sin 2\phi_1 + K_2 \sin 2\phi_2)\sin 2\theta$$

For the right hand side to be equivalent the left hand side

$$K = K_1 \cos 2\phi_1 + K_2 \cos 2\phi_2 \quad \ldots\ldots\ldots \quad (4.4)$$

and $$K_1 \sin 2\phi_1 + K_2 \sin 2\phi_2 = 0$$

or $$\frac{K_1}{K_2} = \frac{\sin 2\phi_2}{\sin 2\phi_1} \quad \ldots\ldots\ldots\ldots\ldots \quad (4.5)$$

From equation (4.5) it is evident, for example, that if the two anisotropies are of equal strength ($K_1 = K_2$) then $\phi_2 = \phi_1$ and the new preferred axis lies midway between them, with, from equation (4.4), a combined anisotropy constant $K = 2 K_1 \cos \alpha$, or mean anisotropy per particle of

$$K_s = K_p \left(\frac{\cos \alpha}{2}\right) \quad \ldots\ldots\ldots \quad (4.6)$$

where K_p is the anisotropy if the particles were parallel. (If in this instance the angle α , between the preferred axes represented by K_1 and K_2 ($K_1 = K_2$) is 90° then there is no net anisotropy. If $K_1 > K_2$ then $\phi_1 < \phi_2$, i.e. the new preferred axis will be closer to that of K_1 the larger K_1 is, relative to K_2).

If this analysis is extended to any number, n, of particles each of the same volume and anisotropy constant when considered in isolation, the combined anisotropy constant can be represented by

$$K_s = K_p \left(\sum_{i=0}^{i=n} \frac{\cos \theta_i}{n}\right) \quad \ldots\ldots\ldots \quad (4.7)$$

$$= Q.K_p$$

which is a generalisation of equation (4.4), where n is the total number of particles, θ_i is the angle of deviation of the preferred axis of the particle from the overall preferred axis and K_p is the anisotropy constant per unit volume if all the particles were parallel.

If the value of K_p for parallel assemblies of particles is

taken from equation (1.32) then equation (4.7) becomes

$$K_s = P\,\frac{(1-P)}{2\mu_o}\,(N_a - N_c)\,(\Delta J_s)^2\,Q \quad \ldots\ldots\ldots \quad (4.8)$$

Where Q is the factor which accounts for the angular distribution of the particle assembly as given in equation (4.7). If two identically shaped particles are considered in equations (4.4) and (4.5) so that K_1, = K_2, = K_p, and the co-ordinate axis is rotated so that ϕ, = 0, putting $2\phi_2 = \beta$ then

$$K = K_p\,(1 + \cos\beta) \quad \ldots\ldots\ldots \quad (4.9)$$

$$K \sin\beta = 0 \quad \ldots\ldots\ldots\ldots\ldots \quad (4.10)$$

This demonstrates that the anisotropy constant K_p for each particle can be separated into two components, an effective part

$$K_{eff} = K_p \cos\beta = K_p \cos 2\phi \quad \ldots\ldots \quad (4.11)$$

which will contain a component in the preferred axis, and $K_p \sin\beta$ which, since its value is zero is directed in $\beta = 90^\circ = 2\phi$, i.e. in all directions at 45° to the preferred axis.

If this treatment is extended to any number of identical particles distributed at random from 0 to some maximum angle ϕ_n from the preferred axis, then this can be represented on a spherical projection as shown in Fig 48 (b). The distribution of the angles of the particle axes over the ranges of ϕ from 0 to ϕ_n and θ from 0 to 2π, where θ is the angle of rotation about the preferred axis, is thus represented by points on the spherical surface enclosed by $\phi = \phi_n$. If the orientations are random then the points on the surface will be evenly distributed.

The total number of particles, X, assuming constant areal density, ρ, will be

$$X = 2\pi r^2 \rho \int_0^{\phi_n} \sin\phi \; d\phi, \quad \ldots\ldots\ldots \quad (4.12)$$

integrating

$$X = 2\pi r^2 \rho\,(1 - \cos\phi_n) \quad \ldots\ldots\ldots \quad (4.13)$$

The maximum occurs at $\phi = 180^\circ$ when $\frac{X}{\rho} = 4\pi r^2$ (i.e. total surface area of the sphere).

In fact, it is envisaged that the actual number of particles, n, and hence the number of orientations to be taken into account will be constant, so that, as the maximum permitted angle of particle axes is reduced from 180°, giving $X = 4\pi r^2 n$, to ϕ_n, the number per unit volume

$$\rho = \frac{n}{(1 - \cos \phi)} \quad \ldots\ldots\ldots (4.14)$$

will increase.

In the same way (i.e. analogous to equations 4.12) the contributions to the total anisotropy itself can be summed. However using, not K_p, but the effective part K_{eff}

$$K = \int_0^{\beta_n} K_{eff} \sin \beta \, d\beta \quad \ldots\ldots\ldots (4.15)$$

converting to ϕ

$$K = \frac{\rho}{2} \int_0^{\phi_n} K_{eff} \sin 2\phi \, d\phi \quad \ldots\ldots\ldots (4.16)$$

(integration through the full range $0 < \beta < 180^\circ$ is equivalent to the summation of the areas of <u>two</u> spheres. The comparison of the integrated energy represented by the areas of these two spheres with the single sphere in Fig 48 (b) and equation (4.14) representing the spherical distribution of orientations, which is necessary in order, ultimately to determine the mean energy, the right hand side of equation (4.15) has been divided by 2 in the equivalent expression is equation (4.16), using equation (4.11)

$$K = \rho \frac{K_p}{2} \int_0^{\phi_n} \cos 2\phi \sin 2\phi \, d\phi \quad \ldots\ldots (4.17)$$

$$= \rho \frac{K_p}{4} \int_0^{\phi_n} \sin 4\phi \, d\phi$$

integrating

$$K = \rho \frac{K_p}{16} (1 - \cos 4\phi)$$

substituting equation (4.14)

$$K = \frac{nK_p}{16} \left(\frac{1 - \cos 4\phi}{1 - \cos \phi} \right) \quad \ldots\ldots\ldots \quad (4.18)$$

where $n K_p = K_{max}$ is the anisotropy constant if all the particles are aligned in the preferred axis.

Values of $\frac{K}{K_{max}}$ for ϕ_n from 0 to 90° are presented graphically in Fig 49 as calculated from equation (4.18)

A similar treatment may (incidentally) be applied to the determination of remanence, J_r, for the same angular distribution of particles assuming that such particles do not mutually interact. The situation is similar with J_r, if it is assumed that after magnetisation to saturation the magnetisation vectors of the individual particles then rotate back to their nearest preferred axis direction. A summation is then simply made of the components of magnetisations of the individual particles in the preferred direction over the range of angles involved i.e. $0 - \phi_n$.

$$J_r = \rho \mu_p \int_0^{\phi_n} \cos \phi \sin \phi \, d\phi \quad \ldots\ldots\ldots \quad (4.19)$$

where ρ is the particle density and μ_p is the saturation magnetic moment of an individual particle.

Integrating and using equation (2.14)

$$J_r = \frac{\rho \mu_p}{4} \left(\frac{1 - \cos 2\phi}{1 - \cos \phi} \right) \quad \ldots\ldots\ldots \quad (4.20)$$

where $\rho \mu_p = J_s$ is the total saturation magnetisations of the particle assembly.

Values of $J_r = J_r/J_s$, calculated from equation (4.20) are also included in Fig 49.

The real situation for equiaxed polycrystalline samples of Alnico or Fe-Cr-Co is that the particles can be in one of the three $\langle 100 \rangle$ within each grain. If it is assumed that the application of a field during annealing or isothermal ageing causes the long axis of the particles to be aligned in the nearest $\langle 100 \rangle$ to that of the

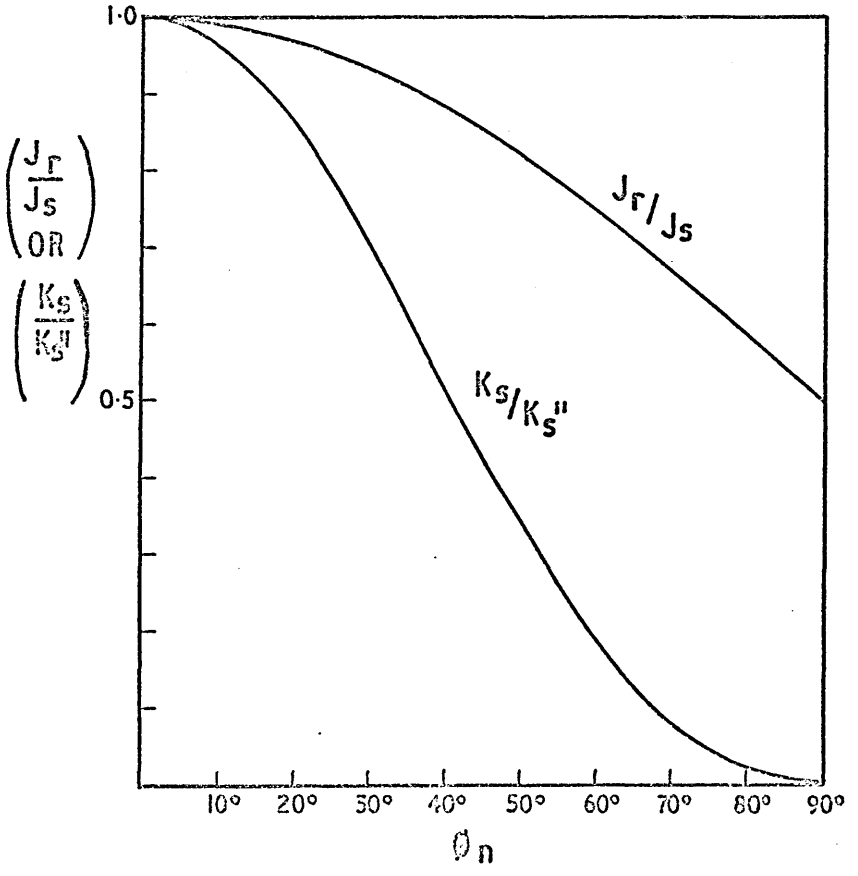

FIG. 49 THE VALUE OF APPARENT REMANENCE AND MAGNETIC ANISOTROPY FOR AN ASSEMBLY OF IDENTICALLY SHAPED PARTICLES WITH LONG AXES DISTRIBUTED UNIFORMALY AT ANGLES UP TO $\emptyset_n$ FROM THE EASY AXIS.

applied field within a given grain, then the two extremes for the orientation of the grain with respect to the field direction are

(a) a grain with <100> in the applied field direction

(b) a grain with <111> in the applied field direction

Any deviation from <111> would mean that at least one of the <100> would then be nearer than the others to the field axis and so would be the preferred one.

The maximum deviation of a particle from the field direction will thus be given by the angle between a <100> and the nearest <111> which is arccos $(1 / \sqrt{3}) = 54.736^{\circ}$. If it is assumed that there are sufficient randomly oriented grains to provide a sufficiently smooth distribution of grain orientations and all orientations up to $\phi_n = 54.736^{\circ}$ are equally likely, then insertion of the above angle (in radians) into equation (4.19) will give the factor which takes into account particle orientations in this situation, i.e. 0.2629. In fact there are four <111> compared with just three <100>. However in equiaxed material both <111> and <100> are evenly distributed and therefore 0.2629 is probably realistic. It is evident then that such a factor, taking into account the distribution of particle orientations can be calculated purely from a knowledge of crystal structure and the effects of the applied field alone. That is, a factor (Q) can be established in the equation for anisotropy, which can then be regarded as a constant so long as crystal structure and the mechanism of field alignment are the same within a given series of experiments.

The above analysis may be an over-simplification in at least two other respects. Firstly, it has been assumed that the long axis of the particle is confined strictly to a <100> when in fact although the electron microscopy and magnetic behaviour completely supports the view, there is at least some evidence that it may be intermediate

between the crystal axis and the field axis during magnetic ageing (69). Secondly, dependant on the details of achieving elongation, the elongation of the particle may be less pronounced in situations where the long axis of the particle is at some larger angle to the field axis, where the component of the field in the long axis is relatively weak and therefore less able to provide the required inducement for elongation.

The first point is less serious because, if the precise function relating field, crystallographic and particle axis were known, then calculations to determine a modified ϕ_n could be made and inserted in equation (4.19) and the orientation factor would still be purely a function of crystal structure and field conditions alone. The second point suggests that Q should also contain some function of $(N_a - N_c)$. However from Fig 50. it may be seen that $(N_a - N_c)$ is a slowly changing function of c/a for modest and higher values of c/a (i.e. $c/a \gtrsim 5$) so that this effect, if it exists at all, may be expected to be relatively small in situations where long particles are required to explain the observed anisotropy.

Given that there are these elements of uncertainty there is little point in attempting more precise calculations for the effect of particle orientation variations until a greater understanding of such effects are available, however it does at least seem reasonable to assume proportionality between K_s and the other factors in equation (4.8) as expressed in equation (4.2) for field aligned polycrystalline samples of Alnico or Fe-Cr-Co, and much of the present work and subsequent analysis is based on this equation.

Factors for volume fraction (p) particle elongation $(N_a - N_c)$, and particle-matrix composition changes represented by changes in ΔJ_s are contained in equation (4.2) so that the behaviour to be expected from the various possible theoretical mechanisms can be compared with

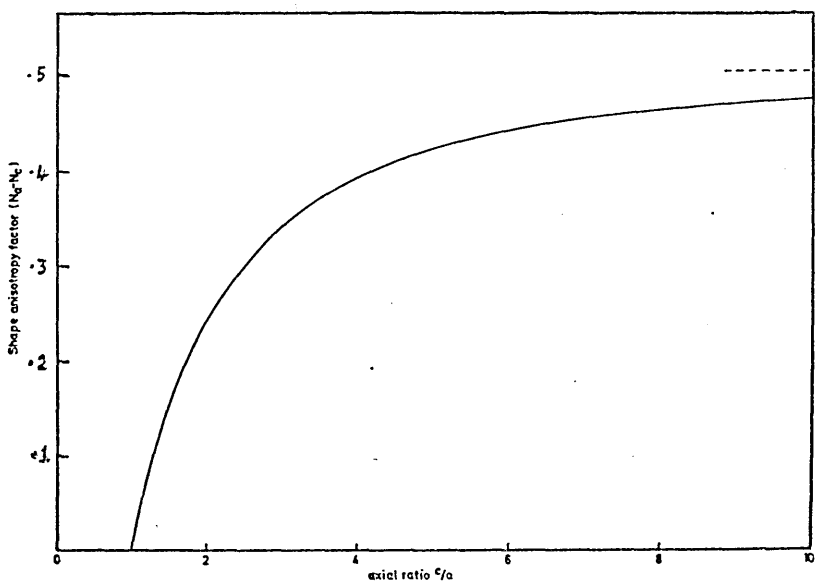

FIG. 50 Variation of shape anisotropy factor (N_a-N_c) with axial ratio of a prolate spheroidial particle

actual changes in anisotropy with ageing. For example if spinodal decomposition occurs then p and $(N_a - N_c)$ should be constant and only variations in ΔJ_s in accordance with the changes in composition of the particle and matrix will occur. Alternatively, for nucleation and growth, in which the particles are visualised as being nucleated already elongated then $(N_a - N_c)$ and ΔJ_s will be fixed and p can be expected to vary with ageing time in accordance with an equation such as (4.1). If spherical particles are initially formed but which subsequently elongate during coarsening in a manner such as suggested by the theory of Zijlstra (51) then in this case p and ΔJ_s will be constant and $(N_a - N_c)$ varies in accordance with the details of the particular theory considered.

It is evident then that measurements of K_s from the earliest stages of isothermal ageing is capable, in principle, of answering both the questions (a) and (b) posed earlier in the chapter and therefore such measurements should be a powerful tool in the investigation of Alnico and Fe-Cr-Co alloys. The investigations reported here are therefore based mainly on torque magnetometry and electron microscopy of an Alnico and on Fe-Cr-Co alloys of analogous composition. Comparison is made between a Fe-Co-Ni-Al alloy similar to Alnico 5 in composition and a Fe-Co-Cr alloy with approximately the same amounts of Fe and Co and an equivalent amount in terms of atomic weight of the "non-ferromagnetic constituent" Cr as there is Ni Al in the Alnico alloy. The idea here was not only to provide information on individual alloys but also to compare the behaviour of equivalent alloys in the two alloy systems.

In addition to torque magnetometry, in which anisotropy and information on rotational hysteresis is determined, other magnetic measurements, including measurements of the technologically important

magnetic parameters B_r, H_{CJ} and (BH) max for various heat treatments as part of the initial magnetic survey of the alloys, and also of B_r, H_{CJ} and J_s and complete magnetic hysteresis curves for these alloys after various isothermal ageing treatments from the solid solution, are determined.

Some microhardness measurements have also been made on the Fe-Cr-Co alloy, and thin foil transmission electron microscopy of both alloys and also samples of commercial Alcomax 111 (anisotropic 25% Cobalt) and Alnico (isotropic 13% Cobalt) for comparison.

Some additional magnetic results have also been obtained on these (particularly Alcomax 111), and other commercial alloys in the Alnico range, where some supporting evidence for general behaviour was required.

CHAPTER 5.

THEORY - 2

Magnetic properties and alloy composition

Certain aspects of the current work have required some further theoretical consideration, e.g., the concept that saturation magnetisation J_s, can be used as a measure of composition and in particular that under certain circumstances J_s is in fact a linear function of composition. The extent to which this may be theoretically justified is explored in section 5.1. In section 5.2. an attempt is made to solve the simultaneous differential equations for particle growth and elongation in a magnetic field as first set out by Zijlstra (51) and first solved by him numerically for a limited range of elongations. Using part of his solution as a first approximation, it was found possible to derive the relationship of anisotropy vs. ageing over a wide range of times.

In section 5.3. the change of composition of elongated particles is considered with reference to the theory involved.

5.1. The magnetisation of the transition metals when alloyed in solid solution with non-ferromagnetic metals.

Stoner (5) first advanced the idea that if a non-ferromagnetic metal such as copper with a completely full 3d band and partly filled 4s band is added to a ferromagnetic transition metal such as nickel which has an unfilled 3d band and a less completely filled 4s band, then the excess electrons in the 4s band of the solute copper atoms may, on alloying, transfer to the 3d band of the solvent nickel atoms leaving the 4s band of the copper atoms filled only to the same extent as for the 4s band of the remaining nickel atoms.

These excess electrons which transfer to the 3d band of the nickel will then, in effect, "neutralise" the effect of an equivalent number of electrons in the positive subband of the 3d band which

would otherwise have contributed to the magnetisation of the alloy.

At some proportion of non-ferromagnetic solute to ferromagnetic solvent these excess electrons will have completely neutralised the remaining "ferromagnetic" electrons originating from the solvent metal atoms (thus reducing the magnetisation to zero at a fixed temperature).

At this point $n_x c' = n_o (1 - c')$ ..... (5.1)

where n_x is the excess electrons/atom of solute of atomic fraction C (which has a critical value c' when equation 5.1 applies) which transfers to the solvent, and in which n_o is the number of electrons per atom of solute which contribute to the magnetisation (which is numerically equal to the magnetisation of the pure solvent metal in Bohr magnetons per atom, i.e. $n_o = \eta_o$ see table 1.). The total number of 4s electrons is $n C$ (where n is the number of 4s electrons per atom) and this must be equal to the number transferred plus the number retained in the 4s band i.e.

$$nc = n_x c + n_s c \quad \ldots\ldots\ldots (5.2)$$

where n_s is the number/atom remaining in the 4s band. When sufficient electrons have transferred to neutralise the ferromagnetic electrons in the 3d band equation (5.1) will apply and therefore

$$c' = n_o (1 - c') + n_s c' \quad \ldots\ldots\ldots (5.3)$$

i.e.
$$n = n_x + n_s$$
$$= n_o \left(\frac{1 - c'}{c'}\right) + n_s \quad \ldots\ldots\ldots (5.4)$$

$$c' = \frac{n_o}{n + n_o - n_s} \quad \ldots\ldots\ldots\ldots (5.5)$$

For copper in nickel $n = 1$, n_o is 0.6, and if the number of 4s electrons/atom of copper remaining in this band n_s is assumed to be the same as that remaining in pure nickel i.e. also 0.6 then c' = 0.6 also.

This equation then predicts that 60% copper is necessary to reduce the magnetisation of nickel to zero and it can be seen from Fig 4. that this is the case in practice. Stoner also noticed that this rule, keeping n_o and n_s the same also held if the solute metal was zinc which has however two 4s electrons i.e. $n = 2$. Substituting these values in equation (5.5), gives a C' for zinc of 0.3. Again this is what is found in practice as in Fig 4.

More suprising however, metals such as aluminium, silicon, tin and antimony which have no 3d or 4s electrons - but instead have valence electrons in other bands such as 3s, 3p in the case of Al and Si, or 5s and 5p in the case of Sn or Sb, also follow this same rule. If n_s in these other bands is kept at 0.6 electrons/atom retained in the valence band, and with n as the total number of the valence electrons/atom, equation (5.5) still gives the appropriate value of C' as confirmed by the data (2,3) in Fig 4.

In order to determine how far these arguments can be extended, the data from Hoselitz (8) (which originated from a large number of sources) has been plotted in Figs 51 and 52. The Figs. present values of magnetisation against composition for nickel as solid solutions with other non-ferromagnetic elements not already shown in Fig 4. and also such solid solutions in both iron and cobalt solvent systems. They are all approximately linear and the linear region in each case is extrapolated to zero magnetisation. These experimental values of this critical composition of solute C' at zero magnetisation are presented for each system in table XlX.

If these values of C together with the appropriate values of n and n_o for each system, are substituted in turn in equation (5.4) then an appropriate value of n_s for the number of electrons retained in the 4_s band of the solute addition is obtained and is

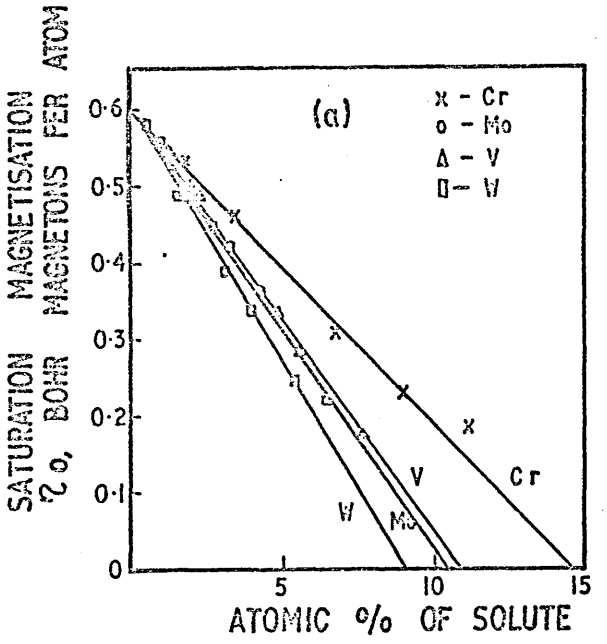

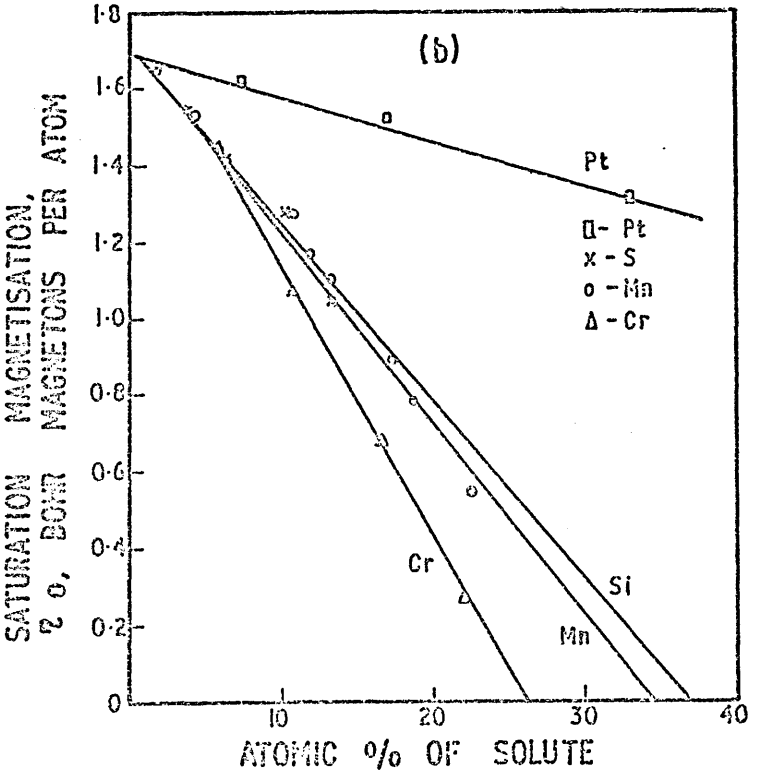

FIG. 51. VARIATION OF SATURATION MAGNETISATION (EXPRESSED IN BOHR MAGNETONS PER ATOM) OF SOLID SOLUTIONS OF VARIOUS METALLIC ELEMENTS IN (a) NICKEL AND (b) COBALT.

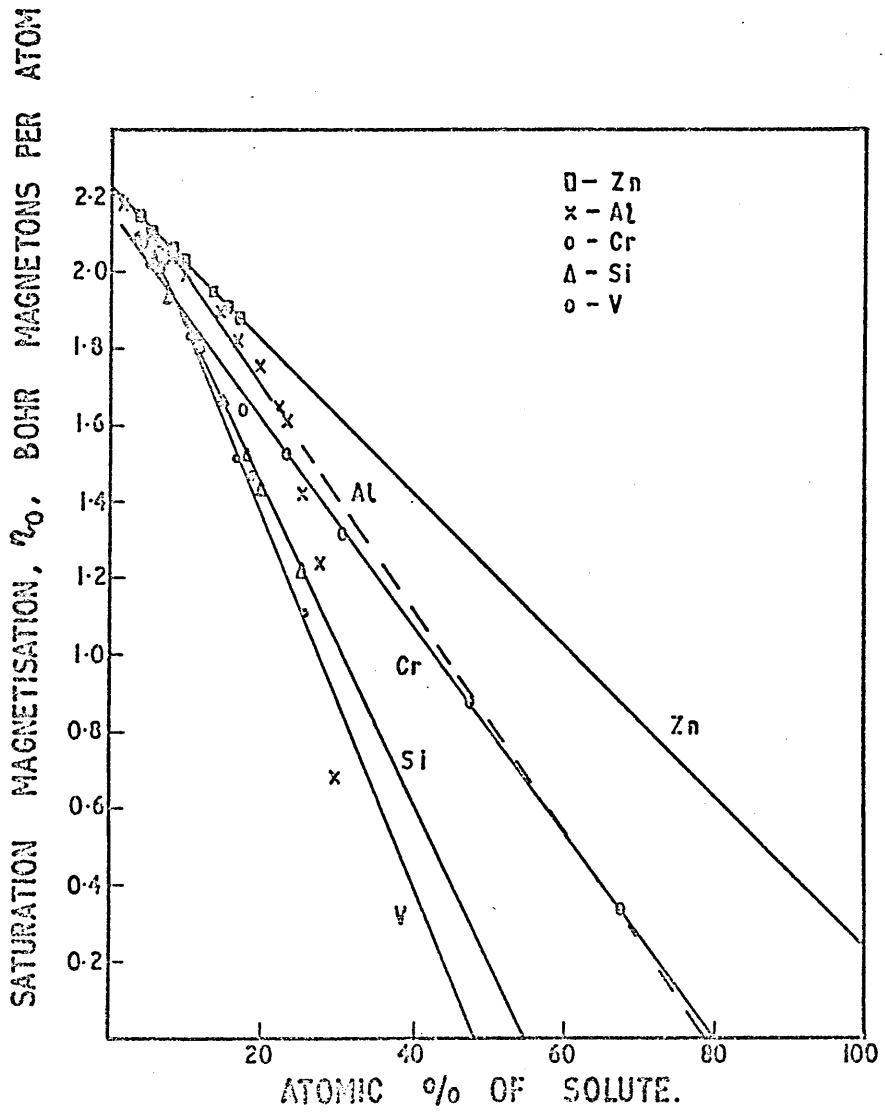

FIG. 52 VARIATION OF SATURATION MAGNETISATION (EXPRESSED IN BOHR MAGNETONS PER ATOM) OF SOLID SOLUTIONS OF VARIOUS METALLIC ELEMENTS IN IRON.

TABLE XIX

Experimental and theoretical prediction for the number of band electrons in the 4S band and the atomic percent of non-ferromagnetic solute element to reduce the magnetisation to zero in two component ferromagnetic solvent metal systems.

Alloy system	No. of valence electrons of solute element (n)	at % solute element to reduce magnetisation to zero (C')		No. of electrons per atom contributing to ferromagnetism in solvent metal. (No)	No. of electrons per atom remaining in 4S band of solute element (Ns)
		from data (8)	Theory		
Ni-Cr	1	58	60	0.6	0.57
Ni-Zn	2	28	30	"	0.46
Ni-Al	3	20.5	20	"	0.67
Ni-Si	4	15	15	"	0.60
Ni-Sn	4	16.5	15	"	0.96
Ni-Sb	5	12	12	"	0.60
Ni-W	6	9	10	"	0.07
Ni-Mo	6	10.5	10	"	0.60
Ni-V	5	11	12	"	0.15
Ni-Cr	6(4)	14.5	(13)	"	0.46
Fe-Al	3	79	73	2.2	2.41
Fe-Zn	2	111	110	"	2.22
Fe-Si	4	55	55	"	2.20
Fe-V	5	48	44	"	2.62
Fe-Cr	6(2)	80	(110)	"	(1.45)
Co-Si	4	37	42.5	1.7	1.11
Co-Mn	5(3d only)	34	34	"	1.84
Co-Cr	6	26	28	"	1.16

No. of excess holes in 3d band of solute compared with solvent.

listed in the end column in table XlX. It is evident that there is some similarity in values of n_o and n_s. Some of the variations may well be due to some inaccuracy in c' which will be amplified especially with small values of c' because this appears as $1/c'$ in equation (5.4). Also n_s is derived as the difference between two numbers of similar size and therefore subject to increased error. A better comparison is perhaps obtained if it is assumed that $n_s = n_o$ in all cases so that for equation (5.5)

$$c' = \frac{n_o}{n} \quad \ldots\ldots\ldots\ldots (5.6)$$

"Theoretical" values calculated from equation (5.6) are placed at the side of the experimental values derived from the data of table XlX. It can be seen quite clearly from a comparison of these values that the same arguments which led Stoner to conclude that the reduction in magnetisation in solid solutions of nickel alloys is explained by a systematic transfer of valence electrons from the solute metal atoms into the 3d band applies generally to iron and cobalt based solid solutions as well. It appears however, in order to explain the values obtained, that the number of electrons per atom of solute n_s retained in the solute 4_s band, needs to be the same as the number of electrons per atoms of solvent, n_o, which are transferred to fill up the 3d band per atom of the solvent. i.e. is an equal division of electrons per atom between the two bands. Details of the co-operative behaviour of electrons in the 3d band, which results in ferromagnetic behaviour in metals and alloys, are still in doubt (168), However, the conduction electrons probably play a part, since they apparently are aligned antiparallel to the 3d + subband electrons (169) and in some way provide the link between these ferro-magnetic 3d electrons.

The conclusion from this analysis i.e. that an equal number of electrons per atom are required in the valence band to, in some way, support sufficient transfer of other valence electrons into the 3d band, to eliminate ferromagnetism in this band is consistant with this idea that valence electrons are somehow involved in an essential way in the ferromagnetic phenomina in metals and alloys.

Future insight into the role that valence electrons play should take this into account i.e. it will be necessary to explain why $n_s = n_o$ in solid solutions of non-magnetic elements in the transition metals Fe,Co and Ni when sufficient solute element is added just to reduce the magnetisation to zero.

Elements which least fit this behaviour tend to be,as might be expected, (because they are antiferromagnetic as pure metals) manganese and chromium alloys, although linear changes of magnetisation with composition are still found. The deviations from the main line in the Slater-Pauling (SP) curve, Fig 3, are in fact mainly alloys of Mn and Cr with one or a fixed proportion of two transition metals.

Suprisingly most of these deviating lines are also linear with approximately the same slope as the main line, but negative.

For instance the main line which is composed mainly of solid solutions of nearest neighbour transition metals Ni Co and Fe can be described by the equation

$$J_s = 10.6 - n_t \quad \ldots\ldots\ldots \quad (5.7)$$

where n_t is the number of (3d + 4s) electrons.

Many of the remaining anomalous lines may be approximated by a set of equations of the form

$$(J_s)_i = a_i + n_t \quad \ldots\ldots\ldots \quad (5.8)$$

where the a_i are constants.

Thus, in the SP curve, the anomalous lines involving Cr, Mn and V are behaving as though it were the difference between the number of electrons/atom in the solute and solvent 3d bands which were involved in the transfer. Or rather, as Cr Mn and V have less electrons in their 3d bands than the other transition metals, a transfer of "holes" will be involved which would account for the negative slope of the anomalous lines in the SP curve. This is accounted for in table XlX where values of n for Cr and Mn in some cases are chosen on this basis.

It is therefore possible to explain in broad outline the saturation magnetisation behaviour - notably the linear change with solute content - of most solid solution alloys of the ferromagnetic transition metals with both themselves and other non-ferromagnetic metals. There is thus a reasonable theoretical basis for expecting a linear change of saturation magnetisation with composition (in atomic percent or fraction).

5.2. An analysis of Zijlstra's simultaneous differential equations for particle coarsening and elongation in a magnetic field.

Zijlstra (51) assumed a simple tetragonal array of ferromagnetic spheroids of equal shape and size with lattice distance b with their long axes all parallel to one lattice axis. The spheroids occupy a fraction, p, of the volume of the whole system which is assumed to be constant during coarsening and elongation in the magnetic field and the compositions of the material of the spheroids and matrix are also assumed constant throughout. The interfacial energy between particles and matrix is assumed constant and independant of the orientation of the interface.

He further assumes that the increase in m, the axial ratio of the particles, during coarsening is due to the decrease in the magnetic (or magnetostatic) free energy as the particles elongate, being greater than the simultaneous increase in the interfacial free energy, σ,

while the increase in the volume of a spheroid, V, is related only to the decrease in σ , since the magnetic free energy is independent of V. This means that when $\sigma = o$, V remains constant while m increases. On the other hand if there is no magnetic free energy, and $\sigma \neq o$, the spheroids will remain spherical and increase in volume V.

Volume diffusion during coarsening was assumed to occur and to be proportional to the area of interface between particle and matrix, the diffusion path being the shortest distance between two spheroids. Zijlstra found that equations derived for coarsening by a surface diffusion mechanism was not consistent with experiment confirming that volume diffusion was dominant.

The two simultaneous differential equations for prolate spheroidal particles derived by Zijlstra are as follows.

$$\frac{dV}{dt} = L_1 A_2 m^{2/3} \left\{ 1 - \left(\frac{6p}{\pi}\right)^{1/3} m^{-\frac{1}{3}} \right\}^{-1}_{p_1^2} \quad \ldots\ldots\ldots (5.9)$$

and

$$\frac{dm}{dt} = -6.75 \; L_1 V^{-2/3} m^{2/3} \; p_1 \left\{ 1 - \left(\frac{6p}{\pi}\right)^{1/3} m^{-\frac{1}{3}} \right\}^{-1} \times (A_1 P_3 + A_2 V^{-\frac{1}{3}} m^{1/3} P_4) \quad \ldots\ldots\ldots (5.10)$$

Where the P_is are known functions of m and L_1 A_1 and A_2 are constants. A complete list of terms is given in Appendix I.

According to Zijlstra the expression $\left\{1 - \left(\frac{6p}{\pi}\right)^{1/3} m^{-2/3} \right\}$ approximates to $0.27\ m^{1/3}$ in the range $3.5 < m < 10$ within 3% if p is taken to be about 0.4. Here we put

$$\left\{1 - \left(\frac{6p}{\pi}\right)^{1/3} m^{-2/3} \right\} = 0.27\ m^{1/3}\ \alpha$$

where α represents any deviations from Zijlstra's simple equation (i.e. approximately equal to unity between $3.5 < m < 10$ if $P = 0.4$, see Appendix 1).

Equations (5.9) and (5.10) then become

$$\frac{dV}{dt} = 3.6\ \alpha^{-1} L_1 A_2 m^{1/3} P_1^{\,2} \quad \ldots\ldots\ldots \quad (5.11)$$

$$\frac{dm}{dt} = -24.3\ L_1 \alpha^{-1} (A_1 m^2 V^{-2/3} P_1 P_3 + A_2 V^{-1} m^{7/3} P_1 P_4) \quad \ldots\ldots\ldots \quad (5.12)$$

Zijlstra obtained approximate numerical solutions of these equations in the range $3 < m < 10$

$$V = V_o t^{1.07} \quad \ldots\ldots\ldots \quad (5.13)$$

and $$m - 0.7 = m_o t^{0.26} \quad \ldots\ldots\ldots \quad (5.14)$$

where V_o and m_o are constants,

However, if these laws are generalised i.e.

$$V = V_o t^{x} \quad \ldots\ldots\ldots\ldots\ldots \quad (5.15)$$

and $$m = m_o t^{y} + a \quad \ldots\ldots\ldots\ldots \quad (5.16)$$

then $$\frac{dV}{dt} = x\ V_o t^{(x-1)} \quad \ldots\ldots\ldots\ldots\ldots \quad (5.17)$$

and $$\frac{dm}{dt} = y\ m_o t^{(y-1)} \quad \ldots\ldots\ldots\ldots\ldots \quad (5.18)$$

If equation (5.11) is substituted in equation (5.12) for part of the second term and putting $-24.3\ L_1 A_1 = K$ then

$$\frac{dm}{dt} + 6.75\ V^{-1} (m^2 P_1^{-1} P_4)\ \frac{dV}{dt} = K \alpha^{-1} V^{-2/3} (m^2 P_1 P_3) \quad \ldots\ldots\ldots \quad (5.19)$$

$$V^{2/3} \frac{dm}{dt} + 6.75\ V^{-1/3} (m^2 P_1^{-1} P_4)\ \frac{dV}{dt} = K\ (\alpha^{-1} m^2 P_1 P_3) \quad \ldots\ldots\ldots \quad (5.20)$$

If now equations (5.15), (5.17) and (5.18) are substituted in equations (5.20)

$$V_o^{2/3}\ t^{(2x/3)}\ y\ m_o t^{(y-1)} + 6.75\ V_o^{-1/3}\ t^{(-x/3)} (m^2 P_1^{-1} P_4) x\ V_o t^{(x-1)} = K/\beta \quad \ldots\ldots\ldots \quad (5.21)$$

where $$\beta = \frac{m^2 P_1 P_3}{\alpha}$$

Substituting $m_o = (m - a)\ t^{-y}$ from equation (5.16)

$$V_o^{2/3}\ t^{2x/3}\ y\ (m-a) t^{-y}\ t^{(y-1)} + 6.75\ V^{2/3}\ x\ t^{(x-1)}\ t^{-x/3}\ m^2 P_1^{-1} P_4\ ) = K/\beta \quad \ldots\ldots\ldots \quad (5.22)$$

$$V_o^{3/3}\, t^{(2x/3-1)}\, y\,(m-a) + 6.75\, V_o^{2/3}\, t^{(2x/3-1)}\, x\,(m^2 P_1^{-1} P_4) = K\beta \quad \ldots\ldots\ldots \quad (5.23)$$

Introducing $\gamma = 6.75 \dfrac{(m^2 P_4)}{P_1}$

$$y\,(m-a) + \gamma x = K V_o^{-2/3} \beta\, t^{(1-2x/3)} \quad \ldots\ldots\ldots \quad (5.24)$$

$$K V_o^{-2/3}\, t^{(1-2x/3)} = \frac{y\,(m-a) + \gamma x}{\beta} \quad \ldots\ldots\ldots \quad (5.25)$$

$$t = \left\{\frac{y\,(m-a) + \gamma x}{K \beta V_o^{-2/3}}\right\}^{1/(1-2x/3)} \quad \ldots\ldots\ldots \quad (5.26)$$

$$t = \left(K^{-1} V_o^{-2/3}\right)^{1/(1-2x/3)} \cdot \left\{\frac{y\,(m-a) + \gamma x}{\beta}\right\}^{1/(1-2x/3)} \quad \ldots\ldots\ldots \quad (5.27)$$

$$= V_{(x)} \cdot t' \quad \ldots\ldots\ldots \quad (5.28)$$

Taking values of m and calculating β, (m-a) and γ and also using Zijlstra's values of a = 0.7, x = 1.07, and y = 0.26, values of t' have been determined. Fig 53 shows a plot of log (m-a) against log t'.

From equation (5.16) $\dfrac{(m-a)}{m_o} = t^y$ so that the slope of the line for x = 1.07, curve A. in Fig 53, should be equal to y. Curve A is linear between m = 2 to m = 30 however the slope given y $\simeq$ 0.22, i.e. inconsistent with the input value initially assumed. However if t' is recalculated with x = 1.00 the slope is then found to be $\sim$ 0.26 over the same range of m (curve B Fig 53) and thus now found to be consistent with the input value.

It is noted that in equation (5.27) t' (or t) is relatively insensitive to the value assumed for y. The equation (for t') can be split into two terms, one proportional to y (m-a) and the other to γ x. Fig 54. shows $\dfrac{y\,(m-a)}{\gamma}$ plotted against $(N_a - N_c)$ and m, from which it is

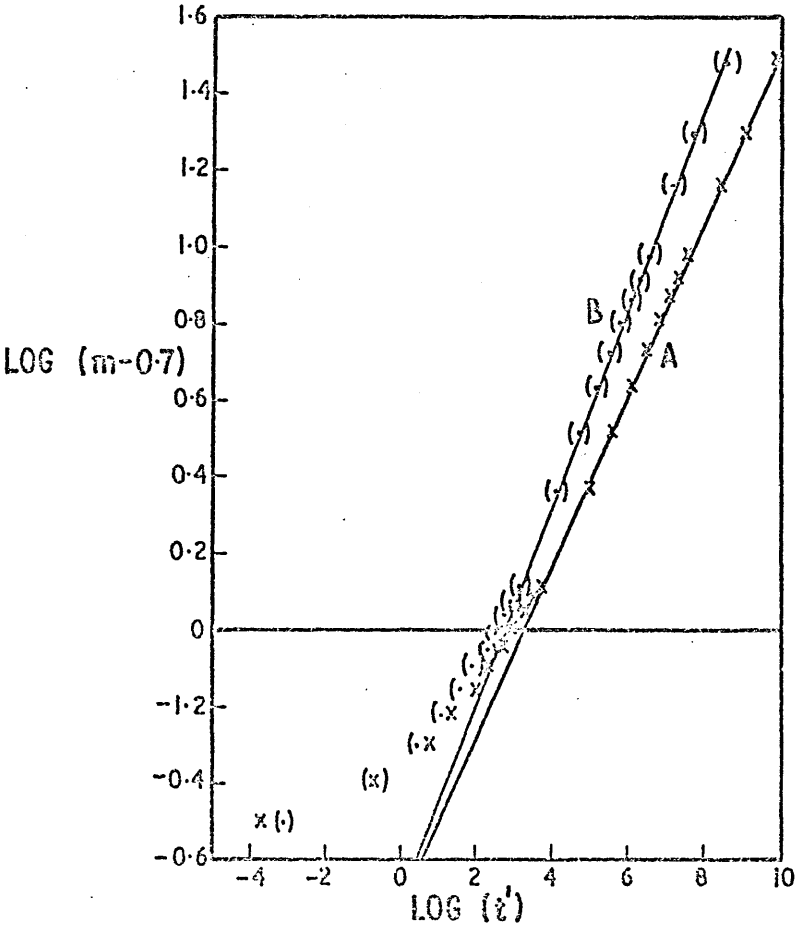

FIG. 53 VARIATION OF LOG (m - 0·7) WITH LOG (t') CURVE A IS FOR ε = 1·07 SUBSTITUTED IN t' WHICH GIVES A SLOPE y = 0·22 — TOO LOW. CURVE B FOR ε = 1·00 GIVES A CONSISTENT VALUE OF y OF 0·26.

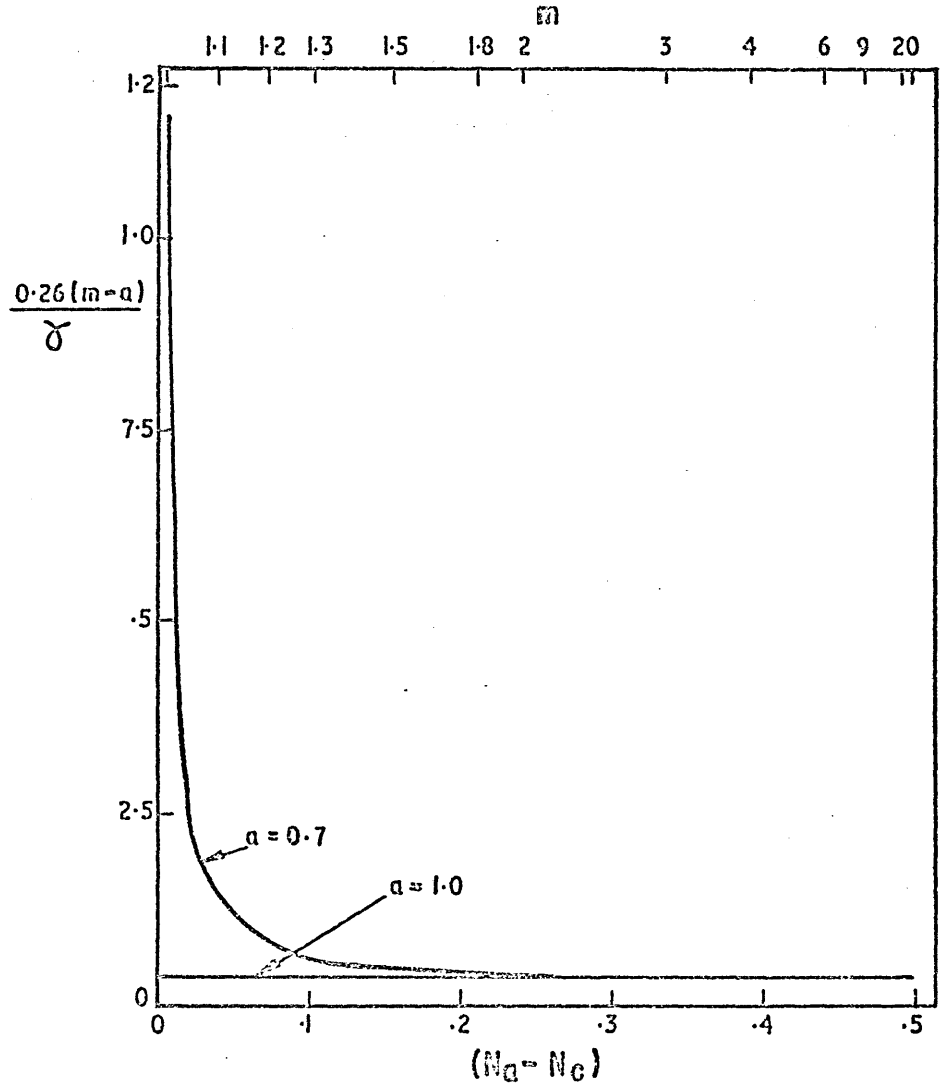

FIG. 54 RATIO OF COMPONENTS OF TERMS MAKING UP t' AS A FUNCTION OF $(N_a - N_c)$

evident that, with $a \simeq 1$, for all values of m the y (m-1) component is only about 3%, and even if a = 0.7 then for $(N - N) > 0.5$ or $m > 1.05$, y (m-a) may be neglected (if $x \simeq 1$). (See also Fig 55).

i.e. $$t'' = \left(\frac{\gamma x}{\beta}\right)^{1/(1-2x/3)} \quad \ldots\ldots\ldots\ldots (5.29)$$

Thus m, the axial ratio of the particles depends mainly only on t and x, and the value to be asigned to y in equation (5.16) appears to depend only on the value given to x. That is, the value given to x in equation (5.15) determines the value to be used for y in equation (5.16) and if x = 1 y = 0.26. Combining equation (5.16) with equation (5.27) or (5.29) gives respectively, putting x = 1, y = 0.26, and a = 0.7.

$$(m - 0.7) = K_{(x,y)} \left\{\frac{0.26\ (m - 0.7) + \gamma}{\beta}\right\}^{0.78} \quad \ldots\ldots (5.30)$$

$$(m - 0.7) \simeq K_{(x,y)} \left(\frac{\gamma}{\beta}\right)^{0.78} \quad \ldots\ldots\ldots\ldots\ldots (5.31)$$

Fig, 55 shows the variation of the right hand side of equations (5.30) and (5.31) with m. From which it is evident that a is actually $\simeq 0.99$ and $K_{(x,y)} = 5.2$, and more importantly it is evident that

$$(m - 1) = 5.2\ (t')^{0.26} \quad \ldots\ldots\ldots (5.32)$$

holds for all values of m from m = 1 up to about m = 25 so long as x = 1. The requirement that x = 1 at all times means that the total volume of a particle must increase directly with time i.e. $V \propto t$

$$\text{i.e.} \quad t \propto r^3 \quad \ldots\ldots\ldots\ldots (5.33)$$

where r is half the mean dimension of the particle.

It is remarkable that this relationship is exactly the one predicted by the Lifshitz - Wagner (142, 143) (LW) theory of particle coarsening already referred to in Chapter 1. and given previously by equations (1.45) and (1.46). The (LW) theory was derived from fundamental chemical solubility theory and has been independantly verified in many solid systems. This lends considerable support to the theoretical

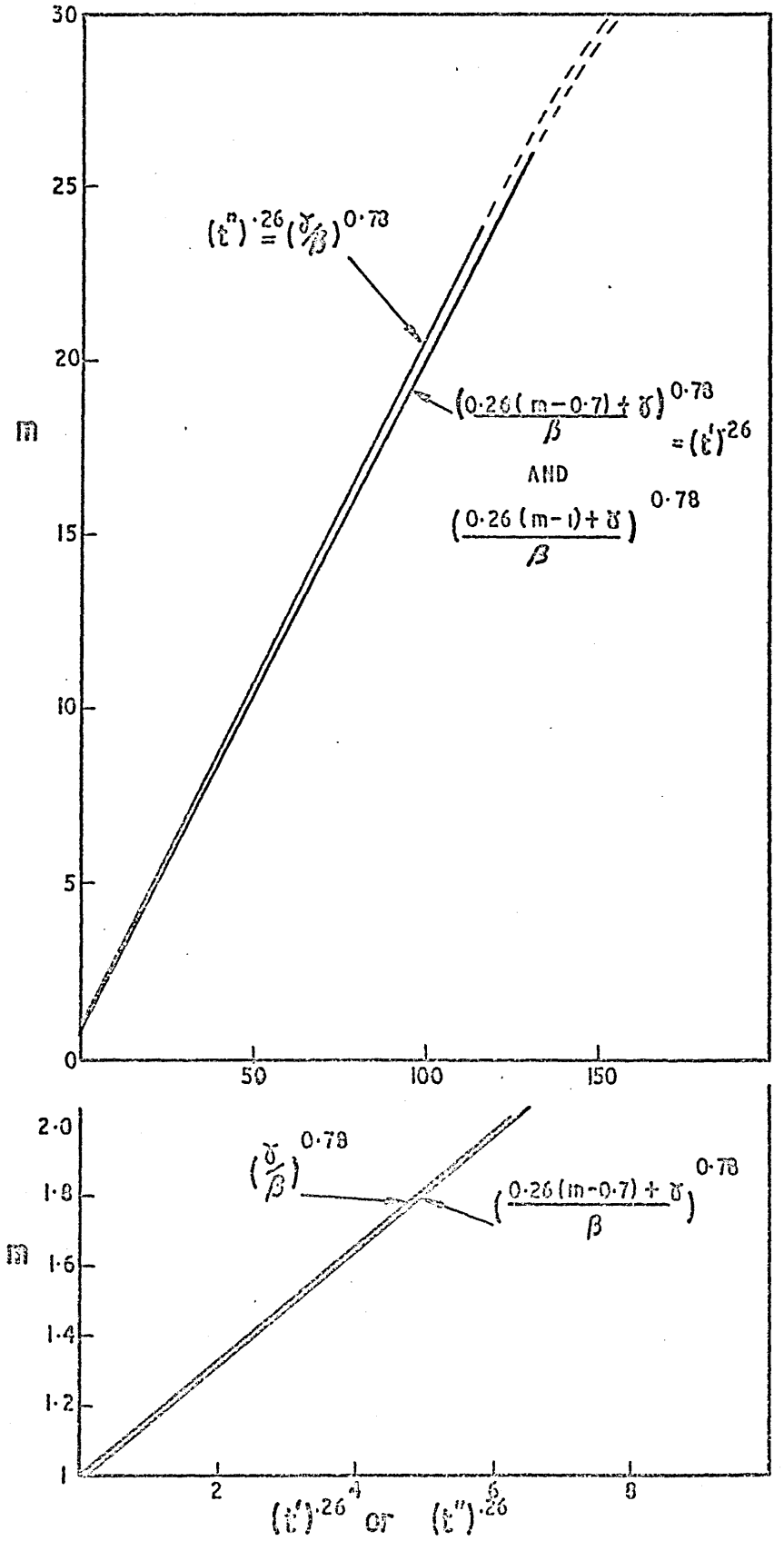

FIG. 55 VARIATION OF PARTICLE DIMENSIONAL RATIO, m, WITH AGEING TIME AS GIVEN BY THE SPECIFIED THEORETICAL PARAMETERS.

soundness of the Zijlstra theory, implying that even when elongation of particles occurs in the presence of a magnetic field, the same law of actual growth in volume with time still applies as in the case where magnetic fields play no part in the coarsening process.

According to the (LW) theory and from equation (1.45) $t \propto (r^3 - r_o^{\ 3}) \propto (V-V_o)$ where r_o and V_o are the radius and volume at the start of coarsening. V_o can be ignored at long ageing times where $V \gg V_o$, but V_o may become important at shorter times when V and V_o have similar values. However, at what stage relationships (5.33) or (1.46) begins to apply is not easily determined.

Recent theoretical work (170) indicates that the simple proportionality between t and r^3 may be established early in the particle growth process when the particles contain only a few atoms so that for all practical purposes in which measurements are taken equation (1.46) may well hold.

In a number of alloy systems in which particles have precipitated and observations and measurements have been made on the growth or coarsening of these particles (110, 146-153), proportionality between t and r^3 was found even in some cases after only a few seconds of ageing and the law seems to apply whether decomposition was initially by nucleation or by spinodal dissociation. It is possible then that Zijlstra's solutions (with x adjusted to 1.00) are good not just over the restricted range of $3.5 < m < 10$ calculated by him, but for any $m \leqslant 30$.

Zijlstra found from the numerical solutions that the anisotropy of the particles should vary linearly with $t^{-.33}$ in the range $3.5 < m < 10$. In this situation (i.e. shape anisotropy) the changes in anisotropy are proportional to changes in $(N_a - N_c)$ due to the change in m. Fig. 56, curve A, is a plot of $(N_a - N_c)$ against

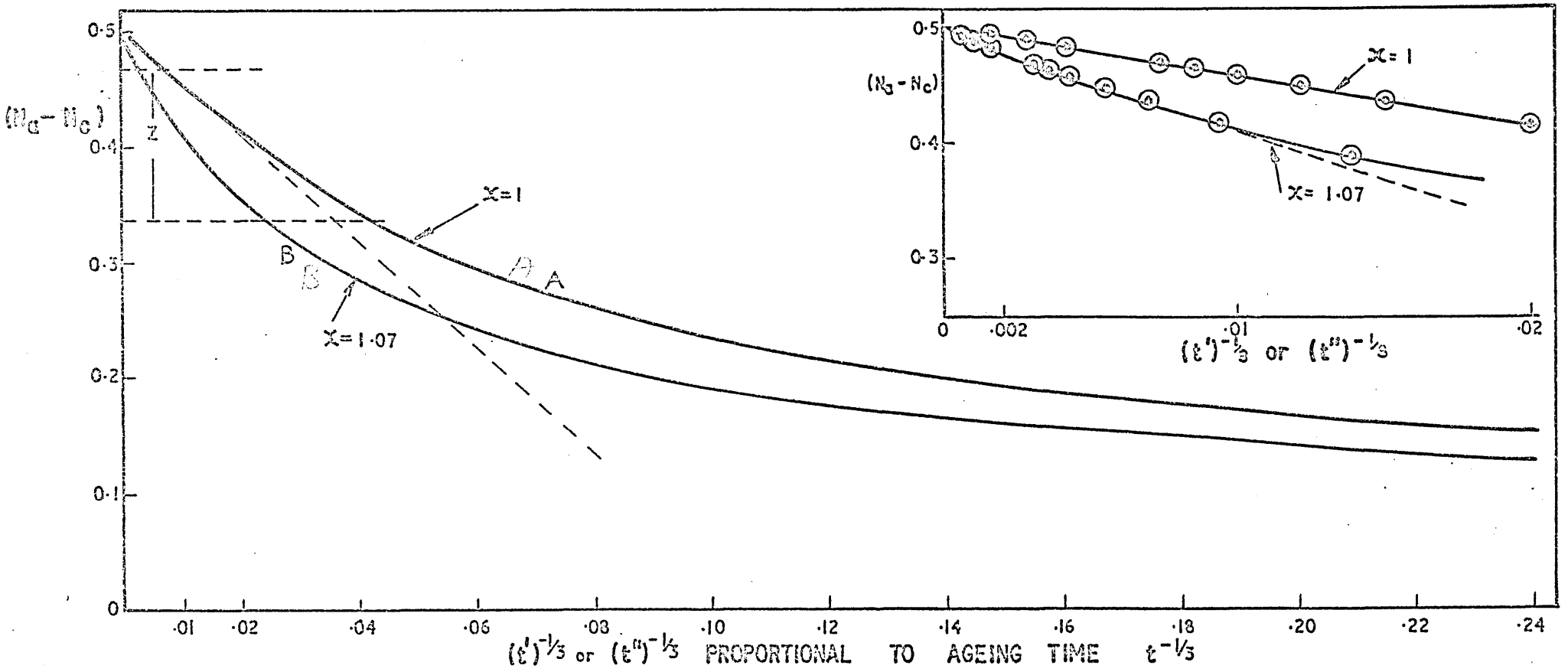

FIG. 56 VARIATION OF (Na - Nc) WITH THE RECIPROCAL CUBE ROOT OF THE AGEING TIME AS MEASURED BY THEORETICAL PARAMETERS t' AND t''.

$(t')^{-1/3} = \dfrac{\beta}{0.26\,(m-1) + \gamma}$ for various values of m. This is effectively a plot of anisotropy against ageing time to the power $-\frac{1}{3}$ with time measured in unspecified units. It is evident that, as found by Zijlstra, there is a linear relationship with $t^{-1/3}$ for long ageing times. The region of m which Zijlstra calculated to be linear i.e. $3.5 < m < 10$ is marked off as region z in Fig 56. In fact the linear region found here is for all $m \geqslant 5$.

If the values of x, (and a) used by Zijlstra, i.e. 1.07 and 0.7 respectively, are used then

$$(t')^{-1/3} = \left\{\frac{\beta}{0.26\,(m - 0.7) + 1.07\gamma}\right\}^{1.1628} \quad \ldots\ldots (5.34)$$

This is plotted against $(N_a - N_c)$ as curve B in Fig 56. from which it is evident that there is no precisely linear part to this curve. It is apparent that t is a very sensitive function of x due to its appearance as a power in equation (5.26) and also because of this t is unlikely to have a linear region in $t^{-1/3}$ except for $x = 1$ when $(1 - \frac{2x}{3})^{-1} = 3$. Non-linearity for $x < 1.0$ can also be demonstrated by calculation as shown for example for $x = 0.93$ which is curve B in Fig. 57.

If equation (5.32) is taken to hold over all measurable values of t then the variation of $(N_a - N_c)$ or anisotropy with t can be obtained by use of equation (1.12) and this is plotted as the solid lines in Fig. 58.

5.3. Diffusion in long particles

5.3.1. Composition changes between particles and matrix

It is known from the work of Clegg and McCaig (96,139) and others (70,83,80) by observing or deducing the Curie points of the individual phases, and the reversible changes in coercivity which

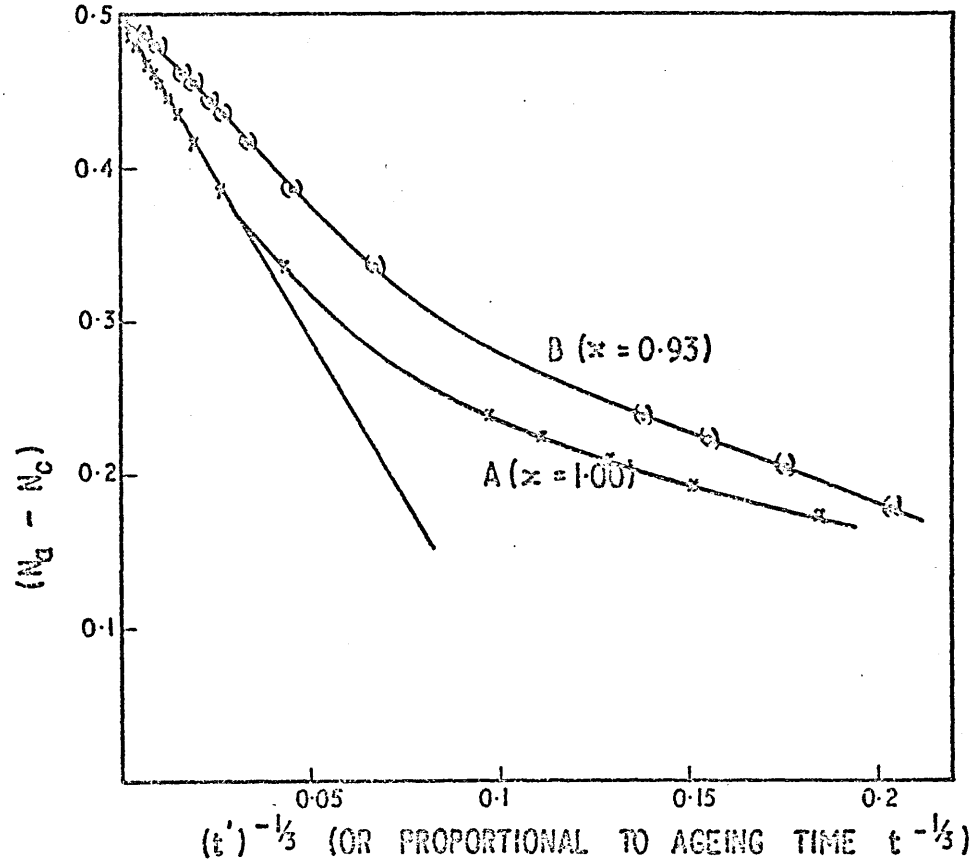

FIG. 57 VARIATION OF $(N_a - N_c)$ WITH THE RECIPROCAL CUBE ROOT OF THE AGEING TIME AS MEASURED BY THE THEORETICAL PARAMETER t'.

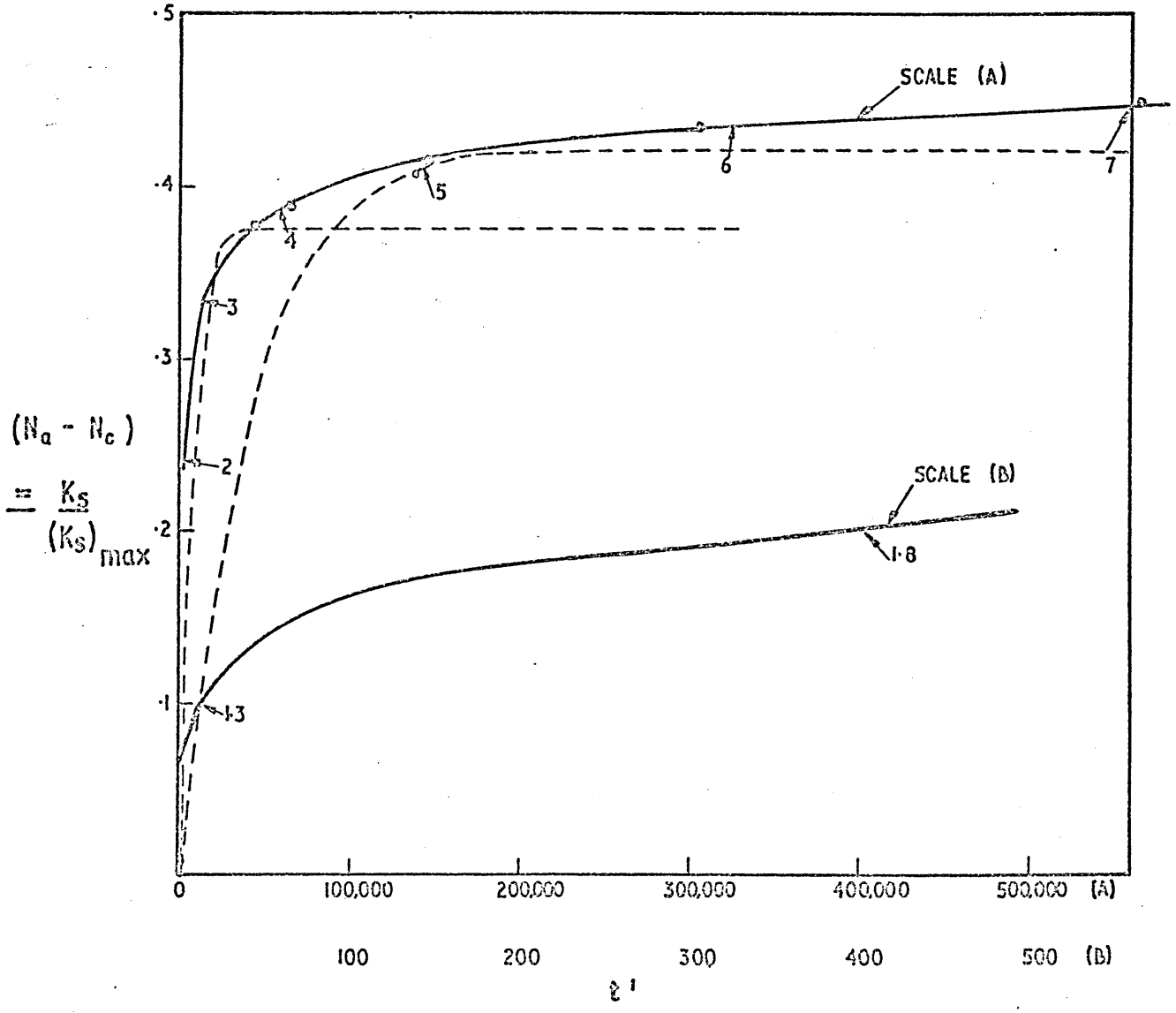

FIG. 58 EXPECTED CHANGES IN ANISOTROPY WITH AGEING TIME (t') FOR ZIJLSTRA'S PARTICLE ELONGATION MECHANISM (SOLID LINES). DOTTED LINES ARE ATTEMPTED FIT OF PARTICLE DIFFUSION MECHANISM ON SAME TIME SCALE. (NUMBERS REFER TO DIMENSIONAL RATIO $m = c/a$ OF PARTICLES).

occur on heating up to 650°C and then re-tempering, that there must be some diffusion resulting in marked changes in composition between particles and matrix in Alnico alloys. Furthermore this reversion of composition appears to be quite reversible depending only on the tempering temperature at each stage so that complete recovery of the original compositions must occur.

This behaviour suggests that a simple non-steady state diffusion based on Fick's second law should apply under these conditions with boundary conditions appropriate to the particle nature of the diffusing system.

It is tempting to speculate how far back to the original decomposition (or nucleation) event this mechanism can be assumed to apply. In fact if the original ageing temperature is considered alone this mechanism is capable of discriminating between spinodal decomposition and nucleation since particles which have nucleated should be either already at the equilibrium composition in which case no diffusion will occur or some intermediate non-equilibrium phase will precipitate initially, and subsequently transform to the final phase leading to some quite complicated anisotropy behaviour.

Spinodal decomposition, however is from the start based on a modified version of Fick's second law given in equation (1.36). This applies only at the very earliest stages of decomposition and later stages require even more additive terms to describe the diffusional behaviour. It may be expected then that this behaviour be equivalent to the basic Fick's second law differential equation

$$\frac{\partial c}{\partial t} = \tilde{D} \frac{d^2 c}{dx^2} \quad \ldots\ldots\ldots (5.35)$$

or its three dimensional analogue with appropriately defined boundary conditions between particle and matrix, at some stage during the

diffusional evolution of the microstructure, assuming that the shape and size of the particles are essentially fixed from the early stages of decomposition (i.e. any growth or elongation of such particles is here considered negligeable).

Sevin and Ellickson (171) using the three dimensional form of equation (5.35) derived a solution which describes the mean concentration c_m of a cylindrical particle as a function of $x/\sqrt{Dt}$. where x is the radius of a cylinder ideally of infinite length. This function may be represented graphically or as a table, and is represented here in table xx and shown as dashed curves in Fig. 58.

From further theoretical work of Olson and Schultz (172) in which the concentrations at the centre of cylindrical (and other shapes) of particles, of varying length, were calculated it was shown that, where the length is greater than about four times the radius, then the function approximates to that of an infinite cylinder. In any case the equivalent function for spherical particles is also similar. This and other relevant work is adequately reviewed by Darken and Gurry (173).

5.3.2. Composition changes in the matrix with particle coarsening

It has already been mentioned in section 1.4.3. of Chapter 1, that as coarsening proceeds in a metallic system of two phases consisting of particles of one phase in another, and as these particles become larger, the solubility of the impurity elements in the matrix phase decreases so that there is some further net transfer of these elements to the particles. This means that a change in the stable composition of the matrix phase occurs with particle growth. For long ageing times this change in composition approaches, asymptotically, a linear relationship between $\Delta C = C - C_e$ representing the change in composition and $t^{-1/3}$ where t is the ageing time, as already

TABLE XX

Fractional Saturation (average composition) of a cylinder during diffusion (173)

Fractional saturation $C = \frac{C_m - C_o}{C_s - C_o}$ where C_m = mean concentration at time, t

C_o = uniform initial concentration

C_s = constant surface concentration

r = radius of cylinder.

D = diffusion coefficient

$k = D/r^2$

kt	C	kt	C
0.005	0.157	0.25	0.832
0.01	0.216	0.30	0.878
0.02	0.302	0.40	0.9316
0.03	0.360	0.50	0.9616
0.04	0.412	0.60	0.9785
0.05	0.452	0.70	0.9879
0.06	0.488	0.80	0.9932
0.08	0.550	0.90	0.9960
0.10	0.606	1.0	0.9979
0.15	0.708	1.5	0.9999
0.20	0.781		

given in equation (1.48). For relatively short ageing times where $C - C_e$ is of the same order of size as $C_o - C_e$ this effect is expected to be relatively minor.

5.3.3. Combination of composition changes due to coarsening with those due to non-steady state diffusion.

The net effect of these two diffusion mechanisms which presumably must be superimposed, may not necessarily cause much confusion since the non-steady state diffusion occurs early in ageing.

This effect rapidly saturates as shown by the dotted lines in Fig 58 , as can be seen from curve A in Fig 59, for which the data from table xx has been replotted against $t^{-1/3}$. A curve for the expected composition modification due to particle coarsening is less easy to draw since all that is known is that the curve will decrease linearly with $t^{-1/3}$ from $t^{-1/3} = 0$ up to some unknown value of $t^{-1/3}$. The slope of the linear region will probably be quite gradual since composition changes based on coarsening are expected to be only relatively slight. Curve B of Fig, 59 gives one possiblity for the shape of the curve plotted on an arbitrary composition scale and the resulting combined effect is shown by curve C. The alternative extreme may be a more gradual linear change over the whole $t^{-1/3}$ range which, in combination, would have the effect of tilting curve A slightly clockwise.

5.3.3. Summary

There are at least three possible mechanisms which can account for at least part of any change in magnetic anisotropy in alloy systems of ferromagnetic particles in a less ferromagnetic matrix.

(a) Elongation of particles in the direction of an applied field which can occur during coarsening if the temperature is sufficiently

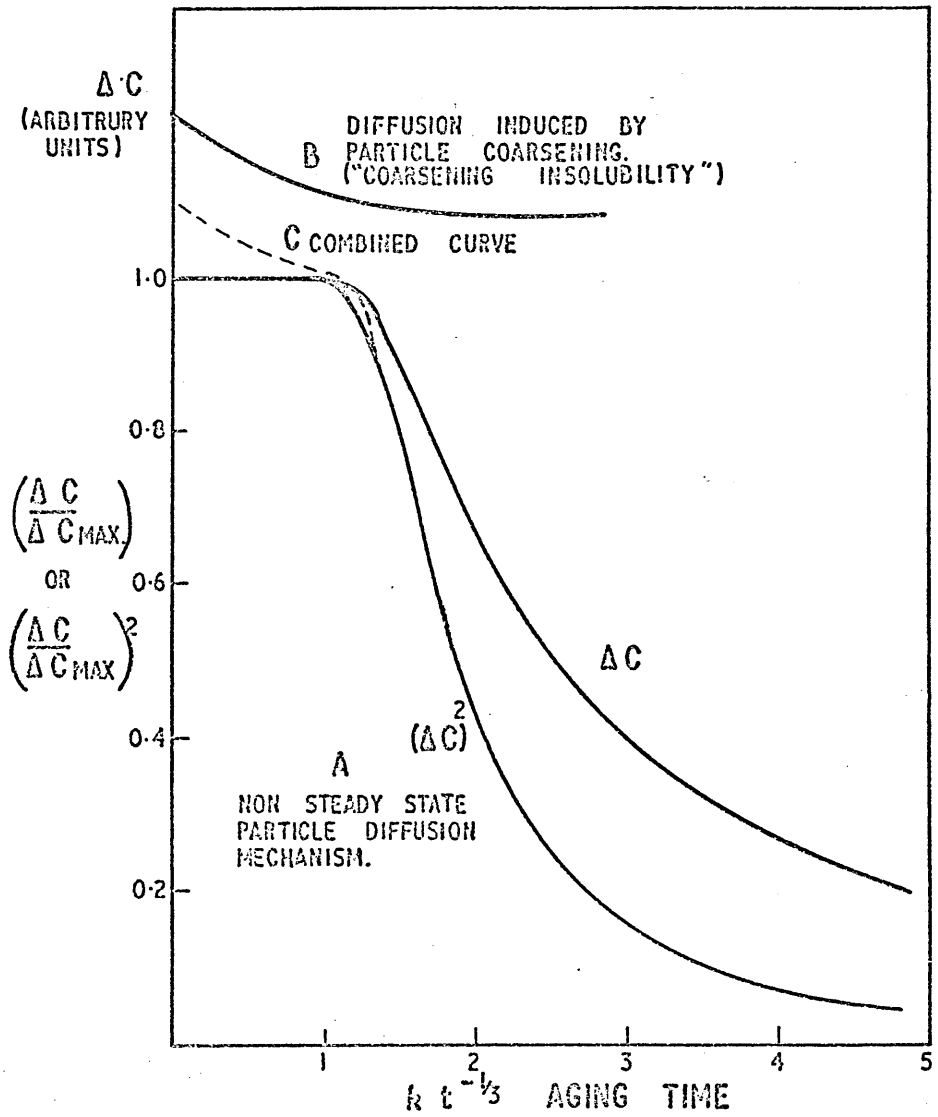

FIG. 59 DIFFUSIONAL BEHAVIOUR FOR A SYSTEM OF PARTICLES FOR VARIOUS MECHANISMS AND POSSIBLE COMBINATIONS OF SUCH MECHANISMS.

high. The basic theory was originally formulated by Zijlstra (51) and in this text will be referred to as the "Zijlstra Mechanism".

(b) Particle coarsening is accompanied by a change in the equilibrium composition of the matrix in which the solubility of any solute elements is reduced the larger the size of the second phase particles. This effect was first pointed out by Ardell (146) some years after the formulation of the Zijlstra mechanisms and therefore not taken into account by him. This extra effect will in this text be referred to as "coarsening insolubility".

(c) Prior to the above effects which can apply during coarsening, the particles themselves must have formed by at least one of two mechanisms either nucleation and growth or spinodal decomposition. The latter mechanisms involve the separation of the initially homogeneous solid solution into two phases by a gradual change of composition from the initial one to the equilibrium compositions of the two phases which are expected to be distributed initially as a periodic fluctuation in composition at right angles to the direction of any applied magnetic field, which thus takes on the appearance of fine highly elongated particles, aligned in the direction of the field. This gradual change in composition, which ultimately leads to the phase separation, must be governed by the usual laws of diffusion i.e. Fick's second law for non-steady state diffusion and will in this text be referred to as the NSS diffusion effect.

(d) The alternative transformation mechanism is of course nucleation and growth, and this is considered further in the next chapter.

CHAPTER 6.

6. Discussion

6.1. Magnetic anisotropy of Alnico and Fe-Cr-Co alloys

The magnetic anisotropy of alloys containing a dispersion of aligned elongated ferromagnetic fine particles is given, as explained in Chapters 1 and 4, assuming the shape of the particles is the only source of the magnetic anisotropy, by

$$K_s = \frac{p(1-p)}{2\mu_o} (N_a - N_c) (\Delta J_s)^2 Q \quad \ldots\ldots\ldots (6.1)$$

This is an interesting equation because it can be separated into factors which are dependent on different mechanisms of the generation and subsequent evolution of the particle system. $(\Delta J_s)^2$ is dependent only on composition difference between particle and matrix and therefore responds to diffusional mechanisms which will occur between the two phases. $(N_a - N_c)$ is a factor which changes with change in elongation of the particles and p (1-p) responds only to changes in quantity of the particle phase.

Thus, for the Zijlstra mechanism of elongation in a magnetic field during coarsening, $(N_a - N_c)$ varies and the other factors are assumed to remain constant. For the diffusional mechanisms a relation between $(\Delta J_s)^2$ and ΔC is also required. Both the experimental observations and theoretical expectations, as explained in section 5.1. are that $\Delta C \propto J_s$ i.e. J_s varies linearly with composition. Fig 60. illustrates schematically the variation of J_s with C, C being the concentration of one component of the alloy system with C_o the untransformed composition and C_α and $C_{\alpha'}$ the equilibrium compositions of the two crystallographically identical phases α and α'.

The miscibility gap in Fig. 60 represents the thermodynamic

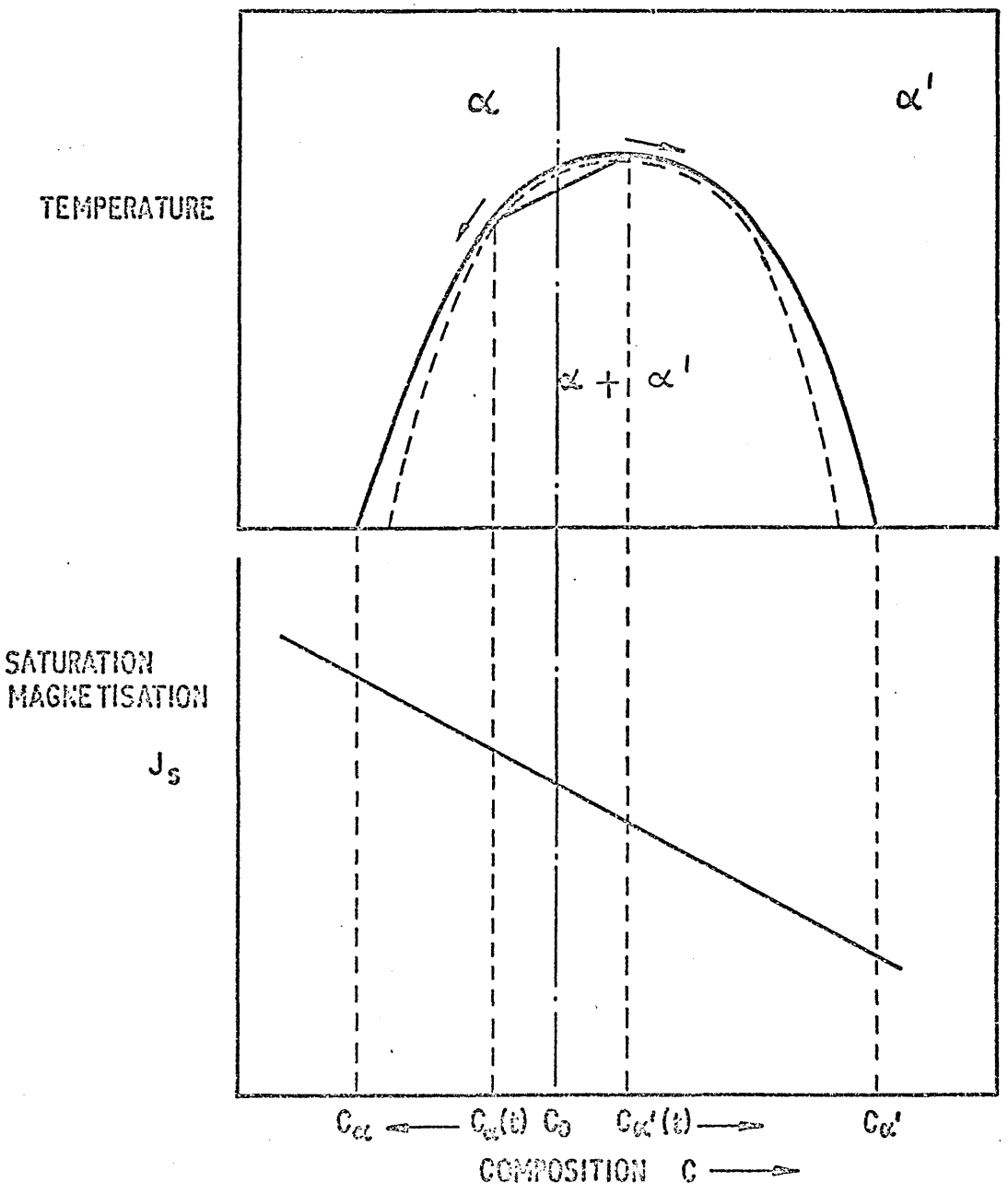

FIG. 60 SCHEMATIC MISCIBILITY GAP - BINARY OR PSEUDOBINARY SECTION AND LINEAR CHANGE OF SATURATION MAGNETISATION WITH COMPOSITION.

condition and the equilibrium situations are governed by this diagram; however the actual composition at time, t, depends on kinetic factors so that C_{α} (t) and $C_{\alpha'}$ (t) may be controlled by diffusional processes.

If there is a linear relationship between J_s and ΔC i.e.

$$J_s = (\Delta C) \frac{\partial J_s}{\partial C} \quad \ldots\ldots\ldots\ldots (6.2)$$

($\frac{\partial J_s}{\partial C}$ assumed constant) This allows magnetic anisotropy to be represented as a function of composition through the factor $(\Delta J_s)^2$ in equation (6.1)

6.1.1. Spinodal Decomposition

Spinodal decomposition, according to Cahn (130-134) gives particles which are rod shaped and ideally are infinitely long from the start of decomposition, so that $(N_a - N_c)$ should be at its maximum value (½) and which, as can be seen from Fig 50. will vary only little with further elongation even if initial elongation is only modest (i.e. $c/a \gtrsim 4$). The proportions of the decomposition products i.e. (p & 1-p) are also fixed from the start so that under these circumstances ΔJ_s is the only variable factor due to changes in composition by diffusion between the two decomposition products.

Cahn's solution for the early stages of decomposition is given from equation (1.37) as -

$$C = A e^{-Rt} \quad \ldots\ldots\ldots\ldots (6.3)$$

for the composition at the centre of the particle, where A and R are constants as explained in section 1.4.1.

As $K_s \propto (\Delta J_s)^2$ then $K_s \propto e^{-R't}$ (where $R' = 2R$).

However it is not expected that any experimental set of data will fit this relationship since it only applies to the earliest stages of decomposition, dependent on the parabolic fit to the free energy -

composition curve in Fig. 21. Equation (6.3), as it stands, predicts ΔC increasing exponentially without limit which is clearly impossible. Figs. 61, 62, and 63 show the magnetic anisotropy data derived from torque curves and previously given in tables XV, XVl and XVll for Alcomax lll (Alnico 5), alloy Al and alloy Cl respectively, plotted against t the ageing time. It is evident that K_s levels off, given sufficient time for ageing, in all these alloys.

Figs. 64 and 65 present the same data but with $\ln \left\{ \frac{K_s}{(K_s)_{max}} \right\}$ plotted against ageing time in accordance with equation (6.3) $(K_s)_{max}$, which is in each case an estimate of the value of K_s to which a given alloy levels off, or saturates, is included only to compare the data (and allow the possibility of a single curve to be drawn through it) and in no way affects the shape of the curve. The curves are not linear, except perhaps at early ageing times as expected from the theoretical arguments.

6.1.2. Particle-matrix interdiffusion during ageing

From the values in Table XX which relates ΔC to $k\, t^{\frac{1}{2}}$ (k being a constant) for non-steady state diffusion between particles and matrix and relation (6.2), a curve can be drawn of K_s against t. Using appropriate values of $(K_s)_{max}$, where $\frac{K_s}{(K_s)_{max}} \propto (\Delta C)^2$, and k. Best fit curves may be drawn to the magnetic anisotropy values from tables XV, XVl and XVll for Alcomax lll, Alloy Al and Alloy Cl respectively. This has been done in Figs. 61, 62 and 63 where the continuous drawn curves are theoretical ones based on this relationship.

It can be seen that, despite some rather large individual discrepancies the data follow the trend of these curves. In the only case where there are apparently sufficient data points at the early stages of ageing, which is Alloy Cl aged at 650°C, there is some indication that the results are linear as predicted by theory.

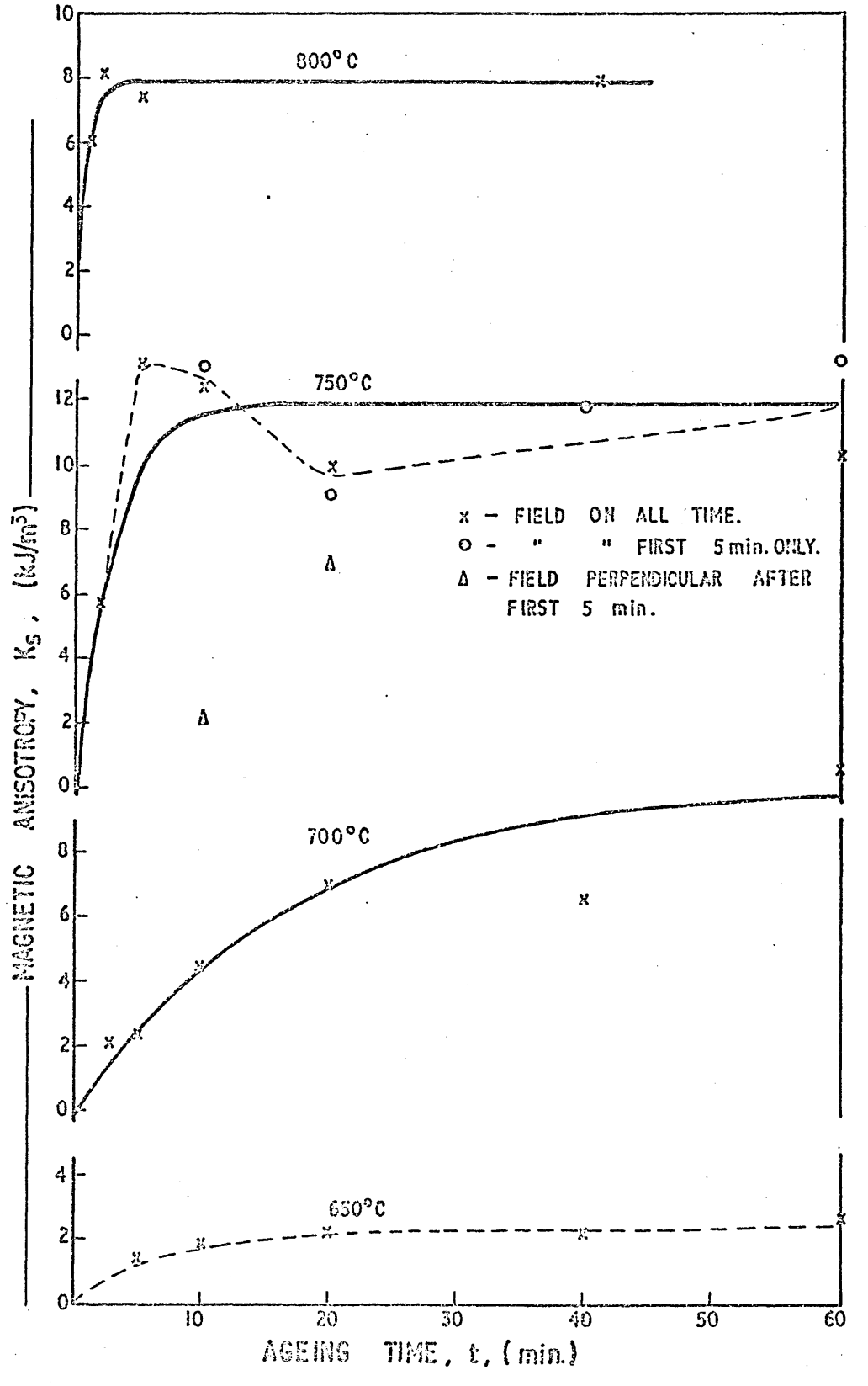

FIG. 61. VARIATION OF MAGNETIC ANISOTROPY WITH AGEING TIME AT THE INDICATED TEMPERATURES FOR ALCOMAX III.

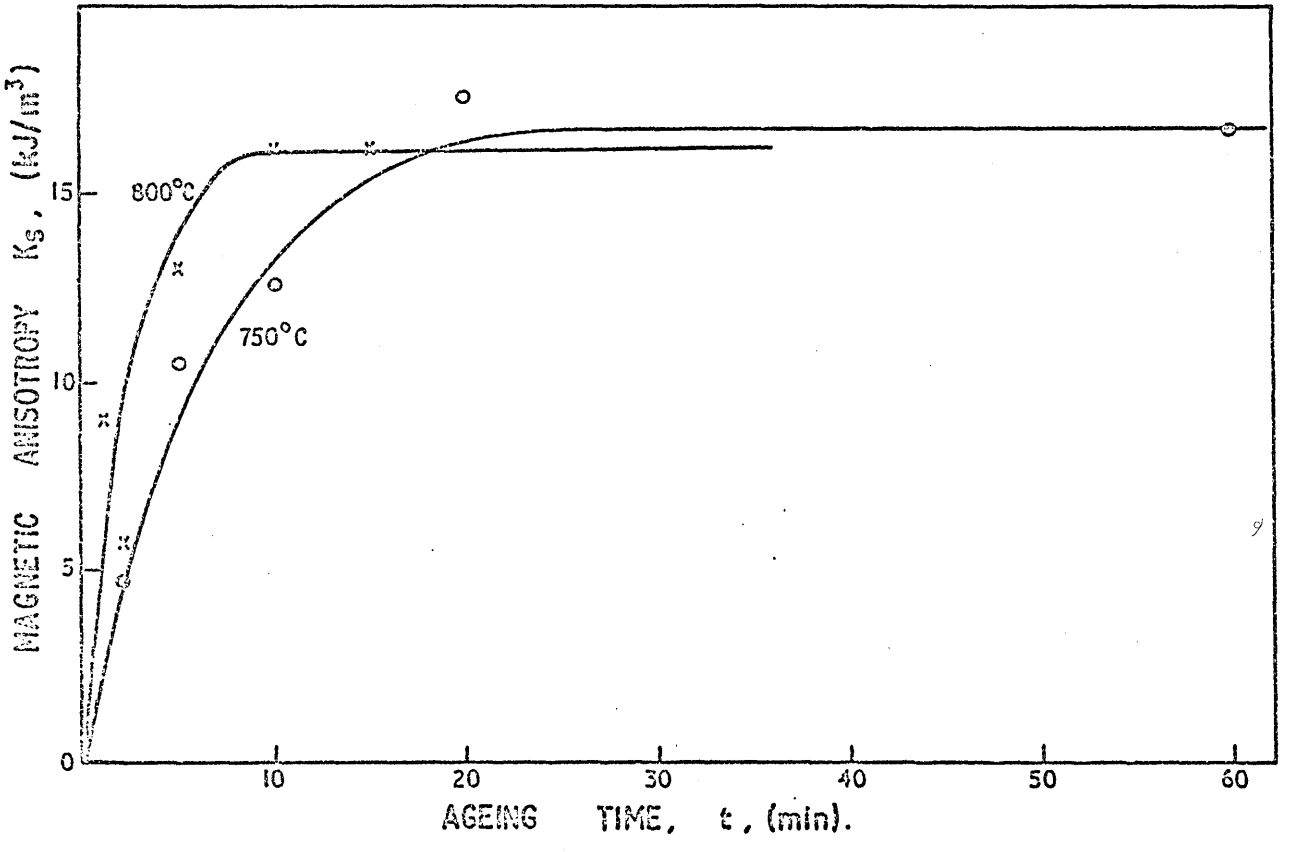

FIG. 62 VARIATION OF MAGNETIC ANISOTROPY WITH AGEING TIME AT 800°C AND 750°C FOR ALLOY A1.

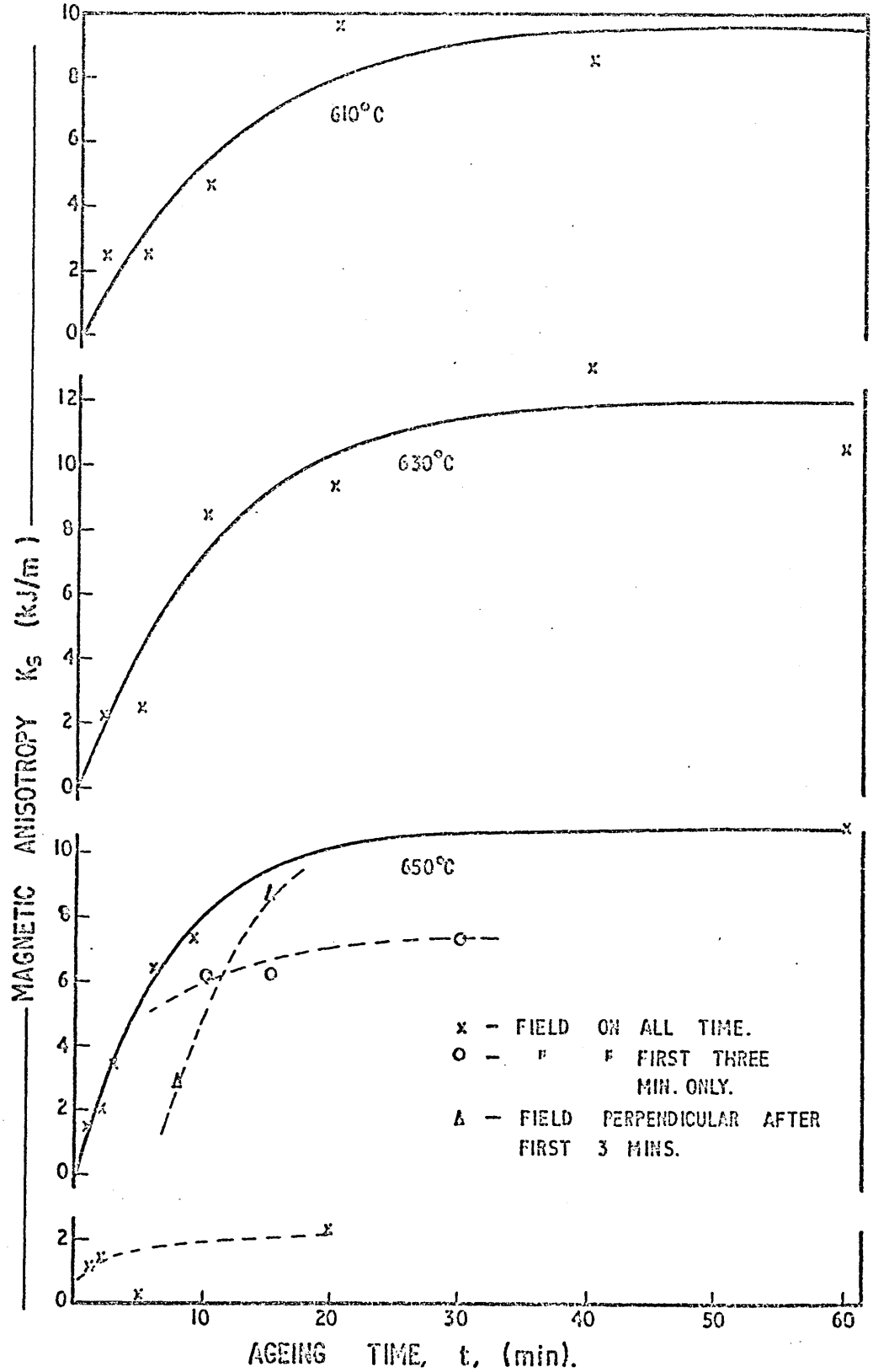

FIG. 63 VARIATION OF MAGNETIC ANISOTROPY WITH AGEING TIME AT THE INDICATED TEMPERATURES FOR ALLOY C1.

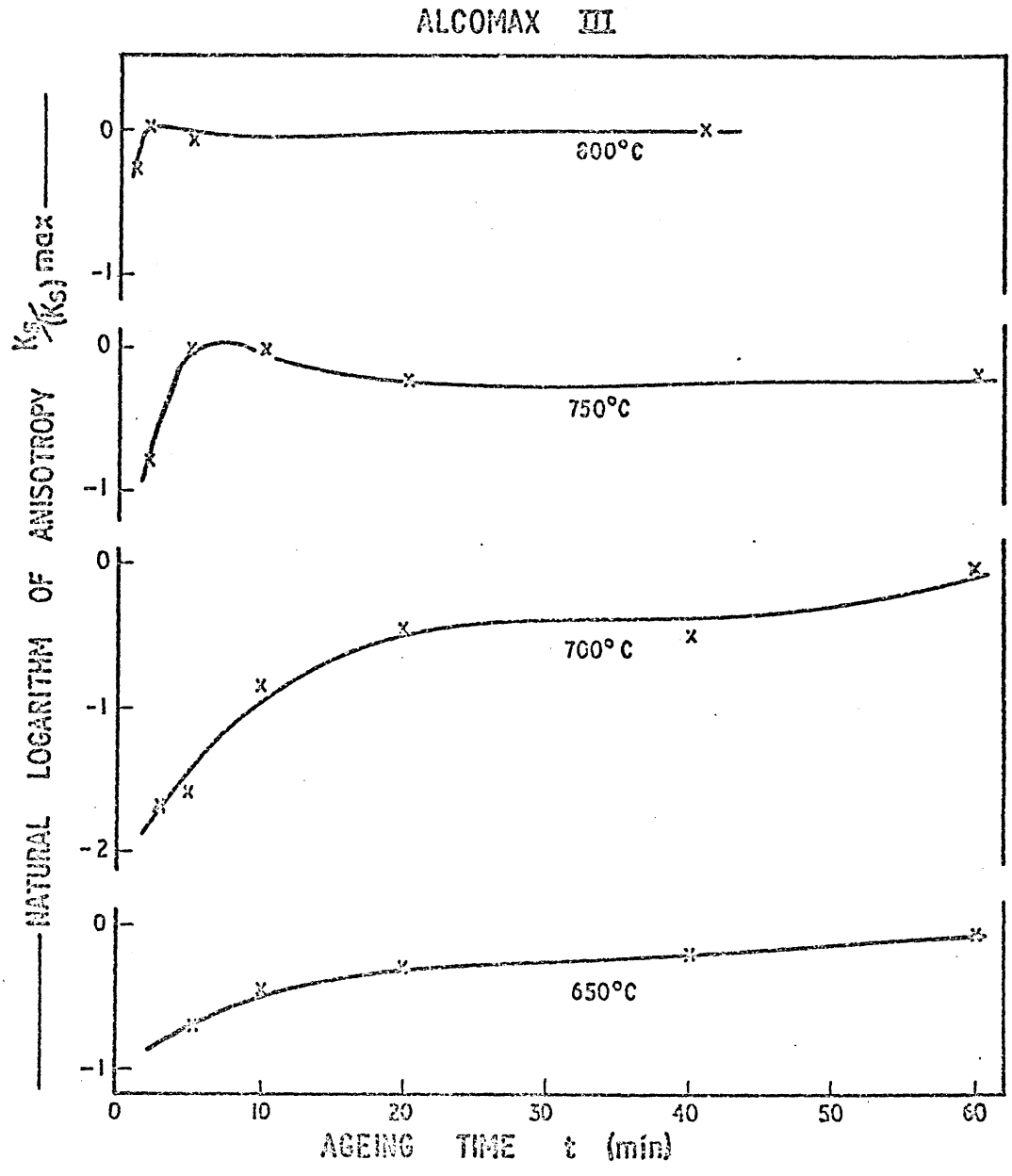

FIG. 64 VARIATION OF THE (NATURAL) LOGARITHM OF THE ANISOTROPY WITH AGEING TIME FOR ALCOMAX III AT THE INDICATED TEMPERATURES.

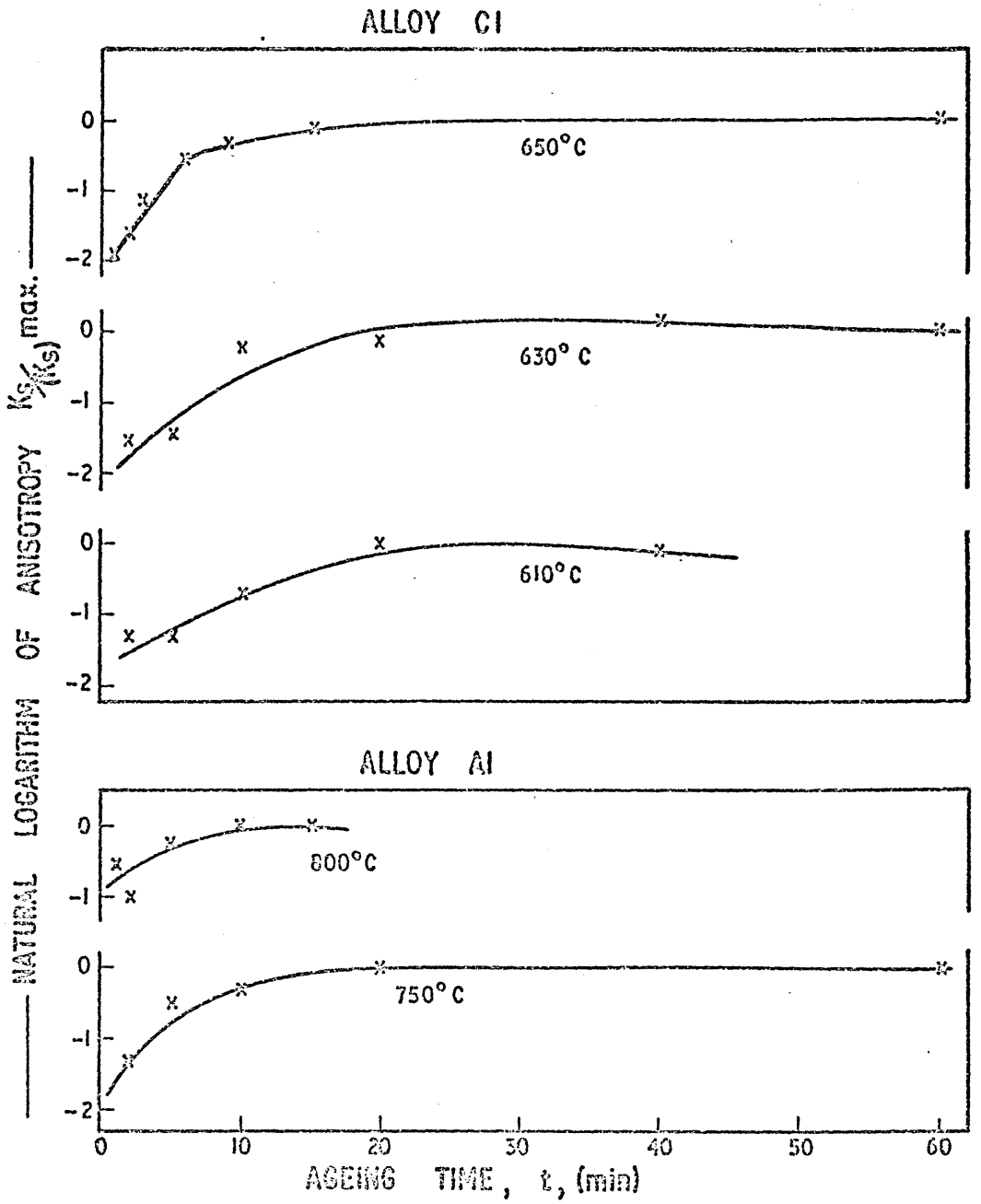

FIG. 65 VARIATION OF THE (NATURAL) LOGARITHM OF THE ANISOTROPY WITH AGEING TIME FOR ALLOYS A1 AND C1 AT THE INDICATED TEMPERATURES.

All the curves demonstrate that there is a levelling off of K_s with sufficiently prolonged ageing time as expected for a simple diffusion mechanism where the composition of the two phases will approach their equilibrium values given sufficient time. Fig 59, indicates the shape of the curve which is to be expected both (A) from non-steady state diffusion as discussed above and in section 5.3.1. and (B) the further adjustments of compositions as the particles coarsen, (sections 1.4.3. and 5.3.2.) if the data is plotted against $t^{-1/3}$.

Figs. 66, 67 and 68 show the same three sets of data as before, this time plotted against $t^{-1/3}$. The shape of many of these curves are again suggestive of mechanism (A), i.e. non-steady state diffusion with a linear region at intermediate values of $t^{-1/3}$ sharply levelling off at low values of $t^{-1/3}$ (i.e. long ageing times).

There is no evidence that coarsening has set in, as there is no further increase in K_s beyond the levelling off point. Indeed, there is some evidence in many of the curves that a slight reduction in K_s is occurring with long ageing times and this is discussed further in section 6.2.4.

6.1.3. Conventional precipitation or nucleation and growth

If transformation is occurring by nucleation and growth, then the kinetics of the reaction will presumably follow a relationship such as the Johnson-Mehl type of equation, the generalised version of which has already been given as equation (4.1).

However an effect on K_s will occur only if the precipitate is nucleated as elongated particles with some alignment relationship with the applied magnetic field, a possibility which was suggested some time ago by Kittel et al (119, 120). If it is assumed that the particles are sufficiently elongated as nuclei, such that $(N_a - N_c)$ is changed little by any further growth of these particles in the period when other

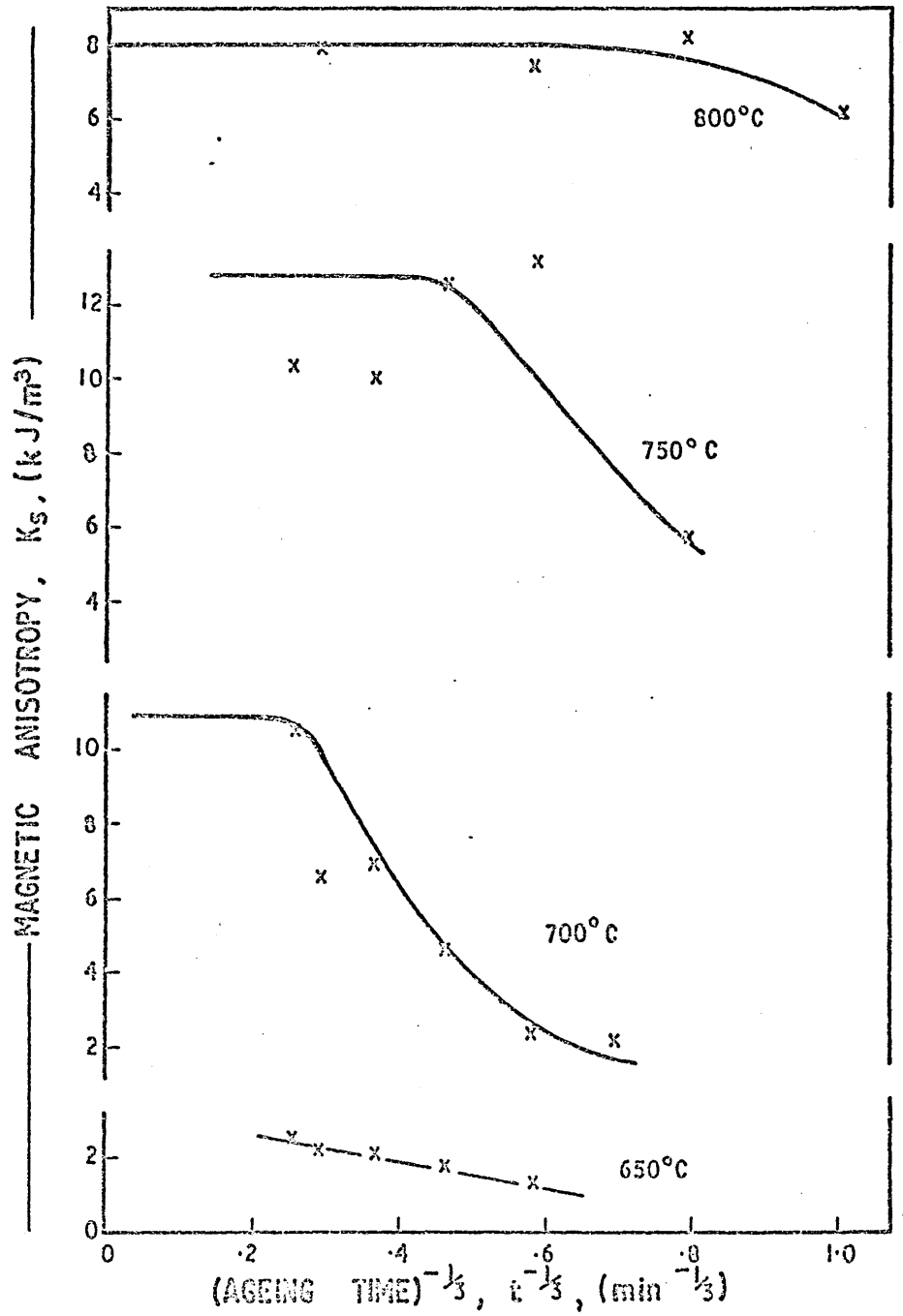

FIG. 66 VARIATION OF MAGNETIC ANISOTROPY OF ALCOMAX III WITH RECIPROCAL CUBE ROOT OF AGEING TIME AT THE INDICATED TEMPERATURES. (SOLID LINES ARE BEST FIT CURVES FOR DIFFUSION MECHANISM.)

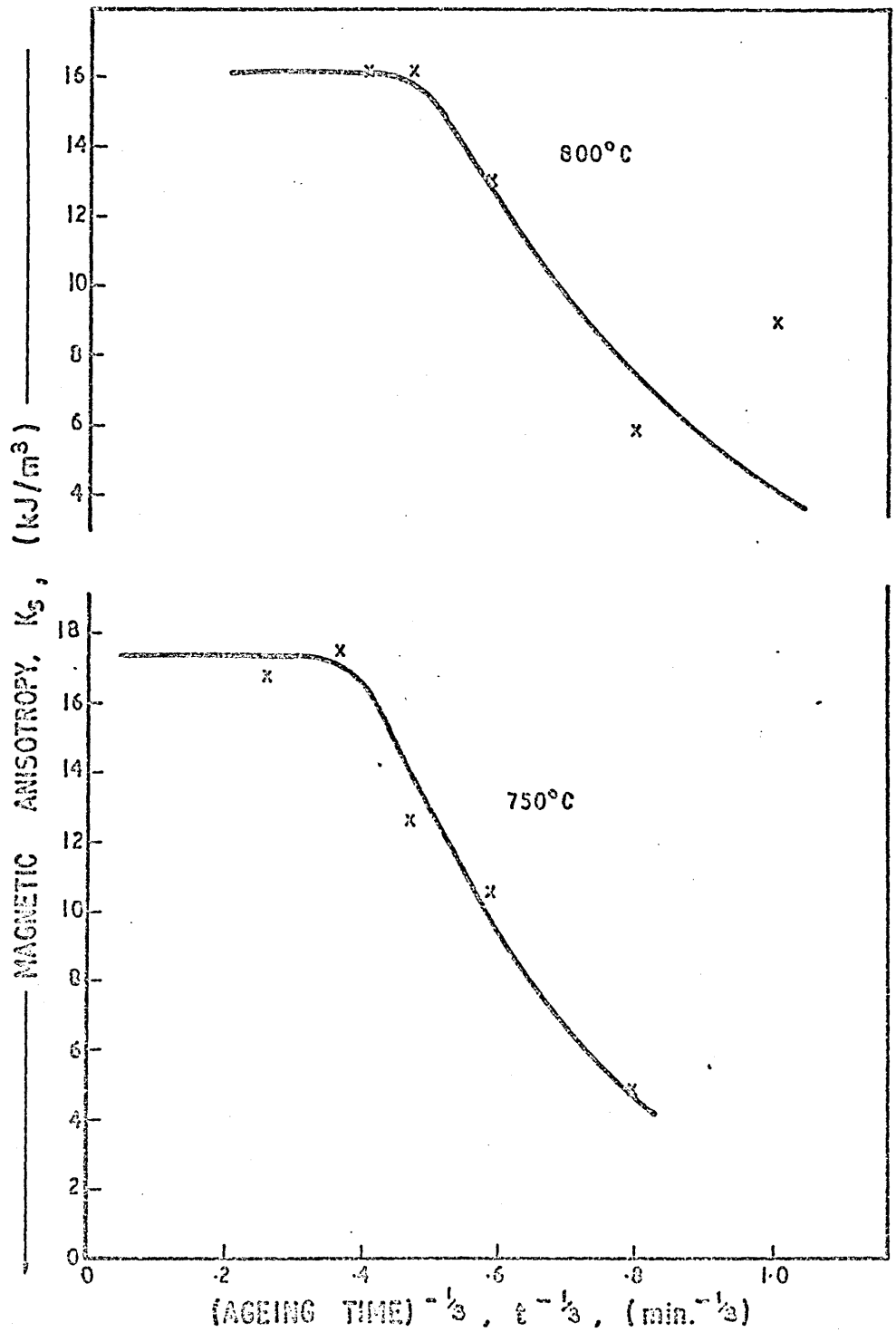

FIG. 67 VARIATION OF MAGNETIC ANISOTROPY OF ALLOY A1 WITH RECIPROCAL CUBE ROOT OF AGEING TIME AT THE INDICATED TEMPERATURES. (SOLID LINES ARE BEST FIT CURVES FOR DIFFUSION MECHANISM.)

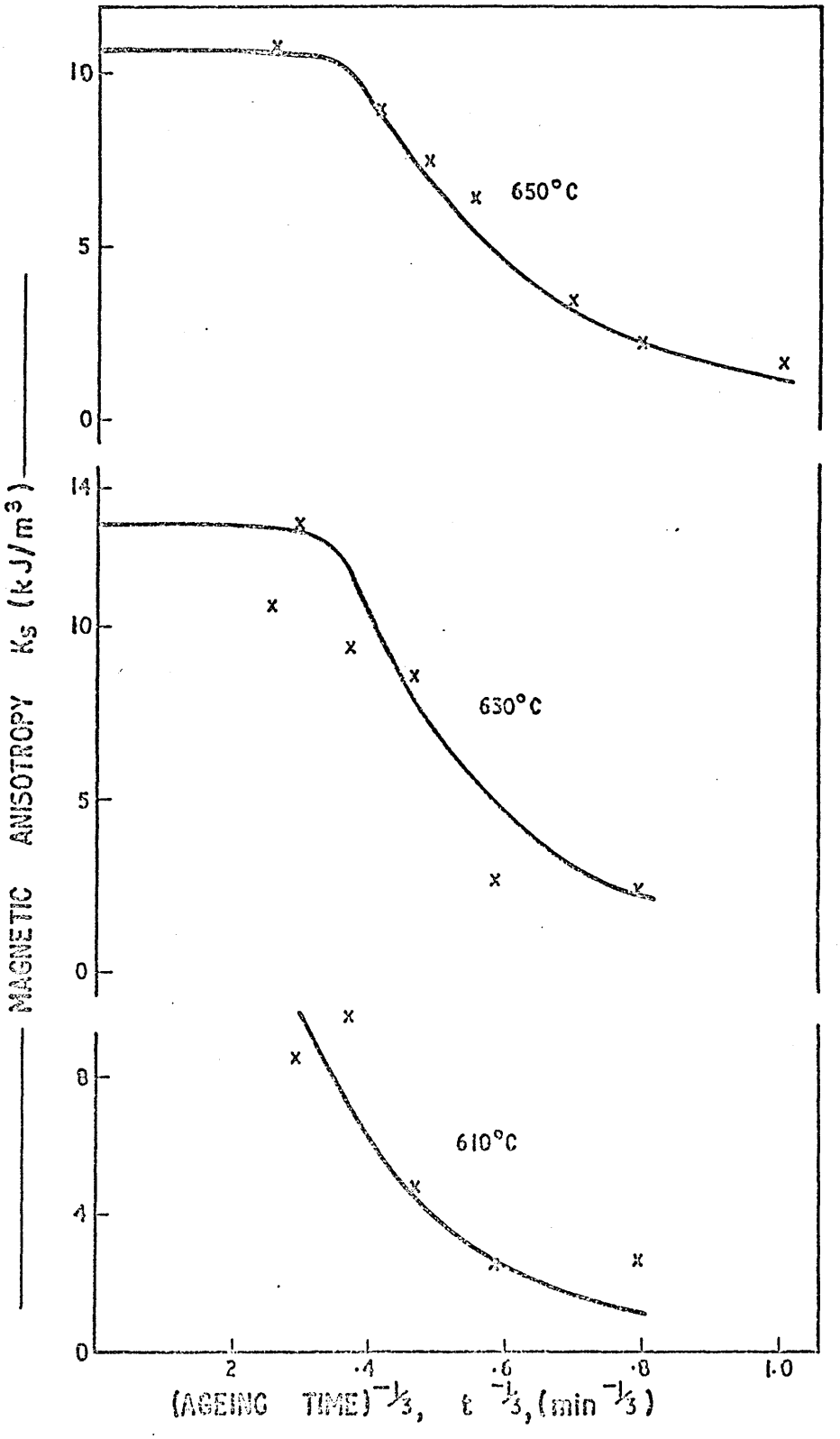

FIG. 68 VARIATION OF MAGNETIC ANISOTROPY OF ALLOY CI WITH THE RECIPROCAL CUBE ROOT OF AGEING TIME AT THE INDICATED TEMPERATURES. (BEST FIT OF PARTICLE DIFFUSION MECHANISM – SOLID LINES.)

such particles are precipitating, or that there is little growth anyway in the time period in which precipitation occurs, then equation (4.1) may give the relationship between the volume fractions of precipitate p at any given time t.

However this cannot be substituted directly as p (1-p) in equation (6.1) because ΔJ_s will also be changing since the composition of the matrix will be changing throughout the precipitation phase. If J_p is the saturation magnetisation of the precipitate phase and J_m that of the matrix i.e. $\Delta J_s = J_p - J_m$, at any moment of time -

$$J_s = p\, J_p + (1-p)\ J_m \quad \ldots\ldots\ldots\ldots \quad (6.4)$$

where J_s is the mean saturation which is at all times a constant because of the expected linear relationship between saturation magnetisation and composition (note this linearity relationship between J_s and composition has almost the status of a conservation law i.e. saturation magnetisation is neither created nor destroyed by and during exchange transformations in such solid solutions of metallic elements).

Rearranging equation (6.4)

$$\frac{J_p - J_s}{(1-p)} = J_p - J_m \quad \ldots\ldots\ldots \quad (6.5)$$

Substituting this in equation (6.1)

$$K_s = \frac{p}{(1-p)} \quad (N_a - N_c)\ (J_p - J_s)^2\ Q \quad \ldots\ldots\ldots \quad (6.6)$$

As J_p and J_s are both constants K_s will vary with $\frac{p}{(1-p)}$.

It should be noted however that p does not approach 1 as its maximum value as implied by the general equation (4.1) but some maximum value p_o less than one and perhaps ~ 0.5 when precipitation is complete so that -

$$p = p_o\ (1 - \exp\ [\ -At^m\ ]\ ) \quad \ldots\ldots\ldots\ldots \quad (6.7)$$

is applicable here, where A and m are constants. substituting equation (6.7) into (6.6)

$$K_s = \frac{(1 - \exp\left[-At^m\right])_m}{(1 - p_o\,(1-\exp\left[-At^m\right]))} \cdot \frac{p_o}{2\mu_o}(N_a-N_c)\,(J_p-J_s)^2 \quad \ldots\ldots(6.8)$$

Considering only the factors which vary with t i.e.

$$\frac{K_s}{(K_s)_{max}} = \frac{(1 - \exp\left[-At^m\right])}{(1 - p_o\,(1-\exp\left[-At^m\right]))}\,\frac{(1-p_o)}{p_o} \quad \ldots\ldots\ldots (6.9)$$

rearranging -

$$\exp\,(-At^m) = 1 - \left(\frac{[1-p_o][K_s]_{max}}{p_o\,K_s} + p_o\right)^{-1} \quad \ldots\ldots\ldots (6.10)$$

A ln ln plot of the right hand side of equation (6.10) against the logarithm of the ageing time, should, if this mechanism is correct, give a straight line plot. In fact the data of tables XV - XVlll when presented in this way gives even more non-linearity than the simpler $\ln\left\{K_s/(K_s)max\right\}$ plots already given in Figs. 64, and 65 (the use of values of p_o ranging from 0.4 to 0.6 makes little difference) in that any linearity at the beginning of ageing is also absent. The same conclusions apply then to this mechanism in that there is no substantial support for it since the curves are not linear, and at long ageing times still level off sharply.

The characteristic shape of the curve (p v. 1-exp $\left[-At^m\right]$) of the curve represented by equation (6.7) is sigmoidal and is expected to contain an "incubation" time period before any precipitation commences. Figs. 61, 62 and 63 show no evidence of any measurable incubation period for the data. Decomposition into already elongated particles appears to begin with the commencement of the ageing treatment.

6.1.4. Particle elongation during ageing in a magnetic field

The final alternative, considered here, that of elongation as the particles coarsen during ageing in a magnetic field, was the mechanism exploited by Zijlstra for ageing of Alnico 5 for long

periods in a magnetic field.

A relationship given in Fig 56. is expected for plots of K_s against $t^{-1/3}$ indicating that linearity and continued increase in K_s is expected for the longest ageing times - i.e. approaching $t^{-1/3} = 0$

where $K_s = (K_s)max - k\, t^{-1/3}$ ..... (6.11)

where k is a constant. However such plots of the data shown in Figs. 66, 67 and 68 indicate that although there is indication of a linearly decreasing region with increasing $t^{-1/3}$ it is not near $t^{-1/3} = 0$, and in fact there is indications of levelling off or some reduction in K_s for the smaller values of $t^{-1/3}$. The curves are more suggestive of the behaviour expected for the NSS diffusion mechanism when plotted against $t^{-1/3}$ as shown in Fig. 59, as already discussed.

6.1.5. Other possible factors affecting magnetic anisotropy variations during ageing

The possibility that the occurrence of other phase transformations, involving other non or lesser ferromagnetic phases, are affecting the magnetic anisotropy or other magnetic properties is ruled out by the trend of the saturation magnetisation with ageing at various temperatures for Alcomax 111 and the A1 and C1 alloys. The saturation magnetisation results from tables XV, XV1 and XV11 are plotted against ageing time at the various ageing temperatures in Fig 69.

At most of the temperatures the trend of the saturation magnetisation for all the alloys can be seen to drop slightly and in a linear manner with increasing ageing time. The slight changes with ageing time probably represent the extent to which composition as measured in atomic fraction or percentage, and saturation magnetisation deviates from linearity over large changes of composition. Alternatively some slight changes in the lattice parameter with long ageing times may occur perhaps connected with the gradual loss of coherency of the particles with the matrix.

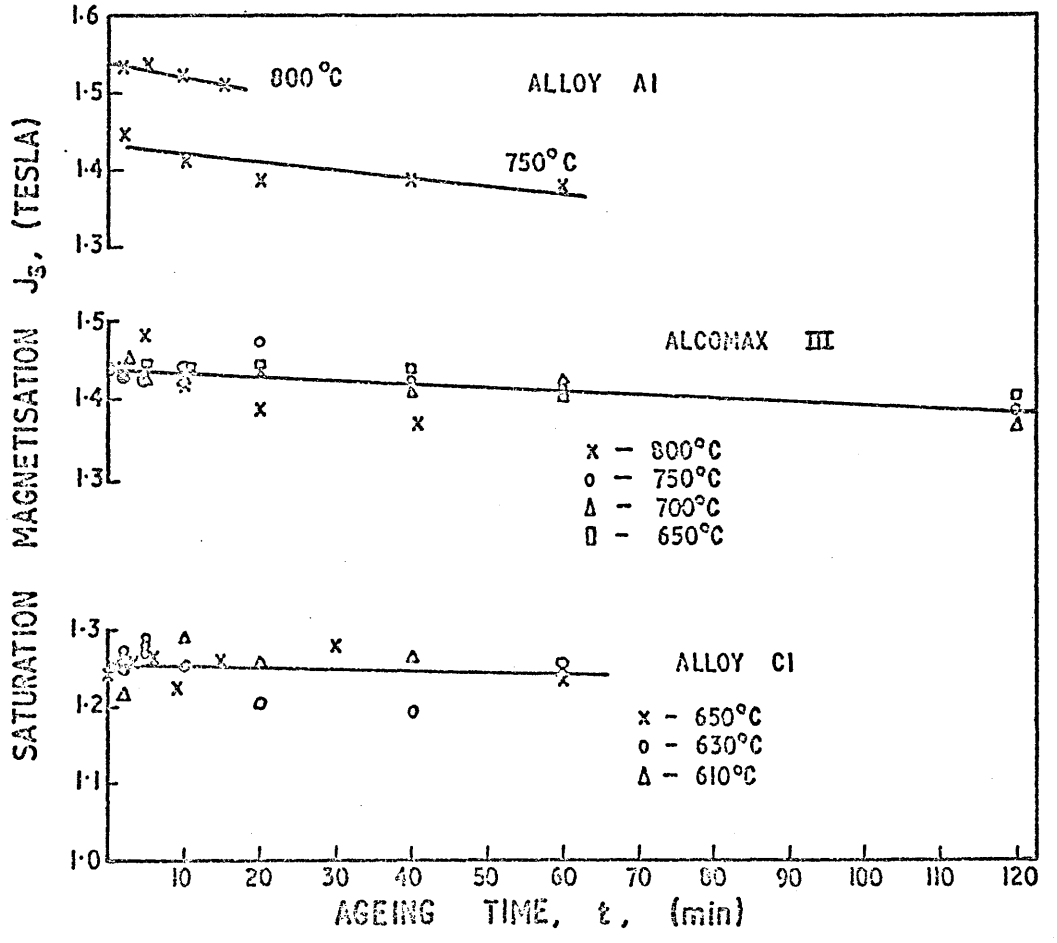

FIG. 69 VARIATION OF SATURATION MAGNETISATION WITH AGEING TIME IN A MAGNETIC FIELD AT THE INDICATED TEMPERATURES FOR ALLOYS AI AND CI AND ALCOMAX III.

Major changes in J_s seem only to occur in Alloy C1 when aged at 675°C. This may presumably be attributed to formation of sigma or σ phase which, according to the Fe-Cr phase diagram in Fig. 19 occurs at such temperatures. According to some recent Russian work (174) on Fe-Cr-Co alloys with 31-32% Cr and 20% Co, the σ phase is present after 4 hour ageing at 650°C and the alloy is completely converted to σ after 24 hours at 650°C, 4 hours at 675°C or 30 min. at 700°C. The phases in this work were identified by neutron and X-ray diffraction. The formation of σ phase begins at the grain boundries and has a cellular structure. Workers at the Permanent Magnet Association Research Laboratory (164), found that both the σ phase and the f.c.c. phase normally found at high temperature (see Fig.20) were both non-ferromagnetic. If either of these phases were formed during ageing then a drastic effect on the saturation magnetisation could therefore be expected. As this did not happen (except for alloy C1 at 675°C) it was concluded that these phases were absent over the ranges of times and temperatures used. Optical and electron microscopy supported this conclusion.

Another possibility, that the occurrence of excessively large grains in certain samples could alter the mean grain orientation factor, Q, was checked by microexamination of a number of samples from each alloy. The samples examined, all had a similar distribution of grain size of 0.15 - 0.25 mm mean dimension. It must be conceded that some chance matching of orientations of grains within individual samples may have accounted for some of the scatter of results, however it cannot account for the main trends of the data.

6.1.6. Further considerations of Zijlstra's magnetic anisotropy results for Alnico 5.

Figs. 25 and 26 show the magnetic anisotropy data obtained by Zijlstra (51) during ageing of both single crystal and polycrystalline

samples of Alnico 5 at various temperatures. Figs. 70 and 71 show the same data when plotted against the reciprocal cube root of the ageing time ($t^{-1/3}$), which, according to the Zijlstra mechanism, involving simultaneous coarsening and elongation of the particles in the magnetic field as discussed in Chapter 5 (section 5.2), should, at low values of $t^{-1/3}$ (i.e. long ageing times), be linear. Figs. 70 and 71 indeed show this expected linearity for his results.

Zijlstra's measurements were actually made at the ageing temperature. At these temperatures the magnetisation of the matrix must be considerably lower than at room temperature since the K_s values obtained are nearly an order of magnitude higher, in general, than the room temperature values of K_s reported here.

Since K_s is proportional to $(J_p - J_m)^2$, J_m, the saturation magnetisation of the matrix needs to be approximately $\frac{1}{3}$ of its room temperature value to explain this effect (assuming J_p, the saturation magnetisation of the particles is roughly the same at both temperatures). De Vos (80) also found that the coercivity of Alnico 5 after ageing for 2 minutes at 830°C and quenching, increased only relatively slowly when measured at increasing temperatures up to about 620°C, but then proceeded to increase much more rapidly (and non-reversibly) from about 8 kA/m at 620°C up to 32 kA/m at about 740°C. The saturation magnetisation of the alloy fell by about 20% over the same temperature range (620-740°C) and a total of about 50% between 620°C and 800°C. Although the difference in saturation magnetisation is apparently large, both phases still remain ferromagnetic in the region 700-800°C, at least for relatively short ageing times since there is no apparent Curie point, i.e. "kink" in the saturation magnetisation temperature curve, representing the matrix phase, in this temperature region and indeed right up to the Curie point for the alloy as a whole, which is about 860°C.

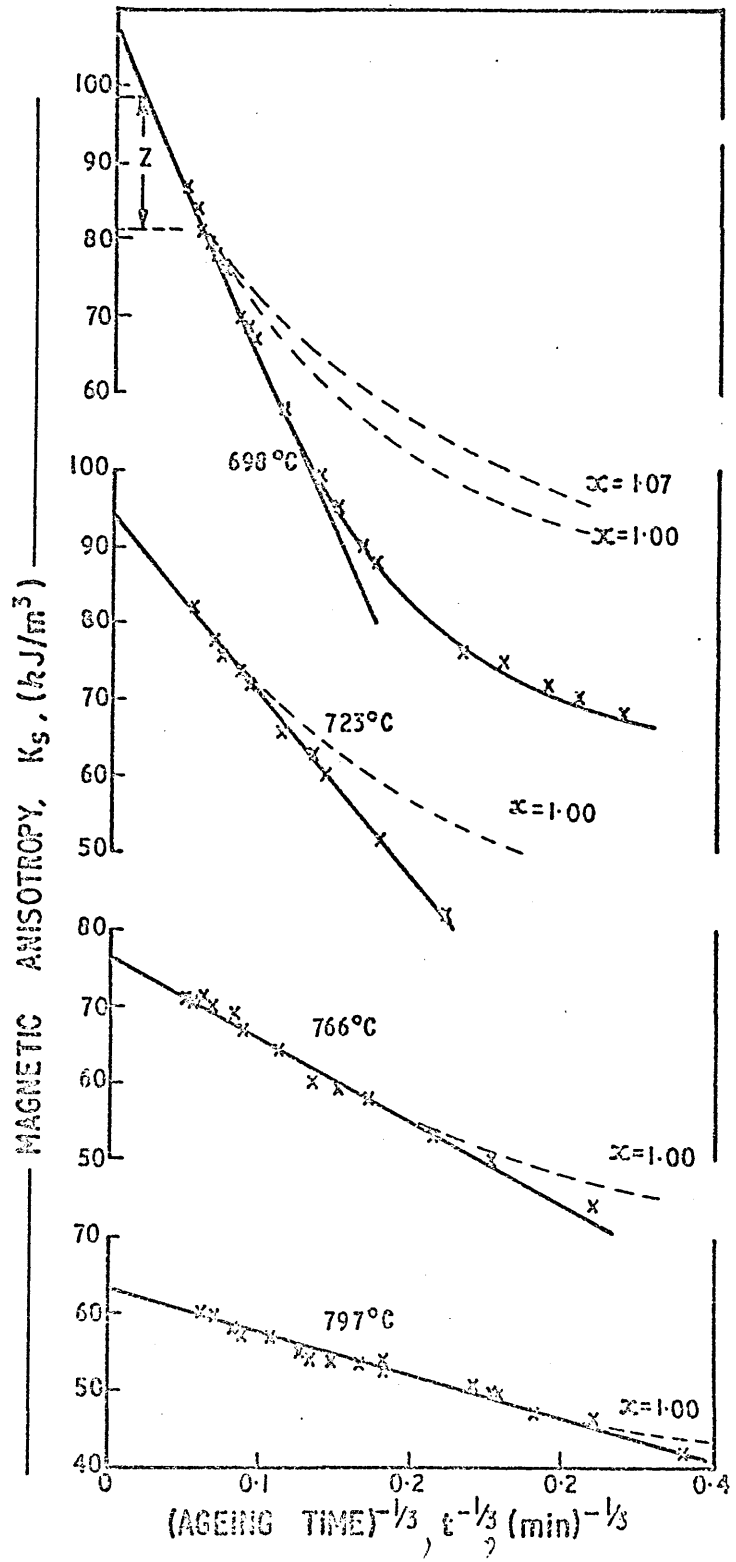

FIG. 70 ZIJLSTRA'S MAGNETIC ANISOTROPY RESULTS [51] FOR POLYCRYSTALLINE ALNICO 5 SAMPLES, PLOTTED AGAINST THE RECIPROCAL CUBE ROOT OF THE AGEING TIME.

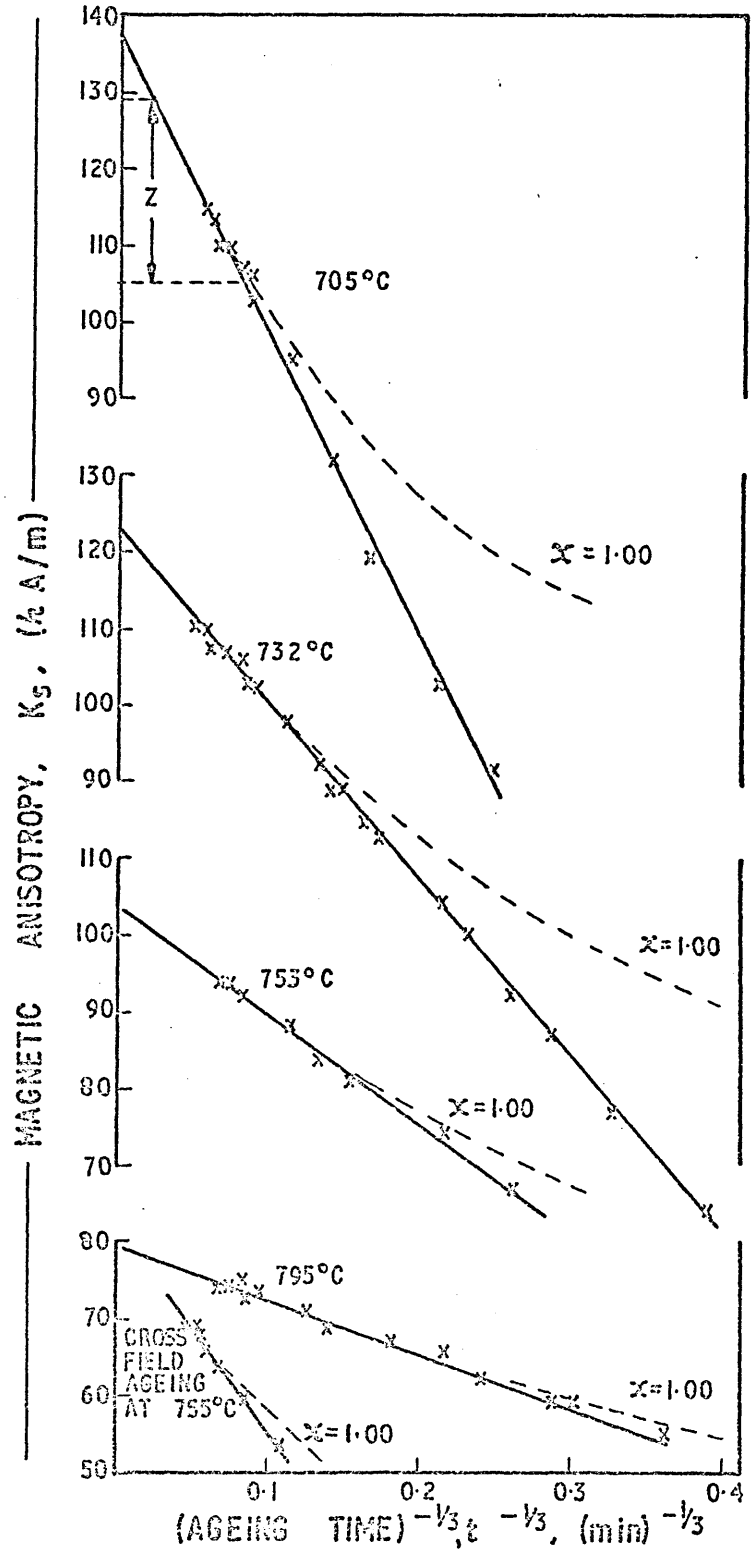

FIG. 71 ZIJLSTRA'S MAGNETIC ANISOTROPY RESULTS [51] FOR SINGLE CRYSTAL SAMPLES OF ALNICO 5, PLOTTED AGAINST THE RECIPROCAL CUBE ROOT OF THE AGEING TIME.

Two compensatory effects can be envisaged in this temperature range. As the temperature is increased, assuming the composition of the particles and matrix remains unchanged (i.e. very fast increase in temperature) the saturation magnetisation of the matrix will be reduced towards zero in the normal way following the J_s - T curve for that particular composition. However, the higher the temperature then the closer the equilibrium compositions of the particles and matrix will be to the top of the miscibility gap, as shown in Fig. 72. Diffusion between the phases will therefore occur so that the compositions of particles and matrix tend to move closer together, i.e. a tendency to reduce the magnetisation of the particles and increase that of the matrix. If the composition of the matrix at T_1 is C_1 with a corresponding saturation magnetisation of J_1 a fast increase of temperature to T_2 will cause the magnetisation of the matrix to be reduced to zero as represented by point x in Fig. 72. Diffusion will then occur changing the composition from C_1 to the equilibrium composition C_2 and the saturation magnetisation of the matrix will move up the J_s composition curve for T_2 from x to J_2.

Although this is a hypothetical situation, such relationships are certainly to be expected in this alloy. According to Oliver and Goldschmidt (82) separation into $\alpha + \alpha'$ in a 24% Cobalt Alnico alloy occurs at 810°C on cooling as determined by X-ray diffractometry, and according to Marcon et al.(175) occurs at about 830°C for Alnico 5, as determined by both dilatometric and differential thermal analysis. The latter workers also determine the Curie point at 850°C for Alnico 5. Such examples from the literature thus confirm that temperatures approaching 800°C are certainly close to both the top of the miscibility gap and the Curie point.

The above conditions also explain why no extra Curie point

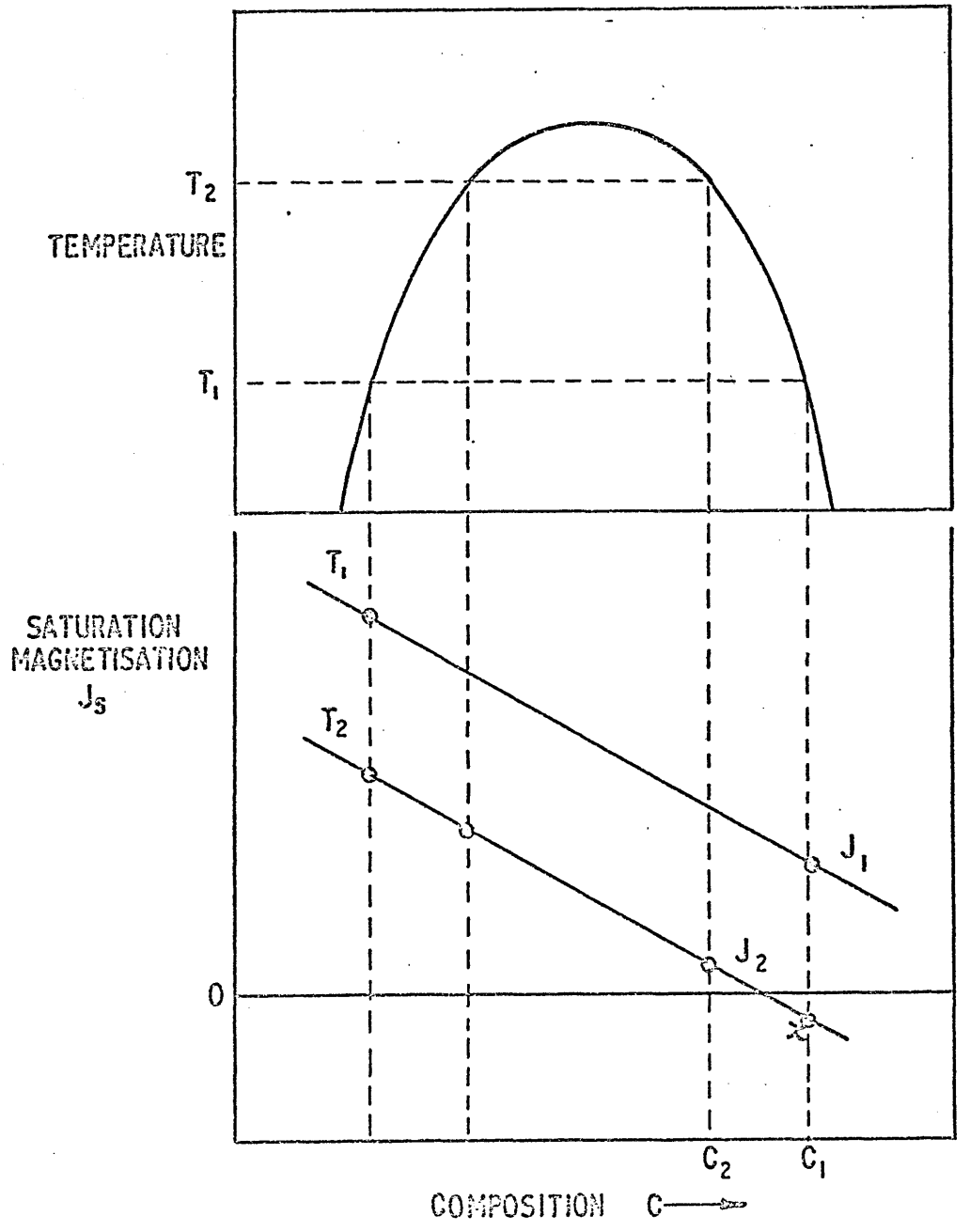

FIG. 72 SCHEMATIC DIAGRAM ILLUSTRATING CHANGES IN SATURATION MAGNETISATION WITH COMPOSITION FOR DIFFERENT TEMPERATURES AND SUBSEQUENT DIFFUSION FOR TWO PHASES WITHIN THE MISCIBILITY GAP.

representing the matrix appears in the J_s temperature curves for Alnico 5. i.e. being small, the particles can change their composition sufficiently rapidly so that reversion to a single phase occurs almost simultaneously with the occurrence of the Curie point.

Zijlstra (51) found that J_s for the alloy as a whole, when measured at room temperature, remained constant with ageing time for periods up to 100 hours, in this temperature range (i.e. 700-800°C). If the matrix had become non-ferromagnetic at sometime during ageing then this constant linear value could not have been expected to continue since the particles would then change in magnetisation by further diffusional transfer of atoms without any compensating magnetic change in the matrix.

A basic assumption in Zijlstra's theory is that the particles are expected to coarsen without any change in the composition of either particles or matrix. However this is contrary to what is expected in coarsening over long periods since, as the smaller particles tend to dissolve and therefore the mean particle size increases, the solubility of the solute elements in the matrix is reduced. The average concentration, C, of a particular solute in the matrix is related to the average particle radius, r, by the Gibbs-Thomson equation (142, 143) -

$$\Delta C = C - C_e = \frac{Z \gamma C_e V_m}{r RT} \quad \ldots\ldots\ldots (6.12)$$

where γ is the interfacial free energy of the particle matrix interface, C_e is the concentration of solute in the matrix in equilibrium with a particle of infinite size, V_m is the molar volume of the particle, and RT has its usual meaning.

The relationship between ΔC and the ageing time, t, is obtained simply by re-writing equation (6.12) for r and substituting into equation (1.45), which is the coarsening relationship for change of r with t.

As already given in equation (148) and discussed in Chapter 1, this substitution reveals that proportionality should exist between ΔC and $t^{-1/3}$ at long ageing times. Also using the expected proportionality between ΔC and ΔJ_s and equation (6.1) it is expected then that $K_s \propto t^{-1/3}$ at long ageing times.

However, only the composition of the matrix C_m, is changing towards some equilibrium value C_e and that of the particles, C_p, is fixed :- $J_s = J_p - J_m = B\,(C_p - C_m)$ with (in this instance) $\Delta C = C_m - C_e$ where B is a constant of proportionality so that $\Delta J_s = (C_p - C_e) - (C_m - C_e)$ therefore -

$$J_s = A - B\,(\Delta C) = A - kt^{-1/3} \propto \sqrt{K_s} \qquad \ldots\ldots\ (6.13)$$

where $A = B\,(C_p - C_e)$ i.e. this is a similar expression to that of Zijlstra (equation 6.11) except that the proportionality for the composition changes is with $\sqrt{K_s}$.

Zijlstra's data is presented as $\sqrt{K_s}$ v. $t^{-1/3}$ in Figs.73 and 74. Most of this data is linear with $t^{-1/3}$ over the complete range of ageing times.

There are thus two effects (or three if the non-steady state diffusion mechanism is included) which predict some linearity for a $t^{-1/3}$ plot i.e. that due to particle elongation as formulated by Zijlstra's original theory, and that expected from changes of matrix composition with particle coarsening irrespective of any elongation effect. Correlation coefficients of the linear parts of the Zijlstra plots and the corresponding coefficients for the same points when plotted against $\sqrt{K_s}$ are very similar indicating no significant improvement in linearity for either mechanism. However, referring back to Fig. 56, which shows the whole theoretical curve for K_s against $t^{-1/3}$, it can be seen that linearity with $t^{-1/3}$, for the particle elongation mechanism should only be expected over a very restricted range, (Zijlstra's original numerical solutions also indicated that linearity could only be expected over the given range), i.e. for relatively small values of $t^{-1/3}$.

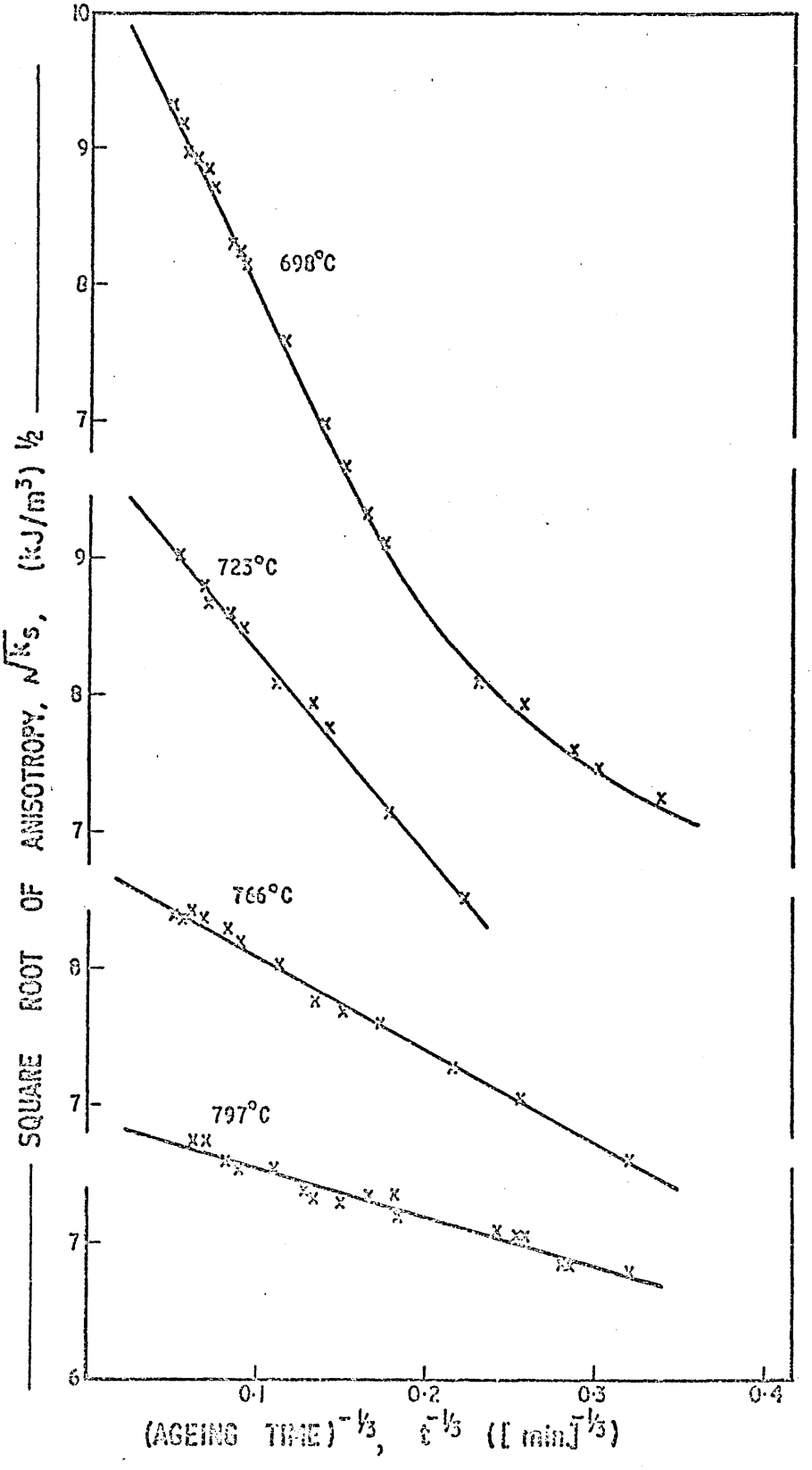

FIG. 73 ZIJLSTRA'S MAGNETIC ANISOTROPY RESULTS FOR POLYCRYSTALLINE ALNICO 5. $\sqrt{K_s}$ v. AGEING TIME TO POWER $^{-1/3}$

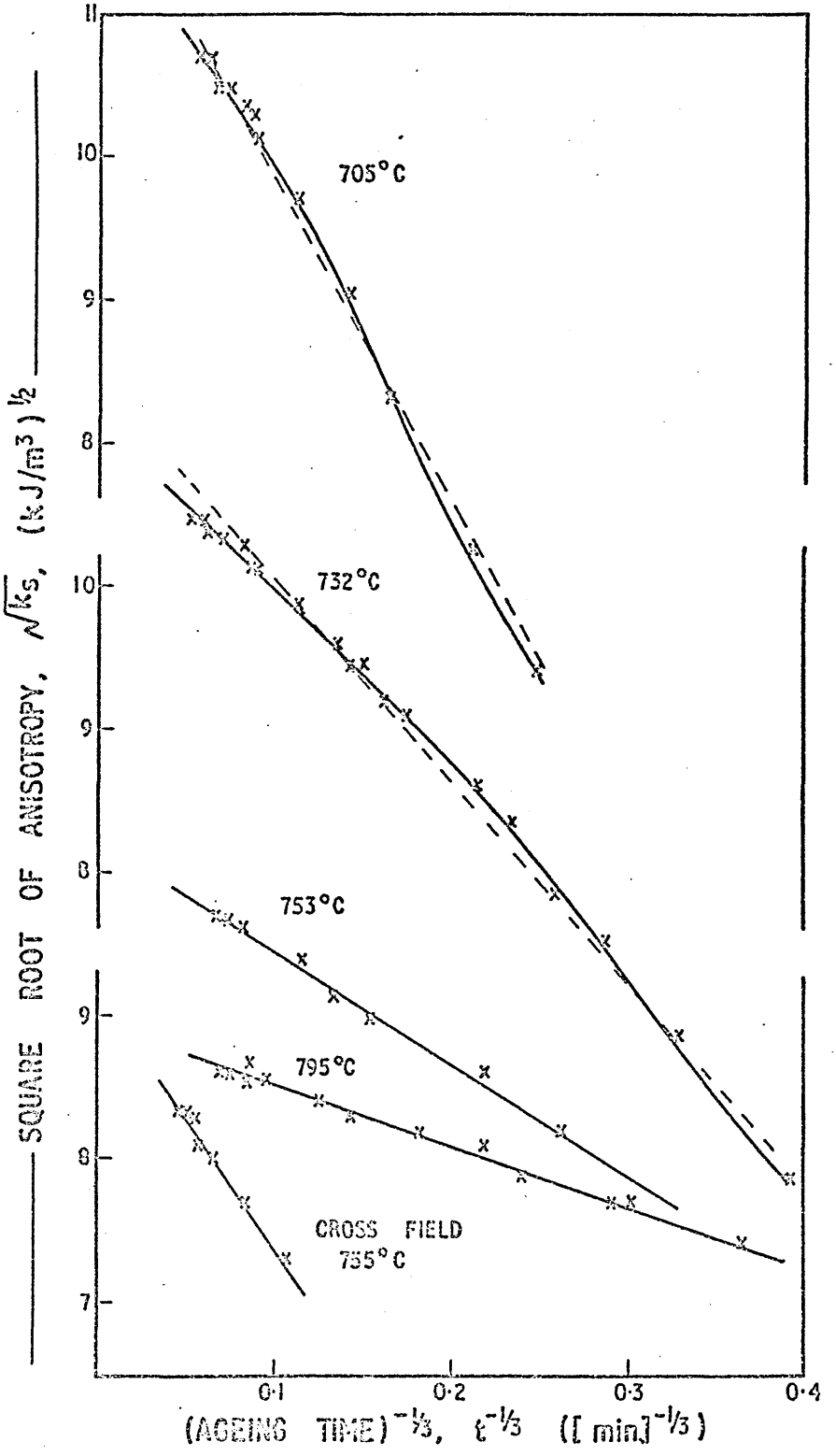

FIG. 74. ZIJLSTRA'S MAGNETIC ANISOTROPY RESULTS FOR SINGLE CRYSTALS OF ALNICO 5. $\sqrt{k_s}$ v AGEING TIME TO POWER $^{-1/3}$

If the maximum values of K_s predicted by Zijlstra's analysis are used to work out a value of $K_s/(K_s)max.$ for each data point, then from equation (6.1).

$$\frac{K_s}{(K_s)max} = (N_a - N_c) \quad \ldots\ldots\ldots \quad (6.14)$$

since the only variable is assumed to be $(N_a - N_c)$ and its maximum value is ½. All values of $(N_a - N_c)$ have a corresponding particle dimension ratio $m = \frac{c}{a}$. Figs. 75 and 76 show these values of m, obtained in this way from K_s, plotted against $t^{0.26}$. To conform with equation (5.32), expected to apply in the Zijlstra theory, the data should be linear with intercept on the m axis of about unity as shown in Fig. 55. (or about 0.7 according to the numerical solutions of Zijlstra (51), which applied over the restricted range of approximately $3 < m < 10$).

At the longer ageing times some deviation from linearity, and in particular a large amount of scatter are evident at the higher ageing temperatures in Figs. 75 and 76. Such scatter is not noticed in a $t^{-1/3}$ plot since for large values of t the points are crowded together.

In an attempt both to isolate a likely mechanism and demonstrate the actual precision of the data, a generalised form of equation 6.11 is considered i.e.

$$K_s^{\,n} = A - Bt^{-q} \quad \ldots\ldots\ldots \quad (6.15)$$

It is not possible to determine the best n or q by plotting the data in logarithmic form since the sum of two terms is involved in equation (6.15). Instead various values of n and q have been assumed and the correlation coefficient calculated for each pair of values from the data of Zijlstra. Fig. 77 shows the variation of the Z transformation of the correlation coefficients for two values of

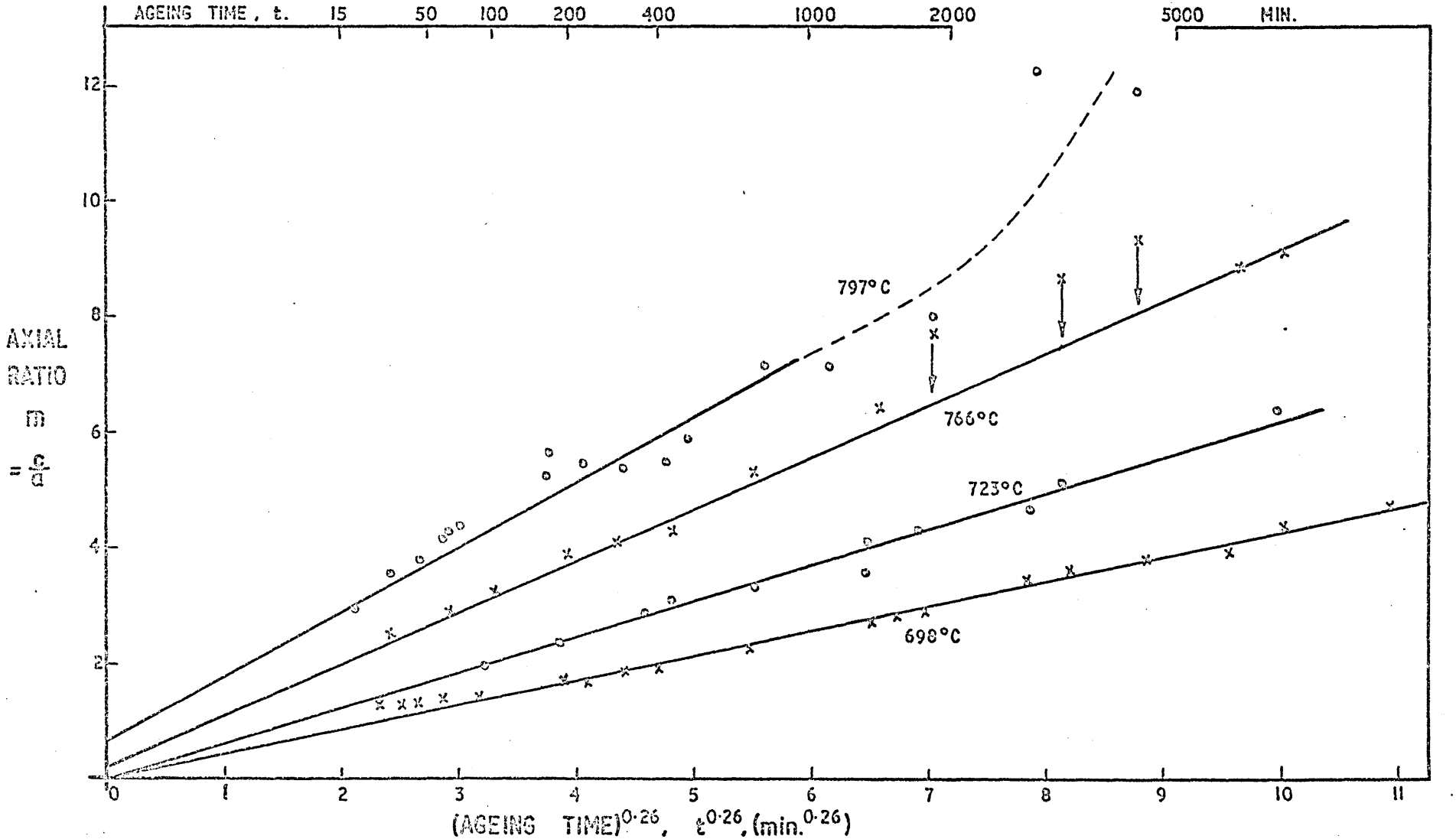

FIG. 75 MEAN AXIAL RATIO OF PARTICLES v AGEING TIME TO THE POWER 0·26 - CALCULATED FROM ZULSTRA'S ANISOTROPY RESULTS [51] ASSUMING INFINITE m FOR EXTRAPOLATION OF $t^{-\frac{1}{3}}$ TO ZERO IN FIG. 70. (FOR POLYCRYSTALLINE SAMPLES)

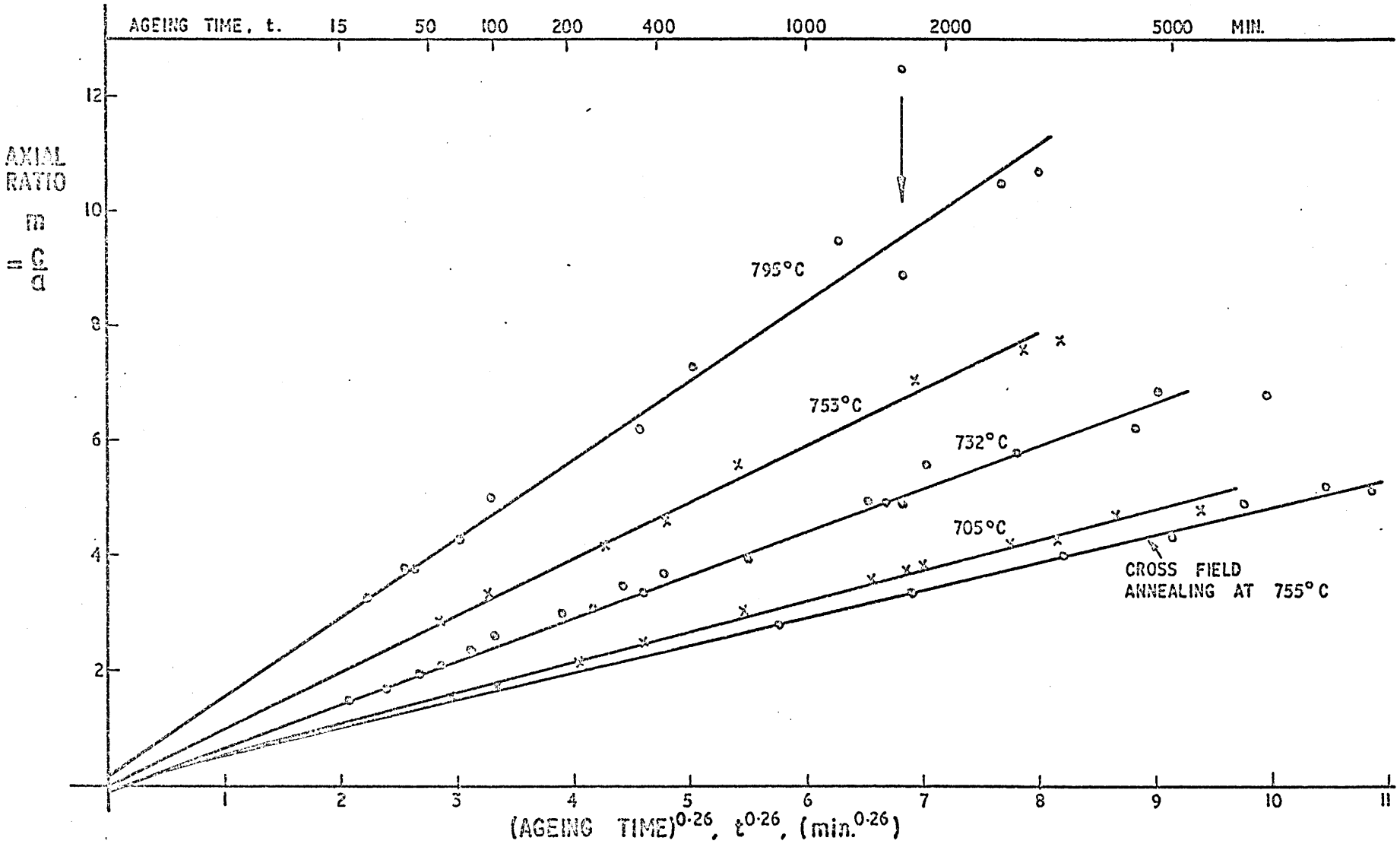

FIG. 76 MEAN AXIAL RATIO OF PARTICLES v AGEING TIME TO THE POWER 0·26 CALCULATED FROM ZIJLSTRA'S ANISOTROPY RESULTS [51] ASSUMING INFINITE m FOR EXTRAPOLATION OF $t^{-1/3}$ TO ZERO IN FIG. 71 (FOR SINGLE CRYSTAL SAMPLES.)

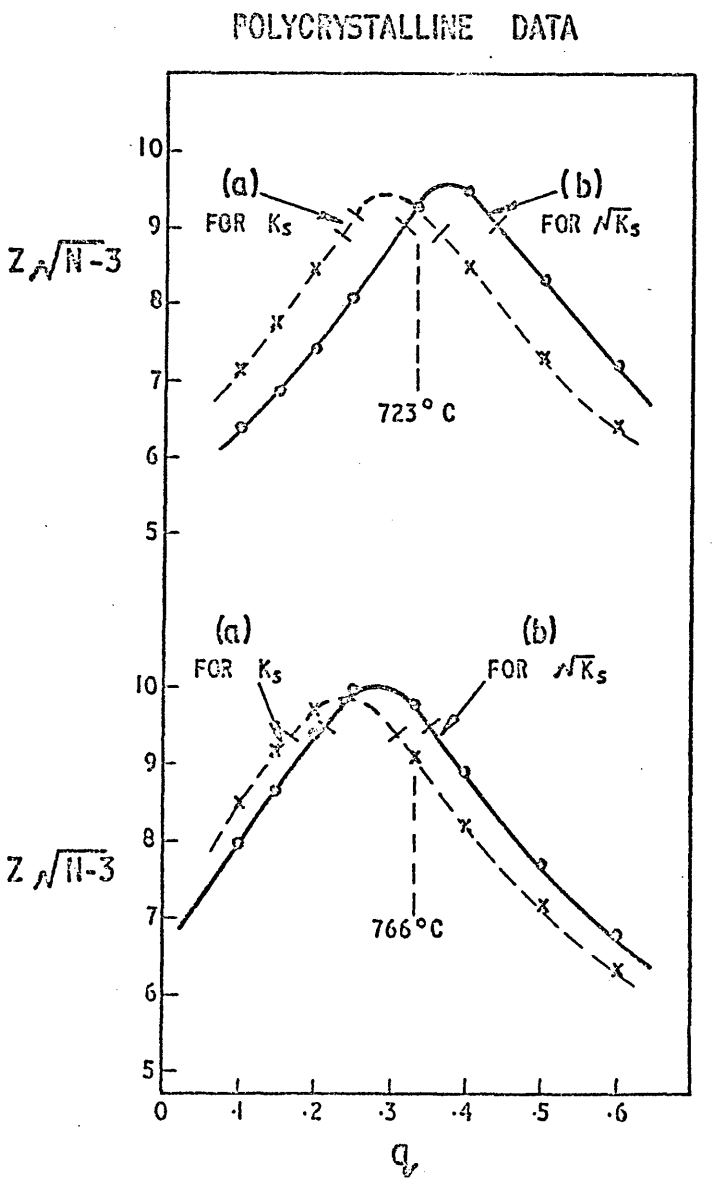

FIG. 77 VARIATION OF Z-TRANSFORMED CORRELATION COEFFICIENT FOR (a) K_S v ℓ^{-q} AND (b) $\sqrt{K_S}$ v ℓ^{-q} Z IS PLOTTED IN UNITS OF VARIANCE = $(N-3)^{-\frac{1}{2}}$ WHERE N IS THE NUMBER OF DATA POINTS.

n, i.e. unity and ½, over values of q from 0.1 to 0.6 for two of the sets of ageing data for the polycrystalline alloy. The Z- transformation is given by -

$$Z = 1.15 \frac{\log (1 + r)}{\log (1 - r)} \quad \ldots\ldots\ldots\ldots \quad (6.16)$$

where r is the correlation coefficient.

r is not distributed normally but Z is, with a variance of $1 / \sqrt{N-3}$ where N is the number of data points. Z is given in Fig.77 in units of the variance so that the variations are comparable from curve to curve and the mathematical significance is more easily assessed. For example a variation which is of the order of unity can be considered to be highly significant. These curves indicate that $t^{-\frac{1}{4}}$ law may be more appropriate for the data when plotted as K_s, whereas when plotted as $\sqrt{K_s}$ the $t^{-\frac{1}{3}}$ law is more reasonable.

Fig. 78 shows the Z- transformations for all of both the polycrystalline and single crystal data for values of n from 0.05 to 1.25 against $t^{-\frac{1}{3}}$.

The ambiguity of data which is only weakly dependant on a particular variable is amply illustrated in many of these curves. As $n \longrightarrow 0$ the condition is being approached where any variation in K_s is being ignored and linearity is established purely by the mathematical restraint imposed (i.e. when n = o, $Bt^{-q} = A-1$ which is represented by a vertical straight line on a plot of K_s against t^{-q}) in Z at low n which is undoubtedly due to this effect. The point where this effect takes over from the true correlation of the variables depends on how rapidly the function varies with respect to the variable being considered and also on the spread or correlation of the data with respect to that variable. The curve for 698°C where all 19 points are included, represents a curve which is highly non linear at n= 1 and approaches the highest level of correlation only at n = 0 with no other maxima.

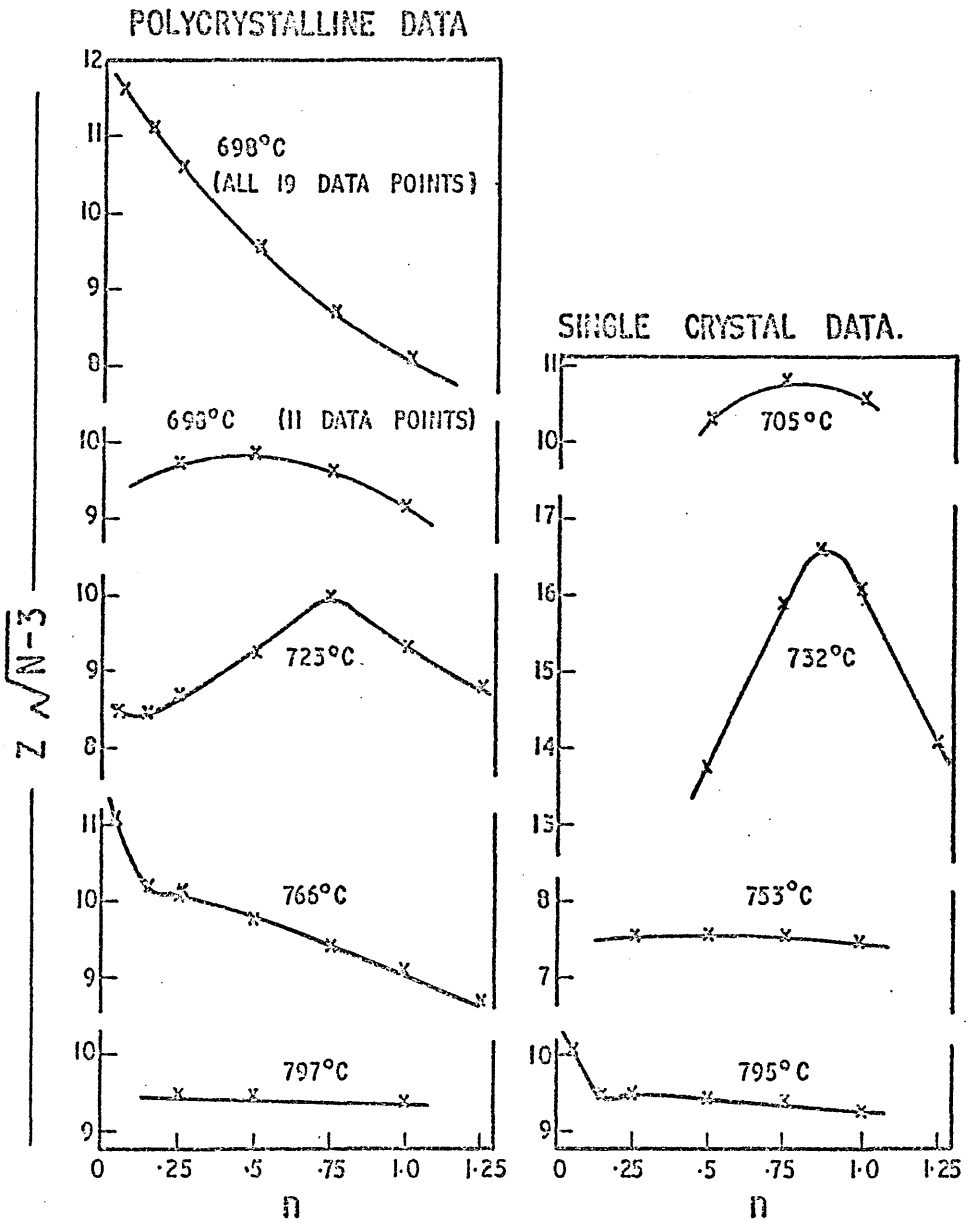

FIG. 78 VARIATION OF Z - TRANSFORMED CORRELATION COEFFICIENT FOR $K_s^n v\ t^{-\frac{1}{3}}$. Z IS PLOTTED IN UNITS OF VARIANCE = $(N-3)^{-\frac{1}{2}}$ WHERE N IS THE NUMBER OF DATA POINTS.

However if only those 11 data points are included which demonstrate a high degree of linearity at n = 1 then it is evident that a broad maximum in Z now occurs at about n = 0.5.

Much of the high temperature data i.e. in the range 750 - 800°C changes so slowly with K_s that any n with $K_s^n = A - Bt^{-1/3}$ will produce a similar correlation. Again it may be assumed that the observed correlation is due to this weak dependance of t rather than any clear behaviour with respect to K_s.

The intermediate temperatures i.e. 700 - 740°C do however indicate a significant extra maximum at a non-zero n, and generally in the range 0.75 - 0.9.

In summary then the Zijlstra data indicates a linear correlation between $t^{-1/3}$ and a power of K_s somewhere between K_s and $K_s^{1/2}$ with stronger support for $K^{1/2}$ rather than K_s. However K_s is favoured if $t^{-1/4}$ rather than $t^{-1/3}$ is chosen as the independent variable. Also it is necessary to note that at intermediate-to-long ageing times the data curves are <u>too</u> linear for strict conformity with the Zijlstra mechanism and for this reason the coarsening insolubility effect is probably the most predominant mechanism for anisotropy change at long ageing times.

6.1.7. Comparison of Zijlstra's data at the shorter ageing times with the current work

It can be seen from Figs. 25 and 26 that the time scale of Zijlstra's experiments is much more extended than in the current work which, because of heating effects associated with the applied field coils during ageing, was limited to from 1 to 120 minutes. Zijlstra's ageing times range from about 20 minutes up to 10,000 minutes, or about seven days at the ageing temperature.

His short term results i.e. 20 - 200 minutes appear to agree qualitatively with current findings for Alcomax 111 and Alloy A1; i.e. that there is a rapid linear increase early in ageing and then an apparent levelling off with increasing time. Zijlstra's data shows that, in each case, K_s stays at the level for times of the order of 15 hours or more before, then very gradually increasing by further relatively small amounts over periods of 1 - 7 days.

Some attempt has been made to fit curves for both the Zijlstra mechanism and the NSS diffusion effect to this data as shown in Figs. 79 and 80. Fig. 58 shows that the Zijlstra mechanism produces an initially more rapid increase in anisotropy than NSS diffusion and then, at longer times, continues to cause a steady (if decelerating) increase in anisotropy when the changes induced by NSS diffusion have levelled off.

It is apparent from Figs. 79 and 80 that NSS diffusion is the most appropriate mechanism at short ageing times at temperatures up to almost 800°C but then the Zijlstra mechanism is becoming more appropriate. At the longer times in these graphs and at all temperatures the anisotropy continues to increase given sufficient time implying the influence of the Zijlstra mechanism at all temperatures. Also neither

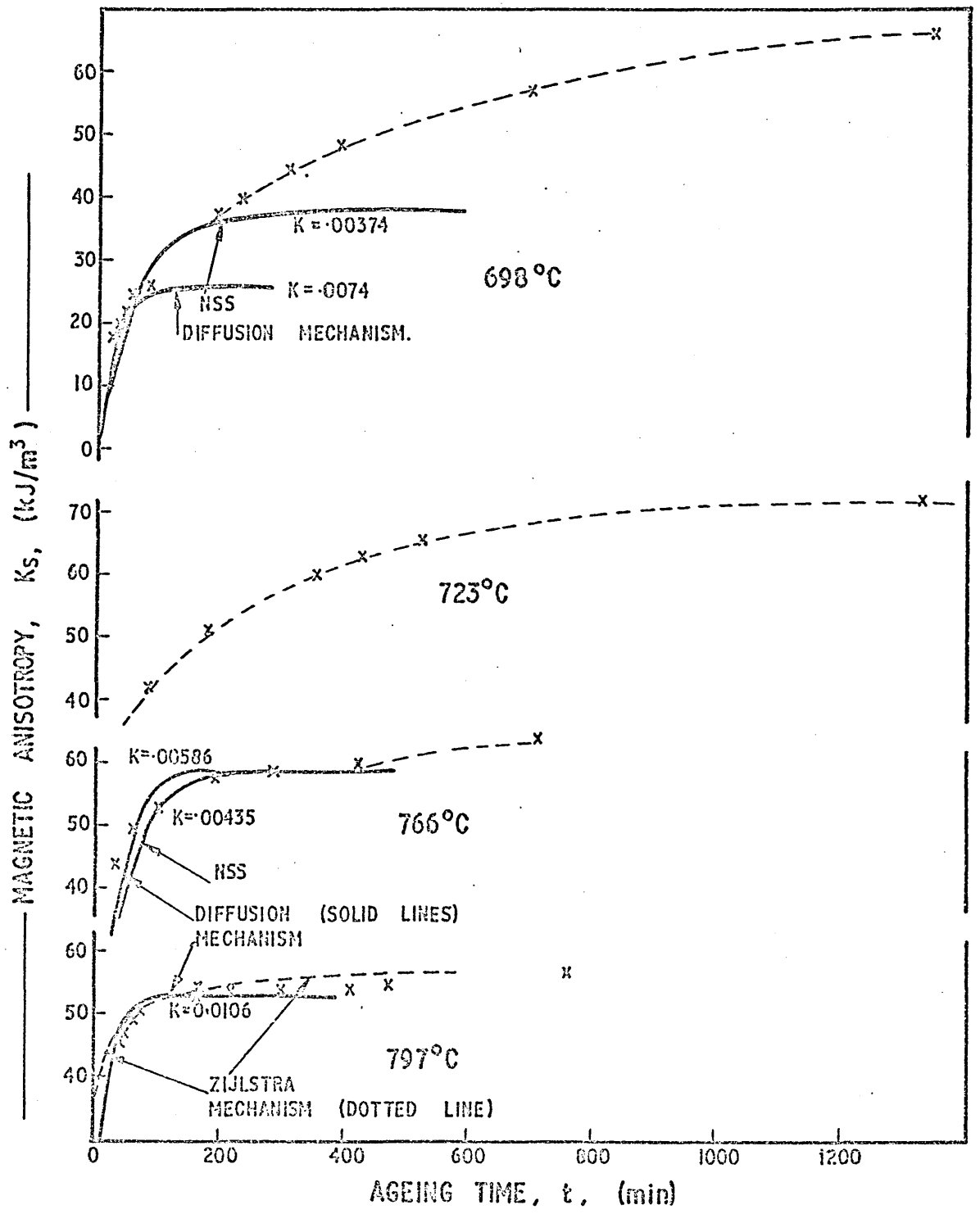

FIG. 79 ZIJLSTRA'S[51] MAGNETIC ANISOTROPY RESULTS AT THE SHORTER AGEING TIMES FOR POLYCRYSTALLINE SAMPLES AND ATTEMPTED FITTING OF SOME OF THIS DATA TO THEORETICAL CURVES.

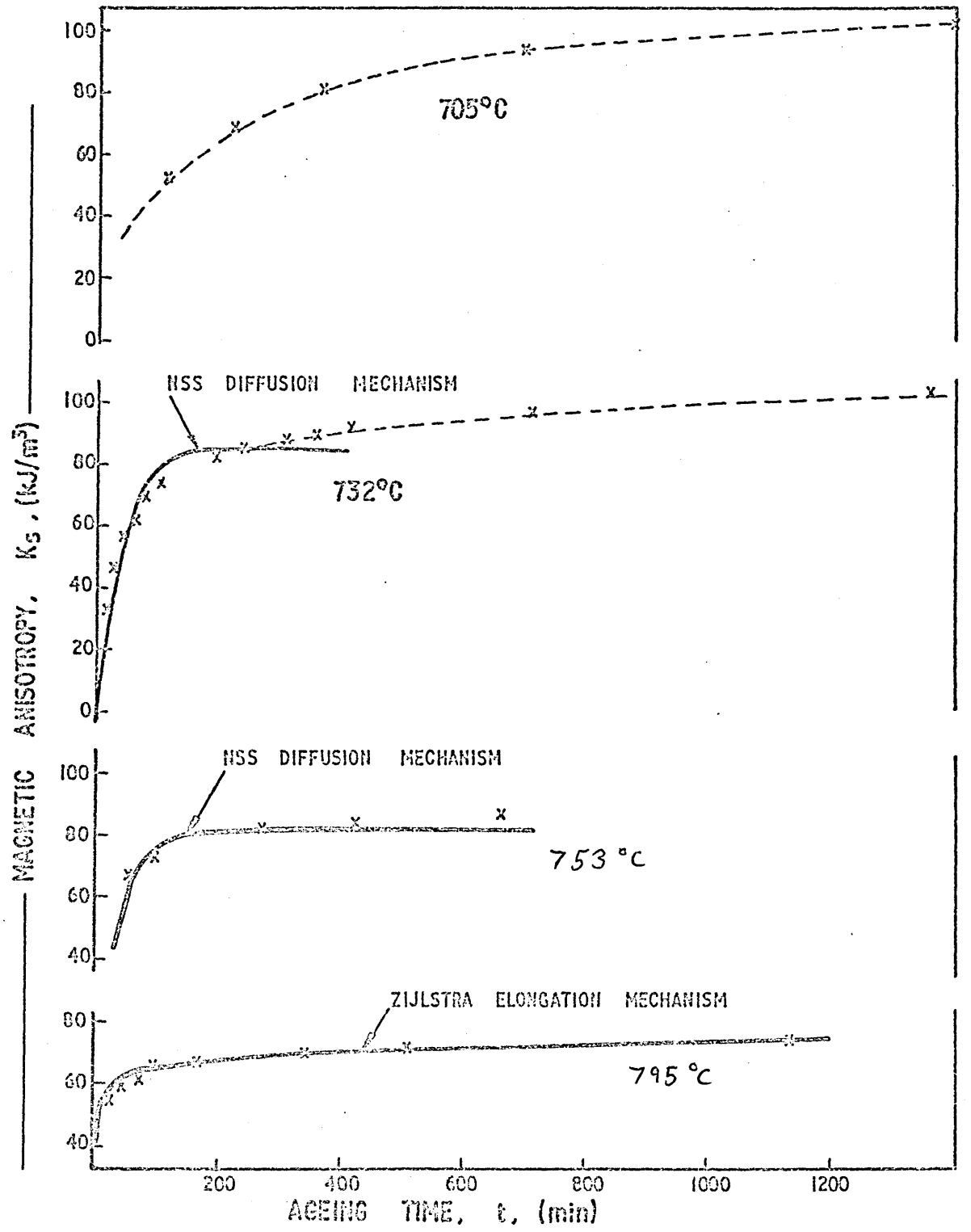

FIG. 80 ZIJLSTRA'S[51] MAGNETIC ANISOTROPY RESULTS AT THE SHORTER AGEING TIMES FOR SINGLE CRYSTAL SAMPLES, AND ATTEMPTED FITTING OF SOME OF THIS DATA TO THEORETICAL CURVES.

mechanism fits the data unambiguously at short times either, and the most reasonable explanation is that both mechanisms are involved with this alloy over approximately the same time range, Zijlstra particle elongation beginning at earlier ageing times with higher temperatures.

From the fitting of the anisotropy data to the NSS diffusion relationship values of $k = D/r^2$ as indicated in table XX can be obtained where r is the radius of the particles and D the diffusion coefficient. In principle values of diffusion coefficient may therefore be obtained from such curves for the atomic species (whatever these may be) involved in the composition adjustments between particles and matrix in each case.

For example alloy A1 aged at 800°C a diffusion coefficient is estimated in this way to be of the order of 10^{-21} or 10^{-22} m/sec. Such results are so imprecise because of the difficulty of estimating a sufficiently accurate mean value of r due to the size and diffuseness of the particles.

In general self-diffusion and mixed diffusion coefficients in the metals such as iron, nickel, cobalts and chromium have been measured by conventional methods only at much higher temperatures. Although extrapolation of such results gives the same general order of magnitudes, it was believed not to be profitable to persue this type of analysis in view of the obvious uncertainties involved. This line of consideration was therefore abandoned.

6.18 Anisotropy after ageing in partial or re-directed fields

Some anisotropy results are given in table XV and X 111 and Figs. 61 and 63 for disc samples of Alcomax 111 and Alloy C1 respectively, which have had similar times and temperatures of ageing as other samples, except that after 3-5 minutes the applied field has been removed or re-directed at 90° to the original direction but still in

the plane of the foil. In fact the samples were removed from the salt bath after 3 minutes in the case of the Alloy C1 samples and 5 minutes in the case of the Alcomax 111 samples and quenched in to iced brine and water respectively.

For the samples which were then held for further times in the salt bath without an applied field, another salt bath was used in which the temperature of the bath was maintained by electrical resistance heating external to the iron crucible and which had no external electro-magnetic circuit, so that there was no danger of residual field external to the magnet influencing the further development of the magnetic anisotropy. The results showed, certainly in the case of Alcomax 111 that the magnetic anisotropy achieved the same level as those samples which had had a continuous magnetic field during ageing. However the magnetic anisotropy is seen to have already reached its maximum level after 5 minutes at 750°C so that no conclusions on any positive effect which the field may have later in ageing could be determined.

For Alloy C1 there was a substantial increase in magnetic anisotropy from its level after 3 minutes at 650°C in a field with continued ageing at this temperature with the field removed, however not so much as with the continuously field aged specimens. The anisotropy constant did still appear to be levelling off with increasing ageing time, but at about 70% of the value of the continuous field ageing data.

It was felt that although the external field had been removed the internal field, as a results of the anisotropy already present, may still be sufficient to promote some elongation in the easy direction. So several samples after the same 3-5 minutes field ageing (and quenching) were re-introduced into the bath with the field at right angles to the original direction of the field. For Alcomax 111 in

Fig. 61 there is seen to be some depression of the anisotropy which can be attributed to preferential elongation of particles with axial alignments well away from the easy axis. The two alloy C1 data results of this kind in Fig. 63 are ambiguous; one shows no increase after the field ageing at right angles compared with the original 3 minute field ageing, but the other is almost equivalent to the magnetic anisotropy of the continuous field ageing treatment.

6.2. Microscopy

At the outset of the description of the microstructures to be described it should perhaps be emphasised here again that there was a general difficulty with all these foils due, it is believed, to the permanent magnet nature of the materials being examined. The differences in magnetisation orientation and its resistance to any change in such orientations mean that the electron beam - or components of the electron beam in the microscope are deflected which results in a blurring of the image.

This problem has been noticed before (63) and many investigators notably de Vos (80), have sought to develop alternative replica techniques. Such a technique, although producing micrographs which contain very sharp outlines of small particle structure of Alnico Alloys, leave some room for doubt that what is being observed is a true representation of what exists in the metal itself. De Vos produced the replicas by electrolytically assisted oxidation of the surface and there is no guarantee that the size or shape of the oxidised areas due to the presence of the particles actually correspond to the morphology of the particles themselves. Thus although the microstructures derived from thin foils of the alloys themselves are clearly of poorer quality than such replica micrographs, it is nevertheless believed that more reliance can be placed on the accuracy

of representation of the structure in thin foils, and accordingly all work has been done by this technique. In addition electron diffraction can and has been regularly made use of to identify particle orientation relationships and identify the presence of ordering and to monitor the quality of the foils.

6.2.1. Alloy C1

Observation of the occurrence of a modulated microstructure basically consisting of aligned evenly spaced "diffuse" particles perhaps 20-60 nm long and less than 10 nm across (the"wavelength" of these modulations appears to be about 16 nm) after only 2 minutes at 650°C in a magnetic field in the plane of the foil is demonstrated in Figs. 81 and 82. Such observations of the structure at this stage was difficult, but was best observed at extinction contours and with dark field illumination. Ageing for longer than 2 minutes in the magnetic field in the plane of the foils (Figs. 83-85) revealed high contrast particles which are believed to be segregates of one of the spinodal products, or perhaps conventional precipitates.

The modulations are not observed when the particles are present. The electron diffraction patterns from these foils show points representing only one b.c.c. lattice with no superlattice points. Evidently the phases which are present have the same lattice parameter within the limit of the electron diffraction image. Their diffraction patterns show that the plane of the foils represented in Figs. 81-85 are all (111) and a correction has been applied to the mean length of the particles as measured from Figs. 81 and 82 taking this into account assuming the particles are aligned in the nearest $\langle 100 \rangle$ to this plane.

As realised for Fe-Cr alloys (176) and Fe-Cr-Co alloys (177) contrast is obtained with such foils by preferential electro-chemical

Fig. 81 Alloy Cl after quenching from solution and ageing for 2 minutes at 650°C in a magnetic field, light field image at extinction contours - plane of foil (111).

Fig. 82 Alloy Cl after 2 minutes at 650°C in a magnetic field, dark field image - plane of foil (111).

Fig. 83 Alloy Cl after 3 **minutes at** 650°C **in** a **magnetic field, - plane of foil (111).**

Fig. 84 **Alloy Cl after** 9 **minutes at** 650°C **in** a **magnetic field, - plane of foil (111).**

Fig. 85 Alloy Cl after 60 minutes at 650°C in a magnetic field, plane of foil (111).

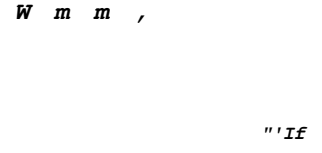

Fig. 86 Alloy Cl after 30 minutes at 650°C in a magnetic field, followed by tempering for 2 hours at 600 C plus 4 hours at 58o°C plus 16 hours at 560°C - plane of foil (111).

attack of compositions either with low Cr content (176) or high Cr content (**177**)* The segregates (or precipitates) are assumed then to have a composition which differs greatly from that of the matrix and therefore electro-chemical thinning of these regions is preferred rather than attack of some composition variation within the modulations which, if due to spinodal decomposition, will be small in comparison with that to be expected for precipitates or segregates.

As already intimated there is some confusion in the literature (176, 177) as to which phase, as observed, is the higher chromium content one, and thus the less ferromagnetic constituent. Houghton et al (177) argue that^because Cr has a lower electrode potential than Fe or Co then;it is the high Cr phase which is preferentially attacked and which therefore appears light in the foil. This would mean that it is the matrix phase which is the highly ferromagnetic phase in both their alloy and also alloy Cl here. Their interpretation of the Mossbauer spectra rests on this belief, i.e. that the particles have a high Cr content but, according to their Mossbauer data, not initially paramagnetic therefore implying a spinodal origin. Obviously if the particles are instead a lov/ Cr constituent then even if produced by nucleation they still will not be paramagnetic and the absence of paramagnetic peaks in the Mossbauer spectra could not then distinguish between nucleation or spinodal dissociation.

The work of Marcinkowski et al. (176) and Williams (113) however, strongly support the opposite conclusion that lov/ Cr alloys are preferentially attacked. First of all Williams leached 33% Cr-Fe chips which had been previously cooled slowly from 330-^72°C and held for 21 days. The leaching solution was a mixture of E C3. and picric acid. This solution preferentially dissolved the high Fe phase and the extracted particles of the high Cr phase could be observed by

electron microscopy. Both solution and particles were chemically analysed to confirm these conclusions.

Marcinkowski et al (176) aged samples of a 47-8 at % Cr-Fe for prolonged periods at 500°C. Both extraction replicas and thin foils again indicated that it was the high Fe matrix phase which was preferentially dissolved. The structure was only observable in the foils at extinction contours i.e. when the foil is oriented for strong diffraction again suggesting that contrast arises from small differences in thickness between the two phases as a result of different dissolution rates. The same explanation would also account for the difficulty of observation of the structure, except at extinction contours, of the present alloy, C1, after 2 minutes at 650°C.

Despite the intermediate appearance of the relatively much larger spherical particles for longer ageing times than 2 minutes at 650°C (Figs. 83-85), Fig. 86, which is from a fully aged and tempered specimen, shows a very similar structural content to the foils which had been aged for only 2 minutes at 650°C, Figs. 81 and 82.

The plane of the foil in Fig. 86 which was actually aged for 30 minutes at 650°C with the magnetic field in the plane of the foil and then tempered for 2 hours at 600°C plus 4 hours at 580°C and then 16 hours at 560°C, corresponding to the optimum magnetic condition is also(111). The modulations have approximately the same mean wavelength as that observed after 2 minutes, however the contrast between the two phases in Fig. 86 is much stronger reflecting what must presumably be the much more distinct difference in composition. There is, after tempering, no sign of the spherical particles observed after longer periods (than 2 min.) at 650°C and it must be presumed that, as the composition amplitude of the modulations increases during tempering, the particles redissolve or become incorporated into the elongated spinodal product.

Fig.87 in which the plane of the foil is (100), is taken from a foil from a bulk specimen which had been annealed for 30 minutes at 650°C with the field in the plane of the foil and then allowed to cool relatively slowly (i.e. aged in the magnetic jig) so that some auto-tempering had taken place. It appears from this plate that the spherical particles are becoming incorporated into the modulations at lower temperatures.

The appearance of rod-like particles oriented in the nearest <100> to that of the field direction at the earliest stages of ageing is consistent with what is predicted by the spinodal decomposition theory of Cahn (132) in the presence of an externally applied magnetic field (133). During the initial stages of decomposition he argues (132) that the amplitude of the composition fluctuations is expected to be less than it would be for the final equilibrium incoherent phases and that nucleation and growth can also occur in the unstable composition region as a competing mechanism.

The microhardness results in Fig. 46 also seem to imply the super-imposition of two mechanisms (there being two peaks in the hardness time curve), and the magnetic hysteresis curves in Fig. 43, plus the magnetic anisotropy data in Fig.63 indicate that some preferentially directed distribution of composition must have taken place at early ageing times as well as the high contrast particles observed in Figs. 83-85 which are spherical.

Houghton et al (177) in their Mössbauer investigation of a Fe - 27.5% Cr - 17.5% Co - 0.5% Al alloy, considered that their results could be interpreted as the gradual spinodal dissociation of two phases with isothermal ageing at 620°C. However they also detected the appearance of an iron rich phase at longer ageing times which they interpreted as a nucleation event. This new phase, which was additional

Fig. 87 Alloy C1 after 30 minutes at 630°C in a magnetic field and cooled in the magnetic jig - plane of foil (100).

Fig. 88 Alloy C2 as quenched showing nitrides on dislocation segments.

to the spinodal phases, has a hyperfine field which closely correspond to that of pure oh-iron, suggesting that some of the Fe from one of the spinodal phases is migrating to form another iron rich phase. This supports what is observed in Figs. 83-83.

6.2.2. Alloy C2

Alloy Cl in the as quenched condition showed no sign of any sub-structure. However samples of Alloy C2 which contained up to 0.073% nitrogen (table IV), as quenched (in iced brine) from the solution temperature (1330°C), indicated the presence of precipitates, either nucleated on dislocation segments or homogeneously, as exemplified in Figs. 88 and 83 respectively.

In order to reduce the nitrogen content, samples were heated in hydrogen up to 1310 C held for approximately 33 minutes and then slowly cooled to 400°C, before removing from the hydrogen atmosphere. The heating and cooling periods were each of approximately seven hours The samples were then held for 1 hour at 1330°C in an argon atmosphere and quenched into iced brine. After ageing for 13 and 30 minutes at 643°C (- 2°C) in the salt bath with the applied magnetic field in the plane of the foil, the structures as shown in Figs. 90 and 91 respectively, were observed by TEM. Again a spherical and, in some cases, elongated precipitate structure is observed even though there was little indication of any directionality.

Fig. 92 is typical of the 30 minute ageing (with a field in the plane of the foils) plus an additional temper for 2 hours at 600 C The magnetically hard nature of the foil is such that there is considerable distortion of the electron beam (see section 6.2.3*)* The distortion is minimised at extinction contours, however, and it is evident that a further finer precipitation of spherical x>articles

Fig, 89 Alloy C2 as quenched showing nitrides homogeneously precipitated.

Fig. 90 Alloy C2 heat treated in hydrogen, solution heated, quenched end then aged for 15 minutes et 6^3 C in a magnetic field.

Fig. 91 Alloy C2 heat treated in hydrogen, solution heated, quenched and then aged for 30 minutes at 643 C in a magnetic field, plane of foil (100).

Fig. 92 Alloy C2 heat treated in hgdrogen, solution heated, quenched, aged for 30 minutes at 643 C in a magnetic field and then tempered for 2 hours at 600 C, plane of foil (110).

has taken place in the matrix phase on tempering at 600°C. It can be seen from table VIII that this kind of microstructure has led to much less than optimum magnetic properties. On the basis of these observations it seems probable then that nitrogen can have at lest two deleterious effects on the microstructure of Fe-Cr-Co alloys. Firstly, in relatively large amounts, nitrogen promotes the formation of the f.c.c. phase which is non-magnetic (164) and in regions where γ phase is not formed, and at intermediate levels of nitrogen, nucleation of iron-rich precipitate is promoted or made easier by the extra nitrogen compared with the situation at nitrogen levels of the order of 0.02% as exemplified by Alloy C1, and plates 81-87.

It may be postulated then that nitrides may provide nuclei for subsequent precipitation of the iron rich phase, i.e. the observed spherical particles may well be hetrogeneously nucleated from such nitride particles in the as quenched alloys, and therefore such nucleation may be expected to be reduced even more by minimisation of the nitrogen content to levels even lower than .02%.

6.2.3. Commercial Alcomax III and Alnico Alloys

Figs. 93 and 94 give an indication of the characteristic microstructure of commercially heat treated Alcomax III and Alnico with nominal compositions as given in table V. Alcomax III is an anisotropic alloy and here heat treated by cooling (at 19.5°C/min from 930°C to 550°C) with the magnetic field applied in the plane of the foil. Alnico is isotropic and therefore here cooled without a field at 260°C per minute from 1250 to 600°C. The bulk specimens of Alcomax III were also tempered for 24 hours at 590°C plus 24 hours at 560°C, and Alnico for 1 hour at 600°C, these were then in their optimum permanent magnet states. In this condition the magnetic nature of the foils are such

Fig, 93 Alcomax 111 solution heated and cooled at 20 C/min in a magnetic field followed by tempering.

Fig. 9^ Alnico solution heated and cooled at about 150°C/min followed by tempering - plane of foil (100).

that there is considerable distortion of the electron beam (i.e. diffraction effects occur due to the magnetic state of the particles) and the detail is usually blurred. This condition applied on all the alloys studied when in their optimum magnetic state, and has been noticed before (63). However, for foils which were aged only, with no additional temper, blurring was not a problem. Electron diffraction gave the usual ordered b.c.c. lattice structure of the C_s Cl type for these alloys, and showed that the plane of the foil in both Figs. 93 and 94 is (100). Several samples of Alcomax 111 were isothermally aged at 800°C in the absence of a magnetic field. Figs. 95, 96 and 97 which all have a (100) plane in the plane of the foil are areas of the foils produced from these samples after 2, 5 and 15 minutes respectively.

Considering spinodal decomposition in cubic crystals with suitable elastic constants, Cahn (132), as a result of his calculations, demonstrated that plane waves of composition variation primarily parallel to all three (100) planes thus results in an initial microstructure at the early stages of decomposition (if the volume fraction of one phase is smaller than the other) of a simple cubic array of octahedral particles whose corners are aligned along the <100> directions.

Fig. 95 Alcomax 111 solution heated, quenched and then aged for 2 minutes at 800 C without a field - plane of foil (100).

Fig. 96 Alcomax 111 aged for 5 minutes without a field - plane of foil (100).

Fig. 97 Alcomax 111 aged for 19 minutes without a field - plane of foil (100).

Fig. 98 Alloy Al, solution heated, quenched and aged for 9 minutes at 800 C in a magnetic field - plane of foil (113).

With increasing volume fraction, these octahedra will come in contact along their corners giving a continuous simple cubic lattice work of truncated octahedra. This seems to describe the detail in Fig. 95, where there is some dependence of structural detail on the degree of preferential dissolution obtained. With presumably greater dissolution at the thinner parts of the foil the cuboid nature of the particles as described above are evident.

Cahn (132) also described what is expected when the volume fraction of the phases are similar , in which case the three plane waves of composition variation in the (100) planes do not interact with one another. The structure then consists of two interlocking systems of <100> rods, one enriched and the other depleted in one of the components. This "maze-like" structure is precisely what is observed in Figs. 96 and 97.

6.2.4. Alloy A1

Figs. 98, 99 and 100 are examples of observations from foils which, as bulk specimens had been aged in the magnetic field at 800°C with the direction of magnetisation in the plane of the foil. Fig. 98 is from a foil previously aged for 5 minutes and Figs. 99 and 100 for 15 minutes.

Unfortunately most of the foils which were successfully prepared from Alloy A1 were found to have their planes in a (110) or more complicated orientations such as (113). In fact Fig. 98 is in a (113) plane and Figs. 99 and 100 are both (110) planes. Because of this and the fact that relatively few foils were successfully prepared because of the extreme brittleness of this alloy, it is difficult to generalise. However, they were all basically modular structures consisting of elongated particles which tend to have a preferred direction in general. There is a definite increase of the length of

Fig. 99 Alloy A1 aged for 15 minutes at 8oO°C in a magnetic field, plane of foil (110).

Fig. 100 Alloy A1 aged for 15 minutes at 8oO°C in a magnetic field, plane of foil (110).

the particles from 5 minutes to 15 minutes ageing and more regular adherence to the <100> directions at the longer ageing times. Some regions of the 15 minute foils showed particles orientated in two mutually perpendicular directions as in Fig. 99 and other regions showed a more obvious preference for one <100> direction as in Fig. 100. Even here there are some "cross linked" particles reminiscent of the models for this kind of system proposed by Paine and Luborsky (98).

One other ageing treatment on Alloy A1- ageing for 48 hours at 600°C in the absence of a magnetic field-revealed a microstructure shown in Fig. 101. This (100) foil shows a highly elongated regular system of particles which occupy most of the foil, i.e. there is little matrix phase. What is most suprising is the high common directionality and extreme length of the particles.

6.2.5. General comments on Microscopy and its relationship to the Magnetic anisotropy data

The anisotropy data discussed in section 6.1 is consistent with decomposition by a spinodal mechanism and additional evidence for this mechanism has also recently been made by Mössbauer spectroscopy (177, 178).

The identification of some additional precipitation in Alloy C1, the Fe-Cr-Co alloy, is however apparent which is consistent with the occurrence of an additional iron rich phase in the Fe-Cr-Co alloy examined by Houghton et al (177). Cremer and Pfeiffer (179) had also earlier postulated the decomposition of the weakly ferromagnetic Cr rich phase into an additional and even weaker magnetic phase, but could not substantiate this from their electron microscopy.

Similar effects involving the occurrence of additional extra decomposition in either the iron rich or Ni Al rich phases have been

Fig, 101 **Alloy Al aged for** 4–8 **hours at 6**oO°C **(without** a **field) - plane of foil (100).**

proposed to occur in the Alnico Alloys (80,84,92,77). De Vos (80), by electron microscopy using replicas, found that by isothermally ageing and then tempering both Fe-Ni-Al and Alnico 5 alloys at a lower temperature, the two phases which had separated during ageing could be further decomposed in the temper. He shows the presence of smaller, presumably Fe rich precipitates particularly noticeable in the Ni Al rich matrix phase. Campbell and Julien (92) detected by X-ray diffraction an additional b.c.c. phase to the two main phases which had a slightly different lattice parameter, and Magat et al (77) again by X-ray diffraction detected the presence of "zones" in several Alnico type alloys as well as the presence of the side bands due to the modular structure in the isothermally aged condition. Koch et al (70) and Pfeiffer (84) both detected an f.c.c. phase within the Ni Al rich b.c.c. phase, in Alnico 5. However this phase apparently only appears after slow cooling or tempering at or below 600°C. In Alnico 5 alloys containing some niobium (e.g. Alcomax 111) Koch et al (70) reported that a Fe_2 Nb phase is precipitated with ageing, over a temperature range from 1200°C down to about 600°C.

In general then, in view of these possibilities, this is a most likely explanation for the decreases in anisotropy found over certain ranges of ageing times, particularly for the Alcomax 111 results in Fig 64 for times greater than 5 minutes, where there is a marked loss of magnetic anisotropy at longer times. This may, for instance, be due to Fe_2 Nb precipitation, although none was detected by electron diffraction or microscopy. There was however some tendency for bridging or material impingement of particles as they grow in length for Alloy A1 as illustrated in Fig. 100 for ageing for 15 minutes at 800°C which would tend also to reduce the anisotropy.

Other magnetic anisotropy data apart from some of the Alcomax

111 points have not shown any consistent departure from NSS particle matrix interdiffusion prediction however, in spite of any extra precipitated phases or particle impingement effects.

Some of the microscopy, microhardness, magnetic anisotropy and other magnetic results have also been published previously (180, 181). Other attempts at measurement of magnetic anisotropy by determintation of the mean area between hysteresis loops from J-H curves measured both parallel and perpendicular to the field alignment direction were made. The areas were determined, using Simpson 's rule and the resulting anisotropy values are given in table XlV. Hysteresis loss was similarly determined from the hysteresis loops for the field alignment direction. The anisotropy and hysteresis energies in this table represent the total for the whole curve and for comparison with the analogous anisotropy constants determined by torque magnetometry for the same alloy in table XVll they must be divided by two.

The two sets of data compare quite well for short ageing times when the hysteresis energy is low i.e. when the curves are narrow. However when the hysteresis is large anisotropy becomes less easy to measure and it is apparent that the anisotropy energy, as measured by the hysteresis loop method, is reduced at the same time that the hysteresis energy is suddenly increased i.e. there is an apparent transfer of energy for anisotropy to hysteresis as the coercivity increases (180). Thus the hysteresis loop method of measurement of anisotropy was considered not to be a satisfactory or reliable method and was abandoned.

6.3. Coercivity

Three broad subclassifications are suggested for mechanisms which could be responsible for coercivity levels in ferromagnetic materials containing particles of a second phase of greater (or lesser)

saturation magnetisation than the matrix phase. These may be conveniently described in terms of the two basic processes of demagnetisation i.e. (i) domain boundary movement and (ii) magnetisation rotation.

The possibilities for demagnetisation are therefore :-

1 domain wall movement, sweeping through both the matrix and particles.

11 domain wall movement through the matrix and (followed by) rotation of magnetisation inside the particles.

111 rotation of particles and (part of) the matrix simultaneously.

Class 1 this is simply general wall movement throughout the material, and the particles can be regarded as having a pinning effect on the mobility of the wall giving a coercivity dependent on the strength of this pinning. The necessary mobility of walls through particles and matrix alike may be expected where the saturation magnetisation of the two phases are similar. Many early theories were put forward to qualify this effect, however those of Néel (22,8) were perhaps the most generally acceptable. These predicted the coercivity to be, in general, proportional to the square of the difference in saturation magnetisation between the particle and matrix phases $\Delta J_s = J_p - J_m$ i.e. $H_{CJ} \propto (\Delta J_s)^2$

Newer theories of this kind lead to more complicated relationships for H_{CJ} with saturation magnetisation (25).

Class 11 reversal mechanisms in which reversal of magnetisation (by wall movement) of the matrix occurs prior to magnetisation reversal in the particles, is perhaps more applicable when the saturation magnetisation of the matrix material is weak relative to that of the particles.

If the reversed matrix magnetisation were the only magnetisation (i.e. the particles were non-ferromagnetic) the position of the particles would be considered as "holes" with a demagnetising energy $\frac{N}{2\mu_o} J_m^2$ per hole. However the presence of the magnetisation inside the particle, in the opposite direction to that of the matrix magnetisation modifies this demagnetising energy per particle to (10)

$$K_s = \frac{N}{2\mu_o} (J_p + J_m)^2 \quad \ldots\ldots\ldots\ldots \quad (6.17)$$

i.e. it behaves as though it were a particle of saturation magnetisation $(J_p + J_m)$ in a non-magnetic matrix and thus associated with a demagnetising field

$$H_d = \frac{-N}{\mu_o} (J_p + J_m) \quad \ldots\ldots\ldots\ldots \quad (6.18)$$

For (Stoner-Wohlfarth) coherent rotation (40) H_{CJ} is proportional to H_d and therefore $H_{CJ} \propto (J_p + J_m)$. But $J_s = p\, J_p + (1-p)\, J_m$ therefore $(J_p + J_m) = \frac{1}{1-p} (J_s + J_p)$, with J_s assumed constant with changes in J_p and J_m due to interdiffusion during ageing or tempering. It can be seen that for this mechanism H_{CJ} will vary linearly with J_p.

If reversal of the particle is incoherent - more likely when the particle magnetisation is large - the most likely incoherent mode is curling in which case, for long particles

$$H_{CJ} = \frac{k\, A}{r^2\, J_p} \quad \ldots\ldots\ldots\ldots \quad (6.19)$$

where r is the radius of the particle, k is a constant near to unity and A is the exchange constant (which of course, despite its name, varies with composition). Fig. 102 shows saturation magnetisation against Curie point, T_c [note :- T_c is proportional to A (8) for various solid solution systems of iron and nickel from the literature (8)]. This indicates that, in general, for this mechanism, because $J_s \propto A$, H_{CJ} should be roughly constant when measured for different stages of ageing or tempering of the same alloy despite the expectation

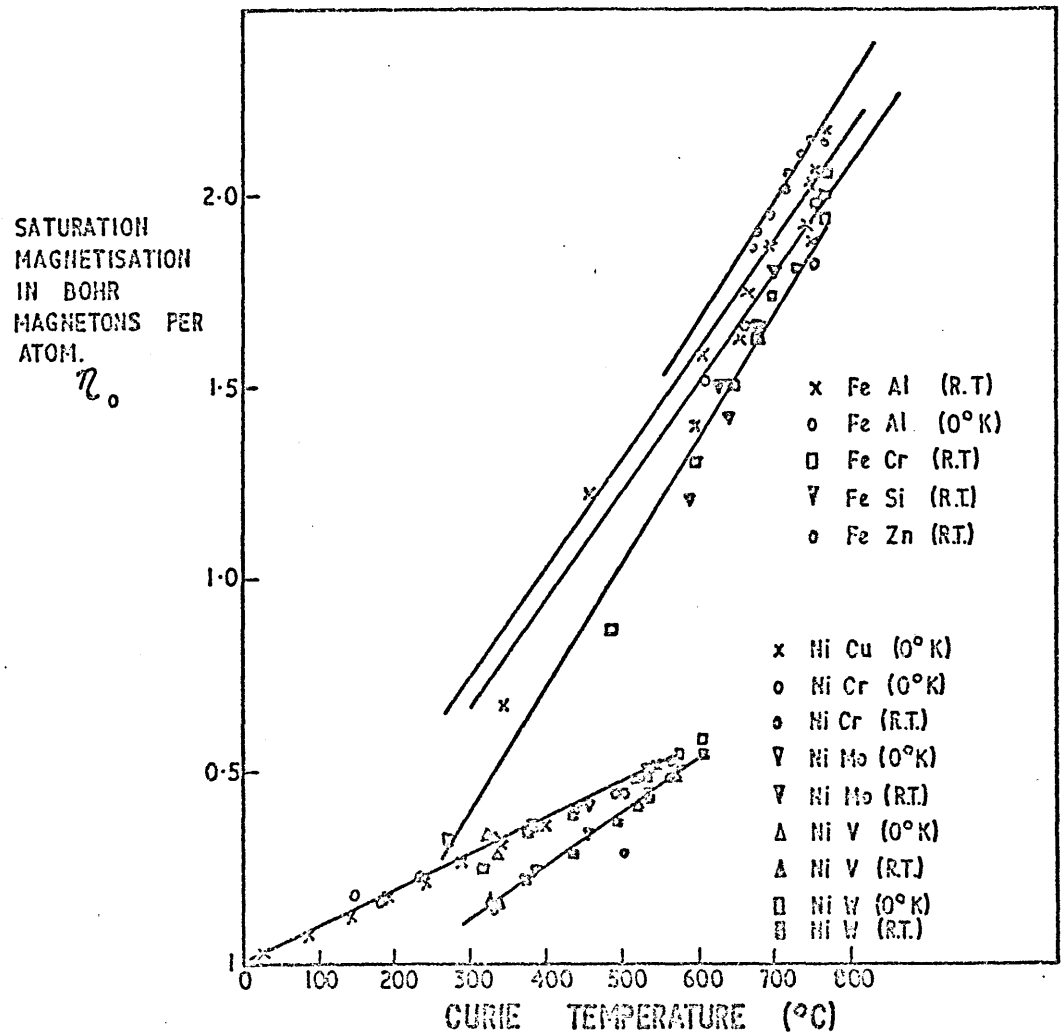

FIG. 102 VARIATION OF CURIE POINT WITH SATURATION MAGNETISATION FOR A NUMBER OF IRON AND NICKEL SOLID SOLUTION SYSTEMS.

that the composition of the particles and matrix will be changing.

Class III magnetisation reversal modes for ferromagnetic particle/matrix systems occur if or when the magnetisation of the matrix rotates with that of the particles during demagnetisation. This situation has already been considered in section 1.2.7., although not catagorised in the way expressed here. This possibility is perhaps appropriate for differences between J_p and J_m which are intermediate to the other two classifications.

In this situation it is the matrix which may be visualised as a "cavity" of depth $J_p - J_m = \Delta J_s$ in a general magnetisation J_p, so that the demagnetising energy is $\frac{N}{2\mu_o} (\Delta J_s)^2$. This time, because the whole system is involved in the reversal

$$H_d = \frac{N}{\mu_o} \frac{(\Delta J_s)^2}{J_s} \quad \ldots\ldots\ldots (6.20)$$

Again, for coherent reversal $H_{CJ} \propto H_d$ therefore, taking J_s, the saturation magnetisation of the system as a whole, to be constant

$$H_{CJ} \propto (\Delta J_s)^2$$

To summarise therefore, H_{CJ} may be expected to vary linearly with $(\Delta J_s)^2$ for either of the two extremes i.e. by either reversal of the particle/matrix system by domain wall motion only, or coherent rotation only. But for coherent reversal of magnetisation of the particles, after the energetically easier reversal of the matrix magnetisation by wall processes, then H_{CJ} may be expected to vary linearly with the saturation magnetisation of one of the constituent phases e.g. J_p (and also the composition of the phase since composition and magnetisation are expected to be linearly related). If the particle magnetisation were to reverse by curling in an otherwise similar situation then H_{CJ} may well be independent of the saturation magnetisation or difference in saturation magnetisation of the two phases.

As ageing or tempering proceeds, some transition from one mechanism to another dependant principally on the saturation magnetisation of the matrix and the difference between the saturation magnetisations of the two phases may occur. In general such a transition effect would be expected to occur with continued ageing or tempering of previously aged specimens. Fig. 103 shows the variation of coercivity with ageing time for alloys A1, C1 and Alcomax 111 from the H_{CJ} results in tables 1X, X, X1 and X111. Figs. 104 and 105 for alloy A1 from the results in tables X and X1 and Fig. 106 from the results in table 1X for Alcomax 111, show the coercivity variation with the square root of tempering time at 600°C after a prior isothermal ageing. It can be seen that there is in general a relatively smooth increase in coercivity levelling out for alloy A1 in Figs. 104 and 105 to values of up to 30 kA/m which is about 60% of the coercivity of optimally heat treated Alcomax 111.

In fact these results have been fitted to the N.S.S. diffusion curve for particles in accordance with the data in table XX and, assuming $H_{CJ} \propto \Delta C$ (i.e, implying $H_{CJ} \propto J_p$). These are the continuous lines in Figs. 104 and 105, and are in general a good fit to the coercivity data. The Alcomax 111 results in Fig. 106 are in general linear with $t^{\frac{1}{2}}$ which is again in accordance with N.S.S. diffusion curve at early times i.e. the diffusion in this alloy has not proceeded to completion. As already discussed in Chapter 1 sections (1.3.2. and 1.4.2. both magnetic (76,83,80,96,139) and Mössbauer (97, 84) data indicate that the changes in properties are due to the diffusion between particles and matrix during tempering, and therefore N.S.S. diffusion behaviour can be expected.

The correlation of ΔC with H_{CJ} which is implied in Figs. 104-106 suggests a simple relationship between H_{CJ} and ΔJ_s or J_p. In fact, a similar distribution of data points are obtained if the

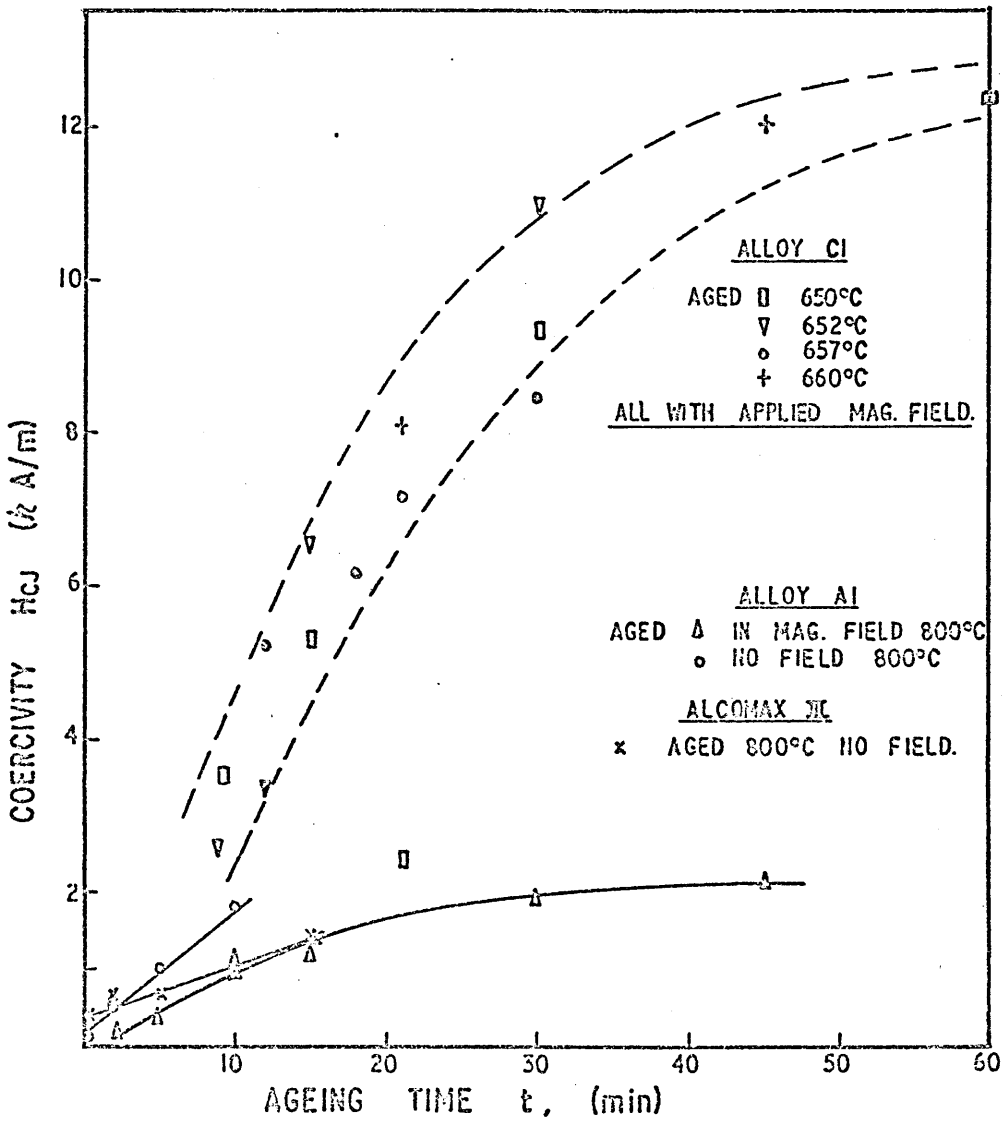

FIG. 103 VARIATION OF COERCIVITY WITH AGEING TIME FOR ALLOY CI AT 650 - 660°C AND ALLOY AI AND ALCOMAX III AT 800°C.

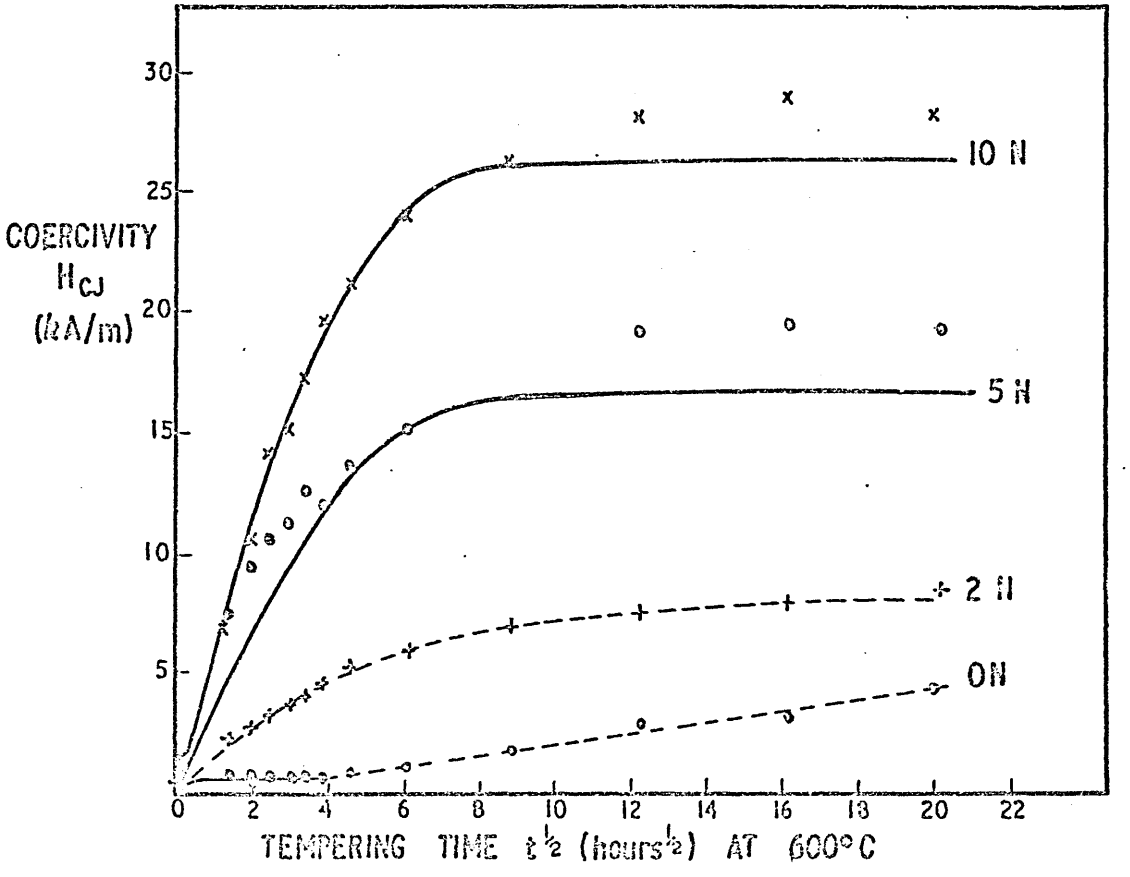

FIG. 104 VARIATION OF H_{cJ} WITH TIME $^{1}/_{2}$ ($t^{1/2}$) OF TEMPERING AT 600°C AFTER PREVIOUS AGEING AT 800°C, (WITHOUT A MAGNETIC FIELD) FOR SAMPLES OF Fe-Ni-Al-20% Co ALLOY A1.

AGED	FOR	0	min.	0N
"	"	2	"	2N
"	"	5	"	5N
"	"	10	"	10N

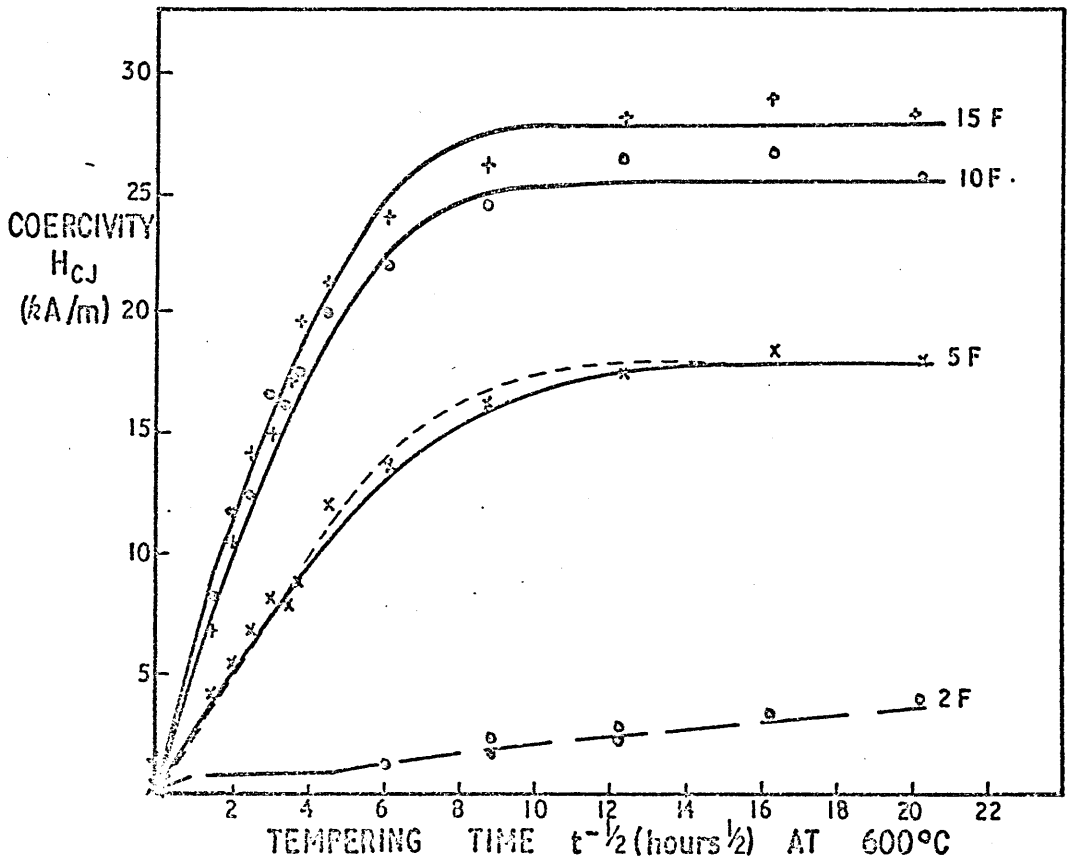

FIG. 105. VARIATION OF H_{cJ} WITH TIME $^{1/2}$ ($t^{1/2}$) OF TEMPERING AT 600°C AFTER PREVIOUS AGEING AT 800°C OF Fe-Ni-Al-20 % Co ALLOY Al IN A MAGNETIC FIELD.

AGED FOR 2 min. 2 F
" " 5 " 5F
" " 10 " 10F
" " 15 " 15F

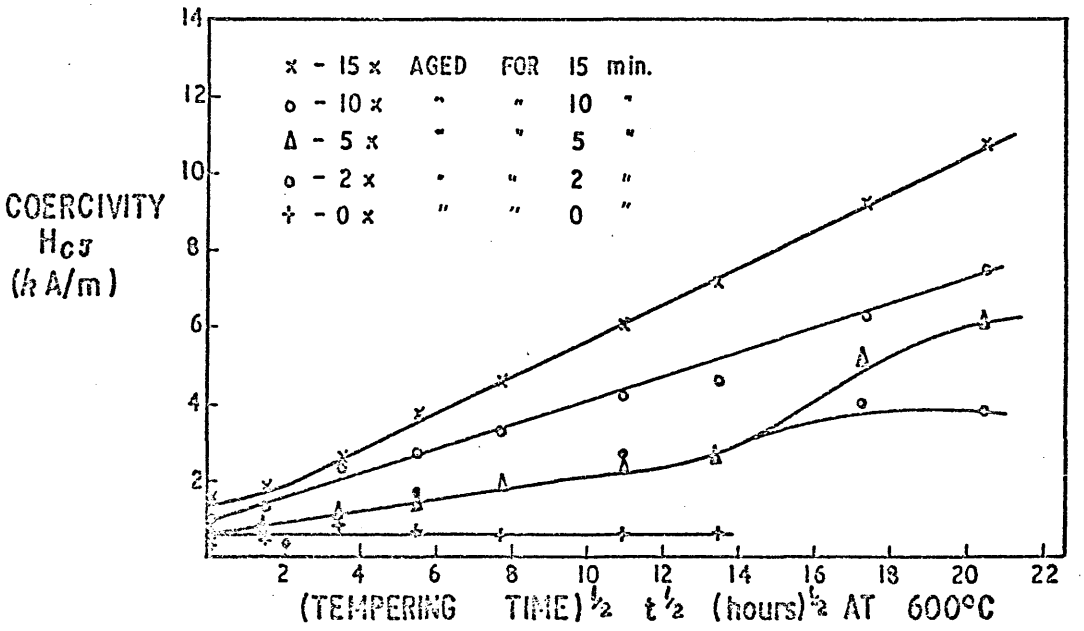

FIG. 106 VARIATION OF H_{cJ} WITH TIME $^{1}/_{2}$ ($t^{1}/_{2}$) OF TEMPERING AT 600°C AFTER PREVIOUS AGEING AT 800°C (WITHOUT A MAGNETIC FIELD) FOR SAMPLES OF ALCOMAX III.

theoretical curves are used for H_{CJ}, assumed proportional to $(\Delta C)^2$ (implying $H_{CJ} \propto (\Delta J_s)^2$). That is, there is a similar inability to separate the various possible mechanisms as there was for magnetic anisotropy in section 6.1. However, the behaviour of H_{CJ} here is very similar to the anisotropy curves, and these coercivity changes, which for the case of tempering are almost certainly due to diffusion, therefore lend support to the diffusion argument for magnetic property changes for the initial ageing behaviour also. Only one mechanism is necessary therefore, to explain in general the magnetic behaviour in both ageing and tempering - with the assumption that the morphology is determined very early in ageing by spinodal decomposition and the requirements that the long time ageing effects, which can be expected to be minimal in normal production heat treatments for these alloys, of particle elongation in the field (51) and the predicted (146) matrix solubility changes, need to be superimposed.

6.4. Remanence

Figs. 107 and 108 show the values of remanence plotted against the coercivity of samples of Alloy A1 and Alcomax 111 as these properties change during tempering at 600°C, after a prior ageing for 2-15 minutes at 800°C with and without a magnetic field, from the data in tables 1X X and X1 respectively. For the results for Alloy A1 in Fig. 107 the data falls into two linear regimes (a) a steep linear increase in J_r with H_{CJ} at low H_{CJ}, i.e. short tempering times, and (b) a slowly decreasing linear regime at the higher H_{CJ} tempers.

The linear increase in region (a) can be explained if it is assumed that all or some (fixed) part of the magnetisation of the matrix can reverse its magnetisation easily i.e. even in a positive field before the applied field is reduced to zero (i.e. at the remanence point). The driving force for this to happen is the

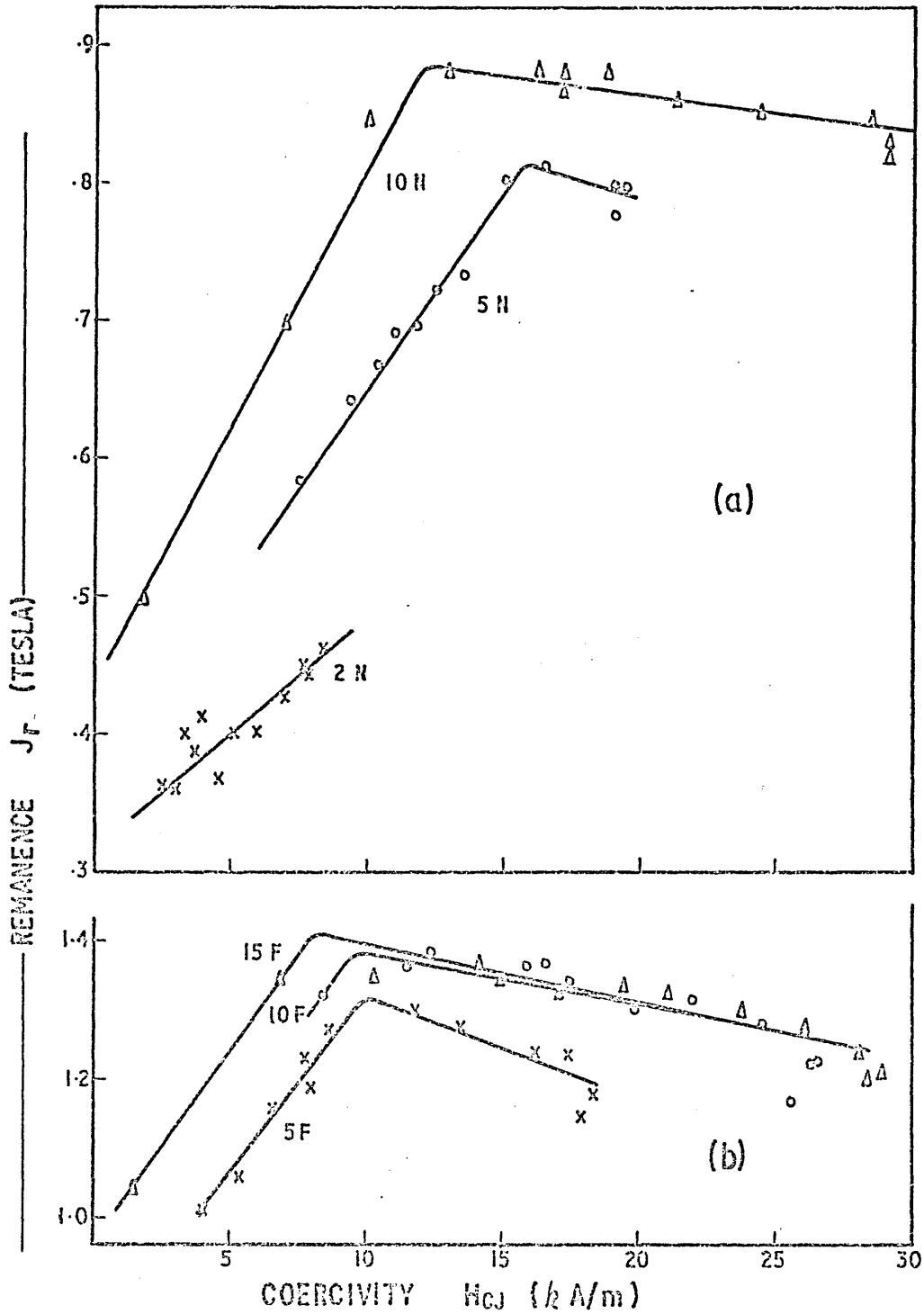

FIG. 107. ALLOY A1 AGED AT 800° C (a) NO APPLIED FIELD AND (b) WITH APPLIED FIELD. J_r AGAINST H_{cJ} FROM THE SAME TEST AFTER TEMPERING PERIODS OF FROM 0-407 HOURS AT 600° C.

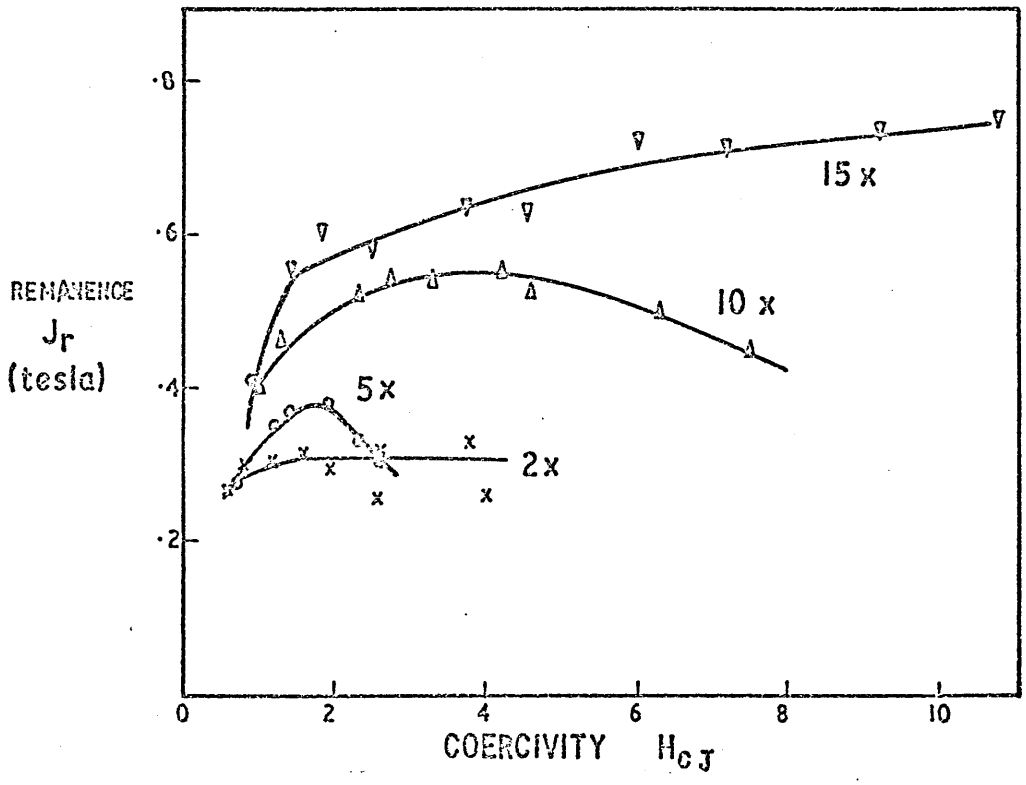

FIG. 108 VARIATION OF REMANENCE WITH COERCIVITY FOR SAMPLES OF ALCOMAX III AGED AT 800° C WITHOUT A MAGNETIC FIELD AND TEMPERED AT 600°C FOR A RANGE OF TIMES FROM 0-420 HOURS.

2 x	AGED	2 min.	AT	800°C
5 x	"	5 "	"	"
10 x	"	10 "	"	"
15 x	"	15 "	"	"

magnetisation of the particles which cannot reverse easily but their flux can "short circuit" back through the matrix, if it too is ferromagnetic. Fig. 109 illustrates what is to be expected in this respect from a single ferromagnetic particle in a lesser ferromagnetic matrix. In reality the amount of flux reversal through the matrix will be limited by an increased energy contribution due to exchange interaction between those adjacent atoms which have non-parallel magnetisation vectors. However if the magnetisation of the particles is only slightly higher than that of the matrix then only a relatively small angular rotation of some of the atomic magnetic moments in the matrix will be sufficient to neutralise the excess magnetisation of the particles. "magnetic ripple" of the magnetisation within domains is easily observed by Lorentz electron microscopy (182) in ferromagnetic alloys. This is thought to be due to such periodic fluctuations in the orientation of the atomic moments perhaps initiated by the need to accommodate the small scale variation in magnetisation which must occur in all practical alloys. This effect is then one possible way in which the excess magnetisation of a particle can be neutralised by flux closure through the immediately surrounding ferromagnetic matrix.

For an ellipsoidal particle, in the presence of a ferromagnetic matrix, the demagnetising energy is $E_p = \frac{N}{2\mu_o} (\Delta J_s)^2$ where N is the demagnetising coefficient, μ_o the magnetic constant and $J_s = J_p - J_m$ the excess saturation magnetisation of the material of the particle, J_p compared with that of the matrix, J_m.

Assuming, initially, that the particle is in a ferromagnetic matrix of unlimited extent such that as much flux reversal as possible through the matrix could occur, subject only to the limitation that the amount of this energy E_e is proportional to the amount of magnetisation which can be reversed through the matrix in this way then the

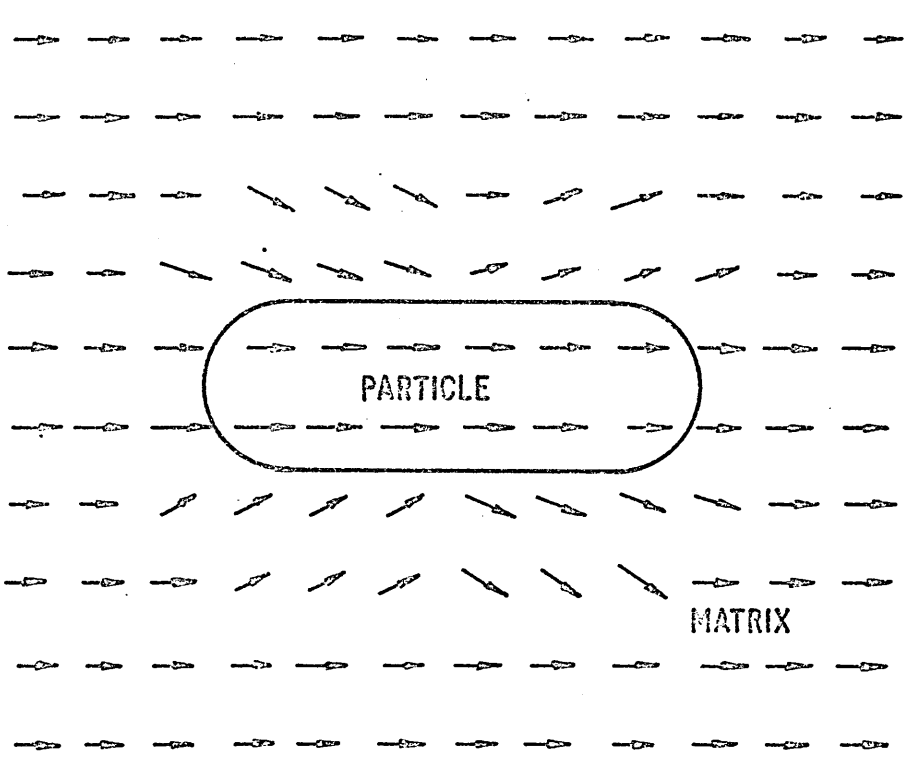

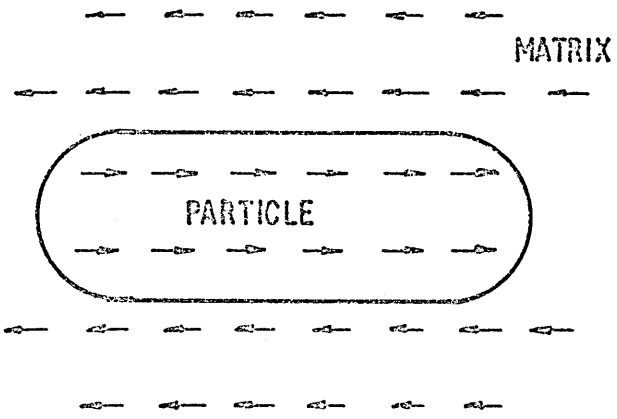

FIG. 109 (a) POSSIBLE WAY IN WHICH THE HIGHER MAGNETISATION INSIDE THE PARTICLE CAN BE CLOSED BY DISPLACEMENT OF MAGNETIC MOMENTS IN THE FERROMAGNETIC MATRIX AROUND THE PARTICLE.

(b) COMPONENTS OF THE MAGNETISATION IN THE DIRECTION OF THE LONG AXIS OF THE PARTICLE AFTER SUBTRACTING THE VALUE OF THE UNDISTURBED MATRIX MAGNETISATION AT EACH POINT.

total energy (remembering that at J_r, H = 0) is

$$E = E_p + E_e =$$

$$\frac{N}{2\mu_o} (\Delta J_e)^2 + C (\Delta J_s - \Delta J_e) \ldots\ldots\ldots (6.20)$$

where ΔJ_e is the magnetisation remaining after part of ΔJ_s has been "short circuited" through the matrix, and C a constant. ΔJ_e will be such as to make E a minimum -

$$\text{i.e.} \quad \frac{dE}{dJ_e} = \frac{N}{\mu_o} \Delta J_e - C = 0 \ldots\ldots\ldots (6.21)$$

$$J_e = \frac{\mu_o}{N} C$$

This implies that ΔJ_e, the effective part of the particle magnetisation at H = 0 is constant and independent of J_p, and J_m, the matrix magnetisation.

From the diagram in Fig. 109 J_r can be supposed to be made up from three parts (a) the magnetisation of the matrix J_m, (b) the excess effective magnetisation of the particle $p J_e$, and (c) less that part of the matrix magnetisation which is carrying the return flux i.e. $- p (\Delta J_s - \Delta J_e)$.

$$J_r = J_m + p \Delta J_e - p (\Delta J_s - \Delta J_e) =$$

$$J_m + p (2 \Delta J_e - \Delta J_s) \ldots\ldots\ldots (6.22)$$

but, the saturation magnetisation of the system as a whole is

$$J_s = J_m + p \Delta J_s \ldots\ldots\ldots\ldots (6.23)$$

substituting equation (6.23)in equation (6.22)

$$J_r = J_s - 2 p (\Delta J_s - \Delta J_e) \ldots\ldots (6.24)$$

This can be seen to decrease with increasing J_p and decreasing J_m which is contrary to what is observed in Fig. 107.

It must be concluded then from the predicted J_r and ΔJ_e on the basis of the above arguments, that the assumption that unlimited amounts of matrix magnetisation are available for flux closure is false. Instead an alternative controlling factor, that ΔJ_s can decrease to an effective level ΔJ_e, not as far as exchange energy

would allow, but only to the extent of the available matrix magnetisation J_m, or some portion of it, is now considered, i.e.

$$p\,(\Delta J_s - \Delta J_e) = (1-p)\,J_m - k\,(\Delta J_e + J_m) \quad \ldots\ldots \quad (6.25)$$

where $(1-p)\,J_m$ is the total matrix magnetic moment per unit volume of the system and $p\,(\Delta J_e + J_m) = p\,J_e$ is the effective part (i.e. that part to be transmitted through the magnetic circuit of the test unit as opposed to that given in equation (6.25) which is carried back through the matrix around the particle) of the magnetic moment of the particle. In order to carry this flux, ΔJ_e, through the network of particles i.e. to avoid the occurrence of free poles inside the material, some of the moments of the matrix material will need always to be aligned in the same way.

If this flux could be measured through a flat plane in the matrix between (i.e. not intersecting) two particles for which the normal is the test direction and the preferred direction of magnetisation e.g. plane A in Fig. 110, then the minimum total flux can be expected to be $p\,(\Delta J_e + J_m)$ i.e. the same as inside the particle. However a similarly oriented plane in the matrix but intersecting the two parallel particles e.g. plane B in Fig. 110 does not necessarily require any matrix flux normal to it in this case. A mean of the sum of all such possible planes as would be obtained on testing assemblies of such particles on a macroscopic scale can thus be expected to give a measure of the proportion of the matrix magnetisation which is involved with the particle flux i.e. $k\,(\Delta J_e + J_m) = k\,J_e$ where k is a fractional constant for a given system of particles, probably smaller than p but depending not just on the volume fraction of particles but also the elongation of the particles and their orientation and parallelism. Obviously long parallel particles will require less of the matrix magnetisation to connect them together (magnetically) than shorter more randomly oriented particles.

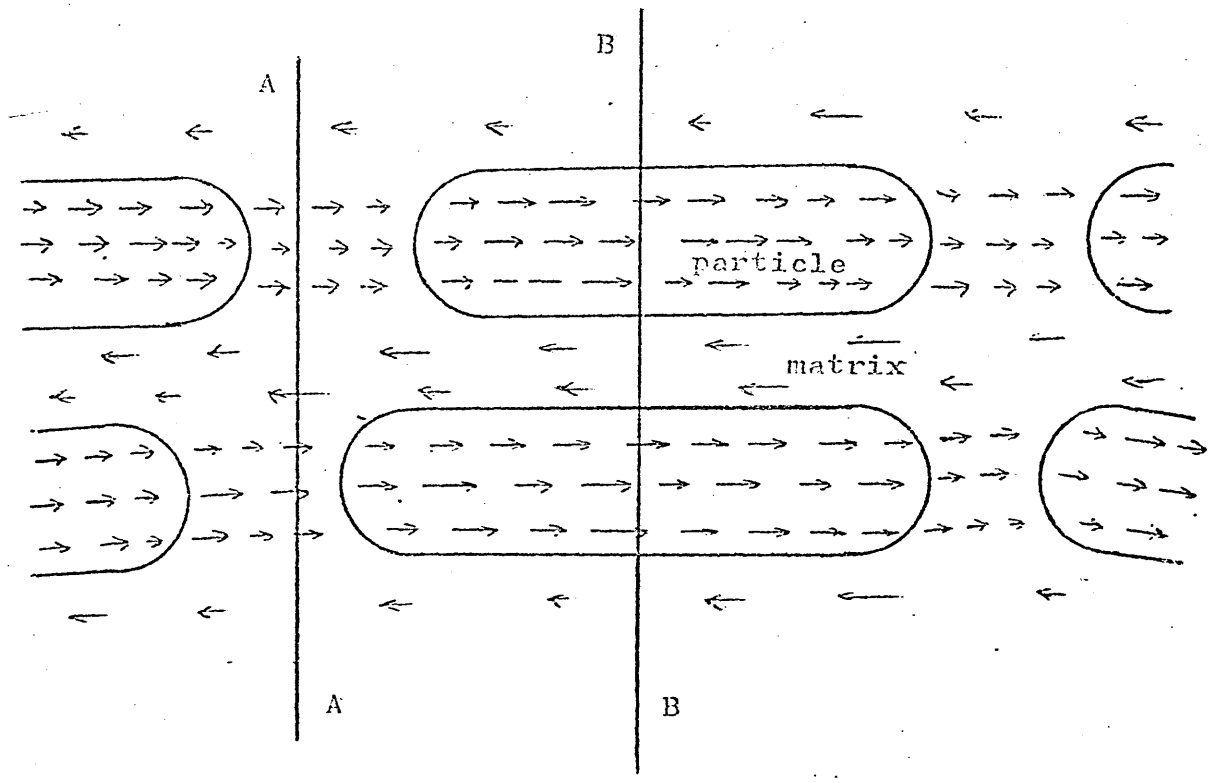

Fig. 110 . Measurement of magnetic flux through two planes in a system containing both ferromagnetic particles and matrix.
For microscopic particles an actual flux measurement will be the mean of a large number of net flux densities from such planes.

The right hand side of equation (6.25) represents the remainder of the matrix magnetisation which can be made available for flux closure for the magnetisation of the particles to provide a minimum effective excess particle saturation magnetisation, ΔJ_e Rearranging equation (6.25)

$$\Delta J_e = \frac{p}{p-k} \Delta J_s - \frac{(1-p-k)}{p-k} J_m \quad \ldots\ldots\ldots (6.26)$$

substituting equation (6.26) into (6.22)

$$J_r = (p + k) \Delta J_s - \frac{(p + k)(1 - 2p)}{(p - k)} J_m \quad \ldots\ldots (6.27)$$

Thus this kind of relationship predicts a linear increase in J_r with change of composition, ΔC, (again assuming linear change of magnetisation with composition and ΔJ_s and J_m related by equation 6.23). Making the assumption, supported by the data as discussed in the last section, that $H_{CJ} \propto \Delta C$, this explains the linear rise in J_r with change in H_{CJ}.

The linear increase in J_r will apply as long as

$$(1-p) J_m \geqslant k \quad (\Delta J_e + J_m) = k J_e \quad \ldots\ldots\ldots (6.28)$$

which is the regime in which equation (6.25) is valid. Once J_m is reduced below the level consistent with the inequality in expression (6.28) then the tendency will be for all the matrix magnetisation to align with the direction of the particle magnetisation to minimise internal free pole formation, and from this point and for lower matrix magnetisations it can be expected to rotate with the particle magnetisation at least near H = 0 in accordance with the Stoner & Wohlfarth theory (40). At higher (negative) H incoherent mechanisms may modify this behaviour.

At these levels i.e. $(1-p) J_m < k J_p$, $J_r = J_s$ for fully aligned particles and matrix i.e. the behaviour of J_r should follow the behaviour of J_s which from tables X, XI, XVI and Fig.69 can be seen to be a linear but slowly decreasing function of tempering time. This is also what is found in regime (b) in Fig. 107 for alloy A1.

In fact the slope is slightly steeper than accounted for by J_s changes alone. This could be expected if there is some small amounts of other phases which are precipitating as already discussed in section 6.2.4.

The J_r - H_{CJ} curves for the Alcomax 111 results are less amenable to analysis principally because there is generally non-linearity and a much larger non-linear decrease in J_r with H_{CJ} in regime (b).

As already suspected from the non-typical behaviour of the magnetic torque curves, Fig. 61, this again could be another effect of some precipitation of a non-magnetic phase such as Fe_2Nb during the course of ageing and tempering, since Alcomax 111 contains Nb whereas Alloy A1 does not.

The basic success of these interpretations of remanence in this section and coercivity in the last section, section (6.3), rests on the assumption that $H_c \propto \Delta C$ i.e. the difference in composition of the ferromagnetic constituents between the two phases which implies $H_c \propto J_s$ or J_p. On the basis of the possibilities considered in section 6.3, an independently and coherently rotating particle system seems to be the most likely reversal mechanism in Alnico 5/Alcomax 111 in the H_{CJ} range 2-15 kA/m.

6.5. Remanence of optimally heat treated alloys

The reduced remanence $j_r = \left(\frac{J_r}{J_s}\right)$, from tables V11, V1 and V for alloy C1, alloy A1 and Alcomax 111 in their optimally heat treated conditions are 0.874, 0.875 and 0.921 respectively. According to Fig.49 and the calculations and considerations in section 4.3, j_r should be 0.789 assuming no particle interaction. The fact that the actual values are higher than theoretical therefore implies that the grains in which there is poor particle alignment because of poor crystallographic <100> alignment with the direction of the applied field, must be influenced by local fields set up by the grains which have better alignment of their preferred axes (i.e. there must be some particle interaction).

One possibility is that, if the particles which are in grains which are less well oriented with respect to the <100> are, because of this, less elongated (which is predicted whatever the decomposition

mechanism), then this will allow the highly elongated particles which are in better oriented grains to influence the magnetisation vectors of the shorter particles to increased co-alignment. Also if the matrix is (even after tempering) still weakly ferromagnetic then this may tend to take the preferred axis.

6.6. Rotational Hysteresis

The measured values of W_r, the rotational hysteresis loss, as given in table XVlll on a disc sample of the Fe-Cr-Co alloy, alloy Cl, are presented in Fig lll as a function of the external field, H_e, as measured in the gap of the electromagnet. The sample bar from which the disc had been prepared had been previously aged in the magnetic field with the field direction in the tranverse plane of the bar for 30 min. at 650°C and then tempered for 2 hours at 600°C, plus 4 hours at 580°C, plus 16 hours at 560°C.This is essentially the optimum heat treatment found by Keneko et al. and also the optimum for alloy Cl as shown in Fig 42.

The effective or internal field H_i inside the disc specimen is given by the external field less the demagnetising field i.e.

$$H_i = H_e - N J \quad \ldots\ldots\ldots (6.29)$$

At high values of H_e, i.e. for $H_e > 2 K_s/J_s$, the sample is fully magnetised and $J = J_s$. At low fields on the other hand, $H_e < K_s/J_s$ for the Stoner Wohlfarth mechanism (40),the direction of magnetisation of the individual particle will vary little from the preferred direction i.e. as the direction of the external field rotates relative to the long axis of the particle,the magnetisation vector makes only small reversible excursions around the easy axis. In both cases there is no rotational hysteresis since changes in direction of J_s are reversible.At intermediate fields irreversible reversals take place which consistitutes the rotational hysteresis in the single domain particle.

In order to obtain H_i,the magnetisation curve of a larger sample of Alloy Cl measured in the direction of field alignment was used to estimate J in equation (6.29). The sample had been heat treated in an identical manner to the disc and the magnetisation curve is given in Fig. 112.

The internal field is determined from the external field in each

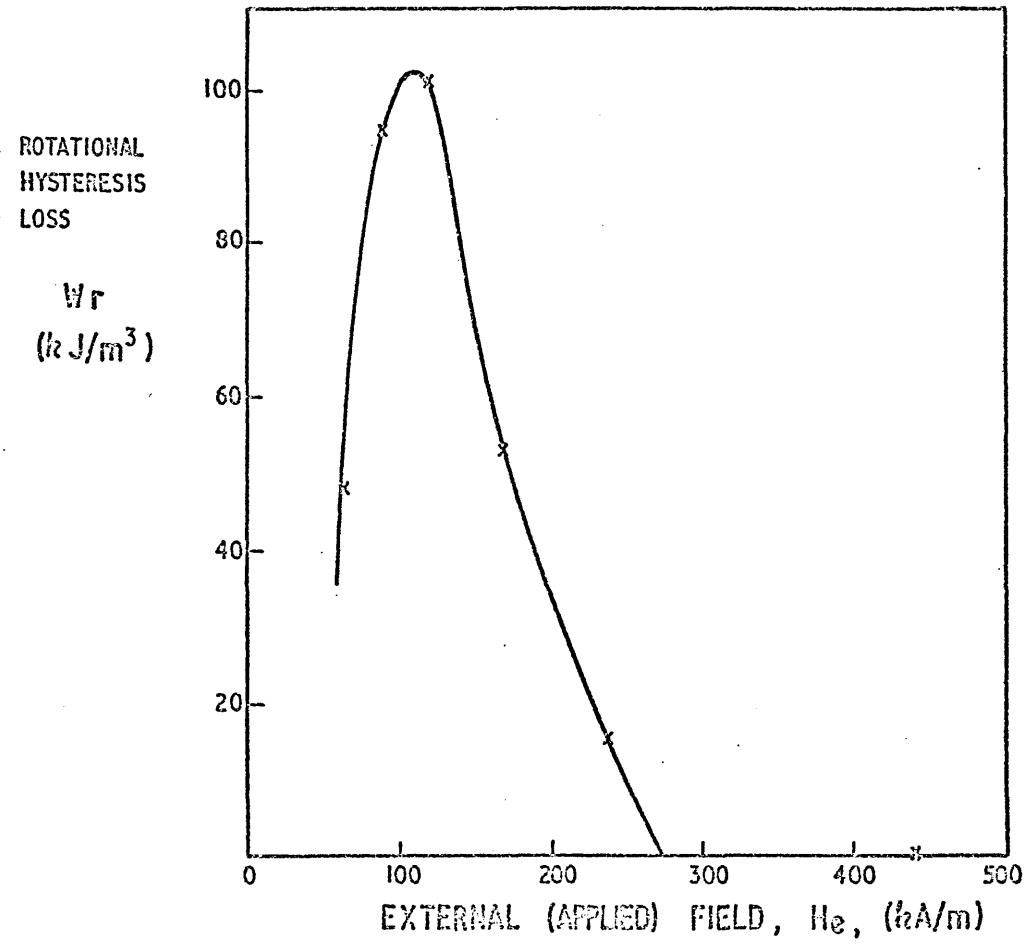

FIG. III. OBSERVED ROTATIONAL HYSTERESIS LOSS AS A FUNCTION OF H_e THE APPLIED FIELD FOR ALLOY C1 SAMPLE DISC, AGED AT 650°C FOR 30 min. IN A FIELD AND TEMPERED (2 h AT 600°C + 4 h AT 580°C + 16 h AT 560°C)

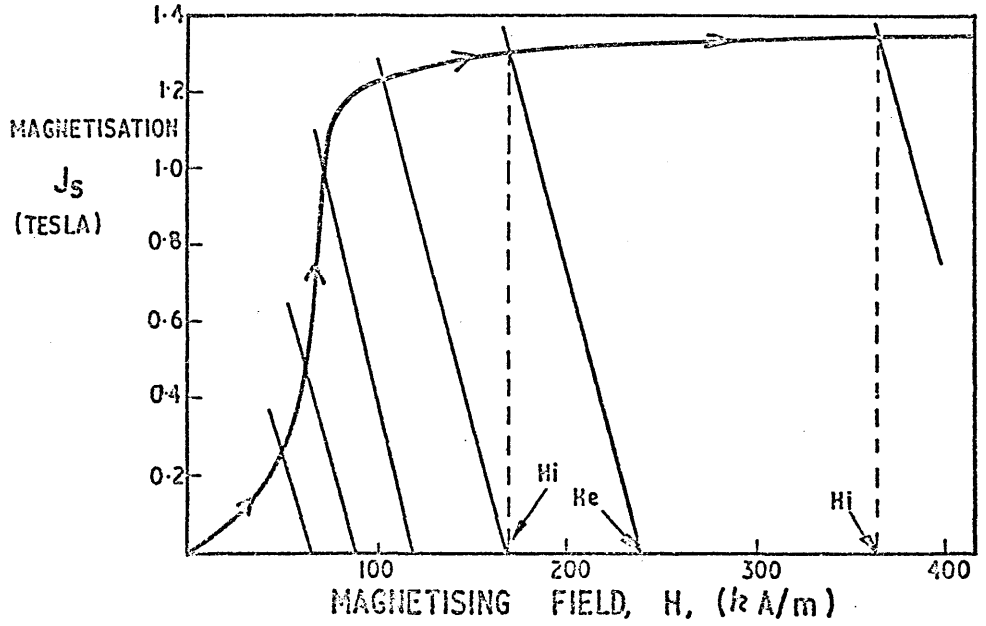

FIG. 112. MAGNETISATION CURVE IN THE DIRECTION OF THE APPLIED FIELD DURING AGEING OF ALLOY C1 AGED FOR 30 MIN. AT 650°C AND TEMPERED FOR 2 HOURS AT 600°C PLUS 4 HOURS AT 580°C PLUS 16 HOURS AT 560°C.

case as shown, by projecting a straight line of slope - $\frac{\mu_o}{N}$ from the abscissa at H_e up through the magnetisation curve. The demagnetisation coefficient N is calculated from the known axial thickness and diameter of the disc sample by interpolation from demagnetising factors (13) assuming an equivalent oblate ellipsoid of the same diameter and thickness. H_i is taken as the value of H at the point of intersection of the permeance line with the magnetisation curve.

The assumption at low fields is again, as for the isolated particle, that the direction of magnetisation will make only small reversible excursions from the preferred direction which is the field alignment direction as measured and shown in Fig. 112. And of course at high fields - $N J_s$ is the demagnetising field, as determined from the magnetisation curve anyway.

Some of the literature which describes rotational hysteresis experiments is vague with respect to the precise method of estimation of H_i (60). It is suspected from the shape of their W_r - H curves, that other workers (183, 184) have used - NJ_s as the demagnetising field at all H. This is certainly so in reference (184) although they have not used the curves to calculate a value of R the rotational hysteresis integral, as described and defined in section 1.2.8. As already stated in that section

$$R = \int_o^\infty \frac{W_r}{J_s} \, d\left(\frac{1}{H_i}\right) \quad \ldots\ldots\ldots (6.30)$$

The method of using the magnetisation curve to calculate H_i is here considered essential to obtain an accurate value of R. Using $H_i = H_e - N J_s$ at all H will have the effect of widening the W_r - $\frac{1}{H}$ curve thus producing too large an estimate of R.

Fig. 113 shows the curve for W_r against H_i and Fig. 114 the curve for the same W_r values plotted against $\frac{1}{H_i}$ in $\left(A/m\right)^{-1} \times 10^6$ from which R could be calculated by determining the area under this

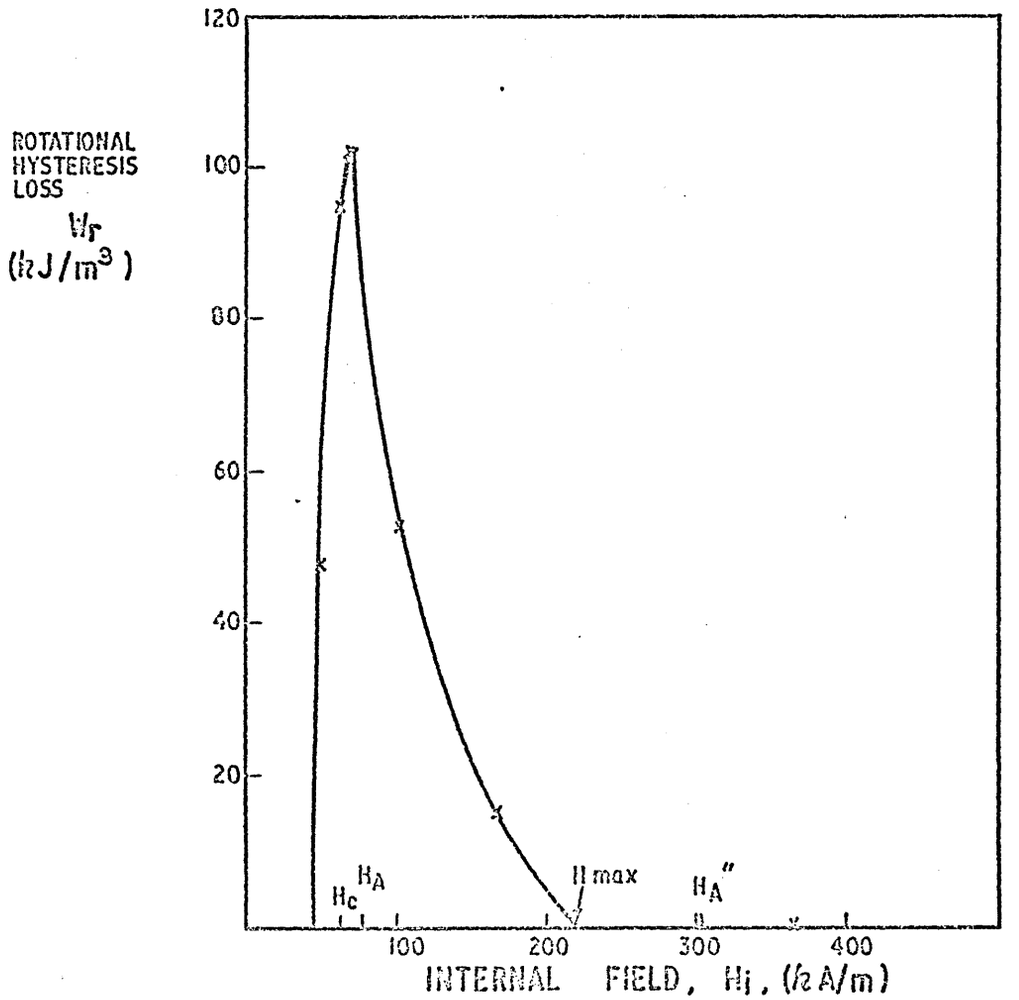

FIG. 113 OBSERVED ROTATIONAL HYSTERESIS LOSS CURVE AS A FUNCTION OF INTERNAL FIELD, Hi, FOR ALLOY C1 SAMPLE, AGED AT 650°C FOR 30 MIN. IN A FIELD AND TEMPERED (2 h 600°C + 4 h 580°C + 16 h 560°C.)

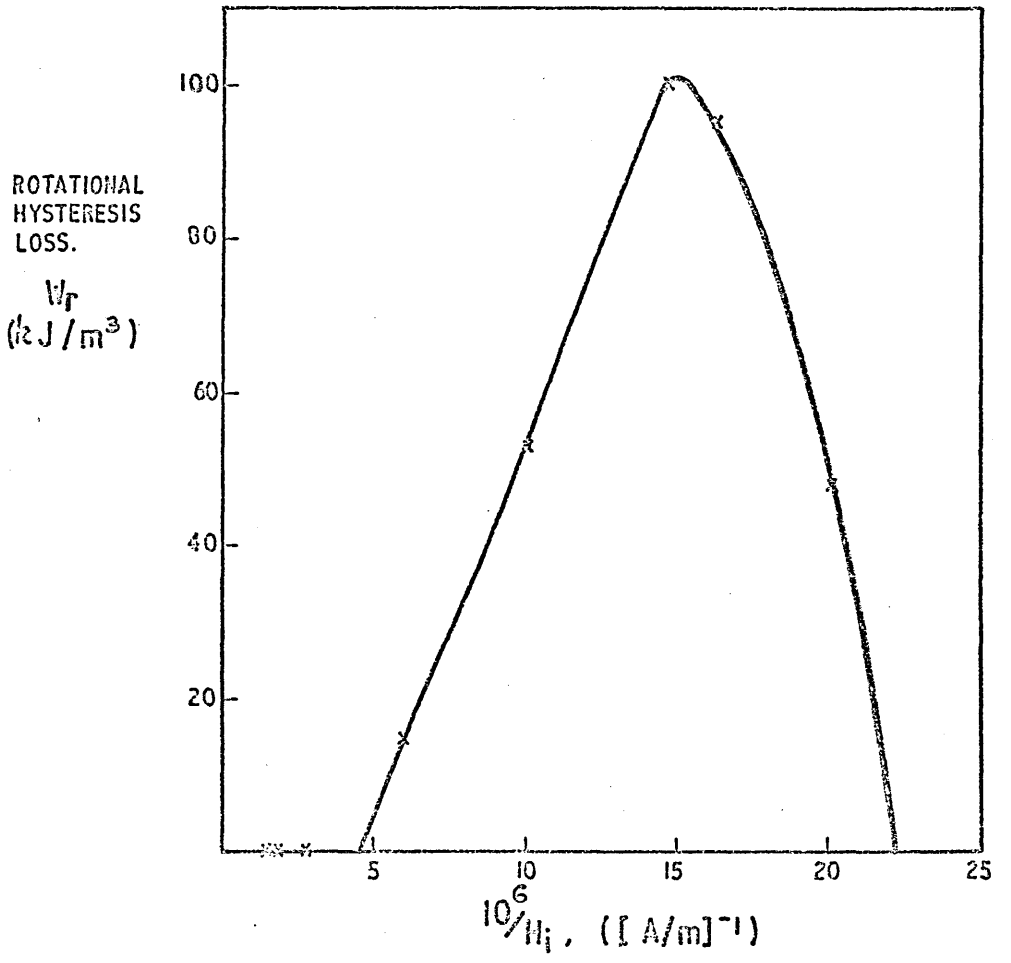

FIG. 114. OBSERVED ROTATIONAL HYSTERESIS LOSS CURVE $W_r - 1/H_i$:, FOR ALLOY CI SAMPLE, AGED AT 650°C FOR 30 min. IN A MAGNETIC FIELD AND TEMPERED (2 h. AT 600°C + 4 h. AT 500°C + 16 h. AT 560°C).

curve (and dividing by J_s). The area was determined by counting the number of 1 mm squares (and part squares) inside the curve on a graph where 1 mm represented a W_r of 10 k/J_m^3 and a reciprocal field of 10^6 $[A/m]^{-1}$.

The value of R was found to be 0.757.

The following values have been marked on the abscissa for the $W_r - H_i$ curve in Fig. 113.

(a) The coercivity H_{CJ} = 62.5 kA/m.

(b) The anisotropy field H_A = 79.3 kA/m corresponding to the measured anisotropy K_s = 53.5 kJ/m^3, as determined from the amplitude of the high field torque curve for the polycrystalline disc of optimally field heat treated alloy C1 (field heat treatment direction in the plane of the discs).

(c) The predicted anisotropy field H_A'' 301 kA/m, corresponding to the predicted value of the anisotropy constant for a perfectly aligned assembly of particles, K_s'', calculated in accordance with the considerations in section 4.3. and specifically equation (4.18) assuming ϕ_n, the maximum angle of deviation of any particle axis from the easy axis, = 54.7°. i.e. $K_s'' = 3.8\ K_s$ [An absolute maximum K_s can also be calculated from equation (1.25) from the saturation magnetisation in this case equal to 1.35 tesla and assuming $(N_c - N_a) = \frac{1}{2}$].

(d) The maximum effective anisotropy field, H_{max} = 220 kA/m, given by the $W_r - H_i$ curve itself. i.e. the field that marks the vanishing of the rotational hysteresis with increasing H_i.

The symbol H_{max} was used to denote this value by Jacobs and Lubosky (60) who also pointed out that the value of H_{max} is independant of the model chosen, as shown in Fig. 115. However H_{max} is here obtained by extrapolation on the $W_r - H_i$ plot as shown in Fig. 113, which, as pointed out by Jacobs and Luborsky, is a useful approximation,

but one which may underestimate the value since the curve may tail off more gradually with H_i.

Clearly H_{max} can be expected to be larger than H_A since the latter is determined from high field measurements which demands complete alignment of magnetisation during the test and therefore is determined strictly by the particle orientations and elongations.

Values of H_i in the region of H_{max} do not necessarily (Fig. 113) produce complete alignment and therefore the hysteresis loss may occur up to the anisotropy field of the individual particles i.e. $H_A^{//}$.

The reduced coercivity h_c defined as the coercivity divided by the anisotropy field is about 0.3 or 0.2 depending upon whether H_{max} or $H_A^{//}$ is used as a measure of the anisotropy field.

As already mentioned the value of H_A is based on the considerations inherent in section 4.3 and particularly on the assumptions that the orientations of the particles are uniformally distributed between 0 and 54.7^o from the measured easy axis in accordance with the crystallography of the alloy system, assuming the particles lie strictly in the nearest <100> to the direction of the applied field during heat treatment of equiaxed polycrystalline samples and that the particles are all exactly the same shape whatever the orientation angle may be. The assumptions have already been called into question in section 6.4.2. by the observed values of remanence which for all the alloys studied are higher than predicted on this basis. The reduced remanence of alloy C1 is about 10.8% higher than predicted from the arguments of section 4.3 using $\phi_n = 54.7^o$. As already pointed out this could be due to magnetic interaction of the particles. However an alternative possibility that some increased alignment due to a slight preference for alignment with the field direction rather than the nearest crystallographic <100> would produce this same effect.

In fact it can be calculated from equation (4.22) that this increase would be produced if the particle orientations were evenly distributed through a solid angle of 42° rather than 54.7°. This implies none of the anomalous increase in j was due to interaction. Calculation of a new K_s using equation 4.18 and from that a value of H_A = 165 kA/m is obtained. This is less than H_{max} and implies that some of the larger than theoretical j is indeed due to interaction at low fields. This demonstrates the uncertainties involved and establishes that H_{max}, as determined from the hysteresis loss curve, is probably the truest estimate of the anisotropy field for the individual particle and h_c = 0.3 is therefore the most accurate estimate of the reduced field.

Fig. 115 shows the theoretical shape of the W_r - H curves for various modes of reversal, i.e. coherent, fanning (60) and curling (48) and Fig, 116 the predicted values of R for these modes (183). Some previously determined values for iron and cobalt particles or "whiskers" are included in the figure. The value of R = .757 found in this work is seen to correspond to a curling mode with a value of S, the reduced particle diameter of about 1.8 which predicts (Fig.12 and 117) a value for h_c (57) of about 0.33. This value is quite close to the previous prediction using H max and the actual coercivity. The measured (W_r/K_s) is about 2.0 which again from Fig. 115 predicts an h_c of about 0.3. H_{max} and R are quite independant values, the latter being the area under the W_r - H curve and the former related more to the actual position of this curve rather than its shape. The consistency of these values lends strong support to the conclusion here that magnetisation reversal occurs by the curling mode.

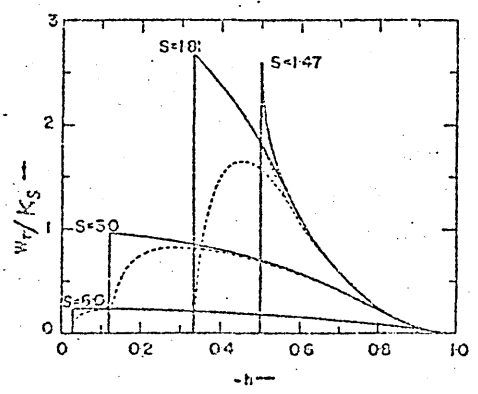

Fig 115. Theoretical curves (48) for rotational hysteresis loss W_r for reversal of magnetisation by curling for aligned (full curves) and random (dashed curves) assemblies of particles as a function of the reduced applied field $h = \frac{J_s^2}{2\mu_0} H$ for long particles. The reduced diameters $s = 2r J_s / 2\mu_0^{\frac{1}{2}} C^{\frac{1}{2}}$, where 2 r is the real diameter and C the exchange constant between two neighbouring spins.

The W_r - H curve for coherent rotation [60] is similar to the above curve for s = 1.47.

The W_r - H curve for fanning [60] is similar to the above curve for s = 1.81.

.....

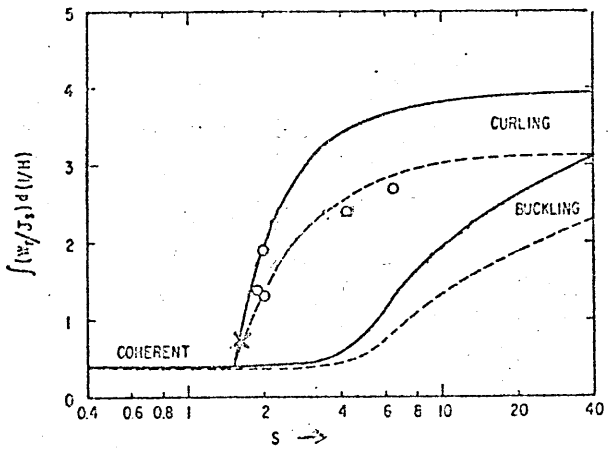

Fig 116. Rotational hysteresis integral $R = \int W_r / J_S \, d\,(1/H)$ for long cylindrical particles reversing magnetisation coherently, by curling or by buckling, calculated for aligned (full curves) and randomly oriented (dashed curves) particles.

Included are experimental points o for plane random dispersions of iron whiskers of various diameters [178] for comparison with × the value determined for alloy C1 assuming the curling mode.

.....

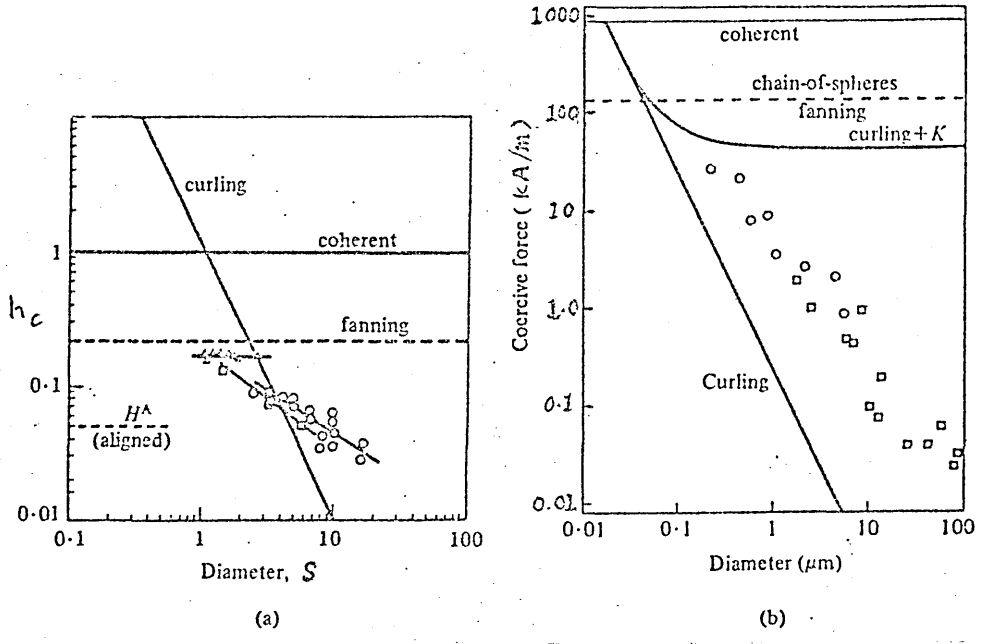

Fig 117 The variation of coercivity with particle diameter for (56,178):-

(a) Δ e.s.d. particles

o iron wire

□ elongated iron particles from the reduction of acicular iron oxides.

In practice [56] for both iron and iron cobalt S is in units of about 12 nm.

The crystal anisotropy field for aligned iron crystals is indicated as H_A

(b) o iron wire

□ iron whiskers [178]

The line marked 'curling + K ' is for the combined effects of shape and crystal anisotropy.

CHAPTER 7.

CONCLUSIONS

1. The most striking observation throughout this work has been the great similarity in magnetic behaviour and metallurgical structure of the Alnico type alloys and the Fe-Cr-Co alloy.

The alloys studied, although they display additional idiosyncrasies peculiar to the individual alloy, all, with the support of TEM observations, behave magnetically (specifically the properties of magnetic anisotropy and coercivity) in a manner consistent with a common transformation mechanism. The evidence supports the view that this mechanism is spinodal decomposition, which initially produces an homogeneous, fine shape-anisotropic particle microstructure, and by subsequent diffusion during heat treatment achieves a highly ferromagnetic state; all of which are necessary conditions for good permanent magnet properties. The results indicates that some contribution to the magnet properties may ensue from further elongation of the particles with prolonged heat treatment. However the evidence indicates that elongated particles aligned, to an extent allowed by crystallographic conditions, with the direction of the applied field during the early stages of heat treatment are produced as the initial spinodal decomposition product, consistent with the theoretical predictions for this mechanism.

2. The rotational hysteresis loss and rotational hysteresis integral specify curling as the mode of magnetisation reversal in alloy C1, the Fe-Cr-Co alloy, after heat treatment to produce the optimum magnetic state.

3. The behaviour of remanence and coercivity for Alcomax 111 and alloy A1 suggested a possible proportional relationship between

coercivity and the saturation magnetisation of the particles during tempering at 600°C. Coherent magnetisation reversal of the particles will give such a relationship at intermediate coercivity levels if it is assumed that some of the matrix magnetisation can reverse prior to the particle magnetisation.

4. Further evidence that, in addition to spinodal decomposition of Fe-Cr-Co alloys, nucleation of Fe rich particles also occurs as a competing mechanism, as found by TEM in alloy C1.

5. The nucleation mode of decomposition becomes more dominant in Fe-Cr-Co alloys with increasing nitrogen contents. The magnetic properties become inferior even at levels of nitrogen which are insufficient to promote markedly increased proportions of f.c.c. phase.

REFERENCES

(1) Stoner, E.C., Proc. Roy. Soc., A154, 656 (1936);
Proc. Roy. Soc., A165, 372 (1938);
Proc. Roy. Soc., A169, 339 (1939).

(2) Cottrell, A.H., "Theoretical Structural Metallurgy"
Arnold, London (1948).

(3) Slater, J.C., J. Appl. Phys. 8, 385 (1937).

(4) Shockley, W., Bell System. Tech. J., 18, 645 (1939).

(5) Stoner, E.C., Phil. Mag[7], 15, 1018 (1933).

(6) Sadron, C., Ann. Physique [10], 17, 371 (1932).

(7) Marian, V., Ann. Physique [11], 7, 459 (1937).

(8) Hoselitz, K., "Ferromagnetic properties of Metals and Alloys"
O.U.P., London (1952).

(9) Weiss, P., J. dePhys., 6, 661 (1907).

(10) Bozorth, R.M., "Ferromagnetism", Van Nostrand,
N.Y & London (1951).

(11) Stoner, E.C., Phil. Mag [7], 36, 803 (1945).

(12) Osborn, J.A., Phys. Rev., 37, 351 (1945).

(13) Cullity, B.D., "Introduction to Magnetic Materials"
Addison - Wesley, London, (1972).

(14) Honda, K., and Kaya, S., Sci.Rep. Tohoku Univ., 15, 721 (1926).

(15) Kaya, S., ibid, 639 and 1157 (1926).

(16) Bloch, F., Z. Phys., 74, 295 (1932).

(17) Zijlstra, H., I.E.E.E. Trans Mag, 6, 179 (1970).
and Van den Brock, J.J., and Zijlstra, H., I.E.E.E.
Trans Mag, 7, 226 (1971).

(18) Brown Jr., W.F., Rev. Mod.Phys. 17, 15 (1945).

(19) Deblois, R.W. and Bean C.P., J. Appl .Phys., 30, 2255 (1959).

(20) Turner, P.A., Stockbridge, C.D., and Theuerer, H.C.,
J. Appl. Phys., 40 1864 (1969).

(21) Barbara, B., Bēcle, C., Lemaire, R., and Paccard, D.,
J. Physique, 32, Collique No.1, 299 (1971).

(22) Nēel, L., Ann. Univ. Grenoble, 22, 299 (1946).

(23) Becker, R., and Döring, W., "Ferromagnetismus", Springer, Berlin (1939).

(24) Kersten, M., "Probleme der technischen magnetisierumgskurve", ed Becker, R., Springer, Berlin (1938). and Phys. Z., 44, 63 (1943).

(25) Friedberg, R., and Paul, D.I., Phys, Rev. Letters 34, 1234 (1974).

(26) Zijlstra, H., Philips. Tech. Rev. 34, No.8, pp 193-207 (1974).

(27) Hadfield, D., "Permanent Magnets and Magnetism " Iliffe, London (1962).

(28) Strnat, K.J. I.E.E.E. Trans. Mag. 6, pp 182-190 (1970).

(29) Kittel, C., and Galt, J.K. Solid State Phys., 3, 437-564 (1956).

(30) Frenkel, J., and Dorfman, J., Nature, 126, pp 274-275 (1930).

(31) Kittel, C., Galt, J.K., and Campbell, W.E., Phys. Rev., 77, 725 (1950).

(32) Luborsky, F.E., J. Appl. Phys. 32, 1715-1835 (1961).

(33) Bean, C.P. and Livingston, J.D., J. Appl.Phys. 30, 1205-1295 (1959)

(34) Adams, E., Rev. Mod.Phys., 25, 306-307 (1953).

(35) Benz, M.G., and Martin, D.L., Appl .Phys. Letters, 17, 176 (1970).

(36) Néel, L., C.R. Acad. Sci. 224, 1550 (1947).

(37) Meiklejohn, W.H., Rev. Mod. Phys., 25, 302 (1953).

(38) Masumoto, H. Kobayashi, T., and Watanabe, K. Trans. Japan Inst. Metals 7, 284 (1966).

(39) Johnson, R.E. PhD Thesis,Sheffield Polytechnic,(1972)Acta Met 20 387 (1972).

(40) Stoner, E.C., and Wohlforth E.P., Phil.Trans.Roy.Soc. A, 240, 599 (1948).

(41) Néel, L., C.R. Acad. Sci.,Paris, 224 1550 (1947).

(42) Néel, L., C.R. Acad. Sci.,Paris, 225, 109 (1948).

(43) Maxwell, J.C., "A Treatise on Electricity and Magnetism" O.U.P. 3rd ed., 2, 69 (1904).

(44) Brown, Jr.,W.F., Am. J. Phys. 28, 542-551 (1960).

(45) Brown, Jr,W.F. and Morrish, A.H., Phys.Rev., 105, 1198-1201 (1957).

(46) Compaan, K., and Zijlstra, H., Phys. Rev., 126, 1722 (1962).

(47) Shtrikman, Thesis, Technion, Haifa (1957).

(48) Aharoni, A., J. App. Phys. 30, 705-795 (1959).

(49) Wohlfarth, E.P., Proc. Roy. Soc. A 232 208-227 (1955).

(50) Wohlfarth, E.P., "Magnetism" Nado, G.T., and Suhl, H., eds. Vol 3 pp. 351-393 Academic Press N.Y. & London (1963).

(51) Zijlstra, H., Thesis, Univ. of Amsterdam (1960).

(52) Adams, E., Hubbard, M.W., and Syeles, J., J. Appl. Phys. 23, 1207-1211 (1952).

(53) Stijts, A.L., Rathenau, G.W., and Weber, G.H., Philips Tech. Rev. 16, No.5, 141-147 (1954).

(54) Sixtus, K.J., Kronenberg, K.J., and Tenzer, R.K., J.Appl.Phys., 27, No.9, 1051-1057 (1956).

(55) Mendelsohn, L.I., Luborsky, F.E., and Paine, T.O., J.Appl.Phys., 26, 1274-1280 (1955).

(56) Luborsky, F.E., J. Appl. Phys., 32, 171S-183S (1961).

(57) Frei, E.H., Shtrikman, S, and Treves, D., Phys. Rev.106, 446-455 (1957).

(58) Jacobs, I.S., and Bean, C.P. Phys. Rev. 100, 1060-1067 (1955).

(59) Shtrikman, S., and Treves, D., "Magnetism", Rado, G.T., and Suhl, H., eds., Vol 3 pp 395-414. Academic Press, N.Y. and London (1963).

(60) Jacobs, I.S., and Luborsky, F.E., Conf. on Mag and Magn. Mat. IEE. 145 (1957).

(61) Bradley, A.J., and Taylor, A., Proc.Roy.Soc.(London) A166, 353 (1938).

(62) Bradley, A.J., J. Iron St. Inst. London, 163, 19 (1949).
ibid 168, 233 (1951).
ibid 171, 41 (1952).

(63) Gould, J.E., "Cobalt Alloy Permanent Magnets", Cobalt Monograph series, Centre D' information Du Cobalt, Brussels (1971).

(64) Mishima, Brit. Pats. 392, 656, to 392, 659 and 392, 661 (1933).

(65) Fried. Krupp A.G., Brit. pat. 425, 455 (1935).

(66) Horsburgh, G.D.L., and Tetley, F.W., Brit. pat.431, 660 (1935).

(67) Oliver, D.A., and Sheddon, J.W., Nature, 142, 209 (1938).

(68) Jonas, B., and Emden, H.J.M., Phillips. Tech. rev.6, 8 (1941).

(69) McCaig, M., J. Appl. Phys., 24, 366 (1953).

(70) Koch, A.J.J., v.d. Steeg, M.G., and de Vos. K.J., Prod. Conf. on Magn. & Mag.Matls. Boston,173 (1956).

(71) Wright, W., and Thomas, A., Cobalt, 13, 24 (1961).

(72) Harrison, J., and Wright, W., Cobalt, 35, 63 (1967).

(73) Köster, W., Arch. Eisenhüttenw., 7, 357 (1933).

(74) Geisler, A.H., Trans. Amer.Soc. Metals, 43, 1 (1951).

(75) Heidenreich, R.D. and Nesbitt, E.A. J. Appl.Phys., 23,352 (1952).

(76) Nesbitt, E.A., Williams, H.J., and Bozorth, R.M., J. Appl. Phys., 25, 1014 (1954).

(77) Magat, L.M., Shur, Ya,S., and Melisheva, E.M., Phys. Metals. Metallog., 17, (2), 130 (1964).

(78) Burgess, W.G., and Snoek, J.L., Physica 2, 1064 (1935).

(79) Snoek, J.L., Physica 6, 321 (1939).

(80) de Vos, K.J., Ph. D. thesis, Univ. of Eindhoven (1966).

(81) de Vos, K.J., Proc. Int. Conf. Mag., Nottingham, 772 (1964).

(82) Oliver, D.A. Goldschmidt, H.J., Elec.Res.Rept. N/T41 (1947).

(83) Shur, Ya. S., Magat, L.M., and Yermolenko,A.S., Phys.Metal Metallog. 14, (3), 117 (1962).

(84) Pfeiffer, I., Cobalt 44, 115 (1969).

(85) Bronner, C., Sauze, J., Planchard, E., Drapier, J.M., Coutsouradis, D., and Habraken, L., Cobalt 36,123 (1967).

(86) Kronenberg, K.J., J. Appl. Phys., 31, 805 (1960).

(87) Nesbitt, E.A., and Heidenreich, R.D., J.Appl.Phys.,23,366 (1952).

(88) Nesbitt, E.A., and Williams, H.J., J. Appl.Phys., 26,1217 (1955).

(89) Fahlenbrach, H., Tech.Mitt. Krupp 12, 177 (1954).

(90) Schultz, D., Exp. Tech. Physik, 4, 193 (1956).

(91) Haanstra, H.B., de Jong, J.J., and Smeets, J.M.G., Philips Tech. Rev., 19, 11, (1957-58).

(92) Campbell, R.B., and Julien, C.A. J. Appl. Phys., 32, 1925 (1961).

(93) Fahlenbrach, H., Stäblein, H., Proc.Int.Conf.Mag.,Nottingham, 767 (1964).

(94) Granovskiy, Ye. B., Pashkov, P.P., Sergeyer, V.V., and Fridman, A.A., Phys.Metals Metallog, 23, (3),55(1967).

(95) Livshitz, B.G., Krizhnik, E.G., Kraposhin, V.S. and Linelsky,Ya.L., I.E.E.E. Trans.Mag., 6, 237 (1970).

(96) Clegg, A.G., and Mc Caig, M., Proc. Phys.Soc., B.70, 819 (1958).

(97) van Wieringen, J.S., and Rensen, J.S., Z. Angew, Physik, 21, 69 (1966).

(98) Paine, T.O., and Luborsky, F.E., J. Appl.Phys., 31, 78S (1960), ibid 31, 66S (1960).

(99) Mason, J.J., Ashall, D.W. and Dean A.V. I.E.E.E. Trans.Mag., 6 191 (1970)

(100) Gladyshev, S.N., Zakharova, M.I., Ilyushin, A.S., and Leonova,G.L., Phys. Metal Metallog., 54, (1972).

(101) Pashkov, P.P., Fridman, A., and Grenovsky, E., I.E.E.E. Trans. Mag, 6, 211 (1970).

(102) Bozorth R.M., "Ferromagnetism", Van Nostrand, N.Y., London (1951).

(103) Keneko, H., Homma, M., and Nakamura, K., Proc. A.I.P. Conf. 5, 1088 (1971).

(104) Keneko, H., Homma, M., Nakamura, K., and Muira, M., I.E.E.E. Trans. Mag., 8, 347 (1972).

(105) Higuchi, A., Kamiya, M., and Suzuki K., Proc.3rd Euro. Conf. on Hard Mag. Mat., Amsterdam,201(1974)

(106) Keneko, H., Homma M., Fukumaga, T., and Ohada, M. I.E.E.E. Trans.Mag., 11, 1440(1975).

(107) McCaig, M., I.E.E.E. Trans. Mag., 11, 1443 (1975).

(108) Becker, J.J., AIME Trans., 209, 59 (1957). ibid 212, 138 (1958).

(109) Livingston, J.D., and Becker, J.J., AIME Trans., 212, 316 (1958).

(110) Livingston, J.D., AIME Trans., 215, 566 (1959).

(111) Wohlfarth, E.P., Advances in Physics, 8, 87 (1959).

(112) Williams, R.O., and Paxton, H.W., J.I.S.I., 185, 358 (1957).

(113) Williams, R.O., AIME Trans., 212, 497 (1958).

(114) Kubaschewski, O., and Chart, T.G., J.I.M., 93, 329 (1964-65).

(115) Rao, M.V., and Tiller, W.A., Scripta Met. 6, 417 (1972).

(116) Chandra, D., and Schwartz, L.H., Met. Trans., 2, 511 (1971).

(117) De Nys, T., and Gielen, P.M., Met. Trans., 2, 1423 (1971).

(118) Nesbitt, E. A, J. Appl. Phys. 21, 879 (1950).

(119) Kittel, C., Nesbitt E.A., and Shockley, W., Phys. Rev. 77, 839(1960)

(120) Nesbitt, E.A., Williams, A.J. Proc.Conf.Magn. and Magn. Mat., Boston, 184 (1956).

(121) Zijlstra, H., J. Appl. Phys. 32 (3), 1945 (1961).

(122) Daniel, V., and Lipson, H., Proc.Roy.Soc. 182, 378, (1943).

(123) Bradley, A.J., Proc. Phys. Soc., 52, 80 (1940).

(124) Hargreaves, M.E., Acta Cryst., 4, 301, (1951).

(125) Butler, E.P., Thomas G., Acta. Met., 18, 347 (1970), and Butler, E.P., Met. Sci. Journal 5, 8 (1971).

(126) Biedermann, E., and Kneller, E., Z. Metallk., 47, 289, 760 (1956).

(127) Phillips, V.A., Inst.of Metals Monograph 33, 11 (1969).

(128) Hillert, M., Acta Met. 9, 525 (1961).

(129) Guiner, A., ibid, 3 510, (1955).

(130) Cahn, J.W., Trans. A.I.M.E., 242, 166 (1968).

(131) Hilliard, J.H, "Phase Transformations" Cahn, J.W., ed. A.S.M.(1970)

(132) Cahn, J.W., Acta Met., 9, 795 (1961), and ibid 10,179 (1962).

(133) Cahn, J.W., J. Appl. Phys., 34, 3581 (1963).

(134) Huston, E.L., Cahn, J.W., and Hilliard, J.E., Acta Met., 14, 1053 (1966).

(135) Cahn, J.W. Acta Met., 14, 1685 (1966).

(136) Morral, J.E., and Cahn, J.W., Acta Met., 19, 1037 (1971).

(137) Bulygina, T.I., and Sergeyer, V.V., Phys.Metals Metallog., 27 (4), 132 (1969).

(138) Magat, L.M., Phys. Metal Metallog., 19, 35 (1965), and ibid 20, (3), 170 (1965).

(139) Jellinghous, W., Arch. Eisenhüttenw., 16, 247 (1943).

(140) Bronner, C, Haberer, J, P., Planchard, E., and Sauze, J., Drapier, J.M., Coutsauradis, D., and Habraken, L., Cobalt, 40, 131 (1968) and Cobalt, 42, 14 (1969).

(141) Imai, Y., Izumiyama, M., and Masumoto, T. J. Japan Inst.Metals, 30, 284 (1966).

(142) Lifshitz, I.M., and Slyozov, V.V., J. Phys.Chem.Solids, 19, 35 (1961).

(143) Wagner, C., Z. Electrochem., 65, 581 (1961).

(144) Oriani, R.A., Acta. Met., 12, 1399 (1964).

(145) Speich, G.R., and Oriani, R.A., Trans AIME., 233, 623 (1963).

(146) Ardell, A.J., Acta Met., 15, 1772 (1967).

(147) Ardell, A.J., and Nicholson, R.B., ibid, 14, 1295 (1966).

(148) Greenwood, G.W., Inst. Metals mon & rept series 33, 103 (1969).

(149) Ardell, A.J., ibid, 33, 111 (1969).

(150) Bower, E.N., and Whiteman, J.A., ibid, 33, 119 (1969).

(151) Faulkner, R.G., and Ralph, B., Acta Met., 20, 703 (1972).

(152) Jack, D.H., and Honeycomb, R.W.K, ibid, 20, 787 (1972).

(153) Flewitt, P.E.J., ibid, 27, 47 (1974).
ibid, 27, 65 (1974).

(154) Gentry, W.O., and Fime, M.E., ibid, 20, 181 (1972).

(155) Sucksmith, W. Proc.Roy.Soc. (London) 170A, 551 (1939).

(156) McCaig, M., "Permanent Magnets" Pentech Press, London (1977).

(157) Scholes, R., J. Scient. Instrum, 1, 1016 (1968).

(158) Greppi, G., and Buzzetti, G., Centro Magneti Perminanti, Milano, Italy (1974).

(159) Klitzing, K.H., Z. Inst. 65, 4 (1957).

(160) Johnson, W.A., and Mehl, R.F., Trans AIME, 135, 416 (1939).

(161) Aurami, M., J. Chem. Phys., 7, 103 (1939).
ibid 8, 212 (1940).
ibid 9, 177 (1941).

(162) Stanley, J.K., and Mehl, R.F., Trans AIME, 150, 260 (1942).

(163) Mehl, R.F., J.I.S.I., 159, 113 (1948).

(164) Gibbs, J.W., collected works, Yale University Press (1948).

(165) Hopper, R.W., and Uhlmann, D.R., Acta Met. 21, 377 (1973).

(166) Langer, J.S., ibid, 21, 1649 (1973).

(167) Gerold, V., and Mertz, W., Scripta Met., 1, 33 (1967).

(168) Feynman, R.P., "The Feynman Lectures on Physics" Vol.3, Addison Wesley, 1963.

(169) Mook, H.A., and Shull, C.G., J. Appl.Phys. 37, 1034 (1966).

(170) Mirold, P., and Binker, K., Acta Met., 25, 1435 (1977).

(171) Serin, B., and Ellickson, R.T., J. Chem. Phys., 9, 742 (1941).

(172) Olson, F.C.W., and Schultz, O.T., Ind.Eng.Chem., 34,879 (1942).

(173) Darken, L.S., and Gurry, R.W., "Physical Chemistry of Metals", McGraw Hill (1953), chapter 18.

(174) Vintaykin, Ye.Z., Urushadze, G.G., Belyatskaya, I.S., and Sukharova, Ye.A., Fiz. Metal. Metalloved, 38, No.5,1012(1974).

(175) Marcon, G., Bronner, C., and Peffen, R., Cobalt, 51, 99 (1971).

(176) Marcinkowski, M.J., Fisher, R.M., and Szirmae, A., Trans. AIME, 230, 676 (1964)

(177) Houghton, M.E., Rossiter, P.L., and Clark, P.E., J.Met.Sci., 13, 155 (1978).

(178) Takara, R., Nakamura, Y., Inagaki, M., and Iwana, Y., "Proc.Int.Conf. on Mössbauer Spectroscopy, Cracow", 1, 107 (1975).

(179) Cremer, R., and Pfeiffer, I., Physica, 80B, 164 (1975).

(180) Gray, P., Hadfield, D., and Rayson, H.W., Proc.3rd. Eur. Conf. on Hard Magn. Mat. (Amsterdam), 193 (1974).

(181) Gray. P., Rayson, H.W., and Hadfield, D., Proc.2nd IEE Conf. Adv. in Magn.Mat. and Appl.(London),153 (1976).

(182) Fuller, H.W., and Hale, M.E., J. Appl. Phys. 31, 238 (1960).

(183) Luborsky, F.E., and Morelock, C.R., J. Appl.Phys., 35,2055 (1964).

(184) Livshitz, B.G., Sumin, V.I., and Lileev, A.S., I.E.E.E. Trans on Magnetics, 6, 169 (1970).

APPENDIX I

(51)

(a) Functions used in Zijlstra Thesis.

symbol used here.	symbol used in Zijlstra if different.	
m	p	Axial ratio of equal shape and size particles arranged in a tetragonal array.
b		Axial separation of particles in a direction normal to that of the long axis of the particles.
t		Ageing time.
V		Total volume of particle
p	δ	Volume fractions of particle i.e. $V = pb^3$
P_1		$= m^{-1} \times m\,(m^2-1)^{-\frac{1}{2}} \arctan\sqrt{m^2-1}$
P_2		$= \frac{N_c}{2} = m(m^2-1)^{-3/2} \ln\left(m+\sqrt{m^2-1}\right) - (m^2-1)^{-1}$
P_3		$= 3m(m^2-1)^{-2} - (2m^2+1)(m^2-1)^{-5/2} \ln\left(m+\sqrt{m^2-1}\right)$
P_4		$= (m^2+2)m^{-2}(m^2-1)^{-1} + (m^2-4)(m^2-1)^{-7/2} \arctan\sqrt{m^2-1}$
P_5		$= m + (m^2-1)^{-1/2} \ln\left(m+\sqrt{m^2-1}\right)$
P_6		$= \frac{1}{2}(m^2-1)^{-1}\left\{m^2(m^2-1)^{-1/2} \arctan\sqrt{m^2-1} - 1\right\}$
P_7		$= (m^2-1)^{-1}\left\{2m^2+1+(1-4m^2)m^{-1}(m^2-1)^{-1/2} \ln\left(m+\sqrt{m^2-1}\right)\right.$
P_8		$= \frac{3}{2} m(m^2-1)^{-2} - \frac{1}{2}(m^3+2m)(m^2-1)^{-5/2} \arctan\sqrt{m^2-1}$
A_1		$= \frac{1}{2}(\Delta J_s)^2 \eta$ (η = factor accounting for mutual interaction of particles)
A_2		$= 0.805\, p\sigma$ (σ = interfacial tension between particles and matrix.)
L_1		= Factor independant of V, m and t
L_2		= unknown constant.

(b) Extra functions used here to solve Zijlstras simultaneous differential diffusion equations for all values of m

Symbol

α Function expressing deviations of l_v as defined by Zijlstra from $l_{v_1} = 0.27 b m^{1/3}$

(see Zijlstra's equations (4-20) and (4.41) and sections 4.33 and 4.5 of ref 51)

α is = 1 in range $3.5 < m < 10$, dependant on m but independant of V & t.

$K = -24.3\ L_1\ A_1$

$\beta = \dfrac{m^2\ P_1 P_3}{\alpha}$

$\gamma = 6.75\ \left(\dfrac{m^2 P_4}{P_1}\right)$

ζ = Function expressing deviation of P_2 from $0.33\ (m - 0.7)^{-1.25}$

$\zeta \doteq 1$ for $3 < m < 10$.

(c) Calculations of factors required in value determination for solutions of Zijlstra's Equations.

m	P_1	P_2	P_3	P_4
1.01	1.9934131	0.330777	-0.2849	0.02073
1.1	1.9405414	0.3082829	-0.235193	0.175040
1.2	1.8928768	0.2861223	-0.208616	0.2921162
1.3	1.8540367	0.2664352	-0.1860578	0.3707452
1.4	1.8219352	0.2488008	-0.1667418	0.4233384
1.5	1.7950787	0.2329596	-0.1500798	0.4579274
1.6	1.7723697	0.2187118	-0.1356217	0.4798831
1.7	1.7529846	0.2057972	-0.1230301	0.4928724
1.8	1.7363018	0.1940566	-0.1119893	0.4994408
1.9	1.7218323	0.1833563	-0.1022760	0.5013875
2	1.7091983	0.1735638	-0.0936786	0.50000
3	1.6389647	0.1087085	-0.0443856	0.4247837
4	1.6113449	0.0754051	-0.0248371	0.347268
5	1.5976758	0.0558190	-0.0153449	0.2895933
6	1.5899199	0.0432229	-0.0102649	0.2470356
7	1.5850970	0.0346079	-0.0073096	0.2148409
8	1.5818939	0.0284255	-0.0052904	0.1898089
9	1.5796580	0.0238276	-0.0040027	0.1698616
10	1.5780365	0.0202802	-0.0031085	0.1536278
15	1.5740999	0.0107341	-0.0011451	0.1036535
20	1.572679	0.0067144	-0.0005522	0.0780802
30	1.5716420	0.0034321	-0.0001929	0.0522207

m	α	β	γ	ζ
1.01	0.3280576	1.765966	0.0716058	0.2318586
1.1	0.4105572	1.3451134	0.7367218	0.2971744
1.2	0.4870576	1.1674869	1.5000286	0.364544
1.3	0.5510925	1.0578605	2.2811176	0.4263512
1.4	0.6053107	0.9836827	3.0740758	0.4827368
1.5	0.6516586	0.9301823	3.874355	0.5341085
1.6	0.6916124	0.8897349	4.6786964	0.5809807
1.7	0.7262978	0.8581685	5.4847648	0.6236278
1.8	0.7566039	0.8326799	6.2908245	0.6624527
1.9	0.7832282	0.8116773	7.095673	0.6978435
2	0.8067317	0.7938961	7.8984398	0.7300861
3	0.9402966	0.6962885	15.745006	0.9330578
4	0.9895445	0.6471038	23.275553	1.0163171
5	1.008023	0.6080261	30.587475	1.0473792
6	1.0128365	0.5800869	37.756398	1.0532822
7	1.0108925	0.5616173	44.829197	1.0467356
8	1.0054101	0.5327243	51.834983	1.033589
9	0.9980355	0.5131627	58.792364	1.0172182
10	0.989666	0.4956546	65.71379	0.9980728
15	0.9451111	0.4291165	100.00874	0.9045264
20	0.9049377	0.3838643	134.04931	0.8605585
30	0.8412837	0.3243289	201.85306	0.7089736

APPENDIX II

Electron Diffractions in the Alnico and Fe-Cr-Co Alloy Systems

The restrictions on the diffracted ray of electrons (or X-rays) is given by the Bragg law

$$n\lambda = 2d \sin \theta$$

representing a beam of electrons of wavelength λ, impinging at an angle θ on a set of crystal planes of spacing d. A beam is reflected at the angle θ only if the rays from each successive plane reinforce each other, and for this to occur the extra distance that a ray scattered from each successive plane has to travel must be equal to an integral number of wavelengths $n\lambda$ where n is an integar from 1 upwards.

It is conventional, when considering cubic crystal lattices, to incorporate or identify the order of reflection, n, with the Miller indices corresponding to the atomic sites in the lattice

$$\text{i.e.} \quad n\lambda = \frac{2a \sin \theta_{hkl}}{\sqrt{h^2 + k^2 + l^2}}$$

The possible values of the angle of diffraction of the beam are determined by the integral values of h, k, and l, in the path difference. If, initially, an ideal simple cubic crystal is considered (A) with an electron beam parallel to a cube edge and a photographic plate placed normal to the incident beam, then a diffraction picture will be obtained from all juxtaposed closely spaced parallel planes in the lattice.

It can be shown that the diffraction under such conditions will consist of spots which lie on hyperbolic or elliptical tracks as shown in (B). However, the curvature of the lines in (B) is exaggerated (for electron beams) and since the wavelength of electrons is so small the hyperbolae approximate to nearly straight lines (and $\sin \theta \simeq 0$).

It is observed that a given spot in the pattern lies in the direction of the plane normal from the origin in the lattice but at a distance which is proportional to the reciprocal of the displacement of the plane from the origin. This is in fact found to be true whichever the orientation of the electron beam with respect to the crystal axes. Thus identification of any orientation can be recognised as corresponding to some plane in the reciprocal lattice composed of a system of points, each of which represents a reflecting plane in the crystal and has the same indices as the corresponding reflecting plane.

The Fe-Cr-Co and Fe-Al-Ni-Co magnet alloys studied here are body centred cubic rather than simple cubic. Thus there is an extra atom introduced as shown in (C) which shows the unit cell and the lattice points projected onto (001). It can be seen that the body centred atoms effectively introduce an intermediate parallel plane of atoms between the (100), and a new plane spacing d_{200} which is half of d_{100}. The new d_{200} will produce half the path difference of d_{100} and therefore destructively interfere. There will therefore, be no spots corresponding to the (100) in the diffractions patterns for B.C.C. crystal structures. If this is taken into account then it is found that the reciprocal lattice for the real B.C.C. lattice is an F.C.C. lattice.

(D) shows some of the sections from the reciprocal lattice for B.C.C. crystals. Indentification of foil planes from selected area diffraction patterns were established by comparison with such patterns, or measurement of angles between spots to establish the corresponding plane in the reciprocal lattice. In addition, if necessary, the orientation of the direction of the long axis of particles in the foil could also be established for such patterns. A rough idea of the lattice parameter could be obtained using the camera constant $L\lambda$ (previously determined for a well known crystal

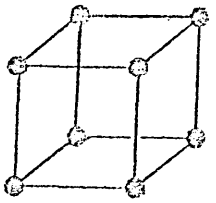

(A)

simple cubic unit cell

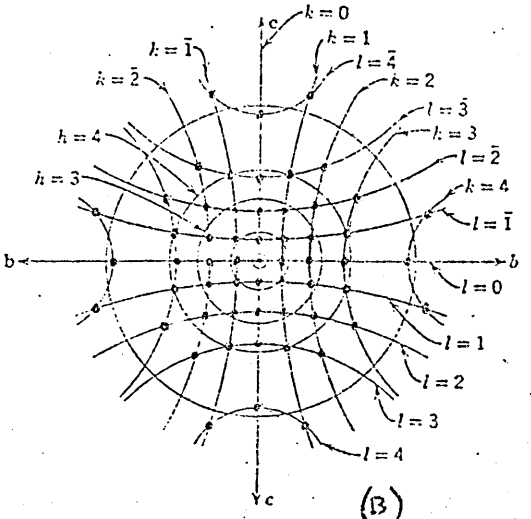

(B)

diffraction pattern from a simple cubic lattice

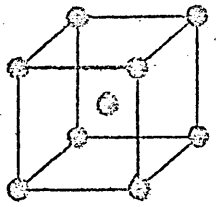

body centred unit cell

(C)

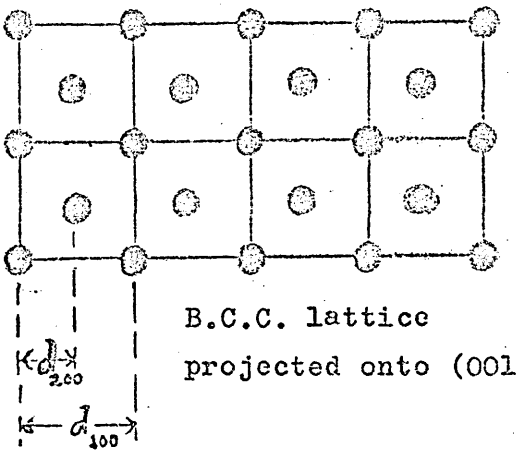

B.C.C. lattice projected onto (001)

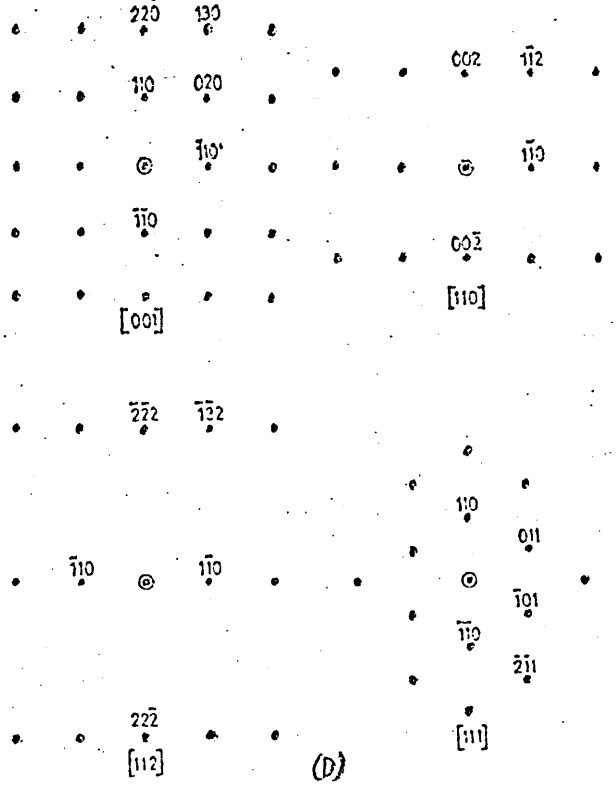

(D)

single crystal electron diffraction patterns with specific zone axes from B.C.C. structures

structure) from $d = \frac{L\lambda}{r}$ where r is half the distance apart of corresponding spots in the single crystal patterns. Such measurements generally confirmed previously measured lattice parameters and <100> alignment of the particles.

The Fe-Al-Ni-Co and Alnico alloys are known to be ordered, (84, 85) or at least one of the phases, the matrix phase which is rich in Ni and Al, is believed to be a preferred site for Al atoms (61). Thus reflections will occur which for the disordered B.C.C. alloy would be forbidden. Diffraction spots corresponding to the (100) will be weaker than the other spots as shown in (E). This was indeed what was observed in Alnico type alloys, as found previously by other investigators (84, 85).

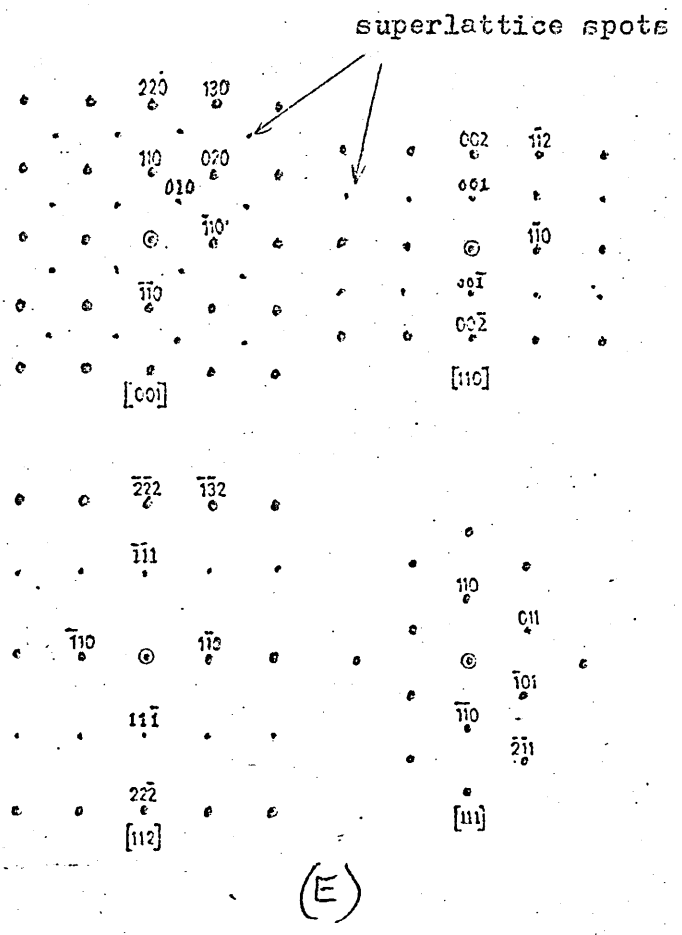

Electron diffraction patterns from B.C.C. structures with regular atomic arrangment of different atomic species at corner and body center sites.